KINETIC AND THERMODYNAMIC STUDIES ON THE EFFECT OF CHAOTROPIC AND KOSMOTROPIC COSOLVENTS ON PROTEINS

A THESIS

submitted to

THAPAR UNIVERSITY, PATIALA

for the degree of

DOCTOR OF PHILOSOPHY

by

Rishu Jain

Regn. No. 901009006

SCHOOL OF CHEMISTRY AND BIOCHEMISTRY

THAPAR UNIVERSITY, PATIALA

PATIALA-147004, PUNJAB (INDIA)

Acknowledgement

If a fellow isn't thankful for what he's got, he isn't likely to be thankful for what he's going to get.

Frank A. Clark

Since childhood I have been told that while standing at start point you should always keep your eye on the final destination so to have a clear picture what exactly you want and taking the second step towards the destination defines that one is ready to pay whatever it takes to achieve that goal with described objectives like time etc. The distance between these points is not less than a goal to be achieved everyday every moment which might not be possible without proper guidance, support and motivation. Standing at this finish line, when I look back throughout the journey between these two points, it brings lots of memories which are precious and unforgettable for me. I want to pay my gratitude to all the people who had been part of my journey and made me to reach here today.

It is impossible to achieve your goal without proper guidance and support for which we need a guide who will stand by us, support us, teach us, describe DO's and DON'T's. Guide is a person who will keep you bound to ultimate goal and make this journey a wonderful stint. I am lucky to have a Guide like **Dr. Rajesh Kumar, Associate Professor, Thapar University, Patiala,** who was always there for me throughout and made me to achieve it today. I am not wrong if I say it would have not been possible without him. He guides me sometimes like parents, sometimes like friend and like a guardian who really wanted me to be here. Though it's not possible to thank him in words still I want to say THANK YOU for making it possible for me, thanks from deep of my heart.

I offer special thanks to **Dr. Bonamali Pal, Head, School of Chemistry and Biochemistry, Thapar University, Patiala** and other faculty members of our department for providing all the necessary lab equipments and facilities in the department. They patiently provided the vision, encouragement and advice necessary for me to move through the doctoral program and complete my dissertation.

I would like to thank all the members of my doctoral committee, **Dr. Susheel Mittal** (Senior Professor, School of Chemistry and Biochemistry), **Dr. Bonamali Pal** (Professor, School of Chemistry and Biochemistry), and **Dr. Siddarth Sharma** (Assistant Professor, Department of Biotechnology) for giving their valuable suggestions in the progress of research work.

Also I want to extend my special thanks to **Dr. Deepak Sharma (Scientist E, Institute of Microbial Technology, Chandigarh)** for his consistent helps and supports throughout my Ph.D research work.

I can never forget to acknowledge the Department of Science and Technology (Govt. of India) for providing me financial assistance in the form of **INSPIRE Fellow** (IF 110240) which supported me to perform my work comfortably.

With heart full feelings I acknowledge my lab mates Mr. Sandeep Kumar and Mr. Rajesh Kumar and many others research scholars here at Thapar University, Patiala.

My special gratitude and love for my elder sister Dr. Anupriya Jain, who had always been with me and keep me motivated towards achievement of my goal. Sometimes I felt half hearted but she always kept me going throughout. She cared for me like Mom Dad and giggled like the best friend. She had been soul of my journey, Thanks a ton and love you Anu.

I owe a special thanks to my family, my Maa and Papa, my Jiju and my younger brother, Bhavesh, who always supported me and helped me throughout my Ph.D. Maa and Papa, I really do not know how to thank you enough for providing me with the opportunity to be where I am today. I dedicate this all work to you. You are indispensible part of my journey and it is for my complete life.

Last but not the least, I would like to pay high regards to Saraswati the Goddess of knowledge who gave me some intellect and wisdom to reach where I am today.

Rishu Jain

CANDIDATE'S DECLARATION

I hereby declare that the work presented in the thesis entitled ***"Kinetic and Thermodynamic Studies on the Effect of Chaotropic and Kosmotropic Cosolvents on Proteins"*** *being submitted in the partial fulfilment of requirements for the award of degree of* ***Doctor of Philosophy*** *submitted in the* ***School of Chemistry and Biochemistry, Thapar University, Patiala*** *is an authentic record of my own work carried out under the supervision and guidance of* ***Dr. Rajesh Kumar,*** *Associate Professor, School of Chemistry and Biochemistry, Thapar University, Patiala. The matter embodied in this thesis has not formed the basis for the award of any other degree of this or any other university.*

Date: 17.7.14

Rishu Jain

Place: Patiala

(Rishu Jain)

This is to certify that above statement made by the student concerned is correct and true to the best of my knowledge.

Dr. Rajesh Kumar

(Supervisor)

Head of the Department

D R & SP

17.07.14

External Examiner

List of Abbreviations

Abbreviation	Description
Ferrocyt *c*	Ferrocytochrome *c*
Ferricyt *c*	Ferricytochrome *c*
Cyt *c*	Cytochrome *c*
Cyt-CO	CO-liganged ferrocytochrome *c*
Mb	Myoglobin
MbCO	Carbonmonoxymyoglobin
Lyz	Lysozyme
CO	Carbonmonoxide
GdnHCl	Guanidine hydrochloride
TMAO	Trimethylamine-*N*-oxide
GB	Glycine betaine
MG	Molten globule
SDS	Sodium dodecyl sulfate
TFE	2,2,2-Triflouroethanol
WT-equation	Wyman-Tanford equation
CD	Circular dichroism
UV	Ultra violet
Trp	Tryptophan
M80	Methionine-80

Contents

Abstract

To find out the effects of alcohols on the low-frequency local motions that control slow changes in structural dynamics of native-like compact-states of proteins, the effects of alcohols on structural fluctuation of M80-containing Ω-loop have been evaluated by measuring the rate coefficients for slow thermally-driven CO-dissociation reaction of a natively-folded carbonmonoxycytochrome *c* (NCO) under varying concentrations of alcohols (methanol, ethanol, 1-propanol, 2-propanol, 3°-butanol, and 2,2,2-trifluoroethanol (TFE)) at pH 7.0. As alcohols concentration is increased within the subdenaturing limit of denaturant, the rate coefficients for CO-dissociation reaction decrease, indicating that subdenaturing concentrations of alcohols decrease the spatial displacement of thermal motion of Ω-loop. The spatial displacement of thermal motion of the Ω-loop is decreased most for TFE and 1-propanol and least for methanol. This finding indicates that the thermal motion of the protein in the subdenaturing limit of alcohols is controlled by the hydrophobicity of alcohol as well as by some specific effects of alcohols. Thermal denaturation studies of ferrocytochrome *c* (Ferrocyt *c*) and myoglobin (Mb) at pH 7.0 and lysozyme (Lyz) at pH 2.3 in the presence of various concentrations of these alcohols suggest that alcohols decrease the thermal stabilities of native and partially denatured proteins. The stabilization free energy ($\Delta\Delta G$) of Ferrocyt *c* and Lyz in alcohols solution was calculated from the slope of the Wyman-Tanford (WT) plot and water activity. The *m*-values obtained from the slope of $\Delta\Delta G$ *vs* [alcohols] plots were found to be more negative for longer and linear chain alcohols, consistent with destabilization of proteins by alcohols through the disturbance of hydrophobic interactions and hydrogen-bonding.

Compatible osmolyte such as glycine betaine (GB) and low concentrations of chaotropic denaturants such as guanidine hydrochloride (GdnHCl) and urea decrease the motional freedom of native Ferrocyt *c* at pH 7.0. This deduction is made from the kinetic and thermodynamic parameters measured for CO-dissociation reaction of NCO under varying concentrations of GB, GdnHCl and urea at pH 7.0. Measurement of the rate coefficients for CO-replacement reaction of carbonmonoxymyoglobin (MbCO) by hexacyanoferrate ions under varying concentrations of GB at pH 7.0 suggests that GB also restrict the internal dynamics of native Mb. The rate coefficients and activation thermodynamic parameters (activation enthalpy and activation entropy) measured for CO-dissociation reaction of NCO under varying concentrations of GdnHCl and urea in the

absence and presence of 1.0 M GB at pH 7.0 indicate that (i) within the subdenaturing limit of denaturants, GB and GdnHCl or urea show a cumulative effect on the constrained dynamics of NCO, and (ii) en route from subdenaturing to denaturing conditions large-scale subglobal unfolding motions come to dominate the dynamics and the inclusion of GB opposes the structural fluctuations that cause unfolding of the protein. Thermal and chemical denaturation studies of ferricytochrome *c* (Ferricyt *c*), Ferrocyt *c* and Mb at pH 7.0 in the presence of different concentrations GB and TMAO at pH 7.0 and at pH 3.8-4.5 suggest that GB and TMAO increase the thermodynamic stability of these proteins at neutral pH, while decrease it at mildly acidic pH. Thermodynamic analysis of thermal and urea-induced unfolding transitions of Ferricyt *c* and Mb measured at different GdnHCl concentrations in the absence and presence of GB or TMAO at pH 7.0 and pH 3.8-4.5 suggests that GB and TMAO counter the deleterious effect of denaturant in native proteins at neutral pH while they show the additive effect on the destabilizing action of denaturant at mildly acidic pH 3.8-4.5.

To determine the effect of chaotropic and kosmotropic salts on the low frequency local motions that control slow changes in structural dynamics of native proteins, the rate coefficients and activation thermodynamic parameters (activation enthalpy and activation entropy) for slow thermally driven CO association reaction of native Ferrocyt *c* have been measured under varying concentrations of salts (NaCl, NaBr, NaI, Na_2SO_4, $NaNO_3$, and $NaClO_4$) at pH 7.0. At low to intermediate salt concentrations, the ions dissociated from both chaotropic and kosmotropic salts decrease the rates of CO association while they increase the activation enthalpy and activation entropy for it. This finding suggests that the low concentrations of chaotropic and kosmotropic ions restrict the internal dynamics of native Ferrocyt *c* (i) by electrostatic screening of the protein charges, and (ii) by lowering the conformational entropy of proteins through binding interactions. At relatively higher salt concentrations, the chaotropic ions modulate the internal dynamics of native proteins according to Hofmeister series (ClO_4^- > I^- > NO_3^- > Br^-). Thermal and chemical denaturation studies of native Cyt *c* and Mb at pH 7.0 and acid-denatured Lyz at pH 2.3 in the presence of various concentrations of these salts suggest that kosmotropic salts increase the thermodynamic stability of the native proteins at pH 7.0 while the chaotropic salts decrease it at pH 7.0 but increase it at pH 2.3. Furthermore, the effect of these salts on the thermodynamic stability of these proteins at pH 7.0 follow the Hofmeister series (SO_4^{2-} > Cl^- > Br^- > NO_3^- > I^- > ClO_4^-). The stabilization free energy ($\Delta\Delta G$) for Ferrocyt *c* in salts solution was calculated from

the slope of the WT plot and water activity. The *m*-values were also estimated from the slope of $\Delta\Delta G$ versus [salts] plots. The *m*-value was found to be most negative for $NaClO_4$ and least for Na_2SO_4, consistent with stabilization of proteins according to the Hofmeister series ($SO_4^{2-} > Br^- > NO_3^- > I^- > ClO_4^-$).

This thesis also evaluates the effects of chaotropic denaturants (GdnHCl and sodium dodecyl sulfate (SDS)) on the stability and dynamics of native and base-denatured proteins. Comprehensive spectroscopic (CD, fluorescence, NMR) studies suggest that the low concentrations of GdnHCl (≤0.2 M) and SDS (≤0.4 mM) transform the base-denatured carbonmonoxycytochrome *c* (Cyt-CO) and Ferricyt *c* to molten globule (MG) states, respectively. Single Trp59 fluorescence experiments show that the interactions of $GdnH^+$ ions dissociated from GdnHCl (≤0.2 M) or Na^+ ions dissociated from SDS (≤0.2 mM) cause the molecular compaction in the base-denatured proteins. The near-UV CD spectra for base denatured protein in the presence of GdnHCl (≤0.2 M) and SDS (≤0.4 mM) suggest that the GdnHCl (≤0.2 M) and SDS (≤0.4 mM) induced MG-states of base-denatured protein have disordered tertiary structures. The far-UV CD spectra for base denatured protein in the presence of SDS (≤0.4 mM) reveal the formation of substantial content of secondary structures in the SDS-induced MG-state of base-denatured protein. Kinetic experiments involving the measurement of the CO association reaction with alkaline Ferrocyt *c* at pH 12.6 and native Ferrocyt *c* at pH 7.0 in the presence of different concentrations of GdnHCl or SDS indicate that the low concentrations of GdnHCl (≤0.2 M) or SDS (≤0.2 mM) restrict the internal dynamics of the native and base denatured proteins. Thermodynamic analysis of the thermal denaturation curves of base-denatured Ferricyt *c* at pH 12.8 (±0.2) and native Ferricyt *c* at pH 7.0 measured in the presence different concentrations of GdnHCl (near-UV CD at 282 nm) and SDS (far-UV CD at 222 nm) indicate that the low concentrations of GdnHCl and SDS increase the thermal stability of base-denatured protein while decrease the thermal stability of native protein.

This thesis work also analyzes the effects pH on the thermodynamic stability and folding dynamics of proteins over the pH range from 3.0 to 13.0. Thermodynamic analysis of the thermal and chemical denaturants (GdnHCl and urea)-induced unfolding transitions of Ferricyt *c*, Ferrocyt *c* and Lyz measured at several different pH values, ranging from pH 3.0 to pH 13.0 reveals that the Ferricyt *c* and Ferrocyt *c* have maximum thermodynamic stability between the pH 8.0-9.5 while the Lyz has maximum thermodynamic stability at pH 4.0. Theoretically

predicted electrostatic unfolding energies of Ferricyt *c* and Lyz over the pH range from pH 0.0 to pH 14.0 also reveal that Ferricyt *c* and Lyz are maximally stable at pH 8.0-9.0 and pH 4.0, respectively. Unfolded Ferrocyt *c* in refolding buffer at pH 7.0 and pH 12.7 refolds rapidly to native-state. Between pH 7.0 and pH 12.7, the activation free energy barrier for folding of Ferrocyt *c* varies by less than 1.0 kcal mol^{-1} while the folding free energy for Ferrocyt *c* which is measured by two-state analysis of GdnHCl-induced unfolding transitions of Ferrocyt *c* varies more than 9.0 kcal mol^{-1}. This finding indicates that the large disparity in thermodynamic, stability of protein between pH 7.0 and pH 12.7 is not strongly reflected in the refolding rates. The classic Wyman-Tanford linkage relation was used to calculate the β^{pH}-value for folding of Ferrocyt *c*, which is less than 0.1 between pH 7.0 and pH 12.7, indicating that the electrostatic interactions are weakly formed in the transition state and exhibit a very small effect on the folding kinetics.

Keywords: Constrained dynamics, *m*-value, water activity, Wyman-Tanford plot, counteraction, cumulative effect, chaotropic salts, kosmotropic salts, molten globule, entropic stabilization, folding kinetics, pH-effect, electrostatic interactions.

Chapter 1

Introduction

Proteins are the biological molecules that carry out vital functions in every cell. To perform their functions, proteins must fold into their 3-dimensional native structure. *In vivo*, protein folding into its functional state is assisted by cellular helper factors such as proline isomerase, protein-protein disulfide isomerase, and molecular "chaperones". Failure of proteins to fold into native structure generally produces inactive or misfolded proteins. The structure of a protein and its ability to carry out the correct function are tightly coupled and thus a small defect in protein structure can cause a number of protein folding related diseases. Protein misfolding and its pathogenic consequences are a major concern in medical science. Protein misfolding is believed to be the major cause of protein related disorders such as Alzheimer's disease, Parkinson's disease, Huntington's disease, Creutzfeldt–Jakob disease, cystic fibrosis, Gaucher's disease and many other degenerative and neurodegenerative disorders. Additionally, protein misfolding is also responsible for various p53-mediated cancers and diseases (*1*).

Both experimental and theoretical research in protein folding is proceeding at an explosive rate worldwide (*2-32*). The process of protein folding while critical and fundamental to virtually all biological processes, still remains primarily an unsolved puzzle. The importance of protein folding problem, perhaps the most multi-disciplinary of all problems in modern science, has been recognized unequivocally. There are several practical applications of protein folding studies including, (i) designing proteins with novel biological functions, (ii) rational engineering of existing proteins, (iii) understanding the molecular basis of many biological malfunctions, (iv) understanding structure-function relationships in proteins, (v) prediction of protein structure from sequence, and (vi) recovery of recombinant proteins from expression medium.

For many decades several physical, chemical, and biological methods have been employed to study thermodynamic, kinetic, and structural aspects of the protein folding reactions *in vitro*. Though these studies have provided some insight, but the basic questions – how does proteins fold into their biologically active states, and how these active states are stabilized remains enigmatic. The characterization of protein properties involves examination of its stability and the forces which lead to its stability and correct folding. It is well recognized that the electrostatic interactions (*33*-

37), hydrophobic interactions (*38-39*) and hydrogen bonding (*40-41*) are responsible for the stability and correct folding of native proteins, however, the relative contributions of each of these factors vary from protein to protein as well as with the neighboring environment such as solvent to which the protein is exposed (*37-39*).

Sugars (*i.e.*, glycerol, sucrose, glucose, etc.) and a number of methylamine solutes, such as trimethylamine-*N*-oxide (TMAO) and glycine betaine (GB) are known as kosmotropic cosolvents that typically stabilize the proteins, but the mechanism by which these kosmotropic cosolvents stabilize proteins is not clearly understood (*42-46*). A specific class of kosmotropic cosolvents (*i.e.*, TMAO, GB, glycerol, trehalose, and other sugars) has been known as protecting osmolytes that typically increase the stability of native proteins and provide protection against denaturing stresses. Increasing evidences indicate that protecting osmolytes such as TMAO and GB counter the deleterious effects of denaturants (guanidine hydrochloride (GdnHCl) and urea) in native proteins at neutral pH (*47-56*), however, the effects of protecting osmolytes on the stability of proteins in the presence of denaturants at mildly acidic pH conditions have remained uncovered. According to few earlier reports, the osmolytes mediated protein stability is due to the preferential ordering of solvent molecules (a solvent-oriented process) which facilitates the protein folding (*42-46*), but the exact mechanism of stabilization remains elusive. Whether the osmolytes modulate the protein stability by direct interactions with protein groups or by involving the indirect interactions by changing the solvent properties, is a matter of current debate (*46, 57*). Further, the functional dependence of structural and energetic properties of proteins with the osmolyte composition is not clear either.

Chemical denaturants such as GdnHCl, urea, sodium dodecyl sulfate (SDS), and monohydric alcohols (methanol, ethanol, 1-propanol, 2-propanol, 3°-butanol and trifluoroethanol (TFE)) are known as chaotropic cosolvents that typically unfold the proteins at higher concentrations. Few previous studies show that these chaotropic cosolvents denature the proteins by direct binding to the particular groups on the protein, for example, to hydrophobic residues in the case of alcohols (*58*) or to peptide groups in the case of urea and GdnHCl (*59-61*). GdnHCl and urea generally unfold the protein through disruption of the both secondary and tertiary structure of proteins. However, the monohydric alcohols disrupt the tertiary structure of proteins, (*62-63*), but enhance secondary structural elements such as helical structure (*64-66*). Despite the routine use of these denaturants in protein folding studies, the exact mechanism of action of these denaturants on proteins is not clearly understood. It is not clear whether the effects of denaturants (urea, GdnHCl,

and alcohols) on proteins are due to direct protein-denaturant interactions (*64, 67-74*) or due to an indirect action, involving changes in the solvent (*i.e.* water) properties by the addition of denaturant (*75-77*). Increasing evidences indicate that the subdenaturing concentrations of denaturants such as GdnHCl, urea and monohydric alcohols can stabilize the native proteins (*62, 67-68, 72-88*). These observations underscore the complexity of the mechanism by which GdnHCl, urea, and alcohols achieve their protein-unfolding action.

Buffer conditions such as pH and salts can modulate the structure, stability and biological functions of proteins (*28, 89-92*). Generally, the pH modulates the protein stability by altering the charges on the ionizable groups of proteins (*93*). Few earlier reports reveal that the salt ions also modulate the stability of the native and partially denatured states of proteins (*34-35, 94-110*). Understanding the effects of salts on the protein stability is important for understanding the thermodynamic properties of biological systems. Increasing evidences indicate that at lower salt concentrations, the salt ions modulate the stability of proteins by varying the electrostatic (Debye-Hückel) screening of Coulombic interactions (*41, 97-98*) while at higher salt concentrations, the Hofmeister effect influences the stability of proteins by increasing the surface tension of solvent that eventually modulates the hydrophobic interactions (*29, 99-100, 111-112*). The Hofmeister series characterizes some properties of ions as cosolvents in protein solutions. This series divides the ions in two groups: the kosmotropic and chaotropic ions (*113*). The Hofmeister series has regular effects on the stability and structures of proteins. Anions show more pronounced effect than cations, and typically follow the order: $F^- \approx HPO_4^{2-} > SO_4^{2-} > CH_3COO^- > Cl^- > NO_3^- > Br^- > ClO_3^- > I^- > ClO_4^- > SCN^-$ and the cations usually follow this order: $NH_4^+ > K^+ > Na^+ > Li^+ > Mg^{2+} > Ca^{2+}$ (*113*). In the anions series, the ions left to the Cl^- are termed as kosmotropes, which generally helps in ordering the water structures and thus stabilize the protein structures (salting out effect) while the ions right to the Cl^- are termed as chaotropes, which break the water structures and thus destabilize the protein structures (salting-in effects) (*114-117*). Although, the effects of Hofmeister series ions on the thermodynamic stability of proteins are extensively studied (*29, 102, 118-119*) but are rarely studied on the internal dynamics of proteins (*102, 119*). A useful summary by which the Hofmeister ions modulate the protein stability is given by Jencks (*120*).

The pH dependence of thermodynamic stability reflects the contribution of electrostatic interactions, which are of great importance for protein structure and function (*121-122*). From the last few decades, there is a fundamental interest in developing theoretical models for the correct

assessment of electrostatic interactions involving conformational changes (*123-126*) and their contribution to protein stability (*123, 127-131*). Although the pH dependence of thermodynamic stability of proteins has been extensively investigated (*128, 132-140*), the pH dependence of folding kinetics of proteins has received meager attention (*137-140*). Few previous reports reveal that the comparison of pH-dependent protein stability profiles and folding rates can provide information related to the development of electrostatic interactions in the transition state of folding (*137-141*).

Proteins denature at extreme pH because of charge repulsions. The salt-induced conformational changes of acid and base-denatured proteins were extensively studied (*97-100, 103-110*). Anions and cations were found to transform the acid- and base-denatured states, respectively to molten globule (MG) states, presumably by a charge screening mechanism (*104-110*). MG state is important for the functioning of proteins in living cells, and involves in various processes at cellular level, for example, the interactions of the proteins with chaperones and membranes. Increasing evidences indicate that low concentrations of GdnHCl and SDS can transform the pH-denatured proteins to MG-states (*78-80, 106-107, 142*). Several previous reports indicate that the monohydric alcohols also induce partially folded states in several proteins (*143-147*). The alcohol-induced partially folded states are biologically significant since they are similar to partially denatured states formed near the membrane surfaces where the pH and dielectric constant are low (*148-151*). Earlier work by Miyawaki et al indicate that the reciprocal form of Wyman–Tanford (WT) equation can also be applied to investigate the role of water activity on the stability of proteins (*25, 152-154*).

In vitro a folded protein can be driven to unfold by using the high concentrations of chemical denaturants that disrupt protein structures. An unfolded polypeptide can also be driven to fold by removing or diluting out the denaturant. This approach is invariably used from many decades to poise the folding-unfolding equilibrium in exploring stability, folding kinetics, and mechanism of protein folding. By using horse heart cytochrome *c* (Cyt *c*) (Figure 1a), horse heart myoglobin (Mb) (Figure 1b), and hen egg lysozyme (Lyz) (Figure 1c), this thesis work examines the effect of pH, chaotropic cosolvents (NaBr, $NaNO_3$, $NaClO_4$, NaI, GdnHCl, urea, SDS, methanol, ethanol, 2-propanol, 1-propanol, 3°-butanol and 2,2,2-triflouroethanol (TFE)) and kosmotropic cosolvents (Na_2SO_4, TMAO, and GB) on the stability, folding and dynamics of proteins. These three proteins are as much paradigamatic for protein folding as the hydrogen atom in physics and chemistry. A brief introduction of these three proteins is given below:

Cyt *c* (molecular mass 12.4 kDa with 104 amino acids residues) acts as an electron carrier (component of the electron transport chain in mitochondria) and is involved in initiation of apoptosis. It can catalyze various reactions (*e.g.* hydroxylation and aromatic oxidation) and also shows peroxidase activity by oxidation of several electron donors. The isoelectric point of Cyt *c* is ~10.0 therefore it is positively charged in an aqueous solution. Being a single domain fast folder protein, Cyt *c* is model in experimental protein folding and dynamic studies (*155-159*). Mb is a single-chain protein, (molecular mass 16.7 kDa with 153 amino acids residues), containing a heme group in the center. Mb has strong affinity for oxygen therefore; it serves as a reserve supply of oxygen and facilitates the movement of oxygen within muscles under the oxygen deficiency conditions such as during anaerobic exercise. Its secondary structure is unusual in that it contains a very high proportion (~75%) of α-helical secondary structure and the isoelectric point is ~7.3. Lyz is a small globular protein (molecular mass 14.3 kDa with 129 amino acids residues) folded in helical and β-sheet domains, containing 18 cationic amino acid residues and 12 anionic residues. In birds, Lyz is present in abundant amounts in eggwhite (hen eggwhite) where it functions as a nutrient and as antibiotic for the early embryogenesis. In vertebrates, Lyz acts as an anti-bacterial agent that helps in the digestion and weakening of the rigid bacterial cell walls, thereby making the bacteria prone to osmotic lysis. The isoelectric point of Lyz is ~11.0 so this protein is positively charged in an aqueous solution.

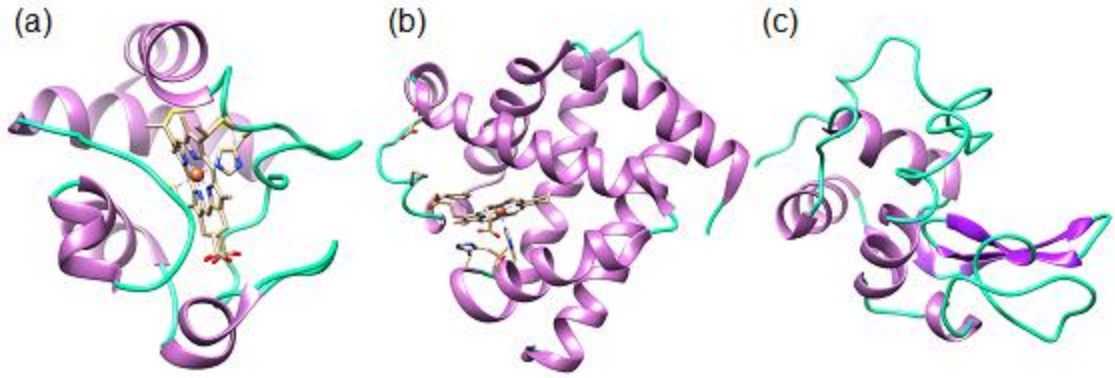

Fig. 1 A ribbon model for (a) horse heart cytochrome *c* (PDB: 1HRC (*160*)), (b) horse myoglobin (PDB: 1YMB (*161*)), and (c) hen egg white lysozyme (PDB: 2LYZ (*162*)).

References

1. Chiti, F., and Dobson, C.M. (2006) *Annu. Rev. Biochem.* **75**, 333–336.
2. Shukla, A., Raje, M. and Guptasarma, P. (2003) *J. Biol. Chem.* **278**, 26505-26510.
3. Kundu, B., and Guptasarma, P. (1999) *Proteins: Str. Func. Bioinf*. **37**, 321-324.
4. Shukla, A., and Guptasarma, P. (2004) *Proteins: Str. Func. Bioinf*. **55**, 548-557.
5. Chandrayan, S.K., and Guptasarma, P. (2008) *Proteins: Str. Func. Bioinf.* **72**, 539-546.
6. Chandrayan, S.K., and Guptasarma, P. (2009) *Biochim. Biophys. Acta: Prot. Proteom.* **1794**, 905-912.
7. Ahmed, S., Shukla, A., and Guptasarma, P. (2008) *Biochim. Biophys. Acta: Prot. Proteom.* **1784**, 916-923.
8. Dalal, V., Bhattacharya, M., Narang, D., Sharma, P.K., and Mukhopadhyay, S. (2012) *J. Phys. Chem. Lett.* **3**, 1783−1787.
9. Bhattacharya, M., and Mukhopadhyay, S. (2012) *J. Phys. Chem. B.***116**, 520-531.
10. Jain, N., Bhattacharya, M., and Mukhopadhyay, S. (2011) *Biophys. J.* **101**, 1720-1729.
11. Bhattacharya, M., Jain, N., and Mukhopadhyay, S. (2011) *J. Phys. Chem. B* **115**, 4195-205.
12. Rao, C.P., Balaram, P., and Rao, C.N.R. (1983) *Biopolymers* **22**, 2091-2210.
13. Chinta, J.P., Acharya, A., Kumar, A., and Rao, C.P. (2009) *J. Phys. Chem. B.***113,** 12075-12083.
14. Francis, A.K., Rao, C.P., Iqbal, M., Nagaraj, R., Vijayan, M., and Balaram, P. (1982) *Biochem. Biophys. Res. Commun.* **106,** 1240-1247.
15. Rao, C.P., Shamala, N., Nagaraj, R., Rao, C.N.R., and Balaram, P. (1981) *Biochem. Biophys. Res. Commun.* **103**, 898-904.
16. Acharya, A., Ramanujam**,** B., Chinta, J.P., and Rao, C.P. (2011) *J. Org. Chem.* **76**, 127-137.
17. Baumann, K. (2014) *Nat. Rev. Mol. Cell Biol.* **15**, 5.
18. Hingorani, K.S., and Gierasch, L.M. (2014) *Curr. Opin. Struct. Biol.* **24**, 81-90.
19. Serohijos, A.W.R., and Shakhnovich, E.I. (2014) *Mol. Biol. and Evol.* **31**, 165-176.
20. Homouz, D. (2014) *Adv. in Exp. Med. and Biol.* **805**, 171-197.
21. Englander, S.W. (2000) *Annu. Rev. Biophys. Biomol. Struct.* **29**, 213-238.
22. Gillespie, B., and Plaxco, K.W. (2004) *Annu. Rev. Biochem*. **73**, 837-859.

23. Mukaiyama, A., Nakamura, T., Makabe, K., Maki, K., Goto, Y., and Kuwajima, K. (2013) *J. Mol. Biol.* **425**, 257-272.
24. Mukaiyama, A., Nakamura, T., Makabe, K., Maki, K., Goto, Y., and Kuwajima, K. (2013) *J. Mol. Biol.* **425**, 273-291.
25. Miyawaki, O., Dozen, M., and Nomura, K. (2014) *Biophys. Chem.* **185**, 19-24.
26. Nakamura, S., and Kidokoro, S. (2012) *J. Phys. Chem. B.* **116**, 1927-1932.
27. Nakamura, S., Seki, Y., Katoh, E., and Kidokoro, S. (2011) *Biochemistry* **50**, 3116-3126.
28. Rosell, F.I., Mauk, M.R., and Mauk, A.G. (2005) *Biochemistry* **44**, 1872-1879.
29. Kumar, R., and Mauk, A.G. (2009) *J. Phys. Chem. B* **113**, 12400–12409.
30. Rosell, F.I., Mauk, M.R., and Mauk, A.G. (2007) *Biochemistry* **46,** 9301-9309.
31. Yasin, U.M., Sashi, P., and Bhuyan, A.K. (2013) *J. Phys. Chem. B* **177**, 12059-12064.
32. Sashi. P., Yasin, U.M., Balasubramanian, H., Sree, M.U., Ramakrishna, D., and Bhuyan, A.K. (2014) *J. Phys. Chem. B* **118**, 717-723.
33. Karshikoff, A., and Ladenstein, R. (2007) In *Methods in Protein Structure and Stability Analysis: Conformational Stability, Size, Shape and Surface of Protein Molecules*; Uversky, V.N., Permyakov, E., Eds.; Nova Biomedical Books: New York, pp 71.
34. Perl, D., Holtermann, G., and Schmid, F.X. (2001) *Biochemistry* **40**, 15501-15511.
35. Jayaraman, S., Gantz, D.L., and Gursky, O. (2006) *Biochemistry* **45**, 4620-4628.
36. Benjwal, S., Jayaraman, S., and Gursky, O. (2005) *Biochemistry* **44**, 10218-10226.
37. Dominy, B.N., Perl, D., Schmid, F.X., and Brooks, C.L. (2002) *J. Mol. Biol.* **319**, 541-544.
38. Jaenicke, R., and Bohm, G. (1998) *Curr. Opin. Struct. Biol.* **8**, 738-748.
39. Pace, C.N. (1995) *Methods Enzymol.* **259**, 538-554.
40. Vogt, G., Woell, S., and Argos, P. (1997) *J. Mol. Biol.* **269**, 631-643.
41. Elcock, A.H., and McCammon, J.A. (1998) *J. Mol. Biol.* **280**, 731-748.
42. Xie, G., and Timasheff, S.N. (1997) *Biophys. Chem.***64**, 25-43.
43. Xie, G., and Timasheff, S.N. (1997) *Protein Sci.* **6**, 222-232.
44. Lin, T.Y., and Timasheff, S.N. (1996) *Science* **5**, 372-381.
45. Gekko, K., and Timasheff, S.N. (1981) *Biochemistry* **20**, 4667-4676.
46. Arakawa, T., and Timasheff, S.N. (1985) *Biophys. J.* **47**, 411-414.
47. Yancey, P.H., and Somero, G.N. (1979) *Biochem. J.* **183**, 317–323.

48. Yancey, P.H., Clark, M.E., Hand, S.C., Bowlus, R.D., and Somero, G.N. (1982) *Science* **217**, 1214–1222.
49. Venkatesu, P., Lee, M.J., and Lin, H.M. (2007) *Arch. Biochem. Biophys.* **466**, 106–115.
50. Timasheff, S.N. (2002) *Proc. Natl. Acad. Sci. USA* **99**, 9721–9726.
51. Tseng, H.C., and Graves, D.J. (1998) *Biochem. Biophys. Res. Commun.* **250**, 726–730.
52. Ortiz-Costa, S., Sorenson, M.M., and Sola-Penna, M. (2008) *FEBS J.* **275**, 3388–3396.
53. Venkatesu, P., Lee, M.J., and Lin, H.M. (2007) *J. Phys. Chem. B* **111**, 9045–9056.
54. Singh, R.K., Haque, I., and Ahmad, F. (2005) *J. Biol. Chem.* **280**, 11035–11042.
55. Singh, L.R., Poddar, N.K., Dar, T.A., Kumar, R., and Ahmad, F. (2011) *Life Sciences* **88**, 117-125.
56. Singh, L.R., Dar, T.A., Rahman, S., Jamal, S., and Ahmad, F. (2009) *Biochim. Biophys. Acta*. **1794**, 929–935.
57. Thirumalai, D., Klimov, D.K., and Dima, R.I. (2003) *Curr. Opin. Struct. Biol.* **13**, 146–159.
58. Timasheff, S.N., and Inoue, H. (1968) *Biochemistry* **7**, 2501-2513.
59. Herskovits, T.T. (1965) *J. Mol. Chem.* **240**, 628-638.
60. Pace, C.N., Laurents, D.V., and Thomson, J.A. (1990) *Biochemistry* **29**, 2564-2572.
61. Schmid, F.X., and Baldwin, R.L. (1979) *J. Mol. Biol.* **133**, 285-287.
62. Brandts, J.F., and Hunt, L. (1967) *J. Am. Chem. Soc.* **89**, 4826-4838.
63. Herskovits, T.T., Gadegbeku, B., and Jaillet, H. (1970) *J. Biol. Chem.* **245,** 2588–2598.
64. Hong, D.P., Hoshino, M., Kuboi, R., and Goto, Y. (1999) *J. Am. Chem. Soc.* **121**, 8427–8433.
65. Hirato, N., Mizuno, K., and Goto, Y. (1998) *J. Mol. Biol.* **275**, 365-378
66. Conio, G., Patrone, E., and Brighetti, S. (1970) *J. Biol. Chem.* **245**, 3335–3340.
67. Povey, J.P., Smales, C.M., Hassard, S.J., and Howard, M.J. (2007) *J. Struct. Biol.* **157**, 329–338.
68. Roccatano, D., Colombo, G., Fioroni, M., and Mark, A.E. (2002) *Proc. Natl. Acad. Sci. USA* **99**, 12179–12184.
69. Makhatadze, G.I., and Privalov, P.L. (1992) *J. Mol. Biol.* **226**, 491-505.
70. Hibbard, L.S., and Tulinsky, A. (1978) *Biochemistry* **17**, 5460-5468.
71. Pike, A.C.W., and Acharya, R. (1994) *Protein Sci.* **3**, 706-710.

72. Dunbar, J., Yennawar, H.P., Banerjee, S., Luo, J., and Farber, G.K. (1997) *Protein Sci*. **6**, 1272-1733.
73. Tanford, C. (1970) *Adv. Protein Chem.* **24**, 1-95.
74. Simpson, R.B., and Kauzmann, W. (1953) *J. Am. Chem. Soc.* **75**, 5139-5152.
75. Onori, G., Passeri, S., and Cipiciani, A. (1989) *J. Phys. Chem.* **93**, 4306-4310.
76. Timasheff, S. N. (1992) *Biochemistry* **31**, 9857-9864.
77. Breslow, R., and Guo, T. (1990) *Proc. Natl. Acad. Sci. U.S.A.* **87**, 167-169.
78. Bhuyan, A.K. (2002) *Biochemistry* **41**, 13386–13394.
79. Kumar, R., Prabhu, N.P., Yadaiah, M., and Bhuyan, A.K. (2004) *Biophys. J.* **87**, 2656-2662.
80. Kumar, R., and Bhuyan, A.K. (2009) *J. Biol. Inorg. Chem.* **14**, 11-21.
81. Martin, S.R., Esposito, V., Rios, P.D.L., Pastore, A., and Temussi, P.A. (2008) *J. Am. Chem. Soc.* **130**, 9963–9970.
82. Walgers, R., Lee, T.C., and Cammers-Goodwin, A. (1998) *J. Am. Chem. Soc.* **120**, 5073-5079.
83. Anderson, N.H., Cort, J.R., Liu, Z., Sjoberg, S.J., and Tong, H. (1996) *J. Am. Chem. Soc.* **118**, 10309-10310.
84. Velicelebi, G., and Sturtevant, J.M. (1979) *Biochemistry* **18**, 1180–1186.
85. Fernandez, A., and Sinanoglu, O. (1985) *Biophys. Chem.* **21**, 163-166.
86. Skukuya, R., and Schwert, G. (1960) *J. Biol. Chem.* **235**, 1658-1661.
87. Fu, L., and Freire, E. (1992) *Proc. Natl. Acad. Sci.USA* **89**, 9335-9338.
88. Cinelli, S., Onori, G., and Santucci, A. (1997) *J. Phys. Chem. B* **101**, 8029-8034.
89. Assfalg, M., Bertini, I., Dolfi, A., Turano, P., Mauk, A.G., Rosell, F.I., and Gray, H.B. (2003) *J. Am. Chem. Soc.* **125**, 2913-22.
90. Rosell, F.I., Harris, T.R., Hildebrand, D.P., Döpner, S., Hildebrandt, P., and Mauk, A.G. (2000) *Biochemistry* **39**, 9047-9054.
91. Konermann, L., Rosell, F.I., Mauk, A.G., and Douglas, D.J. (1997) *Biochemistry* **36**, 6448-6454.
92. Nurizzo, D., Baker, H.M., He, Q.Y., MacGillivray, R.T., Mason, A.B., Woodworth, R.C., and Baker, E.N. (2001) *Biochemistry* 40, 1616-1623.
93. Anderson, D.E., Becktel, W.J., and Dahlquist, F.W. (1990) *Biochemistry* **29**, 2403-2408.

94. Timasheff, S.N. (1998) *Adv. Protein Chem.* **51**, 355-432.
95. Colonna-Cesan, F., and Sander, C. (1990) *Biophys. J.* **57**, 1103-1107.
96. Wills, P.R., Hall, D.R., and Winzor, D.J. (2000) *Biophys. Chem.* **84**, 217-225.
97. Rao, D.K., Kumar, R., Yadaiah, M., and Bhuyan, A.K. (2006) *Biochemistry* **45**, 3412-3420.
98. Kumar, R., Prabhu, N.P., Rao, D.K., and Bhuyan, A.K. (2006) *J. Mol. Biol.* **364**, 483-495.
99. Bhuyan, A.K. (2010) *Biochemistry* **49**, 7774-7782.
100. Bhuyan, A.K. (2010) *Biochemistry* **49**, 7764-7773.
101. Mayr, L.M., and Schmid, F.X. (1993) *Biochemistry* **32**, 7994-7998.
102. Apetri, A.C., and Surewicz, W.K. (2003) *J. Biol. Chem.* **278**, 22187-22192.
103. Arai, M., and Kuwajima, K. (2000) *Adv. Protein Chem.* **53**, 209-282.
104. Goto, Y., and Fink, A.L. (1989) *Biochemistry* **28**, 945-952.
105. Nakamura, S., Seki, Y., Katoh, E., and Kidokoro, S. (2011) *Biochemistry* **50**, 3116-3126.
106. Hagihara, Y., Aimoto, S., Fink, A.L., and Goto, Y.J. (1993) *J. Mol. Biol.* **231**, 180-184.
107. Kuroda, Y., Kidokoro, S., and Wada, A. (1992) *J. Mol. Biol.* **223**, 1139–1153.
108. Nakamura, S., Baba, T., and Kidokoro, S. (2007) *Biophys. Chem.* **127**, 103-112.
109. Hamada, D., Kidokoro, S., Fukada, H., Takahashi, K., and Goto, Y. (1994) *Proc. Natl. Acad. Sci. U.S.A.* **91**, 10325–10329.
110. Hagihara, Y., Tan, Y., and Goto, Y. (1994) *J. Mol. Biol.* **237**, 336-348.
111. Perez-Jimenez, R., Godoy-Ruiz, R., Ibarra-Molero, B., and Sanchez-Ruiz, J.M. (2004) *Biophys. J.* **86**, 2414-2429.
112. Baldwin, R.L. (1996) *Biophys. J.* **71**, 2056-2063.
113. Hofmeister, F. (1888) *Arch. Exp. Pathol. Pharmakol.* **24**, 247-260.
114. Cacace, M.G., Landau, E.M., and Ramsden, J.J. (1997) *Q. Rev. Biophys.* **30**, 241-277.
115. Von Hippel, P.H., and Wong, K.Y. (1964) *Science* **145**, 577-580.
116. Pegram, L.M., and Record, M.T.Jr., (2008) *J. Phys. Chem. B* **112**, 9428-9436.
117. Record, M.T.Jr., Anderson, C.F., and Lohman, T.M. (1978) *Q. Rev. Biophys.* **11**, 103.
118. Villa, A., Zecca, L., Fusi, P., Colombo, S., Tedeschi, G., and Tortora, P. (1993) *Biochem. J.* **295**, 827-831.
119. Kumar, R., and Mauk, A.G. (2012) *J. Phys. Chem. B* **116**, 3795-3807.

120. Jencks, W.P. (1987) *Catalysis in Chemistry and Enzymology*. Dover, Mineola, NY. 358-392.
121. Perutz, M.P. (1978) *Science* **201**, 1187-1191.
122. Warshel, A. (1978) *Proc. Natl. Acad. Sci. U.S.A.* **75**, 5250-5254.
123. Shosheva, A. Miteva, V., Christova, P., and Atanasov, B. (2003) *Eur. Biophys. J.* **31**, 617–625.
124. You, T., and Bashford, D. (1995) *Biophys. J.* **69**, 1721-1733.
125. Alexov, E., and Gunner, M. (1997) *Biophys. J.* **72**, 2075-2093.
126. Rabenstein, B., and Knapp, E.W. (2001) *Biophys. J.* **80**, 1141-1150.
127. Warshel, A. (1991) *Annu. Rev. Biophys. Biophys. Chem.* **20**, 267–298.
128. Yang, A.S., and Honig, B. (1993) *J. Mol. Biol.* **231**, 474–495.
129. Yang, A.S., and Honig, B. (1994) *J. Mol. Biol.* **237**, 602–614.
130. Antoziewicz, J., McCommon, J., and Gilson, M. (1994) *J. Mol. Biol.* **238,** 415–436.
131. Schaefer, M., Sommer, M., and Karplus, M. (1997) *J. Phys. Chem. B* **101**, 1663–1668
132. Bashford, D., and Karplus, M. (1990) *Biochemistry* **29**, 10219–10225.
133. Hendsch, Z.S., and Tidor, B. (1994) *Protein Sci.* **3**, 211-226.
134. Barlow, D.J., and Thornton, J.M. (1983) *J. Mol. Biol.* **168,** 867-885.
135. Kumar, S., and Nussivov, R. (1999) *J. Mol. Biol.* **293**, 1241-1255.
136. Honig, B., and Nicholls, A. (1995) *Science* **268,** 1144-1149.
137. Luisi, D.L., and Raleigh, D.P., (2000) *J. Mol. Biol.* **299,** 1091–1100.
138. Cavagnero, S., Debe, D.A., Zhou, Z.H., Adams, M.W.W., and Chan, S.I. (1998) *Biochemistry* **37**, 3369-3376.
139. LoÂ pez-Arenas, L., SolõÂs-Mendiola, S., and HernaÂndez-Arana, A. (1999) *Biochemistry* **38**, 15936-15943.
140. SolõÂs-Mendiola, S., GutieÂrrez-GonzaÂ lez, L.H., Arroyo-Reyna, A., Padilla-ZuÂnÄ iga, J., Rojo-DomõÂnguez, A., and HernaÂndez-Arana, A. (1998) *Biochim. Biophys. Acta* **1388**, 363-372.
141. Horng, J-.C., Cho, J-.H., and Raleigh, D.P. (2005) *J. Mol. Biol.* **345**, 163–173.
142. Moosavi-Movahedi, A.A., Chamani, J., Goto, Y., and Hakimelahi, G.H. (2003) *J. Biochem.* **133**, 93–102.
143. Hirato, N., Mizuno, K., and Goto, Y. (1998) *J. Mol. Biol.* **275**, 365-378.

144. Kamatari, Y.O., Konno, T., Kataoka, M., and Akasaka, K. (1996) *J. Mol. Biol*. **259**, 512-523.
145. Kentsis, A. and Sosnick, T.R. (1998) *Biochemistry* **37**, 14613-14622.
146. Kamatari, Y.O., Konno, T., Kataoka, M., and Akasaka, K. (1998) *Protein Sci.* **7**, 681-688.
147. Sasahara, K. and Nitta, K. (2006) *Proteins* **63**, 127-135.
148. Bychkova, V.E., Dujsekina, A.E., Klenin, S.I., Tiktopulo, E.I., Uversky, V.N., and Ptitsyn, O.B. (1996) *Biochemistry* **35**, 6058-6063.
149. Kamatari, Y.O., Ohji, S., Konno, T., Seki, Y., Soda, K., Kataoka, M., and Akasaka, K. (1999) *Protein Sci.* **8**, 873-882.
150. Sashi, P., Yasin, U.M., and Bhuyan, A.K. (2012) *Biochemistry* **51**, 3273-3283.
151. Bychkova, V.E., Dujsekina, A.E., Klenin, S.I., Tiktopulo, E.I., Uversky, V.N., and Ptitsyn, O.B. (1996) *Biochemistry* **35**, 6058-6063.
152. Miyawaki, O., Saito, A., Matsuo, T., and Nakamura, K. (1997) *Biosci. Biotechnol. Biochem.* **61**, 466–469.
153. Miyawaki, O. (2007) *Biochim. Biophys. Acta: Prot. Proteom*. **1774**, 928–935.
154. Miyawaki, O. (2009) *Biophys. Chem.* **144**, 46-52.
155. Bhuyan, A.K., and Kumar, R. (2002) *Biochemistry* **41**, 12821-12834.
156. Bhuyan, A.K., and Udgaonkar, J.B. (2001) *J. Mol. Biol.* **312**, 1135-1160.
157. Prabhu, N.P., Kumar, R., and Bhuyan, A.K. (2004) *J. Mol. Biol.* **337**, 195-208.
158. Kumar, R., and Bhuyan, A.K. (2005) *Biochemistry* **44**, 3024-3033.
159. Bhuyan, A.K., Rao, D.K., and Prabhu, N.P. (2005) *Biochemistry* **44**, 3034-3040.
160. Bushnell, G.W., Louie, G.V., and Brayer, G.D. (1990) *J. Mol. Biol.* **214**, 585-595.
161. Evans, S.V., and Brayer, G.D. (1990) *J. Mol. Biol.* **213**, 885-897.
162. Diamond, R. (1974) *J. Mol. Biol*. **82**, 371-391.

Chapter 2

Materials and Methods

2.1 Materials

Hen egg white lysozyme (Lyz) was purchased from calbiochem. Horse heart cytochrome *c* (Cyt *c*) (type VI), horse heart myoglobin (Mb), alcohols (methanol, ethanol, 1-propanol, 2-propanol, 3°-butanol and 2,2,2-triflouroethanol (TFE)), various salts (NaCl, $NaNO_3$, $NaClO_4$, NaBr, NaI, and Na_2SO_4,), sodium dodecyl sulfate (SDS), salts of buffer (sodium acetate, sodium phosphate, Tris-base, and CAPS (3-[Cyclohexylamino]-1-propanesulfonic acid)), osmolytes (glycine betaine (GB), trimethylamine-*N*-oxide (TMAO), and sucrose) and reductant (sodium dithionite) were purchased from Sigma. Chemical denaturants (guanidine hydrochloride (GdnHCl) and urea) were purchased from USB (USA). All other chemicals were of analytical grade. All experiments were done in either 50 mM sodium phosphate buffer or 25 mM Tris-HCl buffer at pH 7.0, 25 mM sodium acetate buffer at pH 2.3-4.5, and 2.0 mM CAPS buffer at alkaline pH 12.6-13.0. The required pH of protein samples were adjusted by using the concentrated HCl and NaOH solutions. The concentrations of GdnHCl and urea stock solutions were determined by refractive index measurements by using an Abbe's Refractometer (*1*). The kinetics and thermodynamic data were analyzed using the program Sigma Plot (v. 9).

2.2 Methods

2.2.1 Preparation of NCO and measurement of CO dissociation kinetics

Ferricytochrome *c* (Ferricyt *c*), initially dissolved in 6.5 M GdnHCl, was deaerated by passing dry N_2 gas and reduced by adding sodium dithionite to a final concentration of ~3.0 mM. The stock solution of sodium dithionite was prepared in a tightly capped glass tube by dissolving 120 mg of solid sodium dithionite in 1 mL of deaerated phosphate buffer, pH 7.0 under nitrogen. Unfolded Ferrocyt *c* (U) thus obtained was liganded with CO by passing the dry CO gas through the protein solution under N_2 atmosphere. The CO-liganded unfolded Ferrocytochrome *c* (Ferrocyt *c*) was then diluted 101-fold into a degassed and dithionite-reduced CO-free refolding buffer containing a desired concentration of alcohol (methanol, ethanol, 1-propanol, 2-propanol, 3°-butanol, and TFE), or osmolyte (GB) or SDS. This method allows complete refolding of UCO

to generate a natively folded CO-liganded Ferrocyt *c*, called NCO. The fast UCO → NCO process, measurable by stopped-flow, precedes the slow NCO → N+CO dissociation. Kinetics of CO dissociation was monitored by 550-nm heme absorbance at pH 7, 25 °C in a Shimadzu UV-visible spectrophotometer (UV-2450). Under denaturing conditions, where the CO dissociation reaction is relatively faster, kinetics were measured by a Shimadzu 2450 spectrophotometer coupled with Applied Photophysics RX 2000 rapid kinetics system stopped-flow mixing accessory.

2.2.2 Kinetic measurements for CO association with Ferrocyt c

Kinetic measurements for CO association with Ferrocyt *c* (Ferrocyt *c*+CO → Ferrocyt *c*-CO) were carried out by using the methods as described earlier (*2-3*). Briefly, Ferricyt *c* was first dissolved in 50 mM phosphate buffer, pH 7.0 and was reduced by adding sodium dithionite under a constant stream of nitrogen. About 25 μl of the reduced protein solution was added to 2 ml of deaerated CO saturated (≈1.0 mM) desired pH buffer containing sodium dithionite and varying concentrations of desired additives (SDS, GdnHCl, NaCl, $NaNO_3$, $NaClO_4$, NaBr, NaI and Na_2SO_4). The kinetics of CO association with Ferrocyt *c* was recorded on Shimadzu (UV-2450) spectrophotometer by monitoring the decrease in absorbance at 550 nm, 25 °C. The final concentrations of protein and sodium dithionite in CO association kinetic experiments were ~8.0-10.0 μM and ~3.0 mM, respectively. The CO association kinetics were also monitored by measuring the decay of the peak height at about ―3.26 ppm (M80 CεH3 resonance) following the addition of a small volume of the protein solution to a CO-saturated aqueous solution containing the desired amount of additives (GdnDCl, NaCl) at pH 7.0, 25 °C on a 400 MHz Bruker Avance (III) spectrometer.

2.2.3 Measurement of CO-replacement kinetics of carbonmonoxymyoglobin (MbCO)

The CO replacement reaction of MbCO complex by using hexacyanoferrate ion ($MbCO+CN^- \rightarrow MbCN+CO$) were carried out in different concentrations of GB. Briefly, Mb (~1 mM) initially dissolved in the native buffer (pH 7.0) was deaerated and reduced by the addition of sodium dithionite. The reduced protein was then liganded with CO by passing a slow stream of dry CO gas under nitrogen atmosphere. A small volume of this CO bound protein was added into a solution of potassium hexacyanoferrate containing a desired concentration of the GB, pH 7.0.

The decrease in the absorbance of the sample solution was monitored at 421 nm on Shimadzu (UV-2450) spectrophotometer at 22°C.

2.2.4 Measurement of the far-UV and near-UV CD spectra of Ferricyt c and Lyz

Far-UV (200-250 nm, 1.0 mm cell, and 10 µM protein) and near-UV (260-300 nm, 5.0 mm cell, and 50 µM protein) CD spectra of Ferricyt *c* (pH 7.0) and Lyz (pH 2.3) were collected in the 0-60% (v/v) range of methanol, 1-propanol, and 2-propanol on a JASCO J810 spectropolarimeter at 25 °C. The near-UV CD spectra for native Ferricyt *c* (~65-70 µM, pH 7) and base-denatured Ferricyt *c* (~65-70 µM, pH 12.8) in the presence of 0.0, 0.2 mM and 0.4 mM SDS; and 0.5 M NaCl were collected at 25°C. The near-UV CD spectra of Ferricyt *c* (~80-100 µM) in the presence of different concentrations of GdnHCl in the 0-4.0 M range were collected at pH 12.6, 25 °C. The near-UV CD spectra of native Ferricyt *c* (pH 7) in the presence of 0.2 M GdnHCl and base-denatured Ferricyt *c* (pH 12.6) in the presence of ~0.2M NaCl were also collected. The far-UV CD spectra of native and denatured (denatured by temperature (90°C)/~5.0 M GdnHCl/~8.0 M urea) states of Ferricyt *c* (~15 µM) were collected at pH 7.0 and pH 3.8 both in the absence and presence of ~1.0 M GB.

2.2.5 Thermal unfolding measurements of Ferricyt c, Ferrocyt c, Mb and Lyz

To determine the effect of alcohols (methanol, ethanol, 1-propanol, 2-propanol, 3°-butanol, and TFE), lyotropic salts (NaCl, $NaNO_3$, $NaClO_4$, NaBr, NaI and Na_2SO_4), osmolytes (GB and TMAO), denaturants (GdnHCl, urea and SDS) and pH on the thermal unfolding of proteins (Ferrocyt *c*, Ferricyt *c*, Mb, and Lyz), the absorbance (550 nm and 415 nm (Ferrocyt *c*); 409 nm (Mb); and 280 nm (Lys)), far-UV CD (222 nm (Ferrocyt *c*, Ferricyt *c*, Lyz) and near-UV CD (282 nm (Ferricyt *c*)) monitored thermal denaturation curves of Ferricyt *c*, Ferrocyt *c*, Mb and Lyz were collected under varying concentrations of these additives at desired pH values on Shimadzu (UV-2450) spectrophotometer and Jasco 810 CD- spectrophotometer. The final protein concentrations for the absorbance, far-UV CD and near-UV CD monitored thermal unfolding experiments were ~8µM, ~12-15 µM and ~50-60 µM, respectively. For thermal unfolding measurements of Ferrocyt *c* the dithionite concentration was ~1-3 mM. For both CD and absorbance measurements, the Peltier-controlled heating rate was 1.0 or 2.0 °C/min. By

assuming a two-state denaturation process, the thermal denaturation data were analyzed by using van't Hoff equation (eq (1)) (*4*) or Gibbs Helmholtz equation (eqs (2) and (3)) (*5-8*),

$$y\,(T)=\frac{\left(y_{\mathrm{F}}+m_{\mathrm{F}}T\right)+\left(y_{\mathrm{U}}+m_{\mathrm{U}}T\right)exp\left[\frac{\Delta H_{\mathrm{m}}}{R}\left(\frac{1}{T}-\frac{1}{T_{\mathrm{m}}}\right)\right]}{1+exp\left[\frac{\Delta H_{\mathrm{m}}}{R}\left(\frac{1}{T}-\frac{1}{T_{\mathrm{m}}}\right)\right]} \qquad (1)$$

$$y\,(T)=\frac{\left(y_{\mathrm{F}}+m_{\mathrm{F}}T\right)+\left(y_{\mathrm{U}}+m_{\mathrm{U}}T\right)exp\left[\frac{-\Delta G_{\mathrm{T}}}{RT}\right]}{1+exp\left[\frac{-\Delta G_{\mathrm{T}}}{RT}\right]} \qquad (2)$$

$$\Delta G_{\mathrm{T}}=\Delta H_{\mathrm{m}}\left(1-\frac{T}{T_{\mathrm{m}}}\right)+\Delta C_{\mathrm{p}}\left((T-T_{\mathrm{m}})-T\,ln(T/T_{\mathrm{m}})\right) \qquad (3)$$

where y (*T*) is the observed variable parameter ($\varepsilon_{550\ nm}$, $\varepsilon_{415\ nm}$, $\varepsilon_{409\ nm}$, $\varepsilon_{280\ nm}$, $CD_{222\ nm}$, $CD_{282\ nm}$), y_F and y_U, and m_F and m_U, represent intercepts and slopes of the folded and unfolded baselines, respectively, *T* represent absolute temperature, ΔC_p represent heat capacity change, *R* is a gas constant, and ΔH_m represent the van't Hoff enthalpy at thermal denaturation midpoint (T_m).

2.2.6 pH titration of Ferricyt c and Ferrocyt c in the absence and presence of CO

For pH unfolding studies, an approximate 10 μM solution of Ferricyt *c*, prepared in an aqueous medium containing 10 mM each of Tris, disodium hydrogen phosphate, and 2 mM CAPS, was titrated to different pH values in the 2.0-13.2 range by the use of concentrated NaOH and HCl solutions. The titration did not upset the uniformity of the protein concentration. To prepare Ferrocyt *c*, the Ferricyt *c* samples were deaerated by using nitrogen gas, and reduced by adding a small volume of freshly prepared dithionite to obtain a final concentration of ~3.0 mM. To prepare CO bound protein, the dithionite-reduced samples were saturated with CO by passing a slow stream of the dry CO gas through the solutions for a minute. These protein samples were then incubated for ~30 minutes in tightly capped glass tubes. Fluorescence emission spectra (ex: 280 nm) were recorded on Perkin Elmer LS-55 fluorescence spectrophotometer (for Ferricyt *c*) and Cary Eclipse Agilent spectrofluorometer (for Ferrocyt *c* in the absence and presence of CO). Optical absorption spectra were recorded on a Shimadzu (UV-2450) spectrophotometer. The pH titration curves were analyzed by using the following transformed Henderson-Hasselbalch equation (eq (4)),

$$y = \frac{c_u + c_f \left[10^{n(pH-C_m)} \right]}{1 + 10^{n(pH-C_m)}} \quad (4)$$

where, c_u and c_f are normalized fluorescence signals for the unfolded and the refolded states, respectively, n is the number of OH^- ions titrated, and c_m is the pH-midpoint for the transition.

2.2.7 Equilibrium unfolding measurements of proteins

For alcohols-induced equilibrium unfolding measurements of Cyt *c*, Mb and Lyz, the samples of Ferricyt *c* (~10μM), Mb (~5μM) and Lyz (~5μM) were prepared in the 0-70 % (v/v) range of alcohols (methanol, ethanol, 1-propanol, 2-propanol, 3°-butanol, and TFE) at pH 7.0 (Cyt *c* and Mb) and at pH 2.3 (Lyz). For GB and salts (NaCl, $NaNO_3$, $NaClO_4$, NaBr, NaI, and Na_2SO_4) dependent denaturant-induced equilibrium unfolding of Cyt *c*, Mb and Lyz, samples of Ferricyt *c* (~5 μM), Mb (~5 μM) and Lyz (~5μM) were prepared at different concentrations of GdnHCl or urea at pH 7.0 and at pH 2.3-3.8, both in the absence and presence of different concentrations of GB or salts.

For equilibrium unfolding measurements of Ferrocyt *c* and Carbonmonoxycytochrome *c* (Cyt-CO) at alkaline pH, the protein concentration was ~10 μM. Stock solutions of the buffer (2 mM CAPS, pH 12.6) and the unfolded protein (4.0-5.0 M GdnHCl, 2.0 mM CAPS, pH 12.6) were mixed appropriately to obtain protein samples containing different concentrations of denaturants. To prepare Ferrocyt *c*, solutions were exhaustively deaerated under nitrogen before the addition of a small volume of concentrated aqueous solution of sodium dithionite to obtain a final reductant concentration of 1-3 mM. The samples were sealed under nitrogen and equilibrated for ~30 minutes at 25(±1) °C. For equilibrium unfolding measurement of Cyt-CO, the dithionite-reduced samples were saturated with CO by passing a slow stream of the dry CO gas through the solutions for a minute.

SDS titration (0-0.6 mM range of SDS) of base denatured Ferricyt *c* (5-6 μM for fluorescence and 13-15 μM for CD) were carried out in CAPS buffer at pH 12.8, 25 °C. For the SDS-induced equilibrium unfolding of Ferrocyt *c*, the protein samples were deaerated by passing the dry N_2 gas and then reduced as described above.

For pH dependent denaturant-induced equilibrium unfolding measurements of Ferricyt *c*, samples of Ferricyt *c* (~5 μM) were prepared in the 0-10.0 M range of urea at different pH values

in the range of 3.0-12.7. In aqueous solution, urea forms cyanate, which can carbamylate lysyl epsilon-amino groups and change the electrostatic properties of a protein (*9-11*). The presence of cyanate in solution could lead to modification of these proteins prior to or during data collection. Therefore, the experiments that employ urea as denaturing agent were used within 2 hours of their preparation to prevent the cyanate formation. For pH dependent equilibrium unfolding measurements of Ferrocyt *c*, the samples of Ferricyt *c* (~5 μM) were prepared in the 0-7.5 M range of GdnHCl at different pH values in the range of 7.0-12.7 and were reduced by adding the freshly prepared sodium dithionite (~3 mM) solution under constant dry nitrogen gas purging. For pH dependent equilibrium unfolding measurements of Lyz, the samples of Lyz (~5 μM) were prepared in the 0-7.5 M range of GdnHCl at different pH values in the range of 2.0-13.0. Protein samples thus prepared were incubated for about half an hour at room temperature. Fluorescence emission (ex: 280 nm) and the far-UV CD spectra of Ferricyt *c*, Mb and Lyz were recorded on Perkin Elmer LS-55 fluorescence spectrophotometer and JASCO J820 spectropolarimeter, respectively. Fluorescence spectra (ex: 280 nm) of Ferrocyt *c* and Cyt-CO samples were collected on Cary Eclipse Agilent spectrofluorometers at 25 °C. The GdnHCl-induced equilibrium unfolding measurements of Ferrocyt *c* at different pH values were also monitored by UV-visible spectrophotometer (UV-2450, Shimadzu). The pH of the protein samples are those measured after the experiments. The data were fitted to a standard two-state equilibrium unfolding eq (5) (*12*).

$$S_{obs} = \frac{(c_f + m_f[D]) + (c_u + m_u[D])\exp(\frac{-\Delta G_D + m_g[D]}{RT})}{1 + \exp(\frac{-\Delta G_D + m_g[D]}{RT})} \qquad (5)$$

where S_{obs} is the observed signal, c_f and c_u, and m_f and m_u represent intercepts and slopes of native and unfolded baselines, respectively, [*D*] is the concentration of denaturant in M, *R* is the gas constant, ΔG_D, the free energy associated with the transition, and m_g, the surface area of the protein exposed by the solvent. C_m, the transition midpoint of denaturant concentration, was calculated as $C_m = \Delta G_D/m_g$.

2.2.8 NMR spectroscopy

Protein samples in D_2O solutions containing the desired additives (NaCl, GdnDCl) were adjusted to the desired pH by adding NaOD/DCl. Protein solutions contained in NMR tubes were then

sealed with sleeved rubber stoppers and equilibrated at 25 °C for ~10 minutes. Spectra were taken at 25 °C on a 400 MHz Bruker Avance (III) spectrometer. Spectra were analyzed by using Topspin 2.1 software.

2.2.9 Laser photolysis and microsecond measurements

About 15 μM cyt *c* solutions, prepared in aqueous NaOH containing GdnHCl in the 0-4 M range, pH 12.7(±0.1), were deaerated and reduced by the addition of 2 mM sodium dithionite, and incubated for ~15 minutes at 25 °C under saturating concentration of CO gas in 1 cm square quartz cuvette. CO photolysis was achieved by irradiation with 50(±10) mJ pulses of the second harmonic output (532 nm) of a Spectra Physics Q-switched Nd/YAG laser (10 Hz). Spectral changes following each photolysis pulse were recorded with a pulsed Xe lamp. The monochromator was set to 421.5 nm. The basic configuration of the instrument is based on the Applied Photophysics laser flash photolysis spectrometer. The sample temperature was maintained by using external water circulating water bath.

2.2.10 Measurement of pH-dependent refolding-unfolding kinetics of Ferrocyt c

Unfolded Ferricyt *c* (~0.5 mM) was obtained by mixing the native Ferricyt *c* in a ~6.3 M GdnHCl solution. To prepare the unfolded Ferrocyt *c*, the unfolded Ferricyt *c* was deareated by passing dry N_2 gas and reduced by adding the freshly prepared sodium dithionite solution. To record the refolding kinetics, unfolded Ferrocyt *c* was mixed rapidly in the refolding buffer in the stopped flow in a desired ratio. To record the unfolding kinetics, native Ferrocyt *c* was mixed rapidly in the deaerated dithionite reduced unfolding buffer in a stopped flow in a desired ratio. The spectrometer was configured for fluorescence detection (ex: 280 nm; em: 340 nm). A two-syringe mixing (1:7; protein: buffer) at a total flow rate of 8 ml/sec was employed. Typically, 10-15 shots were averaged.

2.2.11 Measurement of water activity

The water activity, a_w of a protein solution with a cosolute *Y* can be expressed as a function of the mole fraction of *Y* (X_Y) as (*13-14*):

$$a_W = (1 - X_Y)\exp(\alpha X_Y + \beta X_Y^2 + \gamma X_Y^3) \qquad (6)$$

The experimental parameters, α, β and γ were taken from the literature for methanol, ethanol, 1-propanol, 2-propanol, 3°-butanol, TFE, GdnHCl, and sucrose (*15-16*). The molal concentration range of different lyotropic salts (NaCl, $NaNO_3$, $NaClO_4$, NaBr, NaI and Na_2SO_4) examined was 0 to 2.5 m. The experimental values of osmotic coefficients (ϕ) of salts is defined as

$$\phi = -55.51/m \ln a_w \quad (7)$$

where a_w is the water activity. The values of ϕ as a function of salt concentration were reported in literature (*17*). Thus, using the eq (7), water activities of the salt solutions were calculated.

2.2.12 pKa prediction

The PROPKA 3.1 program (*18*) (http://www.propka.chem.uiowa.edu) was used to predict the pK_a values for all the acidic and basic amino acid residues of 1HRC and 2LYZ used in this study. PROPKA 3.1 utilizes a very fast empirical method to predict pK_a values and is successful in predicting unusual pK_a values. The program uses three factors to determine pK_a perturbations: desolvation, hydrogen bonding, and charge-charge interactions.

2.3 References

1. Pace, C.N., Shirley, B.A., and Thomson, J.A. (1989) in Protein Structure: A Practical Approach (Creighton, T.E., ed.) pp. 311-330, IRL Press, Oxford, UK.
2. Kumar, R., Prabhu, N.P., Yadaiah, M., and Bhuyan, A.K. (2004) *Biophys. J.* **87**, 2656-2662.
3. Rao, D.K., Kumar, R., Yadaiah, M., and Bhuyan, A.K. (2006) *Biochemistry* **45**, 3412-3420.
4. Santoro, M.M., and Bolen, D.W. (1992) *Biochemistry* **31**, 4901-4907.
5. Kumar, R., Prabhu, N.P., Rao, D.K., and Bhuyan, A.K. (2006) *J. Mol. Biol.* **364**, 483-495.
6. Hagen, S.J., Hofrichter, J., Szabo, A., and Eaton, W.A. (1996) *Proc. Natl. Acad. Sci. USA* **93**, 11615-11617.
7. Kuroda, Y., Kidokoro, S., and Wada, A. (1992) *J. Mol. Biol.* **223**, 1139-1153.
8. Strickland, E.H. (1974) *Crit. Rev. Biochem.* **2,** 113-175.
9. Hagel, P., Gerding, J.J., Fieggen, W., and Bloemendal, H. (1971) *Biochim. Biophys. Acta* **243**, 366-373.
10. Stark, G.R. (1972) *Methods Enzymol.* **25**, 103-120.

11. Lin, M.F., Williams, C., Murray, M.V., Conn, G., and Ropp, P.A. (2004) *J. Chromatogr. B Analyt. Technol. Biomed. Life Sci.***803**, 353-362.
12. Santoro, M.M., and Bolen, D.W. (1988) *Biochemistry* **27**, 8063-8068.
13. Miyawaki, O., Saito, A., Matsuo, T., and Nakamura, K. (1997) *Biosci. Biotechnol. Biochem.* **61**, 466–469.
14. Kozak, J.J., Knight, W.S., and Kauzmann, W. (1968) *J. Chem. Phys.* **48**, 675–690.
15. Miyawaki, O. (2007) *Biochim. Biophys. Acta.: Prot. Proteom.* **1774**, 928–935.
16. Miyawaki, O., and Tatsuno, M. (2011) *J. Biosci. Bioeng.* **111**, 198–203.
17. Hamer, W.J., and Wu, Y. (1972) *J. Phys. Chem. Ref. Data* **1**, 1047-1099.
18. Li, H., Robertson, A.D., and Jensen, J.H. (2005) *Proteins: Str. Func. Bioinf.* **61**, 704–721.

Chapter 3

Effects of Alcohols on the Stability and Dynamics of Proteins

3.1 Introduction

The presence of hydrophobic and hydrophilic groups in alcohols is of crucial importance in the perspective of understanding the mechanism of protein folding. Despite various studies, it is not clear whether the effects of alcohols on proteins are due to direct binding of alcohol molecules to different groups in protein (*1-3*) or due to an indirect action, involving changes in solvent (*i.e.* water) properties by the addition of alcohols (*4*). Alcohols are thought to be protein destabilizers, however, the mechanism by which alcohols affect protein stability is not fully understood (*5-7*). It is believed that alcohols destabilize the proteins by weakening hydrophobic interactions between nonpolar residues and/or by disturbing the water structure around the protein molecule (*4, 8-9*). Monohydric alcohols disrupt the tertiary structure of proteins, (*8, 10*), but enhance secondary structural elements such as helical structure (*1, 5, 11*). Although several experimental techniques have been used for quite some time to study fast protein motions that control conformational transitions associated with protein function (*12-13*), very little has been done to record the relatively slow changes in structural dynamics of proteins across the folding-unfolding transition (*14*). Clues to the role of structural dynamics in folding can be obtained by probing the changes in thermal fluctuations at both atomic and large-scale collective level. In order to unravel the exact effect of alcohols on the low-frequency local motions that control the slow changes in structural dynamics of native-like compact state of proteins, we have studied the effects of various alcohols on the structural fluctuations of the M80-containing Ω-loop of Cyt *c* by measuring the rate of thermally-driven CO dissociation from a natively folded carbonmonoxycytochrome *c* (NCO) under conditions of varying concentrations of various alcohols (methanol, ethanol, 1-propanol, 2-propanol, 3°-butanol, and 2,2,2-trifluoroethanol (TFE)). The M80-contaning Ω-loop of Cyt *c* that includes residues 70 to 85 (Fig.1a, Chapter 1) (*15*) has been identified as a partially unfolded subglobal part of the protein (*16-17*).

The NCO state used here resembles the molten globule (MG)-like state which has native-like secondary structure but disordered or dynamic tertiary structure (*18*). The CO dissociation

process (NCO $\rightarrow$ N+CO) is essentially a Fe^{2+}-CO+M80 $\rightarrow$ Fe^{2+}-M80+CO displacement reaction (*5*). For this reaction, the M80-resident segment of the polypeptide, which is linked to the heme iron through the Fe^{2+}-M80 bond in N state, but is free in the NCO state, provides a reacting site. As the neighboring residues of M80 have higher thermal factors (*19*), and the local mobility of the heme ring is suppressed by the intrinsic size and the rigidity of the ring system (*20*), the collective motion of the Ω-loop is expected to be the key determinant of the CO dissociation processes. As alcohols concentration is increased, CO-dissociation from NCO is decelerated in the subdenaturing region and then accelerated as the protein is taken from subdenaturing to denaturing milieu. The alcohol modulation of CO dissociation rates reveal the way the collective motion of the Ω-loop responds to alcohol content in the reaction medium. Since atomic fluctuations or high-frequency local motions involve only small spatial displacements, the thermal motion viewed here must be of collective character in which groups of atoms in a part or in the entire Ω-loop move in a correlated manner or as a unit. The observation that it responds to increments of alcohol implies that it is a local or subgobal unfolding motion, and hence is a low-frequency (τ, millisecond or longer) large-amplitude mode (several Å) (*21*). Thus, the CO-dissociation reaction data show a progressive decrease in spatial displacement of thermal fluctuation of a subglobal unit as the protein is taken from native to subdenaturing milieu. As compared to methanol, the spatial displacement of thermal fluctuation is reduced to a greater extent by TFE and 1-propanol. Both activation energy and conformational entropy loss for CO-dissociation reaction increase in the presence of subdenaturing concentrations of alcohols, which indicate the reduced motional freedom of the protein in the presence of subdenaturing concentrations of alcohols relative to that in the absence of alcohols. This finding confirms that the internal motions of the protein are decreased in the subdenaturing limit. When the concentration of the alcohol is increased above subdenaturing limits, the large-scale subglobal unfolding motions come to dominate the dynamics.

Protein stability characterization has an extreme importance for a number of applications ranging from protein-based pharmaceutical formulation to protein misfolding diseases. In order to determine the exact effects of subdenaturing concentrations of alcohols on the thermal stability of native proteins, we have also examined the effects of various alcohols (methanol, ethanol, 1-propanol, 2-propanol, 3°-butanol, and TFE) on the thermal denaturation of Ferrocyt *c*,

Mb and Lyz. Analysis of the thermal unfolding transitions of Ferrocyt *c*, Mb, and Lyz indicates that upon increasing the chain size or concentration of alcohols, the values of T_m for these proteins are decreased. Water plays an important role in the stabilization of the folded protein and in the control of their dynamics (*22*). For example, it is very crucial for many biological functions, such as protein architecture and enzymatic activity (*22*). Water activity also plays a major role in protein stability (*23-25*). In accordance with the earlier work by Miyawaki et al (*23-26*), the reciprocal form of Wyman–Tanford (WT) equation have been applied to investigate the role of water activity on the stability of Ferrocyt *c* at neutral pH (7.0) and of Lyz at mildly acidic pH (2.3). From this, the stabilization energy of the proteins (Ferrocyt *c* and Lyz) in alcohols solution was calculated and the *m*-values of protein stability were obtained. The longer and linear chain alcohols showed more negative *m*-values, suggesting that protein destabilization by alcohols is mainly due to the disturbance of hydrophobic interactions and hydrogen-bonding.

3.2 Results

3.2.1. Effect of alcohols on the ΔG_D, m_g and C_m of proteins

Fig. 1a, Fig. 1b, and Fig. 1c present the fluorescence monitored normalized various monohydric alcohols induced equilibrium unfolding curves of Ferrocyt *c*, Mb, and Lyz, respectively at 25 °C. The alcohol-induced equilibrium unfolding transitions of Ferrocyt *c* (Fig. 1a), Mb (Fig. 1b) and Lyz (Fig. 1c) were analyzed assuming a two state transition between the folded (N) and unfolded (U) conformations of proteins by using two-state equation (chapter2, eq (5)) (*27*). The resulting free energy of denaturation (ΔG_D), surface area exposed by solvent (m_g), and midpoint alcohol concentration (C_m) for unfolding of Ferrocyt *c*, Mb and Lyz by various alcohols monitored by Trp fluorescence (ex: 280 nm) are provided in Table 1.

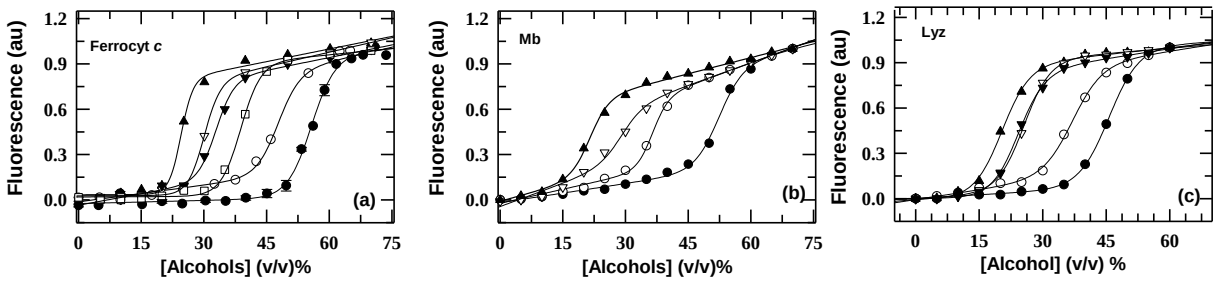

Fig. 1 Equilibrium stability curves: (a) The alcohols-induced equilibrium unfolding of Ferrocyt *c* (•, methanol; o, ethanol; □, TFE; ▲, 1-propanol; ▼, 2-propanol; and ▽, 3°-butanol) at 25 (±1)°C, pH 7.0. (b) The alcohols-induced equilibrium unfolding of Mb (•, methanol; o, ethanol; ▲, 1-propanol; and ▽, 3°-butanol) at 25 (±1)°C, pH 7.0. (c)

The alcohols-induced equilibrium unfolding of Lyz (•, methanol; o, ethanol; ▲, 1-propanol; ▼, 2-propanol; and ▽, 3°-butanol) at 25 (±1)°C, pH ~2.3. The solid curves in panels (a), (b), and (c) represent nonlinear least-squares fits to two-state equation (chapter 2, eq (5)) (*27*).

Table 1. ΔG_D, m_g, and C_m values for alcohols-induced unfolding of Ferrocyt *c* and Mb at pH 7.0 and of Lyz at pH 2.3, monitored by Trp fluorescence (ex: 280 nm).

	Ferrocyt *c*			Mb			Lyz		
Alcohols (M)	ΔG_D (kcal mol^{-1})	m_g (kcal mol^{-1}M^{-1})	C_m (v/v) %	ΔG_D (kcal mol^{-1})	m_g (kcal mol^{-1} M^{-1})	C_m (v/v) %	ΔG_D (kcal mol^{-1})	m_g (kcal mol^{-1} M^{-1})	C_m (v/v) %
Methanol	11.5	0.21	55.7	10.6	0.20	53.0	7.6	0.17	45.6
Ethanol	10.7	0.22	47.7	11.2	0.31	36.1	6.2	0.17	37.0
TFE	9.5	0.25	38.7	-	-	-	-	-	-
2-propanol	9.0	0.27	32.9	-	-	-	4.5	0.19	24.1
3°-butanol	9.0	0.30	29.9	6.4	0.22	29.1	4.9	0.19	25.6
1-propanol	10.0	0.40	24.4	5.5	0.26	21.2	3.6	0.18	20.2

*The uncertainties of m_g and ΔG_D values reported here are ±0.2 kcal mol^{-1} M^{-1} and ±1.0 kcal mol^{-1}, respectively. The uncertainty of C_m values reported here is ±0.3 (v/v) %.

3.2.2 Thermal dissociation of CO from natively folded carbonmonoxycytochrome c (NCO) and alcohols dependence of k_{diss}

The α-band (550 nm) in the electronic absorption spectrum of Ferrocyt *c* at 25 °C, pH 7.0 is the main characteristics of native Fe^{2+}-M80 bond of Ferrocyt *c* (*28-29*). The CO-dissociation from the NCO raises the intensity of the α-band (Fe^{2+}-CO+M80 → Fe^{2+}-M80+CO) (Fig. 2a,b). Fig. 2b typifies the kinetics of the NCO → N+CO dissociation in the presence of ~0.06M GdnHCl. The increase in absorbance at the heme $\pi \rightarrow \pi^*$ α-band (550 nm) in a single exponential is due to slow dissociation of CO (τ=18.5 min; Fig. 2b).

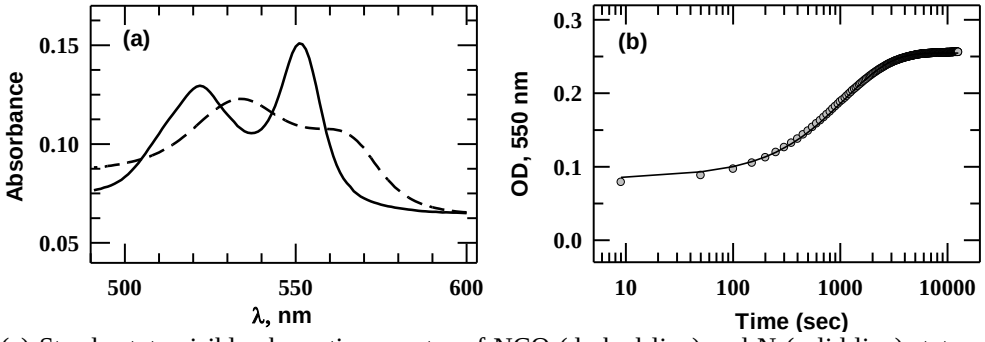

Fig. 2 (a) Steady-state visible absorption spectra of NCO (dashed line) and N (solid line) states. The spectra were recorded in 10mM Tris-HCl buffer, pH 7, containing ~0.06M GdnHCl and 5% (v/v) methanol at 25°C. (b) The slow single-phase CO dissociation reaction, NCO → N+CO (τ=18.5 min, ~0.06M GdnHCl, 25 °C) monitored by 550 nm heme absorbance.

Fig. 3a shows the rate coefficient for dissociation of CO from NCO in the 0-60 (v/v) % range of various alcohols (methanol, ethanol, 1-propanol, 2-propanol, 3°-butanol, and TFE) concentration. Given the midpoint of alcohols-induced unfolding transitions of Ferrocyt *c* (C_m ≈55.7, 47.7, 38.7, 32.9, 29.9, and 24.4 (v/v) % for methanol, ethanol, TFE, 2-propanol, 3°-butanol, and 1-propanol, respectively) (Fig. 1a, Table 1), at 25 °C these data provide an opportunity to analyze the thermodynamic properties of the protein in subdenaturing and denaturing limits. Fig. 3a shows that as final concentration of alcohols in the reaction medium is changed from strongly-native like conditions to denaturing conditions, the values of k_{diss} initially decrease in the subdenaturing regions and then increase, displaying a broad minimum around 5-15 (v/v) % of alcohols.

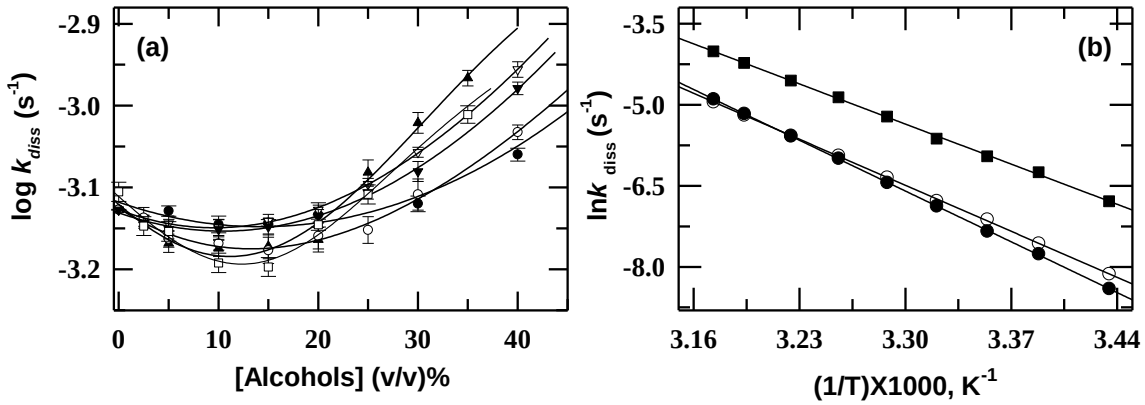

Fig. 3 (a) Alcohols dependence of k_{diss} obtained for Ferrocyt *c* (•, methanol; o, ethanol; □, TFE; ▲, 1-propanol; ▼, 2-propanol; and ▽, 3°-butanol) at 25(±1)°C, pH 7.0. The lines through the data in panel (a) have been drawn by inspection only. (b) Arrhenius plots for the CO dissociation reaction of Ferrocyt *c*, 10 mM Tris-HCl, pH 7.0, with 0.0 (o), 10 (•) and 60 (■) (v/v) % of methanol.

The decrease in k_{diss} values in the subdenaturing limit suggests that alcohols tend to block dissociation of CO from NCO. This finding provides a primary evidence for the reduced motional freedom of the protein or part of it in the subdenaturing limit of alcohols. In the subdenaturing limit of alcohols, the decrease in the k_{diss} value is more pronounced for TFE and 1-propanol and least for methanol, which suggests that the CO-dissociation from the NCO is controlled by the hydrophobicity of alcohols as well as by specific interactions of alcohols with the protein groups. The increase in k_{diss} values above 15 (v/v) % of alcohols concentration can be interpreted to arise from protein destabilization and structural unfolding that would facilitate CO dissociation process. The increase in k_{diss} values in the denaturing limit are more pronounced for longer and linear chain alcohols (*i.e.*, 1-propanol) (Fig. 3a), which suggest that at relatively

higher alcohol concentrations, the hydrophobic interactions play a vital role in controlling the dissociation of CO from the NCO state.

3.2.3 Dependence of activation enthalpy and entropy of CO-dissociation on the concentration of alcohols

The observation that the logarithm of k_{diss} decreases initially with increment in concentration of alcohols around 5-15 (v/v) % and then increases gradually at higher concentration of the alcohols (Fig. 3a) warrants a thermodynamic analysis of the CO dissociation reaction. If the decrease in the magnitude of the rate coefficient of CO-dissociation from the NCO is the result of internal motional constraints of protein by the alcohols, the decrease in entropy in the presence of alcohols must be compensated by an increase in activation enthalpy of the CO dissociation reaction. As discussed in previous works (*30-31*), this follows from,

$$\frac{H_{diss}}{RT} = ln\left(\frac{v}{k_{diss}}\right) + \frac{S_{diss}}{R} \qquad (1)$$

where v is the vibrational frequency, H_{diss} and S_{diss} are changes in activation enthalpy and activation entropy, respectively, between the relevant reactants and transition state. From eq (1) and Arrhenius equation ($k_{diss} = A\exp(-E_a/RT)$) one can obtain:

$$E_a = H_{diss}$$

$$ln\left(\frac{A}{v}\right) = \frac{S_{diss}}{R} \qquad (2)$$

Fig. 3b shows the Arrhenius plots for the CO dissociation reaction of NCO in the presence of 0.0, 10 and 60 (v/v) % of methanol. The data in Table 2 clearly shows that in the presence of 10 (v/v) % of alcohols, the activation energy increases (Table 2).

Fig. 4a shows the methanol distribution of H_{diss} for the CO dissociation reaction. The peak value of H_{diss} appears at ~10 (v/v) % of methanol. The quantity ΔS_{diss} (*i.e.*, conformational entropy loss for NCO in the presence of methanol relative to the entropy of the protein in the absence of methanol) was calculated according to eq (3) (*30-31*),

$$\Delta S_{diss} = k_B \, ln\frac{A_x}{A_{ref}} \qquad (3)$$

Here, A_{ref} and A_x are the front factor in the absence and the presence of x concentration of alcohol. ΔS_{diss} (in Boltzmann units (k_B)) obtained from eq (3) are plotted in Fig. 4b as a function of methanol concentration. Clearly, the ΔS_{diss} increases upto ~10% (v/v) of methanol and thereafter it decreases. The increase in ΔS_{diss} at subdenaturing concentrations of methanol is due likely to internal motional constraints of the protein caused by methanol. The decrease in ΔS_{diss} at higher concentrations of methanol is most likely due to structural unfolding of the protein by alcohol (Table 2).

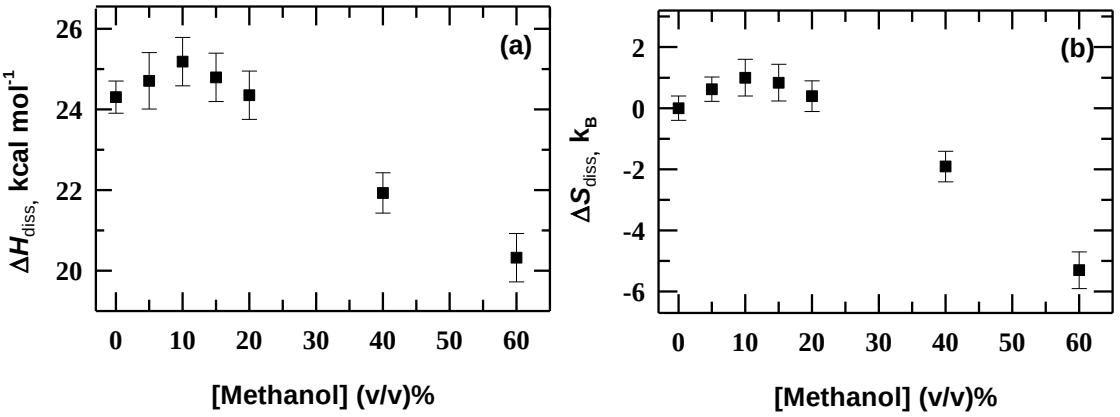

Fig. 4 Methanol distribution of (a) activation enthalpy (H_{diss}), and (b) conformational entropy loss by NCO relative to the entropy of the protein in the absence of methanol (ΔS, eq (3)) for CO dissociation reactions (NCO → N+CO). The peaks of both distributions appear at the same methanol concentration where the minimum of the log k_{diss}-methanol space (Fig. 3a) occurs.

Table 2. Activation energies (E_a) or Activation enthalpies (H_{diss}), Frequency factor (A), and Conformational entropy loss (ΔS_{diss}) for CO-dissociation from NCO in 25 mM Tris-HCl, pH 7.0.*

additive	alcohols (v/v)%	E_a (=H_{diss}) (kcal mol^{-1})	log A (s^{-1})	ΔS_{diss} (k_B)
GdnHCl	0.06	24.3	14.6	0.0
Methanol	10	24.9	15.1	1.2
	60	20.3	12.3	-5.3
Ethanol	10	25.8	15.6	2.3
1-propanol	10	25.3	15.3	1.6
2-propanol	10	25.2	15.2	1.4
3°-butanol	10	25.1	15.2	1.4
TFE	10	25.9	15.7	2.5

*Errors in values of E_a and log A are <0.5 kcal mol^{-1} and 0.6 s^{-1}, respectively, and the corresponding errors in ΔS_{diss} are ~0.5 k_B. The errors values were determined from two or more independent measurements.

3.2.4 Alcohols dependence of far-UV CD and near-UV CD

In the far-UV region (200-240 nm), the CD spectrum of native protein is characterized by two negative Cotton effects at 210 nm and 222 nm, typical of proteins with α-helix structure. Fig. 5a

and Fig. 6a show the far-UV CD spectra of Ferricyt *c* and Lyz, respectively, in the absence and presence of 20 or 30 % (v/v) aqueous solutions of methanol, 1-propanol, and 2-propanol. Fig. 5a and Fig. 6a show the increase of the far-UV CD signal towards the more negative value in the presence of alcohols, which is the usual feature for all folded proteins because alcohols are known to enhance helical secondary structures (*32-38*). However, the efficiencies for the enhancement of helical secondary structure vary significantly depending on the concentration and type of alcohol used. Fig. 5a and Fig. 6a show that the far-UV CD spectra of native Ferricyt *c* and Lyz are not greatly affected in 20 or 30 % (v/v) aqueous solutions of methanol, but they showed a significant increase in the far-UV CD signal in the presence of 20 or 30 % (v/v) of 1-propanol or 2-propanol.

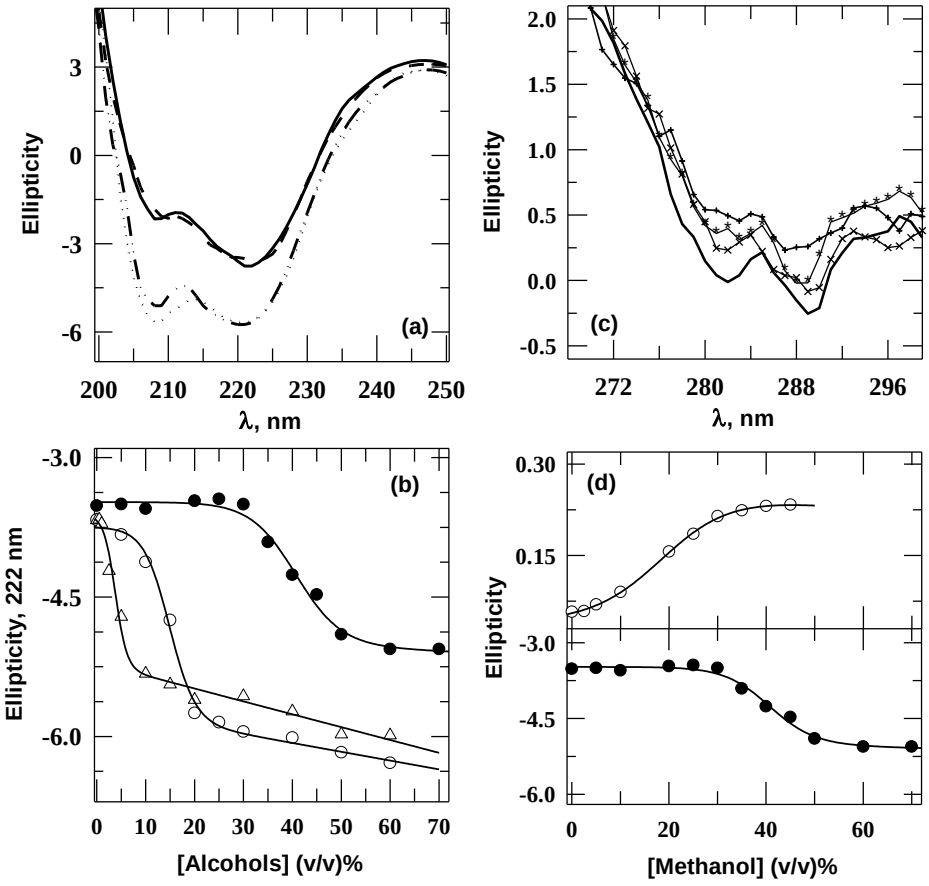

Fig. 5 (a) The far-UV CD spectra of Ferricyt *c* in the absence (——) and in the presence of 20 (v/v) % aqueous solutions of methanol (– – –), 1-propanol (— · · —), and 2-propanol (·····) at pH 7.0, 25 °C. (b) The alcohols (methanol (●), 1-propanol (Δ), and 2-propanol (o)) dependence of the far-UV CD at 222 nm, pH 7.0, 25 °C. (c) The near-UV CD spectra of Ferricyt *c* in the absence (——) and in the presence of 20 (v/v) % aqueous solutions of methanol (××××××), 1-propanol (++++++), and 2-propanol (******) at pH 7.0, 25 °C. (d) The methanol dependence of the near-UV CD at 280 nm (upper panel) and far-UV CD at 222 nm (lower panel), pH 7.0, 25 °C.

Fig. 5b and Fig. 6b compare the alcohols dependence of the far-UV CD ellipticity of Ferricyt *c* and Lyz, respectively at 222 nm. The effectiveness of the three alcohols (methanol, 1-propanol, and 2-propanol) is investigated in inducing changes in helical secondary structures of Ferricyt *c* (Fig. 5b) and Lyz (Fig. 6b) as a function of increasing the hydrocarbon chain size and branching. This is shown in Fig. 5b and Fig. 6b that comparatively higher amount of methanol (40.6 (v/v) % for Ferricyt *c* and 54.2 (v/v) % for Lyz) is required to induce one half of the maximum change in ellipticity in far-UV CD region compared to the 2-propanol (14.7 (v/v) % for Ferricyt *c* and 36.4 (v/v) % for Lyz) and 1-propanol (3.8 (v/v) % for Ferricyt *c* and 21.6 (v/v) % for Lyz)).

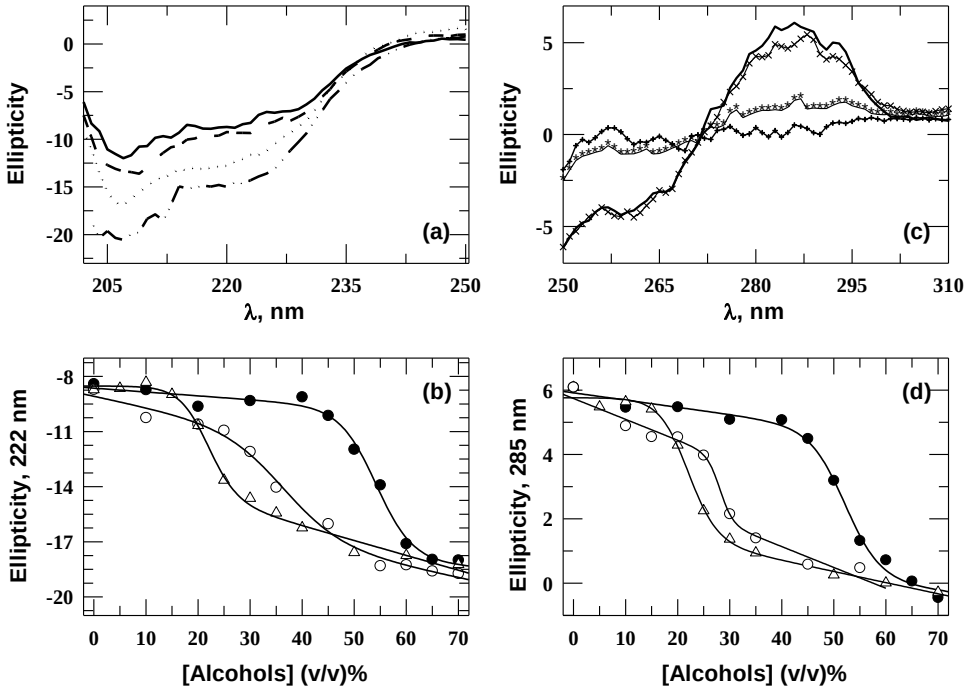

Fig. 6 (a) The far-UV CD spectra of Lyz in the absence (——) and in the presence of 30 (v/v) % aqueous solutions of methanol (– – –), 1-propanol (— · · —), and 2-propanol (·····) at pH 2.3, 25 °C. (b) The alcohols (methanol (●), 1-propanol (Δ), and 2-propanol (o)) dependence of the far-UV CD at 222 nm, pH 2.3, 25 °C. (c) The near-UV CD spectra of Lyz in the absence (——) and in the presence of 30 (v/v) % aqueous solutions of methanol (××××××), 1-propanol (++++++), and 2-propanol (******) at pH 2.3, 25 °C. (d) The alcohols (methanol (●), 1-propanol (Δ), and 2-propanol (o)) dependence of the near-UV CD at 285 nm, pH 2.3, 25 °C.

In the near-UV region (250–300 nm), the CD spectrum of native Ferricyt *c* is characterized by two negative bands between 280 nm and 290 nm, while that of Lyz is characterized by a positive band at 285 nm. Fig. 5c and Fig. 6c show the near-UV CD spectra of Ferricyt *c* and Lyz, respectively, in the absence and in the presence of 20 or 30 % (v/v) aqueous solutions of methanol, 1-propanol, and 2-propanol. Fig. 5c and Fig. 6c reveal that intensity of the two

negative bands between 280 nm and 290 nm of Ferricyt *c* and of a positive band at 285 nm of Lyz decrease in the aqueous solution of alcohols. This is because alcohols are known to disrupt tertiary structures of folded proteins (*39*). The near-UV CD spectra in ~20 % (v/v) of methanol for Ferricyt *c* and ~30 % (v/v) of methanol for Lyz showed that the two negative bands between 280 nm and 290 nm (Fig. 5c) and positive band at 285 nm (Fig. 6c) are not completely missing. However, these bands are almost lost in the presence of ~20% (v/v) of 1-propanol for Ferricyt *c* (Fig. 5c) and ~30 % (v/v) of 1-propanol for Lyz (Fig. 6c).

Fig. 5d compares the methanol dependence of the near-UV CD of Ferricyt *c* at 280 nm (upper panel) and far-UV CD of Ferricyt *c* at 222 nm (lower panel). This comparison shows that, while the CD signals at 280 nm changes mainly from 5 to 35% methanol (upper), the primary changes of the CD signals at 222 nm occur at methanol concentrations >35% (lower), *i.e.*, when the change of CD signals at 280 nm are almost over. Fig. 6d compares alcohols dependence of the near-UV CD at 285 nm for Lyz. The effectiveness of the three alcohols (methanol, 1-propanol, and 2-propanol) is investigated in disrupting the tertiary structures of Lyz (Fig. 6d) as a function of increasing the hydrocarbon chain size and branching. This is shown in Fig. 6d that almost ~52.1 (v/v) % of methanol is required to induce one half of the maximum change in ellipticity in near-UV CD region, while the corresponding figures are only ~29.1 (v/v) % for 2-propanol and ~22.4 (v/v) % for 1-propanol.

3.2.5 Alcohol-dependent thermal stability of proteins in aqueous solutions

To determine the effect of alcohols on the thermal stability of proteins, we have collected the absorbance-monitored thermal unfolding curves of Ferrocyt *c* (550 nm), Mb (409 nm) and Lyz (280 nm) in the presence of varying concentrations of monohydric alcohols. Fig. 7a and Fig. 7b show the representative thermal denaturation curves for native Ferrocyt *c* and Mb, respectively, taken at various methanol concentrations, at pH 7.0 and Fig. 7c shows the representative thermal denaturantion curves of Lyz taken at various 1-propanol concentrations at pH 2.3. To simplify the comparison of various thermal transitions, the fraction of unfolded protein (Fig. 7d,e,f) were calculated from the eq (4),

$$Fraction\,Unfolded = \frac{y(T) - (m_F T + y_F)}{(m_U T + y_U) - (m_F T + y_F)} \qquad (4)$$

By assuming a two-state denaturation process, the thermal denaturation data were analyzed by van't Hoff equation (chapter 2, eq (1)) (*40*). The resulting midpoint transition temperatures, T_m, and the enthalpy of denaturation, ΔH_m, for thermal unfolding of Ferrocyt *c*, Mb and Lyz under various alcohols concentrations are provided in Table 3, Table 4 and Table 5, respectively.

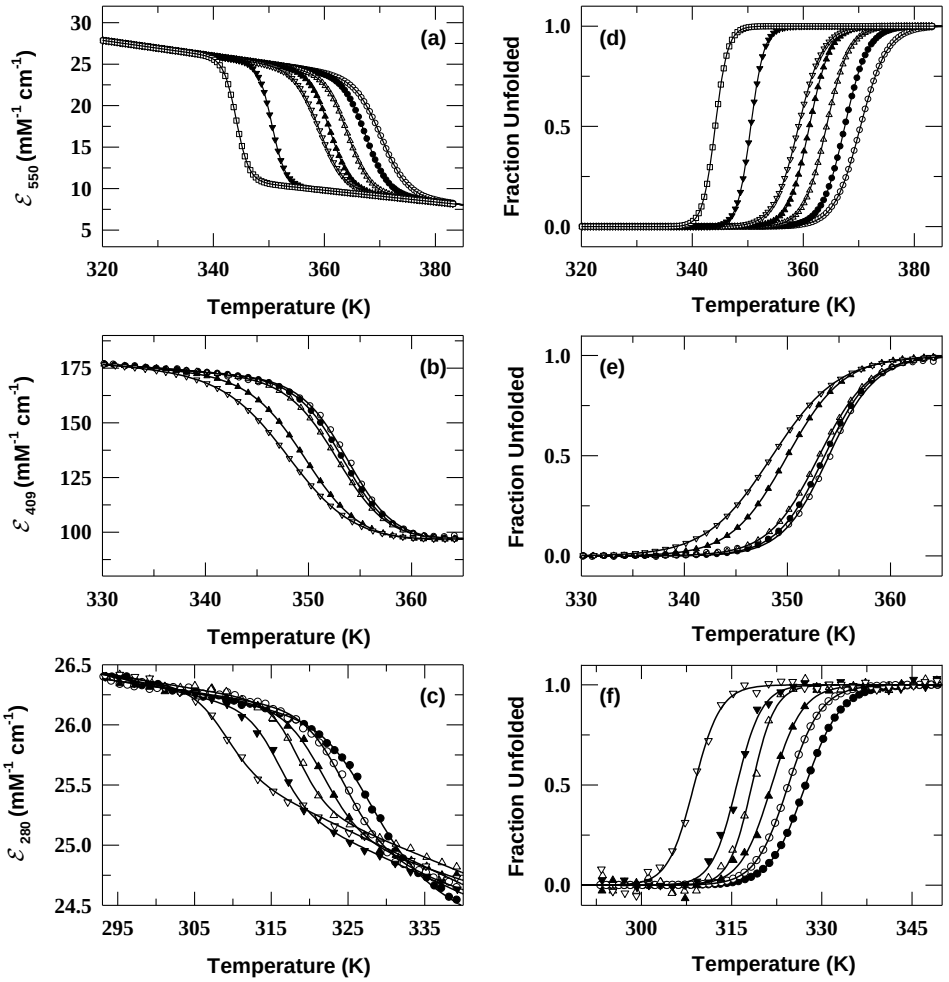

Fig. 7 (a) Thermally induced unfolding of Ferrocyt *c* monitored at 550 nm as the change in excitation coefficient in the presence of 0.0 (o), 5.0 (•), 10.0 (Δ), 15.0 (▲), 20.0 (∇), 30.0 (▼), and 40 (□) (v/v) % methanol, pH 7.0. (b) Thermally induced unfolding of Mb at 409 nm as the change in extinction coefficient in the presence of 0.0 (o), 2.5 (•), 5.0 (Δ), 7.5 (▲), and 10.0 (v/v) % methanol, pH 7.0. (c) Thermally induced unfolding of Lyz monitored at 280 nm as the change in excitation coefficient in the presence of 0.0 (•), 2.5 (○), 5.0 (▲), 7.5 (Δ), 10.0 (▼), and 15.0 (∇) (v/v) % 1-propanol, pH 2.3. To simplify the comparison of various thermal transitions, the extent of protein denaturation is presented as a fraction of unfolded protein (550 nm, panel (d); 409 nm panel (e); and 280 nm panel (f)) calculated from the eq (4). The solid curves represent nonlinear least-squares fits of the data to van't Hoff equation (*40*) (chapter 2, eq (1)).

3.2.6 Alcohols dependence of the T_m and ΔH_m

Fig. 8a, Fig. 8b and Fig. 8c show the effects of the type of alcohols and their concentrations on T_m for Ferrocyt *c*, Mb and Lyz, respectively. In agreement with earlier work (*4*, *6*, *26*) we found

that the T_m of proteins is linearly decreased upon increasing concentrations of alcohols (Fig. 8a,b,c).

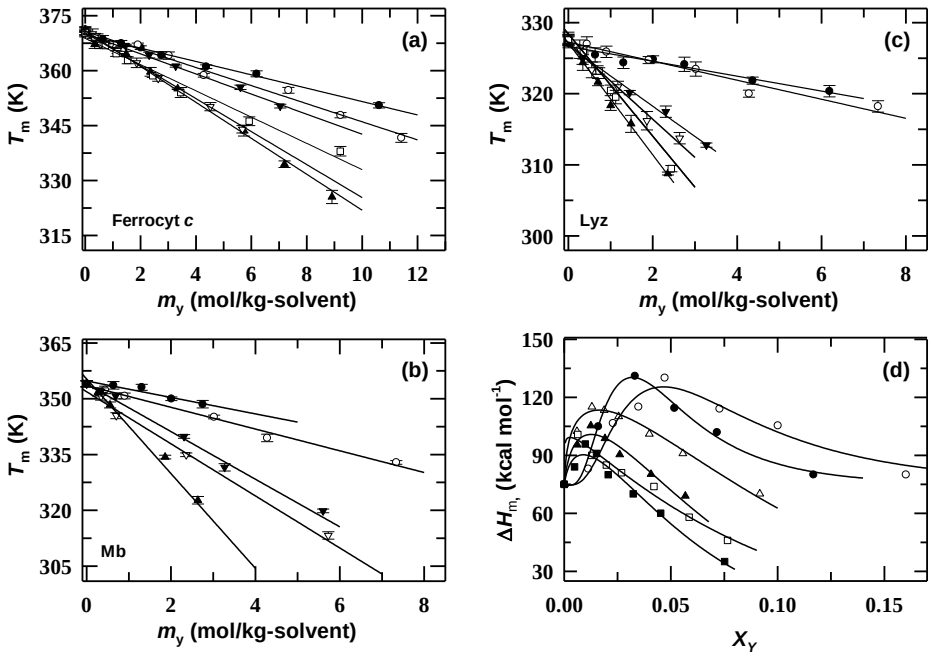

Fig. 8 (a) Effect of alcohols concentration (•, methanol; o, ethanol; □, TFE; ▲, 1-propanol; ▼, 2-propanol; and ▽, 3°-butanol) on T_m of Ferrocyt *c* at pH 7.0. (b) Effect of alcohols concentration (•, methanol; o, ethanol; ▲, 1-propanol; ▼, 2-propanol; and ▽, 3°-butanol) on T_m of Mb at pH 7.0. (c) Effect of alcohols concentration (•, methanol; o, ethanol; □, TFE; ▲, 1-propanol; ▼, 2-propanol; and ▽, 3°-butanol) on T_m of Lyz, at pH 2.3. The solid curves in panels (a), (b) and (c) represents linear least-squares fitting. (d) Alcohol (o, methanol; •, ethanol; □, TFE; ▲, 1-propanol; Δ, 2-propanol; and ■, 3°-butanol) dependence of enthalpy change, ΔH_m for Ferrocyt *c* at pH 7.0 (550 nm). The solid lines through the data have been drawn by inspection only.

Fig. 8d shows the effects of the type of alcohols and their concentrations on ΔH_m for Ferrocyt *c* at pH 7.0. Clearly, the ΔH_m varies with nature and amount of alcohol present (Fig. 8d). When concentration of alcohol is increased, ΔH_m initially increases until a maximum value is reached at a mole fraction, x_Y^* of about 0.047, 0.033, 0.013, 0.012, 0.009, and 0.006 for methanol, ethanol, 2-propanol, 1-propanol, 3° -butanol, and TFE, respectively, and thereafter decreases continuously. The maximum in the values of ΔH_m occurs at a lower alcohol concentration in the order methanol, ethanol, 2-propanol, 1-propanol, TFE ≈3°-butanol, that is, increasing hydrophobic character of the alcohol added. Velicelebi et al (1979) (*6*) had also studied the thermal denaturation of Lyz at pH 2.0 in aqueous mixture of methanol, ethanol, and 1-propanol by DSC and observed the similar plot of ΔH_{cal} for methanol, ethanol, and 1-propanol. Parodi et al

(1973) (*7*) have reported similar plot of ΔH_m for methanol, ethanol, and 1-propanol for thermal denaturation of Lyz at pH 3.

Table 3. Alcohol (methanol, TFE, ethanol, 1-propanol, 2-Propanol, and 3°-Butanol) dependence of thermodynamic parameters for thermal denaturation of Ferrocyt *c* as monitored by absorbance at 550 nm and 415 nm.*

Additive [Alcohols] (v/v)%	Methanol (550 nm)			Methanol (415 nm)		TFE (550 nm)			TFE (415 nm)	
	ΔH_m	T_m	ΔG_D	ΔH_m	T_m	ΔH_m	T_m	ΔG_D	ΔH_m	T_m
0	75	371.2	4.5	70	370.2	75	371.2	4.5	75	371.2
5	107	367.5	10.7	95	366.9	90	366.9	7.6	91	368.4
10	130	364.2	15.0	115	363.6	81	362.8	6.2	108	363.7
15	114	361.1	12.1	105	359.6	74	358.6	5.2	79	359.8
20	105	359.1	10.5	95	355.9	58	354.0	2.9	68	359.0
30	80	350.5	-	95	348.6	46	346.2	1.7	30	351.4
40	-	344.1	-	85	341.3	-	338.0	-	-	-
Additive [Alcohols] (v/v)%	Ethanol (550 nm)			Ethanol (415 nm)		1-propanol (550 nm)			1-propanol (415 nm)	
0	75	371.2	4.5	70	370.2	75	371.2	4.5	70	370.2
5	105	367.2	10.4	130	368.8	105	366.9	10.5	130	366.7
10	131	364.1	15.2	146	364.2	90	359.7	8.0	119	359.1
15	114	358.7	12.0	119	360.1	80	355.1	6.4	84	355.6
20	102	354.6	9.9	115	355.9	69	343.6	4.9	69	347.7
30	80	347.9	6.3	108	350.6	-	334.4	-	-	-
40	-	341.6	-	-	339.0	-	325.5	-	-	-
Additive [Alcohols] (v/v)%	3°-Butanol (550 nm)			3°-Butanol (415 nm)		2-propanol (550 nm)			2-propanol (415 nm)	
0	75	371.2	4.5	70	370.2	75	371.2	4.5	70	370.2
5	96	367.2	8.7	140	367.0	115	366.9	10.5	121	369.9
10	80	362.2	6.1	91	362.0	110	359.7	8.0	113	365.3
15	70	362.9	4.6	50	362.7	101	355.1	6.4	99	360.6
20	60	357.9	3.5	38	359.5	91	343.6	4.9	57	355.7
30	35	350.2	1.0	49	338.8	70	334.4	-	-	345.6
40	-	344.0	-	36	340.5	-	325.5	-	-	338.5

*ΔH_m and ΔG_D (25 °C) are reported as kcal mol^{-1}. The uncertainties of ΔH_m and ΔG_D (25 °C) values reported here are ±5.0 and ±1.0 kcal mol^{-1}, respectively. T_m is reported in K. The uncertainty of T_m values reported here is ±0.5 °C.

Table 4. Alcohol (methanol, Ethanol, 1-propanol, 2-Propanol, 3°-Butanol) dependence of the thermodynamic parameters for thermal denaturation of Mb as monitored by absorbance at 409 nm at pH 7.0*.

Additive [Alcohol] (v/v)%	Methanol		Ethanol		1-propanol		2-propanol		3°-butanol	
	ΔH_m	T_m	ΔH_m	T_m	ΔH_m	T_m	ΔH_m	T_m	ΔH_m	T_m
0	109.8	354.0	109.8	354.0	109.8	354.0	109.8	354.0	109.8	354.0
2.5	108.4	353.6	95.4	352.4	73.4	351.7	171.8	351.9	98.2	350.6
5	101.5	353.1	105.1	350.8	99.6	348.3	108.7	350.8	83.4	345.5
7.5	90.0	350.0	83.3	345.1	80.2	334.3	77.2	339.9	55.3	334.9
10	75.8	348.5	72.1	339.5	70.4	322.7	71.9	331.6	37.6	313.2
15	-	-	70.3	332.9	-	-	73.2	319.9	-	-

*ΔH_m is reported here as kcal mol^{-1}. The uncertainties of ΔH_m values reported here are ±5.0 kcal mol^{-1}. T_m is reported in K. The uncertainty of T_m values reported here is ±0.5 °C.

Table 5. Alcohol (methanol, TFE, Ethanol, 1-propanol, 2-Propanol, 3°-Butanol) dependence of the thermodynamic parameters for thermal denaturation of Lyz as monitored by absorbance at 280 nm, pH 2.3*.

Additive [Alcohol] (v/v)%	Methanol		Ethanol		1-propanol	
	ΔH_m	T_m	ΔH_m	T_m	ΔH_m	T_m
0	66.6	327.6	66.6	327.6	66.6	327.6
2.5	90.8	325.5	79.5	327.0	78.4	324.4
5	72.5	324.4	82.5	325.9	80.9	321.6
7.5	81.8	324.8	79.7	324.7	107.6	318.4
10	82.2	324.1	86.0	323.5	100.3	315.8
15	92.8	321.8	96.8	320.0	87.2	308.8
20	99.8	320.3	173.6	318.2	-	-
	2-propanol		TFE		3°-butanol	
0	66.6	327.6	66.6	327.6	66.6	327.6
2.5	87.1	325.0	82.8	325.8	86.7	326.3
5	119.7	323.3	91.6	323.2	109.5	323.4
7.5	123.6	320.2	92.5	320.5	101.1	321.0
10	97.2	317.5	99.5	319.5	109.0	316.2
15	156.8	312.8	98.4	309.5	136.9	313.8
20	-	-	-	-	71.9	303.7

*ΔH_m is reported here as kcal mol^{-1}. The uncertainties of ΔH_m values reported here are ±5.0 kcal mol^{-1}. T_m is reported in K. The uncertainty of T_m values reported here is ±0.5 °C.

3.2.7 Analysis of thermal unfolding behavior of proteins in various alcohol solutions with varied water activity

Tanford (*41*) theoretically analyzed the effect of hydration and the binding of cosolute on protein unfolding in a solution (eq (5)),

$$N + \Delta i\, W + \Delta j\, Y \rightarrow U \qquad (5)$$

where *W* is water and *Y* is a cosolute that binds to protein upon unfolding, *N* and *U* are native and unfolded states, respectively, Δi is the change in the hydration number per protein molecule, Δj is the change in the bound-cosolute molecules per protein molecule. The reciprocal form of the WT equation can be used to obtain the Δi value of protein (*24, 42*),

$$dlnK_{U,S}/dlna_W = \left[\Delta i - \left(X_W/X_Y\right)\Delta j\right] \qquad (6)$$

where $K_{U,S}$ (=[U]/[N]), and X_W and X_Y are molar fraction of water and cosolute, respectively. a_W is water activity and it must be known as a function of cosolutes concentrations to utilize eq (6). The water activity, a_W of a protein solution with a cosolute *Y* can be expressed as a function of the mole fraction of *Y* (X_Y) as (*23, 43*):

$$a_W = (1 - X_Y)\exp(\alpha X_Y + \beta X_Y^2 + \gamma X_Y^3) \qquad (7)$$

The experimental parameters, α, β and γ were taken from the literature for methanol, ethanol, 1-

propanol, 2-propanol, 3°-butanol, TFE, GdnHCl, sucrose, and glycerol (*23*, *26*) and are summarized in Table 6 to describe a_W.

Table 6. Parameters in eq (7) to describe water activity of alcohol solutions.*

Solute	α	β	γ
Methanol	-	-0.9888	-
Ethanol	-	-2.029	-
1-propanol	-	0.0281	-
2-propanol	-	-2.075	-
3°-butanol	-	-3.548	-
TFE	-	0.2234	-
Sucrose	-	-7.405	-
GdnHCl	-0.6462	6.560	-20.97

* From reference (*23*, *26*)

Fig. 9a and Fig. 9b show the typical reciprocal WT plot for unfolding of Ferrocyt *c* at pH 7.0 and Lyz at pH 2.3, respectively, in which the logarithm of $K_{U,S}$ of the protein is plotted against the logarithm of a_W of solutions at a fixed temperature. The slope (Δi-(X_w/X_Y)Δj) determined for each alcohol from linear regression fits to eq (6). It was observed that the slope depends on the kind of alcohols (Fig. 9a,b and Table 7). For both Ferrocyt *c* and Lyz, the sugars such as sucrose showed a positive slope while the denaturants such as monohydric alcohols and GdnHCl showed the negative slopes (Table 7). Among sugars, it has been reported that slopes of the reciprocal WT plot of reducing and non-reducing sugars are much different (*24-25*). At high temperatures, the reducing sugars interact with the proteins groups, however, the non reducing sugars do not exhibit such type of protein-sugar interactions (*25*). Being a nonreducing sugar, sucrose does not exhibit interactions with the protein groups and hence is preferentially excluded from the protein surface (*44-45*). Therefore, the term (X_W/X_Y)Δj in eq (6) is negligible for sucrose (*24-26*). Consequently, the value of Δi is determined from the slope of the WT plot (eq (6)) (*24, 26, 44*). The Δi,s thus determined, are 68.3 and 40.2 mol/ mol-protein for Ferrocyt *c* and Lyz, respectively. When the Δi, in eq (6) is obtained, the term, (X_W/X_Y)Δj for alcohols can easily be determined from the slope in Fig. 9a and Fig. 9b (Table 7) and Δi. By fixing the cosolute concentration, the value of Δj can easily be calculated from (X_W/X_Y)Δj. Table 8 summarizes the calculated values of Δj's at cosolute concentration of 1 mol/kg-solvent. Among various alcohols used, the Δj is highest for longer chain alcohols such as 1-propanol (3.82 and 4.96 for Ferrocyt *c* and Lyz, respectively), but this value is found to be minimum for the methanol (2.17 and 1.20 for

Ferrocyt *c* and Lyz, respectively) suggesting that hydrophobic interaction play an important role in thermal unfolding of the proteins (Table 8).

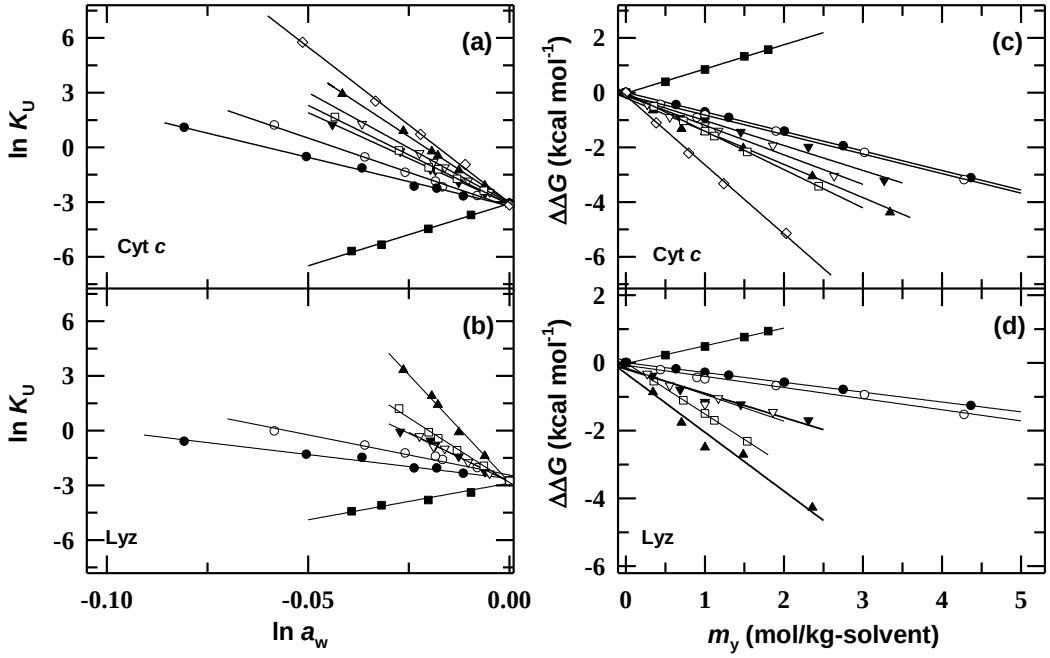

Fig. 9 (a) and (b) Reciprocal form of WT plot: Effect of water activity on unfolding ratio of Ferrocyt *c* (pH 7.0) and Lyz (pH 2.3), respectively, in aqueous solution of alcohols (•, methanol; o, ethanol; □, TFE; ▲, 1-propanol; ▼, 2-propanol; and ▽, 3°-butanol), GdnHCl (◊), and sucrose (■). (c) and (d) $\Delta\Delta G$ is plotted as a function of cosolute concentration (m_y) (•, methanol; o, ethanol; □, TFE; ▲, 1-propanol; ▼, 2-propanol; ▽, 3°-butanol; ◊, GdnHCl; and ■, sucrose) by eq (12) for thermal unfolding of Ferrocyt *c* (pH 7.0) and lyz (pH 2.3), respectively. The solid curves represent linear least-squares fitting of the data.

Table 7. Slope of the reciprocal WT plot for Ferrocyt *c* and Lyz (eq (6))*.

	Methanol	Ethanol	1-propanol	2-propanol
Ferrocyt *c*	-53.1	-75.2	-145.0	-100.5
Lyz	-26.3	-44.01	-235.5	-104.8
	3°-butanol	TFE	Sucrose	GdnHCl
Ferrocyt *c*	-119.3	-108.6	68.3	-170.7
Lyz	-108.9	-141.7	40.2	-

*The uncertainties in the value of slope reported here is ±0.2.

Table 8. Number of change in bound-cosolute molecules upon protein unfolding, Δj, at cosolute concentration of 1 mol/kg-solvent for Ferrocyt *c* and Lyz.

	Methanol	Ethanol	1-propanol	2-propanol
Ferrocyt *c*	2.17	2.57	3.82	3.02
Lyz	1.20	1.52	4.96	2.61
	3°-butanol	TFE	Sucrose	GdnHCl
Ferrocyt *c*	3.36	3.17	0.00	4.28
Lyz	2.68	3.27	0.00	-

3.2.8 Thermodynamic analysis for protein conformational stability in the presence of alcohols

Tanford (*46*) has given a transfer model (eq (8)) to analyze the conformational stability of protein in solution,

$$\Delta\Delta G = \Delta G_{U,S} - \Delta G_{U,0} = \sum \alpha_k n_k \delta g_{tr,k} \qquad (8)$$

where $\Delta\Delta G$ is the difference of free energies for protein unfolding in a solution ($\Delta G_{U,S}$) and in water ($\Delta G_{U,0}$). Green and Pace (*47*) and Pace (*48*) proposed a linear extrapolation model (LEM) for $\Delta\Delta G$:

$$\Delta\Delta G = m[m_Y] \qquad (9)$$

where m_Y is the concentration of cosolute (mol/kg-solvent) and m is an empirical parameter.

The value of m is positive for protein stabilizers and negative for protein destabilizers. Neither Tanford transfer model (*46*) nor Green and Pace (*47-48*) linear extrapolation model theoretically provides the direct effect of cosolute concentration on $\Delta\Delta G$. To evaluate the exact effect of cosolute concentration on $\Delta\Delta G$, we have applied eq (10) as Miyawaki et al used earlier for analyzing the value of Δi in sugar and alcohol solutions (*25-26*).

$$\Delta lnK_U - \Delta lnK_{U,0} = \left[\Delta i - \left(X_W/X_Y\right)\Delta j\right] lna_W \qquad (10)$$

Further, the role of water activity in protein stability can be obtained from the following expression (eq (11)) (*25-26*).

$$\Delta\Delta G = -RT\left(\Delta lnK_U - \Delta lnK_{U,0}\right) = -RT\left[\Delta i - \left(X_W/X_Y\right)\Delta j\right] lna_W \qquad (11)$$

As $\ln a_W$ is zero or negative ($a_W \leq 1$), therefore the hydration term Δi typically functions to stabilize proteins (eq (10)). While the term, $(X_W/X_Y)\Delta j$ always destabilizes proteins unless Δj is negative (*49-50*). From eqs (1) and (11), one can directly relate the effect of cosolute concentration on $\Delta\Delta G$ of Ferrocyt *c* and Lyz (eq (12))

$$\Delta\Delta G = -RT\left[\Delta i - \left(X_W/X_Y\right)\Delta j\right]\left[ln\left(1 - X_Y\right) + \alpha X_Y + \beta X_Y^2 + \gamma X_Y^3\right] \qquad (12)$$

$\Delta\Delta G$ was calculated from eq (12) as a function of cosolute concentration. $\Delta\Delta G$ was found to depend linearly on m_Y (Fig. 9c,d) indicating the applicability of LEM model. The slope (*m*-value) determined for each alcohol from linear regression fits to eq (9) (Fig. 9c,d). The *m*-value was found to depend on the kind of alcohol (Table 9).

Table 9. *m*-value of alcohols and sucrose for Ferrocyt *c* and Lyz unfolding (eq (9)).

	Methanol	Ethanol	1-propanol	2-propanol
Ferrocyt *c*	-0.71	-0.72	-1.2	-0.9
Lyz	-0.29	-0.33	-1.74	-0.72
	3°-butanol	TFE	Sucrose	GdnHCl
Ferrocyt *c*	-1.07	-1.4	+0.9	-2.5
Lyz	-0.79	-1.51	+0.52	-

*The *m*-value is reported as kcal mol^{-1} m^{-1}. The uncertainties of *m*-value reported here is ±0.2 kcal mol^{-1} m^{-1}.

3.3 Discussion

The results obtained from various kinetic and thermodynamic studies of Ferrocyt *c* in the presence of various alcohols indicate that the internal motions of Ferrocyt *c* are reduced in the subdenaturing limit of alcohols. The probable explanations for the constrained dynamics of Ferrocyt *c* at low concentrations of alcohols are discussed. The possible role of water activity on protein (Ferrocyt *c*, Mb and Lyz) stability in aqueous alcohols solutions and the mechanisms by which alcohols modulate the protein stability are also discussed in details.

3.3.1 How could protein-alcohols interactions constrain the internal dynamics of native proteins?

Several previous reports suggest that the alcohol−protein interactions are predominantly hydrophobic in nature (*7, 32-33, 50*) which affects both local and nonlocal structures (*35, 51*). A particularly interesting situation arises when the alcohol−protein interactions eventually constrain the internal dynamics of native proteins in the subdenaturing limit of alcohols. A comprehensive study of the effect of TFE on Lyz suggested that low concentrations of TFE increases the internal protein interactions by interacting with oxygen atom of –C=O group and hydrophobic groups on the protein surface (*2*). It is evident that the low concentrations of TFE (~10 (v/v) %) increase the NMR-NOE contacts of native Lyz and thus compacts and tightens the structural contacts of native protein (*2*). The other alcohols (methanol, ethanol, 1-propanol, 2-propanol, and 3°-butanol) may also compact and tighten the structural contacts at low concentrations (*52*), but the evidence supporting "increased NMR-NOE contacts of native protein at low concentrations of these alcohols" are lacking.

Our global observation reported here support current hypothesis regarding TFE action on protein structure (*1-3*) that at low concentrations, the polyfunctional interactions between the protein group and TFE increases the internal protein interactions and thus restrict the dynamics

of protein. The decrease in the rate coefficient of CO dissociation reaction in the presence of subdenaturing concentrations of alcohols could be due to the increase in the internal protein interactions resulting from some form of alcohol-protein interactions. Such an increase in intramolecular interactions within protein molecules by subdenaturing concentrations of alcohols can constrain the internal dynamics of protein or part of it. In subdenaturing limit of alcohols, the magnitude of decrease in the rate coefficient of the CO dissociation reaction is found higher for TFE and 1-propanol and is least for methanol. This finding provides two important information, (i) the internal motional freedom of Ferrocyt *c* is decreased more by TFE and 1-propanol and least by methanol, and (ii) in the subdenaturing limit, the CO-dissociation from the NCO is controlled by the hydrophobicity of alcohol as well as by some specific effects of alcohols as discussed above.

If the internal motions of protein are constrained by increase in the internal protein interactions due to some form of alcohol-protein interaction, the restricted thermal fluctuations then decrease the rate of CO dissociation by increasing the activation energy barrier. The physical origin of atomic fluctuations and local entropy are similar, therefore, the interactions of fewer alcohol molecules with the hydrophobic groups on the surface of proteins or on a part of it will result in the conformational entropy reduction. The data in Table 2 clearly shows that in the presence of subdenaturing concentrations of alcohols (~10 (v/v) %), both the activation energy and conformational entropy loss increases. This finding suggests that the internal motional freedom of the protein is reduced in the presence of subdenaturing concentrations of alcohols. The substantial reduction in the amplitudes of thermal motions in the presence of subdenaturing amounts of alcohols conceivably reduces the magnitude of subglobal unfolding motions, and thus stiffens the protein. Thus, the resultant conformation is dynamically constrained and is lower in entropy.

3.3.2 How could alcohol-water interactions stabilize the native proteins?

It has been reported that the low concentrations of typical monohydric alcohols (*i.e.*, methanol, ethanol, and 1-propanol) stabilize the native proteins at low temperatures but they destabilize the protein at higher temperatures (*6, 8, 53*), but the exact reasons about these observations are still not clearly understood. The possible molecular mechanism that brings about a prominent

relationship between temperature and the effect of alcohols on protein stability can be easily speculated. At high temperatures, the nonpolar groups are buried under the tightly folded structures but at sufficiently low temperature, these tightly folded structures unfold and expose the buried nonpolar groups to water (*54*). Furthermore, the high temperature transition is not significantly dependent on hydration of apolar protein side chains (*55*). Recently, a comprehensive study of the effect of alcohols on cold denaturation of yeast frataxin suggested that alcohols may compete with apolar groups of the proteins for water solvation, effectively making the hydration process of the aploar side chains more difficult (*54*).

The competition of alcohols with the apolar groups of the protein core for hydration is in good agreement with general view of water-alcohol interactions (*56*) intertwined with the introduction of the hydrophobic force as one of the main factor contributing to protein stability (*57*). A number of studies on the dissolution of small nonpolar molecules in water had revealed that the hydration of these molecules leads to a significant decrease in entropy of the system, primarily due to increase in the orderness of water molecules (*56-58*). At the molecular level, such a decrease in entropy was attributed to formation of iceberg-like structures of water molecules next to the nonpolar molecule (*58*). Along the same line, we can explain that entropy of the system increases much less than expected for an ideal solution of alcohol and water. In this scenario, monohydric alcohols mediated stabilization of proteins, akin to low-temperature stabilization; originate by formation of highly ordered water structure which will provide solvation for nonpolar side chains with little or no reduction of water-water hydrogen bonds but at a considerable cost of entropy that can stiffen the protein.

3.3.3 Effect of alcohols on protein structures

The existence of highly helical conformations and disrupted tertiary structures induced by alcohols has been reported for many proteins (*10, 39, 59-61*). It is interesting to determine the mechanism by which alcohols enhance the secondary structural elements such as helical structure on one hand, and disturb the tertiary structure on the other (*5, 62-63*). For Ferrocyt *c* and Lyz, the order of effectiveness towards the increase of helical structures and the disruption of tertiary structure typically follows as: 1-propanol > 2-propanol > methanol (Fig. 5 (Ferricyt *c*) and Fig. 6 (Lyz)). This order of effectiveness towards the enhancement of helical structures and

the disruption of tertiary structure for Ferricyt *c* and Lyz appear the same as reported in the literature for other proteins (TFE > propanol > ethanol > methanol) (*10*, *61*, *64*).

3.3.4 The role of water activity on protein stability

Equation (12) shows that the water activity plays a vital role in protein stability. $\Delta\Delta G$ varies linearly with alcohols, sucrose, and GdnHCl concentrations and the *m*-values for these cosolutes for protein unfolding were obtained from the slopes of these linear plots (Table 9). The effect of cosolute on protein stability is indicated by the *m*-value. In general, for kosmotropic cosolute the *m*-value is positive while for the chaotropic cosolute the *m*-value is negative (*26*). With increasing the hydrophobicity of alcohol, the *m*-value becomes more negative, which indicates that the disruption in hydrogen-bonding and hydrophobic interactions play a crucial role in destabilization of protein by alcohols. The destabilizing power of GdnHCl, which is a typical protein denaturant, is stronger than the alcohols used. The *m*-value for TFE is not so high in spite of its strong α-helix forming power, (*65-67*) indicating that TFE is a weaker protein destabilizer at higher concentration and stronger stabilizer in subdenaturing concentrations.

3.4 Conclusion

On going from the native to strongly unfolding conditions the thermal motion of the Ferrocyt *c* first decreases and then increases as the protein is taken from subdenaturing to denaturing or unfolding milieu. In the subdenaturing limit of alcohols, the extent of decrease in amplitudes of thermal motions of the protein is found to be higher for TFE and 1-propanol and is least for methanol, indicating that the internal dynamics of Ferrocyt *c* is constrained to a greater extent by TFE and 1-propanol and least by methanol. This finding further suggests that the thermal motion of the protein in the subdenturing limit of alcohols is controlled by the hydrophobicity of alcohol as well as by some specific effects of alcohols. The first phase of motional constraint is due likely to intramolecular protein cross-linking effect of the alcohols, while the second phase reflects promotion of selective unfolding of the protein or a structural unit of it (*i.e.*, M80 containing-Ω-loop). The increase in intramolecular interactions within protein molecule by subdenaturing concentrations of alcohols results in conformational entropy reduction, and thus stiffens the protein. As compared to methanol, the extent of conformational entropy reduction is more for TFE and 1-propanol. Analysis of thermal unfolding curves of Ferrocyt *c*, Mb, and Lyz

show that the value of T_m decreases with increase in alcohols concentration, indicating that alcohol decrease the thermal stability of proteins. The T_m-values for Ferrocyt *c*, Mb, and Lyz were found to decrease more for longer and linear chain alcohols, indicating that the destabilization of proteins by alcohols is due to the disturbance of hydrophobic interactions. The reciprocal form of WT equation was used to determine the effect of water activity on Ferrocyt *c* and Lyz stability. From this, $\Delta\Delta G$ of protein in alcohol solution was determined. The *m*-values were determined from the slope of $\Delta\Delta G$ *vs* [alcohols] plot. The *m*-values were found more negative for longer and linear chain alcohols, consistent with destabilization of proteins by alcohols through the disturbance of hydrophobic interactions and hydrogen-bonding.

3.5 References

1. Hong, D.P., Hoshino, M., Kuboi, R., and Goto, Y. (1999) *J. Am. Chem. Soc.* **121**, 8427–8433.
2. Povey, J.P., Smales, C.M., Hassard, S.J., and Howard, M.J. (2007) *J. Struct. Biol.* **157**, 329–338.
3. Roccatano, D., Colombo, G., Fioroni, M., and Mark, A.E. (2002) *Proc. Natl. Acad. Sci. U.S.A.* **99**, 12179–12184.
4. Onori, G., Passeri, S., and Cipiciani, A. (1989) *J. Phys. Chem.* **93**, 4306-4310.
5. Hirato, N., Mizuno, K., and Goto, Y. (1998) *J. Mol. Biol.* **275**, 365-378.
6. Velicelebi, G., and Sturtevant, J.M. (1979) *Biochemistry* **18**, 1180–1186.
7. Parodi, R.M., Bianchi, E., and Ciferri, A. (1973) *J. Biol. Chem.* **248**, 4047–4051.
8. Brandts, J.F., and Hunt, L. (1967) *J. Am. Chem. Soc.* **89**, 4826-4838.
9. Franks, F., and Eagland, D. (1975) *CRC crit. Rev. Biochem.* **3**, 165-219.
10. Herskovits, T.T., Gadegbeku, B., and Jaillet, H. (1970) *J. Biol. Chem.* **245,** 2588–2598.
11. Conio, G., Patrone, E., and Brighetti, S. (1970) *J. Biol. Chem.* **245**, 3335–3340.
12. Frauenfelder, H., Parak, F., and Young, R.D. (1988) *Ann. Rev. Biophys. Biophys. Chem.* **17**, 451-479.
13. Schlichting, I., Berendzen, J., Phillips, G.N., and Sweet, R.M. (1994) Crystal *Nature* **371**, 808-812.
14. Bai, Y., Sosnick, T.R., Mayne, L., and Englander, S.W. (1995) *Science* **269**, 192-197.

15. Leszczynski, J.F., and Rose, G.D. (1986) *Science* **234**, 849–855.
16. Hoang, L., Maity, H., Krishna, M.M.G., Lin, Y., and Englander, S.W. (2003) *J. Mol. Biol.* **331**, 37-43.
17. Xu, Y., Mayne, L.C. and Englander, S.W. (1998) *Nature Struct. Biol.* **5**, 774-778.
18. Yadaiah, M., Kumar, R., and Bhuyan, A.K. (2007) *Biochemistry* **46**, 2545-2551.
19. Berghuis, A.M., and Brayer, G.D. (1992) *J. Mol. Biol.* **223**, 959–976.
20. Morgan, J.D., and McCammon, J.A. (1983) *Biopolymers* **22**, 1579–1593.
21. Petsko, G.A., and Ringe, D. (1984) *Ann. Rev. Biophys. Bioeng.* **13**, 331-371.
22. Bellissent-Funel, M. (1999) Hydration Processes in Biology, IOS Press, Amsterdam.
23. Miyawaki, O., Saito, A., Matsuo, T., and Nakamura, K. (1997) *Biosci. Biotechnol. Biochem.* **61**, 466–469.
24. Miyawaki, O. (2007) *Biochim. Biophys. Acta: Prot. Proteom.* **1774**, 928–935.
25. Miyawaki, O. (2009) *Biophys. Chem.* **144**, 46-52.
26. Miyawaki, O., and Tatsuno, M. (2011) *J. Biosci. Bioeng.* **111**, 198–203.
27. Santoro, M.M., and Bolen, D.W. (1988) *Biochemistry* **27**, 8063-8068.
28. Margoliash, E., and Frohwirt, N. (1959) *Biochem. J.* **71**, 570-572.
29. Varhac, R., Antalik, M., and Bano, M. (2004) *J. Biol. Inorg. Chem.* **9**, 12-22.
30. Kumar, R., Prabhu, N.P., Yadaiah, M., and Bhuyan, A.K. (2004) *Biophys. J.* **87**, 2656-2662.
31. Filiaci, M., and Nienhaus, G. U. (1997) *Eur. Biophys. J.* **26**, 209-214.
32. Tanford, C. (1968) *Adv. Protein. Chem.* **23**, 121-282.
33. Timasheff, S.N. (1970) *Acc. Chem. Res.* **3**, 62-68.
34. Wilkinson, K.D., and Mayer, A.N. (1986) *Arch. Biochem. Biophys.* **250**, 390-399.
35. Alexandrescu, A.T., Ng, Y-L., and Dobson, C.M. (1994) *J. Mol. Biol.* **235**, 587-599.
36. Ptitsyn, O.B., Bychkova, V.E., and Uversky, V.N. (1995) *Philos. Trans. R. Soc. London B Biol. Sci.* **348**, 35-41.
37. Shiraki, K., Nishikawa, K., and Goto, Y. (1995) *J. Mol. Biol.* **245**, 180-192.
38. Kaminsky, L.S., Yong, F.C., and King, T.E. (1972) *J. Biol. Chem.* **247**, 1354-1359.
39. Bychkova, V.E., Dujsekina, A.E., Klenin, S.I., Tiktopulo, E.I., Uversky, V.N., and Ptitsyn, O.B. (1996) *Biochemistry* **35**, 6058-6063.
40. Santoro, M.M., and Bolen, D.W. (1992) *Biochemistry* **31**, 4901-4907.

41. Tanford, C. (1969) *J. Mol. Biol.* **39**, 539–544.
42. Jenkins, W.T. (1998) *Protein Sci.* **7**, 376–382.
43. Kozak, J.J., Knight, W.S., and Kauzmann, W. (1968) *J. Chem. Phys.* **48**, 675–690.
44. Lee, J.C., and Timasheff, S.N. (1981) *J. Biol. Chem.* **256**, 7193–7201.
45. Kendric, B.S., Chang, B.S., Arakawa, T., Peterson, B., Randorf, T.W., Manning, M.C., and Carpenter, J.F. (1997) *Proc. Natl. Acad. USA* **94**, 11917–11922.
46. Tanford, C. (1970) *Adv. Protein. Chem.* **24**, 1–95.
47. Greene, R.F., and Pace, N. (1974) *J. Biol. Chem.* **249**, 5388–5393.
48. Pace, C.N. (1986) *Meth. Enzymol.* **131**, 266–280.
49. Kaushik, J.K., and Bhat, R. (2003) *J. Biol. Chem.* **278**, 26458–26465.
50. Gerlsma, S.Y. (1968) *J. Biol. Chem.* **243**, 957−961.
51. Fan, P., Bracken, C., and Baum, J. (1993) *Biochemistry* **32**, 1573−1582.
52. Sashi, P., Yasin, U.M., and Bhuyan, A.K. (2012) *Biochemistry* **51**, 3273-3283.
53. Brandts, J.F. (1969) *Structure and Stability of Biological Macromolecules* (Timasheff, S. N., Fasman, G. D., Ed.), pp 213-290, Dekker, New York.
54. Martin, S.R., Esposito, V., Rios, P.D.L., Pastore, A., and Temussi, P.A. (2008) *J. Am. Chem. Soc.* **130**, 9963–9970.
55. Privalov, P.L. (1990) *Crit. Rev. Biochem. Mol. Biol.* **25**, 281–305.
56. Frank, H.S., and Evans, M.W. (1945) *J. Chem. Phys.* **13**, 507–532.
57. Kauzmann, W. (1959) *Adv. Protein Chem.* **14**, 1–63.
58. Frank, H.S., and Wen, W-.Y. (1957) *Disc. Faraday. Soc.* **24**, 133–140.
59. Kamatari, Y.O., Konno, T., Kataoka, M., and Akasaka, K. (1998) *Protein Sci.* **7**, 681-688.
60. Kamatari, Y.O., Ohji, S., Konno, T., Seki, Y., Soda, K., Kataoka, M., and Akasaka, K. (1999) *Protein Sci.* **8**, 873-882.
61. Bianchi, E., Rampone, R., Tealdi, A., and Ciferri, A. (1970) *J. Biol. Chem.* **245**, 3341-3345.
62. Walgers, R., Lee, T.C., and Cammers-Goodwin, A. (1998) *J. Am. Chem. Soc.* **120**, 5073-5079.
63. Anderson, N.H., Cort, J.R., Liu, Z., Sjoberg, S.J., and Tong, H. (1996) *J. Am. Chem. Soc.* **118**, 10309-10310.
64. Perham, M., Liao, J., and Stafshede, P.W. (2006) *Biochemistry* **45**, 7740-7749.

65. Kentsis, A., and Sosnick, T.R. (1998) *Biochemistry* **37**, 14613–14622.
66. Brooks, C.L., and Nilsson, L. (1993) *J. Am. Chem. Soc.* **115**, 11034–11035.
67. Luo, P., and Baldwin, R.L. (1997) *Biochemistry* **36**, 8413–8421.

Chapter 4

Effect of Compatible Osmolytes on the Stability and Dynamics of Proteins

4.1 Introduction

Proteins are complex systems that show extensive structural variability in their native state (*1*). The native conformation of proteins under external stress such as dehydration, temperature variations, variable pH, freezing, high salinity, and internal stress such as high concentrations of denaturants can be stabilized by the accumulation of low-molecular-weight organic molecules, termed as osmolytes or osmoprotectants (*2-7*). Under protein stabilization conditions, many physicochemical approaches have provided significant evidences for the interaction of osmolytes with proteins (*8-18*). However, due to the multifarious structures of the native proteins, an exact molecular explanation of the interaction of osmolytes with functional groups of proteins is not reported. The osmolytes can interact with the proteins both directly (*19-22*) as well as indirectly (*16,22-24*). Few previous studies suggest that the unfavorable interactions between the hydration surfaces of proteins and osmolytes stabilizes native conformation of proteins (*5,7,25-30*).

The interrelationships between protein function, stability, and dynamics can play important roles in protein engineering and biological processes. The stability of a protein is the outcome of equilibrium between the interactions of the functional groups of proteins with each other and with the solvent environment. Generally, the stability and dynamics of proteins in solution are strongly coupled to the dynamics of solvent (*31-35*). Addition of osmolytes into the protein solution can alter the stability and internal dynamics of proteins (*7,12,20-23,25-27,30,36-39*). Compatible osmolytes such as TMAO and GB have been shown to do the following: (i) increase the thermodynamic stability of proteins (*2,3,5,8,17,29-30,40-42*), (ii) counteract the destabilizing effects of denaturants (*2,3,5,8,17,29-30,40-42*), salts (*18,40*), and hydrostatic pressure (*19-20,40*), and (iii) refold the partially denatured proteins (*9-12,40,43*). Few earlier reports have also shown that the compatible osmolytes such as TMAO and sucrose can restrict the internal dynamics of proteins (*36-38*). This chapter investigates the effect of a compatible osmolyte such as GB and TMAO on the thermodynamic stability and internal dynamics of Cyt *c* and Mb.

GB and TMAO are the best excluder from the protein surface and are the most potent osmoprotectants (*3,5,7,27-28,30,44-45*). It has been found that GB and TMAO not always

stabilize the proteins but their effects on protein stability depend on the pH of solution, concentration of the osmolyte, and the types of protein (*40-42*). Few earlier studies have shown that the effects of GB and TMAO on the stability of Lyz, α-lactalalbumin, and RNase-A are pH dependent (*40,42*). This chapter shows that GB and TMAO increase the thermodynamic stability of Cyt *c* and Mb at neutral pH while decrease the thermodynamic stability of these proteins at mildly acidic pH. In addition, this chapter also demonstrates that GB and TMAO counter the deleterious effect of denaturants (GdnHCl and urea) at neutral pH while they show cumulative effect on the deleterious effect of denaturants at mildly acidic pH. While the counteraction effects of osmolytes on the deleterious effect of denaturants (GdnHCl and urea) are studied extensively (*2,5,7,12-16,23,29*) the additive effects of osmolytes on the denaturing effects of denaturants on proteins are not studied so far.

Though, fast protein motions that control conformational transitions responsible for biological functions have been extensively studied (*46-47*), however, only few studies are available which show the relatively slow changes in structural dynamics of proteins across the folding-unfolding transition (*48*). By probing the changes in thermal fluctuations at both atomic and large-scale collective level, the possible roles of structural dynamics in folding can be obtained. Although, the effects of denaturants (urea and GdnHCl) on the internal dynamics of native Cyt *c* and Mb have been investigated, (*49-54*), the effect of osmolytes such as GB on the on the internal dynamics of natively folded carbonmonoxycytochrome *c* (NCO) and carbonmonoxymyoglobin (MbCO) are not studied so far. Furthermore, the effect of GB on the structural fluctuation of the Ω-loop of NCO across the folding-unfolding transition of the protein also remains elusive. In this chapter, the effects of GB on the internal dynamics of NCO and MbCO have been studied by measuring the rates of CO dissociation from NCO and CO replacement from MbCO by hexacyanoferrate ion under conditions of varying concentrations of GB at pH 7.0. In addition, in this chapter the effects of GB on the structural fluctuation of the Ω-loop of NCO across the folding-unfolding transition have been studied by measuring the rates of thermally-driven CO dissociation from NCO under varying concentrations of denaturant (GdnHCl or urea) both in the absence and presence of 1.0 M GB at pH 7.0. The current results show that GB constrains the internal dynamics of NCO and MbCO at neutral pH. The major endeavor of this work is to demonstrate that within the subdenaturing limit of denaturants, GB and GdnHCl or urea show a cumulative effect on the restricted dynamics of NCO while in the subdenaturing to denaturing milieu, the large-scale unfolding fluctuations dominate the dynamics

and the inclusion of GB opposes the structural fluctuations that cause the unfolding of the protein.

4.2 Results

4.2.1 Thermal dissociation of CO from NCO and CO replacement from MbCO by hexacyanoferrate ion

CO dissociation from the natively folded CO-liganded Ferrocyt *c* (NCO) raises the intensity of the α-band (Fe^{2+}-CO+M80 → Fe^{2+}-M80+CO) (chapter 3, Fig. 2a). The CO dissociation reaction (NCO→N+CO) described here is thermally-driven and hence is slow. Fig. 1a shows a representative CO dissociation kinetic profile of NCO in the presence of ~0.06 M GdnHCl (τ =23 min) at 25 °C.

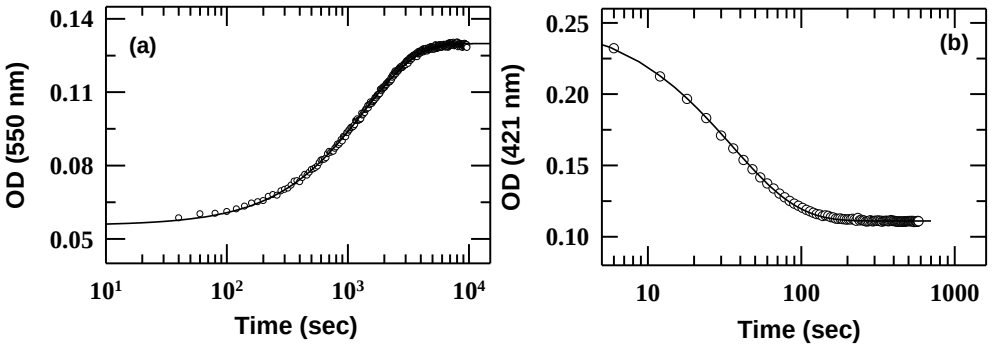

Fig. 1 (a) The slow single-phase dissociation of CO from NCO, NCO → N+CO (τ =23 min., 0.06 M GdnHCl, 25°C). The NCO → N+CO reaction was probed at 550 nm, the λ_{max} of the N-state spectrum. (b) The slow single-phase replacement of CO from MbCO, MbCO+CN → MbCN+CO (τ=0.6 min., 0.0 M GB, 22°C). The MbCO+CN → MbCN+CO reaction was probed at 421 nm.

The CO replacement reaction of MbCO by hexacyanoferrate ions, which is obtained by $K_3[Fe(CN)_6]$ can be described as:

$$\text{MbCO} + \text{CN}^- \underset{k_{on}}{\overset{k_{off}}{\rightleftharpoons}} \text{Mb} + \text{CO} + \text{CN}^- \underset{k_{-CN}}{\overset{k_{+CN}}{\rightleftharpoons}} \text{MbCN} + \text{CO}$$

where the displacing ligand CN^- has a higher affinity for Mb because $k_{-CN} \ll k_{off}$. After the addition of MbCO into $K_3[Fe(CN)_6]$ solution, the pseudo-first order condition can be used to estimate the k_{off}.The observed rate constant $k_{app,}$ is then given by (*55*),

$$k_{app} = \frac{k_{off}k_{+CN} + k_{-CN}k_{on} + k_{off}k_{-CN}}{k_{on} + k_{+CN} + k_{-CN}} \qquad (1)$$

Since CN^- binds much faster and dissociates much slower than CO, so $k_{+CN} \gg k_{on}$, and $k_{-CN} \ll k_{off}$. Further, $k_{-CN} \ll k_{+CN}$. The eq (1) then simplifies to $k_{app} \sim k_{off}$. Fig. 1b presents the single phase CO replacement kinetic profile of MbCO in the absence of GB at 22 °C (k_{off} = 0.028 s^{-1}).

4.2.2 GB dependence of the log k_{diss}, $\Delta H_{diss/off}^{\ddagger}$ and $\Delta S_{diss/off}^{\ddagger}$

Fig. 2a and Fig. 2b show the variation of the log k_{diss} and log k_{off} for NCO and MbCO, respectively, as a function of GB concentration. As GB concentration is increased from 0.0 to 2.0 M, the values of log k_{diss} (for NCO) and log k_{off} (for MbCO) decrease monoexponentially, indicating that GB restricts the internal dynamics of native Ferrocyt *c* and Mb at pH 7.0. To further investigate the effect of GB on the internal dynamics of these proteins, the GB dependence of the activation enthalpy ($\Delta H_{diss/off}^{\ddagger}$) and activation entropy ($\Delta S_{diss/off}^{\ddagger}$) for the CO dissociation and CO replacement reactions of NCO and MbCO, respectively were determined at pH 7.0. The logic is that if the internal dynamics of these proteins are restricted at some concentration of GB, then the activation energy barriers or activation enthalpies for these reactions will be relatively higher. Fig. 2c and Fig. 2d show the Eyring plots for the CO dissociation and CO replacement reactions of NCO and MbCO, respectively, in the absence and presence of ~1.0 M GB at pH 7.0. To estimate the GB effect on the activation enthalpies and activation entropies for the CO dissociation and CO replacement reactions of NCO and MbCO, respectively, the Eyring plots in Fig 2c and Fig. 2d were analyzed by using the Eyring equation (eq (2)) (*54,56*),

$$\ln(k_{diss/off} h/k_B T) = (\Delta S_{diss/off}^{\ddagger}/R) - (\Delta H_{diss/off}^{\ddagger}/RT) \qquad (2)$$

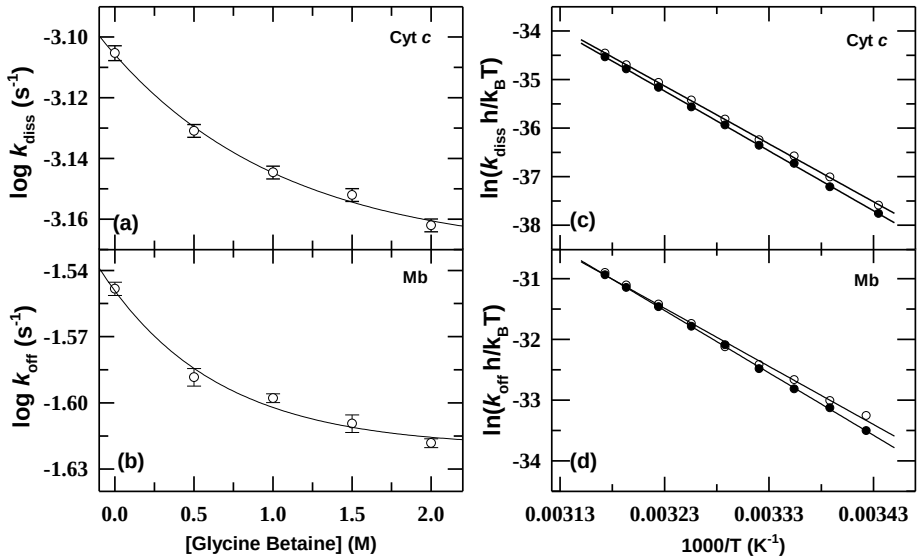

Fig. 2 Panels (a) and (b) show the effects of GB on the rate of the CO dissociation reaction, NCO → N+CO and CO replacement reaction, MbCO+CN^- → MbCN+CO, respectively, at pH 7.0. The line through data has been drawn to guide the eye only and do not represent a functional dependence of rate constant on the GB concentration. Panels (c) and (d) present the Eyring plots for the CO dissociation reaction and CO-replacement reaction, respectively, 50 mM phosphate buffer, pH 7.0, with no additives (o), and in the presence of 1.0 M GB (•). The solid lines in panels (c) and (d) are the linear least square fit to the data.

As expected, relative to in the absence of GB, the values of $\Delta H_{diss}^{\ddagger}$ and $\Delta H_{off}^{\ddagger}$ increase in the presence of 1.0 M GB (Fig.2c,d and Tables 1a-1b), which indicates that the GB decreases the motional freedom of the native proteins at neutral pH.

Table 1a. Activation enthalpy ($\Delta H_{ass}^{\ddagger}$) and activation entropy ($\Delta S_{ass}^{\ddagger}$) for CO dissociation reaction of NCO in the absence and presence of 1.0 M GB at pH 7.0*

Additive	Additive concentration, (M)	$\Delta H_{diss}^{\ddagger}$	$\Delta S_{diss}^{\ddagger}$
Control	0.0	23.9(±0.2)	6.8(±0.5)
GB	1.0	24.7(±0.1)	9.2(±0.5)

*$\Delta H^{\ddagger}_{diss}$ and $\Delta S^{\ddagger}_{diss}$ are reported as kcal mol^{-1} and cal mol^{-1} K^{-1} respectively. The uncertainty (standard error) is indicated in parenthesis.

Table 1b. Activation enthalpy ($\Delta H_{ass}^{\ddagger}$), activation entropy ($\Delta S_{ass}^{\ddagger}$) for CO replacement reaction of MbCO in the absence and presence of 1.0 M GB at pH 7.0*

Additive	Additive concentration, (M)	$\Delta H_{diss}^{\ddagger}$	$\Delta S_{diss}^{\ddagger}$
Control	0.0	19.1 (±0.002)	-1.0 (±0.01)
GB	1.0	20.6 (±0.003)	3.4 (±0.01)

*$\Delta H^{\ddagger}_{diss}$, and $\Delta S^{\ddagger}_{diss}$, are reported as kcal mol^{-1}, and cal mol^{-1} K^{-1}, respectively. The uncertainty (standard error) is indicated in parenthesis.

4.2.3 Effect of GB on the ΔG_D and denaturants-dependent log k_{diss} of NCO

Fig. 3a shows the fluorescence-monitored normalized GdnHCl and urea denauration curves of Ferrocyt *c* in the absence and presence of 1.0 M GB at pH 7.0, 25 °C. Both in the absence and presence of 1.0 M GB, Ferrocyt *c* is completely unfolded in the presence of 6.0 M GdnHCl (Fig. 3a), while within the limit of the aqueous solubilities of urea, Ferrocyt *c* exhibits incomplete unfolding (Fig. 3a) (*54-56*). Fig. 3a also shows that the GdnHCl-induced unfolding curve of Ferrocyt *c* shift towards the higher concentration of GdnHCl in the presence of 1.0 M GB. Two-state analysis (chapter 2, eq (5)) of the GdnHCl-induced unfolding curves of Ferrocyt *c* (*57*) in the absence and presence of 1.0 M GB yields denaturation free energy, ΔG_D = 17.1 kcal mol^{-1} and surface area exposed by solvent, m_g =3.3 kcal mol^{-1}M^{-1} in the absence of GB while ΔG_D =18.4 kcal mol^{-1} and m_g =3.2 kcal mol^{-1} M^{-1} are obtained in the presence of 1.0 M GB. This finding suggests that GB increases the thermodynamic stability of the protein.

To test the effect of GB on the structural fluctuation of the M80 containing Ω-loop of the native and denatured-state of Ferrocyt *c*, the rate coefficients of CO dissociation from NCO were measured as a function of GdnHCl or urea concentrations both in the absence and presence of 1.0 M GB. Fig. 3b shows the effect of GB on the denaturant (urea or GdnHCl) dependence of log k_{diss}. When the concentration of denaturant in the reaction medium is raised starting from 0.0 to

4.5 M GdnHCl or 9.5 M urea, the value of log k_{diss} initially decreases and then increases, displaying inflections centered at ~2.5 M GdnHCl or ~5.5 M urea in the absence of GB. The decrease in log k_{diss} in the subdenaturing limit of denaturants has been taken as an evidence for internal motional constraints of the protein in the subdenaturing limit of denaturant (*51*), which tends to block the CO dissociation from the NCO.

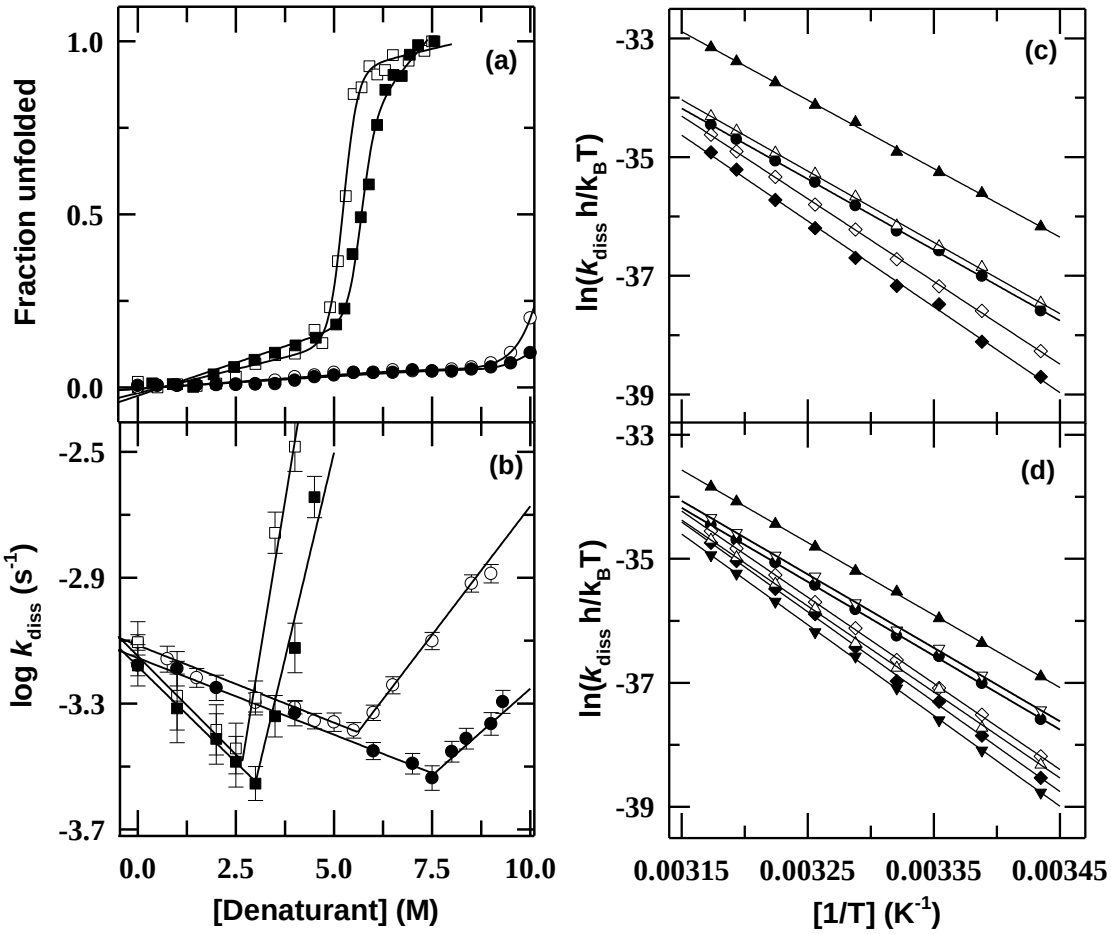

Fig. 3 (a) Denaturant (GdnHCl and urea)-induced fluorescence monitored equilibrium unfolding curves of Ferrocyt *c* measured in the absence (GdnHCl (□), urea (○)) and presence of 1.0 M GB (GdnHCl (■), urea (●)) at pH 7.0, 25 °C. The continuous curves are the fit of the data to two-state equation (chapter2, eq (5)) (*59*). The values of ΔG_D and m_g obtained are ~17.1 kcal mol^{-1}, 3.3 kcal mol^{-1} M^{-1} and ~18.4 kcal mol^{-1}, ~3.2 kcal mol^{-1} M^{-1} for GdnHCl in the absence and presence of 1.0 M GB, respectively. (b) GdnHCl and urea-dependence of log k_{diss} in the absence (GdnHCl (□), urea (○)) and presence of 1.0 M GB (GdnHCl (■), urea (●)) at pH 7.0, 25 °C. (c) Eyring plots for the CO dissociation reaction, 50 mM phosphate buffer, pH 7.0, with no additive (•); 2.5 M GdnHCl in the absence (◊) and presence (♦) of 1.0 M GB; 4.0 M GdnHCl in the absence (▲) and in the presence (Δ) of 1.0 M GB (d) Eyring plots for the CO dissociation reaction, 50 mM phosphate buffer, pH 7.0, with no additive (•), 5.5 M urea in the absence (◊) and presence (♦) of 1.0 M GB; 7.5 M urea in the absence (▽) and presence (▼) of 1.0 M GB; 9.0 M urea in the absence (▲) and presence (Δ) of 1.0 M GB. Activation enthalpies, activation entropies, and conformational entropy loss relative to native-state entropy are listed in Table 2.

Since both GB and subdenaturing concentrations of GdnHCl (<2.5 M GdnHCl) or urea (< 5.5 M urea) individually decreases the rates of CO dissociation (Fig. 2a and Fig. 3b), the coexistence of the two in the reaction medium is expected to produce a cumulative effect on the rates of CO dissociation. The denaturants dependence of the log k_{diss} in the absence and presence of 1.0 M GB is shown in Fig. 3b. Fig. 3b clearly shows that the rate-denaturant profile is shifted vertically down to lower log k_{diss} in the presence of 1.0 M GB (Fig. 3b). A horizontal shift toward higher concentration of denaturant is also apparent in the presence of 1.0 M GB (Fig 3b). Both vertical and horizontal shifts indicate that within the subdenaturing limit of denaturant, GB shows a cumulative effect with denaturant on the decrease of structural fluctuations of the Ω-loop of the protein. In the subdenaturing to denaturing region, the increase in log k_{diss} (Fig. 3b) can be interpreted to arise from protein destabilization and structural unfolding action of denaturant (*51*) that would facilitate the CO dissociation from the NCO. The log k_{diss} increases to a lesser extent in the presence of 1.0 M GB than in the absence (Fig. 3b), which indicates that the inclusion of GB opposes the structural fluctuations that cause the structural unfolding of the protein. To investigate the effect of GB on the structural fluctuations of the native and denatured states of Ferrocyt *c* further, the values of $\Delta H_{diss}^{\ddagger}$ and $\Delta S_{diss}^{\ddagger}$ for the CO dissociation reaction at different denaturant (GdnHCl or urea) concentrations both in the absence and presence of 1.0 M GB were estimated. Fig. 3c shows the Eyring plots for the CO dissociation reaction in the presence of 0.05 M GdnHCl in the absence of GB, and 2.5 and 4.0 M GdnHCl both in the absence and presence of 1.0 M GB. The Eyring plots for the CO dissociation reaction in the presence of 0.05 M GdnHCl in the absence of GB, and 5.5, 7.5 and 9.0 M urea both in the absence and presence of 1.0 M GB are shown in Fig. 3d. The Eyring plots in Fig. 3c and Fig. 3d were analyzed by using the Eyring equation (eq (2)) (*54,56*). The estimated values of $\Delta H_{diss}^{\ddagger}$ and $\Delta S_{diss}^{\ddagger}$ are summarized in Table 2. The conformational entropy loss, $\Delta\Delta S_{diss}^{\ddagger}$ for NCO in the presence of additive relative to the entropy of the protein in the absence of additive was calculated and summarized in Table 2. The data in Table 2 clearly show that in the subdenturing limit of denaturants, the values of $\Delta H_{diss}^{\ddagger}$ and $\Delta\Delta S_{diss}^{\ddagger}$ increase, while in the denaturing limits, the values of these thermodynamic parameters decrease. Remarkably, within the subdenaturing limit of denaturant, the values of $\Delta H_{diss}^{\ddagger}$ and $\Delta\Delta S_{diss}^{\ddagger}$ increase to a greater extent in the presence of GB

than in the absence of GB. However, within the denaturing limits of denaturants, the value of $\Delta H_{diss}^{\ddagger}$ and $\Delta\Delta S_{diss}^{\ddagger}$ decrease to a lesser extent in the presence of GB than in the absence of GB.

Table 2. Activation enthalpy ($\Delta H_{ass}^{\ddagger}$), activation entropy ($\Delta S_{ass}^{\ddagger}$) and conformational entropy loss ($\Delta\Delta S_{ass}^{\ddagger}$) for for CO dissociation reaction of NCO at pH 7.0*

Additive	Additive concentration, (M)	$\Delta H_{diss}^{\ddagger}$	$\Delta S_{diss}^{\ddagger}$	$\Delta\Delta S_{diss}^{\ddagger}$
Control	0.0	23.9(±0.2)	6.8(±0.5)	0.0
GB	1.0	24.7(±0.1)	9.2(±0.5)	2.4(±0.1)
GdnHCl	2.5	27.9(±0.2)	19.2(±0.6)	12.4(±0.1)
GdnHCl+1 M GB	2.5	28.9(±0.4)	21.9(±1.0)	15.1(±0.5)
GdnHCl	4.0	23.1(±0.3)	7.0(±0.8)	0.2(±0.3)
GdnHCl+1 M GB	4.0	24.0(±0.3)	7.6(±0.8)	0.8(±0.3)
Urea	5.5	27.8(±0.2)	19.1(±0.5)	12.3(±0.1)
Urea+1 M GB	5.5	29.0(±0.3)	22.5(±1.0)	15.7(±0.5)
Urea	7.5	23.7(±0.3)	6.6(±0.8)	-0.2(±0.3)
Urea+1 M GB	7.5	29.3(±0.2)	23.0(±0.5)	16.2(±0.1)
Urea	9.0	23.4(±0.1)	6.5(±0.4)	-0.2(±0.1)
Urea+1 M GB	9.0	27.7(±0.4)	18.6(±1.2)	11.8(±0.7)

*$\Delta H^{\ddagger}_{diss}$, $\Delta S^{\ddagger}_{diss}$, and $\Delta\Delta S^{\ddagger}_{diss}$ are reported as kcal mol^{-1}, cal mol^{-1} K^{-1}, and cal mol^{-1} K^{-1}, respectively. The uncertainty (standard error) is indicated in parenthesis.

4.2.4 Effect of GB on the secondary structures of native- and denatured states of Ferricyt c at neutral pH 7.0 and mildly acidic pH 3.8

Far-UV CD spectrum of Ferricyt *c* at 25 °C exhibits a negative Cotton effect at 222 nm that reflects the secondary structure of the native protein at pH 7.0 (Fig. 4a) or pH 3.8 (Fig. 4b). On raising the temperature from 25 to 90 °C or denaturant concentration from 0.0 to 5.0 M GdnHCl, the negative Cotton effect is eliminated at pH 7.0 (Fig. 4a) or pH 3.8 (Fig. 4b), indicating that the secondary structure of the protein is significantly disrupted. The effect of GB on the far-UV CD spectra of native and denatured (by ~5.0 M GdnHCl or ~8.5 M urea) states of Ferricyt *c* at pH 7.0 and pH 3.8, are shown in Fig. 4c and Fig. 4d, respectively. Fig. 4c and Fig. 4d clearly shows that at both pH 7.0 and pH 3.8, the far-UV CD signals of native state of Ferricyt *c* do not change significantly in the presence of 1.0 M GB, indicating that the GB does not greatly affect the secondary structure of native protein (Fig. 4c and Fig. 4d). However, in the presence of 1.0 M GB, the denatured-protein gains some far-UV CD signals at pH 7.0, indicating that the GB induces the secondary structures of denatured protein at pH 7.0 (Fig. 4c).

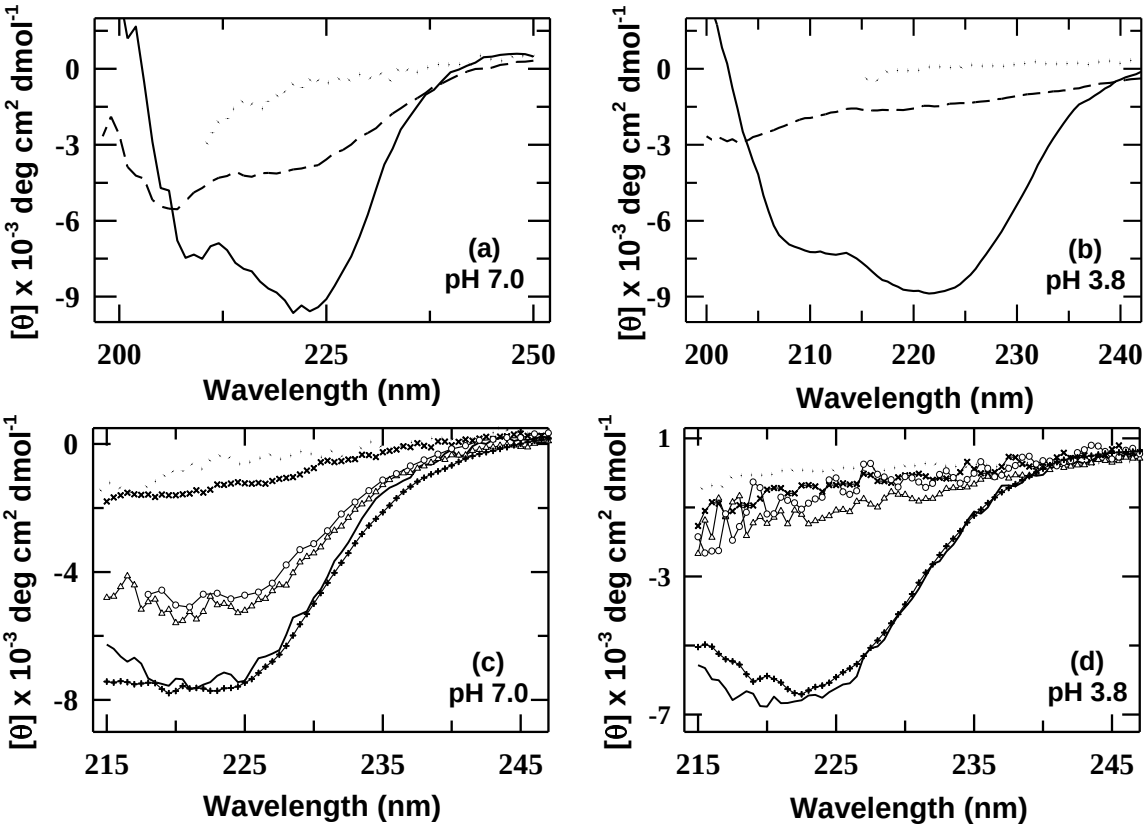

Fig. 4 The effect of GB on the native and denatured states of Ferricyt *c*. Panels (a) and (b) present far-UV CD spectra of native (solid line, 25°C) and temperature (dashed line, 90°C) and GdnHCl (dotted line, 5.0 M GdnHCl)-denatured states of Ferricyt *c* collected at pH 7.0 (panel (a)) and pH 3.8 (panel (b)). The far-UV CD spectra of native Ferricyt *c* in the absence (–––) and presence of 1.0 M GB (+++) are shown in panels (c) and (d) at pH 7.0 and 3.8, respectively. Panels (c) and (d) also show the far-UV CD spectra of denaturant-induced denatured state of Ferricyt *c* (8.0 M urea and 5.0 M GdnHCl) both in the absence (urea (xxxx) and GdnHCl (·····)) and presence of 1.0 M GB (urea (ΔΔΔΔ) and GdnHCl (○○○)) at pH 7.0 and 3.8, respectively.

4.2.5 Effect of GB and TMAO on the T_m, ΔH_m and ΔG_T of Cyt c and Mb in aqueous solution

Fig. 5a and Fig. 5b show the heme absorption (550 nm) and far-UV CD (222 nm) monitored thermal denaturation curves of Ferrocyt *c* (pH 7), respectively, in the absence and presence of 1.0 M GB. The representative absorbance (409 nm) monitored thermal unfolding curves of Mb in the absence and in the presence of 1.0 M GB and 1.0 M TMAO at pH 7.0 and pH 4.5 are shown in Fig. 5c and Fig. 5d, respectively. The representative far-UV CD (222 nm) monitored thermal unfolding curves of Ferricyt *c* both in the absence and presence of 1.0 M GB at pH 7.0 and pH 3.8 are shown in Fig. 5e and Fig. 5f, respectively. It is clear from Fig. 5 that in the presence of 1.0 M GB or 1.0 M TMAO, the thermal unfolding curves get shifted to higher temperatures at pH 7.0 (Fig. 5a,b,c,e) while they get shifted to lower temperatures at pH 3.8 or pH 4.5 (Fig. 5 d,f). The thermal unfolding curves were analyzed for thermal denaturation midpoint (T_m), enthalpy of denaturation (ΔH_m), and heat capacity change (ΔC_p) by using a non-linear least

squares method according to the Gibbs Helmholtz equation (chapter 2, eqs (2) and (3)). For Ferrocyt *c*, Ferricyt *c*, and Mb the resulting T_m, ΔH_m and ΔC_p in the absence and presence of GB or TMAO are provided in Table 3, Table 4, and Table 5, respectively. The T_m values increase in the presence of GB or TMAO at pH 7.0 while they decrease at pH 3.8-4.5 (Tables 3-5). By using ΔH_m, T_m, and ΔC_p values and eq (3) (chapter 2), the ΔG_T values at 25 °C were determined as a function of GB and TMAO concentration and are given in Tables 3-5.The ΔG_T value increases linearly with GB and TMAO concentration at pH 7.0 (Insets of Fig. 5c,e) while it decreases at pH 3.8-4.5 (Insets of Fig. 5d,f). This finding indicates that GB and TMAO increase the thermodynamic stability of the proteins at neutral pH while decrease it at mildly acidic pH.

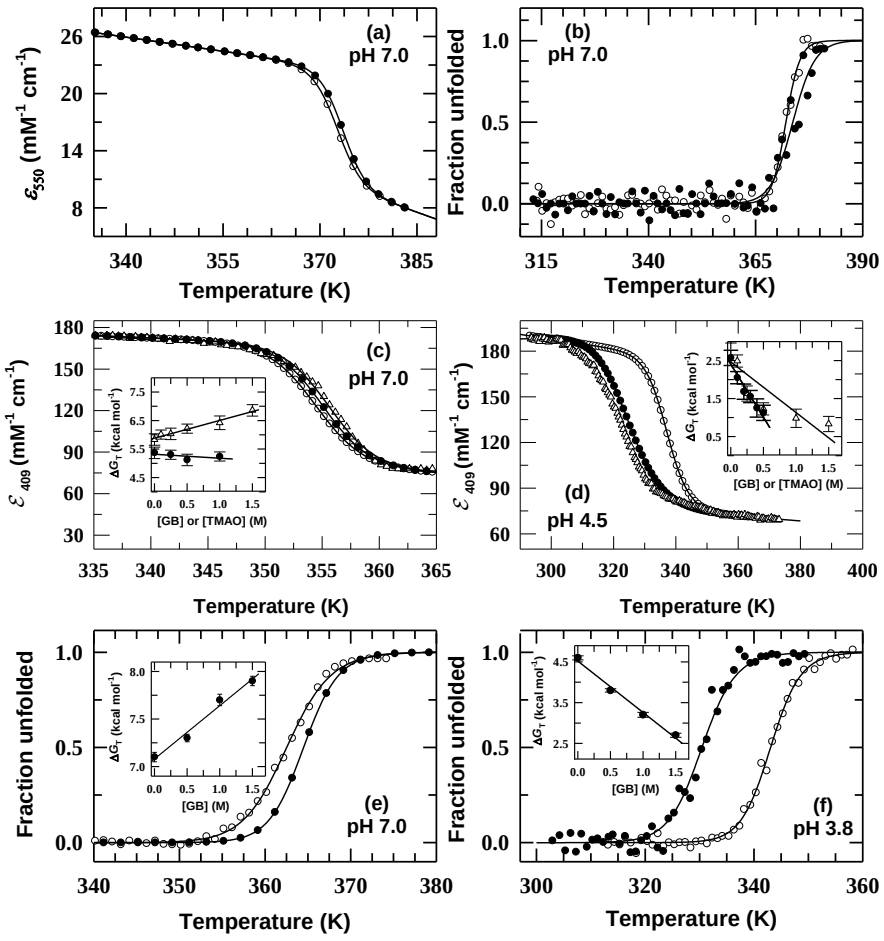

Fig. 5 (a) Thermally induced unfolding of Ferrocyt *c* monitored at 550 nm in the Soret region as the change in excitation coefficient in the absence (○) and presence of 1.0 M GB (●), pH 7.0. (b) Thermally induced unfolding of Ferrocyt *c* monitored at CD-222 nm in the absence (○) and presence of 1.0 M GB (●), pH 7.0. (c) Thermally induced unfolding of Mb monitored at absorbance-409 nm as the change in excitation coefficient in the absence (○) and presence of 1.0 M GB (●) and 1.0 M TMAO (Δ), pH 7.0. (d) Thermally induced unfolding of Mb monitored at 409 nm as the change in excitation coefficient in the absence (○) and presence of 1.0 M GB (●) and 1.0 M TMAO (Δ), pH 4.5. Panels (e) and (f) present far-UV CD monitored thermal unfolding curves of Ferricyt *c* measured at pH 7.0 and pH 3.8, respectively, in the absence (○) and presence of ~1.0 M GB (●).The solid curves in panels (a), (b),

(c), (d), (e) and (f) represent non-linear least-squares fit to the Gibbs Helmholtz equation (chapter 2, eqs (2) and (3)). Insets of panels (c) and (d) show the variation of change in thermal unfolding free energy, ΔG_T of Mb with GB (●) and TMAO (Δ) concentration at pH 7.0 and pH 4.5, respectively. Insets of panels (e) and (f) show the variation of change in thermal unfolding free energy, ΔG_T of Ferricyt *c* with GB (●) concentration at pH 7.0 and pH 3.8, respectively. The solid lines in insets of panels (c), (d), (e) and (f) represent linear least-squares fit of the ΔG_T *vs* [osmolyte] data.

Table 3. GB dependence of the T_m, ΔH_m, ΔC_p and ΔG_T for thermal unfolding of Ferrocyt *c* (absorbance 550 nm) at pH 7.0. *

GB (M)	T_m (K)	ΔH_m (Kcal mol^{-1})	ΔC_p (Kcal mol^{-1} K^{-1})	ΔG_T (Kcal mol^{-1})
0.0	372.8	115.0	1.5	12.6
1.0	373.4	121.8	1.5	13.3

*The uncertainties of T_m, ΔH_m, ΔG_T and ΔC_P values reported here are ±0.5 °C, ±2.0 kcal mol^{-1}, ±0.5 kcal mol^{-1} and ±0.2 kcal mol^{-1} K^{-1}, respectively.

Table 4. GB dependence of the T_m, ΔH_m, ΔC_p and ΔG_T for thermal unfolding of Ferricyt *c* (CD 222 nm) at pH 7.0 and 3.8.*

	pH 7.0					pH 3.8			
GB (M)	T_m (K)	ΔH_m (Kcal mol^{-1})	ΔC_p (Kcal mol^{-1} K^{-1})	ΔG_T (Kcal mol^{-1})		T_m (K)	ΔH_m (Kcal mol^{-1})	ΔC_p (Kcal mol^{-1} K^{-1})	ΔG_T (Kcal mol^{-1})
0.0	362.9	83.5	1.3	6.9		342.8	65.7	1.1	5.2
0.5	363.4	85.0	1.2	7.8		336.6	60.1	1.1	4.4
1.0	364.5	86.0	1.3	7.3		330.9	54.7	1.1	3.6
1.5	365.5	87.0	1.2	8.1		325.5	45.2	1.0	2.6

*The uncertainties of T_m, ΔH_m, ΔG_T and ΔC_P values reported here are ±0.5 °C, ±2.0 kcal mol^{-1}, ±0.5 kcal mol^{-1} and ±0.2 kcal mol^{-1} K^{-1}, respectively.

Table 5. GB and TMAO dependence of the T_m, ΔH_m, ΔG_T and ΔC_p for thermal unfolding (absorbance 409 nm) of Mb, at pH 7.0 and 4.5*

		pH 7.0						pH 4.5			
Additive	Conc. (M)	T_m (K)	ΔH_m (Kcal mol^{-1})	ΔC_p (Kcal mol^{-1} K^{-1})	ΔG_T (Kcal mol^{-1})		Conc (M)	T_m (K)	ΔH_m (Kcal mol^{-1})	ΔC_p (Kcal mol^{-1} K^{-1})	ΔG_T (Kcal mol^{-1})
GB	0.0	354.0	101.9	2.3	5.4	GB	0.0	337.3	43.9	1.2	2.3
	0.25	354.0	101.5	2.3	5.3		0.1	334.9	39.1	1.2	1.8
	0.5	353.1	99.7	2.3	5.1		0.2	331.1	35.1	1.2	1.5
	1.0	353.7	100.9	2.3	5.2		0.3	329.3	33.6	1.2	1.4
							0.4	326.8	30.1	1.2	1.1
							0.5	322.8	28.3	1.2	1.0
TMAO	0.0	354.0	101.9	2.3	5.4	TMAO	0.0	337.3	43.9	1.2	2.3
	0.1	354.8	103.6	2.3	5.5		0.1	332.8	38.6	1.2	1.8
	0.25	355.2	104.0	2.2	6.0		0.25	325.6	30.9	1.1	1.3
	0.5	355.4	105.3	2.1	6.7		0.5	320.8	26.9	1.0	1.1
	1.0	356.0	107.0	2.1	6.9		1.0	315.3	25.2	0.9	0.9
	1.5	358.2	111.0	2.1	7.4		1.5	312.7	23.9	0.9	0.8

*The uncertainties of T_m, ΔH_m, ΔG_T and ΔC_P values reported here are ±0.5 °C, ±2.0 kcal mol^{-1}, ±0.5 kcal mol^{-1} and ±0.2 kcal mol^{-1} K^{-1}, respectively.

4.2.6 Effect of GB and TMAO on the denaturant-dependent T_m, ΔH_m and ΔG_T of Cyt c and Mb

Fig. 6a shows the representative heme absorption (550 nm) monitored normalized denaturant (GdnHCl and urea) dependent thermal unfolding curves of Ferrocyt *c* both in the absence and presence of 1.0 M GB at pH 7.0. The representative absorbance (409 nm) monitored GdnHCl dependent normalized thermal unfolding curves of Mb both in the absence and presence of 0.25 M GB and 1.5 M TMAO at pH 7.0 and 0.5 M TMAO at pH 4.5 are shown in Fig. 6b and Fig. 6c, respectively. The representative far-UV CD (222 nm) monitored GdnHCl dependent normalized thermal unfolding curves of Ferricyt *c* both in the absence and presence of 1.0 M GB at pH 7.0 and 3.8 are shown in Fig. 6d and Fig. 6e, respectively. At pH 7.0 and pH 3.8-4.5, the thermal unfolding curves shift to lower temperatures in the presence of denaturant (Fig. 6a-e). However, in the presence of GB or TMAO, the denaturant-induced shift in the thermal unfolding curve is less pronounced at pH 7.0 (Fig. 6a,b,d) while it is more pronounced at pH 3.8 or pH 4.5 (Fig. 6c,e).

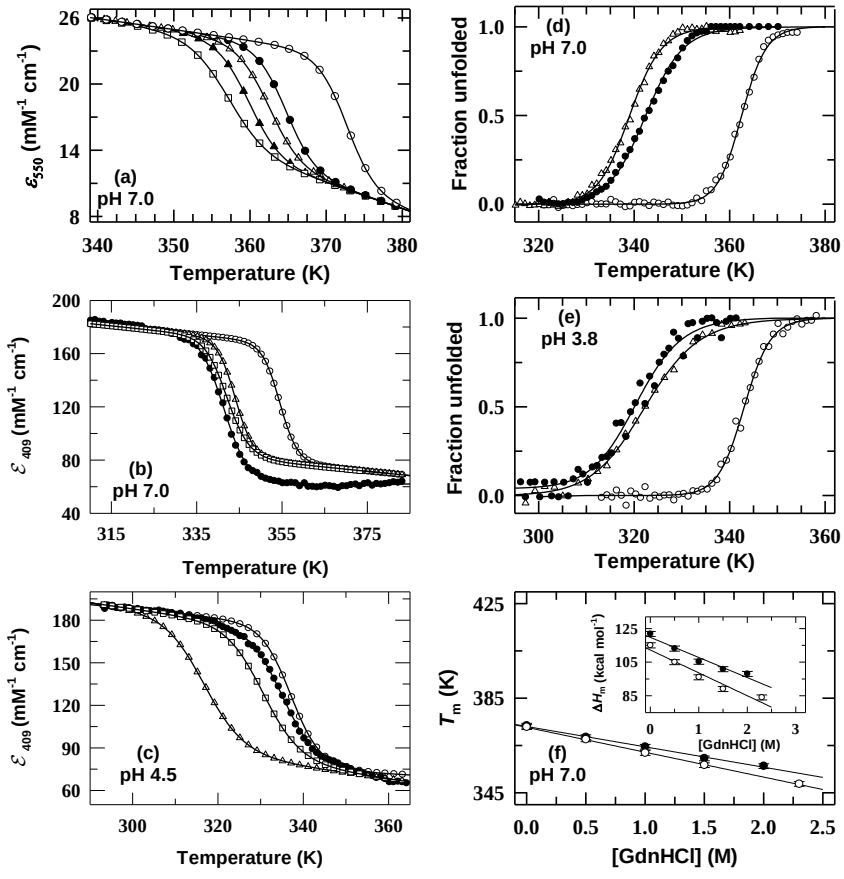

Fig. 6 (a) Thermally induced unfolding of Ferrocyt *c* monitored at 550 nm in the Soret region as the change in excitation coefficient at pH 7.0, in the absence (○); in the presence of 3.0 urea (Δ); in presence of 3.0 M urea with 1.0 M GB (•); in the presence of 1.5 M GdnHCl (□); and in the presence of 1.5 M GdnHCl with 1.0 M GB (▲). (b) Thermally induced unfolding of Mb monitored at 409 nm in the Soret region as the change in extinction coefficient

at pH 7.0, in the absence (○); in the presence of 0.5 M GdnHCl (•); in the presence of 0.5 M GdnHCl with 1.5 M TMAO (Δ), and in the presence of 0.5 GdnHCl with 0.25 M GB (□). (c) Thermally induced unfolding of Mb monitored at 409 nm in the Soret region as the change in extinction coefficient at pH 4.5, in the absence (○); in the presence of 0.05 M GdnHCl (•); in the presence of 0.05 M GdnHCl with 0.5 M TMAO (Δ), and in the presence of 0.05 GdnHCl with 0.25 M GB (□). Panels (d) and (e) represent the far-UV CD (222 nm) monitored thermal unfolding curves of Ferricyt *c* at pH 7.0 and 3.8, respectively, no additive (○); in the presence of 1.5 M GdnHCl (Δ); in the presence 1.5 M GdnHCl with 1.0 M GB (•). The solid curves in panels (a), (b), (c), (d) and (e) represent non-linear least-squares fit of the data to Gibbs Helmholtz equation (chapter 2, eqs (2) and (3)). Panel (f) show the variation of thermal unfolding midpoint, T_m of Ferrocyt *c* as a function of GdnHCl concentration, in the absence (o) and presence of 1.0 M GB (•) at pH 7.0. Inset of panel (f) shows the variation of ΔH_m of Ferrocyt *c* at pH 7.0 as a function of GdnHCl concentration in the absence (o) and presence of 1.0 M GB (•).

To determine the effect of GB and TMAO on the denaturant dependence of ΔH_m, T_m and ΔC_p, the thermal unfolding curves of Ferrocyt *c*, Ferricyt *c* and Mb collected at various GdnHCl or urea concentrations both in the absence and presence of GB and TMAO were analyzed by using Gibbs Helmholtz equation (chapter 2, eqs (2) and (3)). The resulting T_m, ΔH_m and ΔC_p values are provided in Tables 6-8. At pH 7.0 and pH 3.8-4.5, both in the absence and presence of GB and TMAO, the values of T_m and ΔH_m were found to decrease linearly with GdnHCl concentration (Fig. 6f and Fig. 7a-d). However, in the presence of GB or TMAO, the decrease in T_m and ΔH_m with GdnHCl concentration are less pronounced at pH 7.0 (Fig. 6f and Fig. 7a,b) while more pronounced at pH 3.8 or pH 4.5 (Fig. 7c,d).

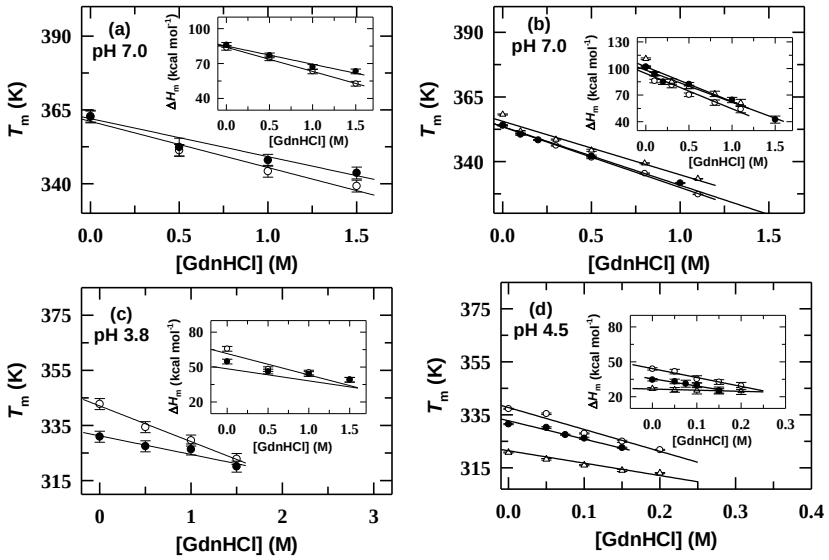

Fig. 7 Panels (a) and (c) show the variation of T_m of Ferricyt *c* at pH 7.0 and pH 3.8, respectively, as a function of GdnHCl concentration in the absence (o) and presence of 1.0 M GB (•). Panel (b) shows the variation of T_m of Mb at pH 7.0, as a function of GdnHCl concentration in the absence of osmolytes (o), in the presence of 0.25 M GB (•) and in the presence of 1.5 M TMAO (Δ). Panel (d) shows the variation of T_m of Mb at pH 4.5, as a function of GdnHCl concentration in the absence of osmolytes (o), in the presence of 0.25 M GB (•) and in the presence of 0.5 M TMAO (Δ). Insets of panels (a) and (c) show the variation of ΔH_m of Ferricyt *c* at pH 7.0 and pH 3.8, respectively, as a function of GdnHCl concentration in the absence (o) and presence of 1.0 M GB (•). Insets of panels (b) and (d) show the variation of ΔH_m of Mb at pH 7.0 and pH 4.5, respectively, as a function of GdnHCl concentration in the absence of osmolyte (o), in the presence of 0.25 M GB (•) and in the presence of 0.5 M (pH

4.5) or1.5 M (pH 7.0) TMAO. The solid lines in panels (a), (b), (c) and (d) and in insets of panels (a), (b), (c) and (d) represent linear least-squares fit of the data.

The dependence of the ΔH_m on T_m obtained by thermal unfolding of proteins in the presence of various concentrations of GdnHCl both in the absence and presence of GB and TMAO at pH 7.0 (Fig. 8a,b) and pH 3.8 (Fig. 8c) and pH 4.5 (Fig. 8d) are shown in Fig. 8. From the ΔH_m *vs* T_m plots, the ΔC_p values both in the absence and presence of GB and TMAO were determined by linear least-squares fit of the data to equation, $\Delta H_m = \Delta C_p T_m + b$ (*58-60*).

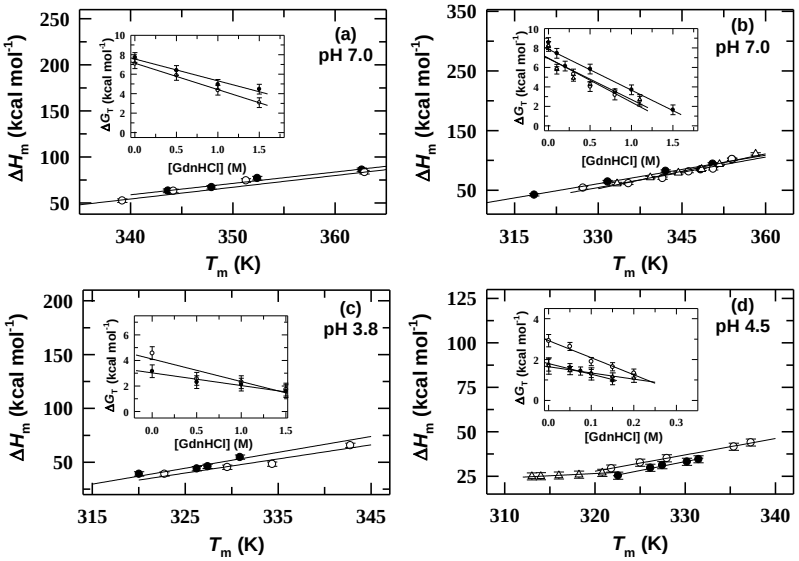

Fig. 8 Panels (a) and (c) show the variation of ΔH_m as a function of T_m of Ferricyt *c* (CD-222 nm) at pH 7.0 and 3.8, respectively, obtained at different GdnHCl concentrations in the absence (○) and presence of 1.0 M GB (●). The insets of panels (a) and (c) show the variation of ΔG_T of Ferricyt *c* as a function of GdnHCl concentrations at pH 7.0 and 3.8, respectively, in the absence (o) and presence (●) of 1.0 M GB. (b) Variation of ΔH_m as a function of T_m of Mb (absorbance 409 nm) at pH 7.0 obtained at different GdnHCl concentrations in the absence of osmolyte (○), in the presence of 0.25 M GB (●), and in the presence of 1.5 M TMAO (Δ). (d) Variation of ΔH_m as a function of T_m of Mb (absorbance 409 nm) at pH 4.5 obtained at different GdnHCl concentrations in the absence of osmolyte (○), in the presence of 0.25 M GB (●), and in the presence of 0.5 M TMAO (Δ). The insets of panels (b) and (d) show the variation of ΔG_T of Mb as a function of GdnHCl concentrations at pH 7.0 and 4.5, respectively, in the absence of osmolyte (o), in the presence of 0.25 M GB (●) and in the presence of 0.5 M (pH 4.5) or1.5 M (pH 7.0) TMAO (Δ).

By using the Gibbs Helmholtz equation (chapter 2, eq (3)) and ΔC_p values, the ΔG_T values were determined at 25 °C as a function of GdnHCl concentration both in the absence and presence of GB and TMAO (Tables 7-8). The ΔG_T *vs* [GdnHCl] plots in the absence and presence of GB and TMAO at pH 7.0 (Insets of Fig. 8a,b) and pH 3.8 and pH4.5 (Insets of Fig. 8c,d) are shown in the insets of Fig.8a-d. Both in the absence and presence of GB and TMAO, the ΔG_T values decrease linearly with GdnHCl concentration (Insets of Fig.8a-d). However, in the presence of GB or TMAO, the ΔG_T decrease to a lesser extent at pH 7.0 (Insets of Fig.7a,b) while it is decreased to a greater extent at pH 3.8 and pH 4.5 (Insets of Fig.7c,d). These findings indicate that the GB and TMAO counteract the destabilizing action of the denaturants on the thermal

stability of the protein at neutral pH while at mildly acidic pH, the osmolytes (GB or TMAO) and GndHCl show a cumulative effect on the thermal destabilization of protein.

Table 6. Denaturant (GdnHCl, Urea) dependence of the T_m, ΔH_m, ΔC_p and ΔG_T for thermal unfolding of Ferrocyt *c* (absorbance 550 nm) both in the absence and presence of 1.0 M GB at pH 7.0.*

Additive	Concentrations of Denaturant (M)	T_m (K)	ΔH_m (Kcal mol^{-1})	ΔC_p (Kcal mol^{-1} K^{-1})	ΔG_T (Kcal mol^{-1})
GdnHCl	0.0	372.8	115.0	1.5	12.6
	0.5	367.6	105.0	1.4	10.7
	1.0	361.8	96.0	1.4	9.1
	1.5	356.7	89.0	1.4	7.8
	2.3	348.7	84.0	1.4	7.0
GdnHCl+1 M GB	0.0	373.4	121.8	1.5	13.2
	0.5	368.5	113.1	1.5	11.5
	1.0	364.4	105.3	1.5	10.2
	1.5	359.6	100.8	1.4	9.4
	2.0	356.3	98.0	1.4	9.0
Urea	0.0	372.8	115.0	1.5	13.0
	1.5	366.4	110.0	1.4	12.0
	2.5	363.3	105.0	1.4	11.0
	3.5	360.6	100.0	1.4	10.1
	4.5	358.0	97.0	1.4	9.5
Urea+1 M GB	0.0	373.4	121.8	1.5	13.3
	1.0	370.5	118.0	1.5	12.5
	2.0	366.4	114.0	1.5	11.8
	3.0	364.5	110.0	1.4	11.1
	4.0	362.4	106.0	1.4	10.4

*The uncertainties of T_m, ΔH_m, ΔG_T and ΔC_P values reported here are ±0.5 °C, ±2.0 kcal mol^{-1}, ±0.5 kcal mol^{-1} and ±0.2 kcal mol^{-1} K^{-1}, respectively.

Table 7. GdnHCl dependence of the T_m, ΔH_m, ΔG_T and ΔC_p for thermal unfolding of Ferricyt *c* (CD 222 nm) both in the absence of presence of 1.0 M GB at pH 7.0 and 3.8*

Additive	Conc. (M)	T_m (K)	ΔH_m (Kcal mol^{-1})	ΔC_p (Kcal mol^{-1} K^{-1})	ΔG_T (Kcal mol^{-1})	ΔC_p (Kcal mol^{-1} K^{-1})	ΔG_T (Kcal mol^{-1})
		pH 7.0					
GdnHCl	0.0	362.9	83.5	1.3	6.9	1.3	7.1
	0.5	351.3	74.5	1.1	6.6		5.9
	1.0	344.2	63.2	1.1	4.9		4.4
	1.5	339.2	52.6	1.1	3.5		3.1
GdnHCl+	0.0	364.5	86.0	1.3	7.3	1.1	7.7
1 M GB	0.5	352.4	77.0	1.1	7.0		6.4
	1.0	347.9	67.1	1.1	5.5		5.0
	1.5	343.6	63.3	1.1	4.9		4.5
		pH 3.8					
GdnHCl	0.0	342.8	65.7	1.1	5.2	1.3	4.6
	0.1	334.3	48.2	1.1	3.0		2.6
	0.2	329.5	45.3	1.0	2.8		2.3
	0.3	322.8	39.1	1.0	2.0		1.7
GdnHCl+	0.0	330.9	54.7	1.1	3.6	1.4	3.2
1 M GB	0.1	327.4	46.1	0.7	3.2		2.3
	0.2	326.2	44.0	1.0	2.5		2.1
	0.3	320.0	39.1	1.0	1.9		1.6

*The uncertainties of T_m, ΔH_m, ΔG_T and ΔC_P values reported here are ±0.5 °C, ±2.0 kcal mol^{-1}, ±0.5 kcal mol^{-1} and ±0.2 kcal mol^{-1} K^{-1}, respectively.

Table 8. GdnHCl dependence of the T_m, ΔH_m, ΔG_T and ΔC_p for thermal unfolding of Mb (absorbance 409 nm) both in the absence of presence of 0.25 M GB, and TMAO (1.5 M at pH 7.0 and 0.5 M at pH 4.5) at pH 7.0 and 4.5*

Additive	Conc. (M)	pH 7.0					
		T_m (K)	ΔH_m (Kcal mol^{-1})	ΔC_p (Kcal mol^{-1} K^{-1})	ΔG_T (Kcal mol^{-1})	ΔC_p (Kcal mol^{-1} K^{-1})	ΔG_T (Kcal mol^{-1})
GdnHCl	0.0	354.0	101.9	2.3	5.4	1.7	8.2
	0.1	350.6	85.9	2.0	4.6		5.8
	0.3	346.2	81.3	2.0	4.3		5.3
	0.5	341.5	70.3	2.0	3.2		4.0
	0.8	335.4	61.5	2.0	2.5		3.2
	1.1	327.3	54.0	2.0	2.1		2.5
GdnHCl+	0.0	354.0	101.5	2.3	5.3	1.6	8.6
0.25 M	0.1	350.5	94.1	2.3	4.6		7.5
GB	0.2	348.3	84.9	2.3	3.5		6.1
	0.5	342.1	82.2	2.3	3.8		5.8
	1.0	331.7	64.4	2.3	2.5		3.7
	1.5	318.5	42.3	2.3	1.2		1.6
GdnHCl+	0.0	358.2	111.0	2.1	7.4	1.9	8.2
1.5 M	0.1	351.7	93.5	2.3	4.3		5.9
TMAO	0.3	348.5	85.3	2.3	3.5		4.9
	0.5	344.4	79.2	2.3	3.2		4.3
	0.8	339.3	71.3	2.3	2.7		3.6
	1.1	333.4	61.2	2.3	2.0		2.7
		pH 4.5					
GdnHCl	0.0	337.3	43.9	1.2	2.3	0.9	2.9
	0.05	335.4	41.6	0.7	3.1		2.6
	0.1	328.0	35.1	0.7	2.2		1.9
	0.15	325.0	32.6	0.5	2.1		1.6
	0.2	321.8	29.3	0.5	1.7		1.3
GdnHCl+	0.0	331.5	34.5	1.2	1.4	1.0	1.7
0.25 M	0.05	330.2	33.1	1.1	1.4		1.6
GB	0.075	327.5	31.2	0.8	1.7		1.4
	0.1	326.1	29.7	0.7	1.7		1.3
	0.15	322.6	25.3	0.6	1.3		1.0
GdnHCl+	0.0	320.8	26.9	0.6	1.4	0.3	1.7
0.5 M	0.05	318.2	25.9	0.5	1.3		1.5
TMAO	0.1	316.0	25.4	0.5	1.2		1.3
	0.15	314.0	25.0	0.4	1.1		1.2
	0.2	313.0	24.9	0.4	1.0		1.1

*The uncertainties of T_m, ΔH_m, ΔG_T and ΔC_P values reported here are ±0.5 °C, ±2.0 kcal mol^{-1}, ±0.5 kcal mol^{-1} and ±0.2 kcal mol^{-1} K^{-1}, respectively.

4.2.7 Effect of GB on the ΔG_D and C_m of Ferricyt c in aqueous solution

Fig. 9a and Fig. 9b show the fluorescence-monitored normalized urea-induced unfolding curves of Ferricyt *c* at pH 7.0 and pH 3.8, respectively, in the absence and presence of ~0.3, 0.5, and 1.0 M GB at 25 °C. The urea-induced unfolding curves of Ferricyt *c* shift towards the higher concentration of urea in the presence of GB at pH 7.0 while they shift towards lower concentration of urea at pH 3.8. Two-state analysis (*57*) of the urea-induced unfolding curves of Ferricyt *c* in Fig 9a (pH 7.0) and Fig 9b (pH 3.8) provided the ΔG_D and m_g values at different

concentrations of GB (Table 9). The urea unfolding midpoint, C_m (=$\Delta G_D/m_g$) for different concentration of GB was also calculated (Table 9). As GB concentration is increased from 0.0 to 1.0 M, the ΔG_D and C_m values increase at pH 7.0 while they decrease at pH 3.8 (Fig. 9c,d). The increase in ΔG_D in the presence of GB at pH 7.0 indicates that the GB increases the thermodynamic stability of native protein at neutral pH. On the other hand, the decrease in ΔG_D in the presence of GB at pH 3.8 suggests that GB decreases the thermodynamic stability of native protein at mildly acidic pH.

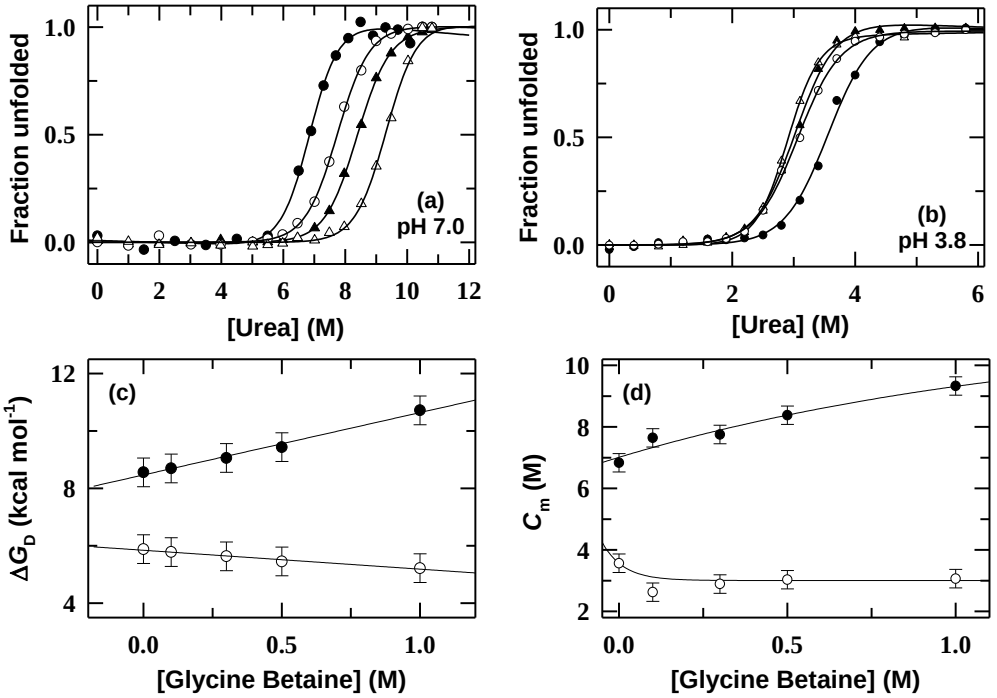

Fig. 9 Panels (a) and (b) show the fluorescence-monitored normalized equilibrium urea-induced unfolding curves of Ferricyt *c* at pH 7.0 and pH 3.8, respectively, in the presence of 0.0 (•), 0.3 (○), 0.5 (▲), and 1.0 M GB (Δ) at 25 °C. The solid curves represent non-linear least-squares fit according to the standard two-state equation (chapter 2, eq (5)) (*57*). (c) Variation of change in unfolding free energy, ΔG_D of Ferricyt *c* with GB concentration at pH 7.0 (•) and pH 3.8 (o). (d) Variation of the urea unfolding midpoint, C_m of Ferricyt *c* with GB concentration at pH 7.0 (•) and pH 3.8 (o).

Table 9. Dependence of the ΔG_D, m_g and C_m of Ferricyt *c* on GB concentration at pH 7.0 and pH 3.8 as monitored by Trp fluorescence (ex: 280; em: 365 nm)*.

Additive	Conc. (M)	pH 7.0			Conc. (M)	pH 3.8		
		C_m (M)	ΔG_D (kcal mol^{-1})	m_g (kcal mol^{-1} M^{-1})		C_m (M)	ΔG_D (kcal mol^{-1})	m_g (kcal mol^{-1} M^{-1})
GB	0.0	6.8	8.6	1.25	0.0	3.6	5.9	1.7
	0.1	7.6	8.7	1.14	0.1	2.6	5.8	2.2
	0.3	7.8	9.1	1.13	0.3	2.9	5.6	2.0
	0.5	8.4	9.4	1.13	0.5	3.0	5.5	1.8
	1.0	9.3	10.7	1.14	1.0	3.1	5.2	1.7

*The uncertainties associated with ΔG_D, m_g, and C_m are ±0.5 (kcal mol^{-1}), ±0.2 (kcal mol^{-1} M^{-1}), and ±0.2 (M), respectively.

4.2.8 Effect of GB on the denaturant-dependent ΔG_D **and** C_m *of Ferricyt c*

Fig. 10a and Fig. 10b show that at both pH 7.0 and pH 3.8, the inclusion of GdnHCl shifts the urea-induced unfolding curve to lower urea concentrations. However, in the presence of 0.5 M GB, the GdnHCl-triggered shift in the urea-induced unfolding curve is less pronounced at pH 7.0 (Fig. 10a) while it is more pronounced at pH 3.8 (Fig. 10b). To determine the effect of GB on the GdnHCl dependence of ΔG_D and m_g, the urea-induced unfolded curves of Ferricyt *c* collected at various GdnHCl concentrations both in absence and presence of 0.5 M GB were analyzed by using two-state equation (chapter 2, eq (5)) (*57*). The resulting ΔG_D and m_g values are provided in Table 10.

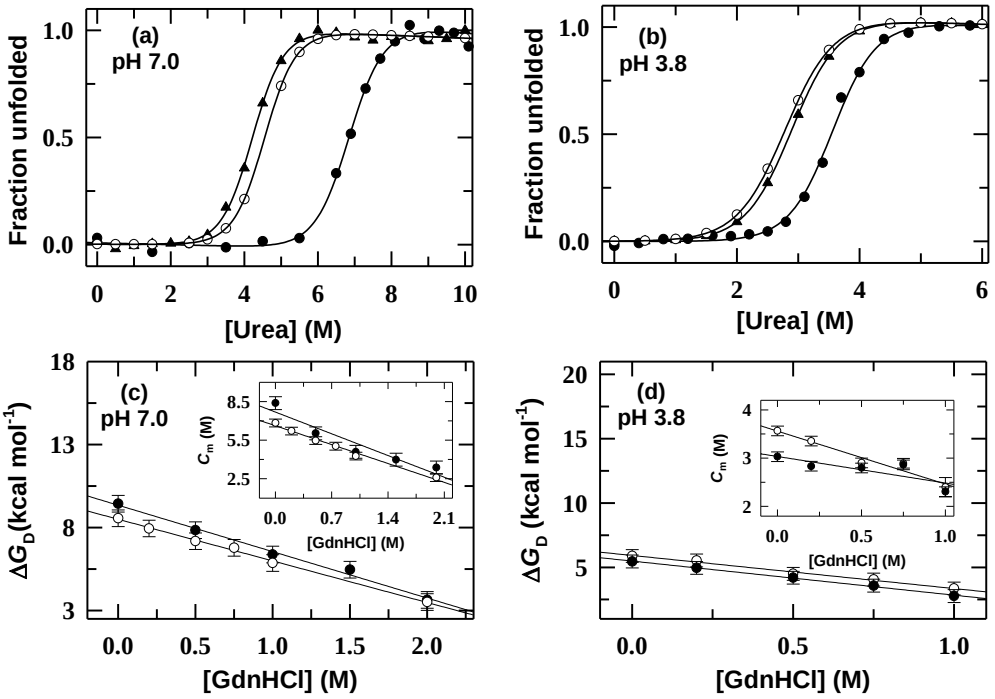

Fig. 10 Panel (a) shows the urea-induced denaturation curves of Ferricyt *c* at pH 7.0, 25 °C; in the absence of additive (•), in the presence of 1.0 M GdnHCl (▲), and in the presence of 1.0 M GdnHCl with 0.5 M GB (○). (b) Urea-induced denaturation curves of Ferricyt *c* at pH 3.8, 25 °C; in the absence of additive (•), in the presence of 0.5 M GdnHCl (▲), and in the presence of 0.5 M GdnHCl with 0.5 M GB (○). The solid curves in panels (a) and (b) represent non-linear least-squares fit of data according to the standard two-state equation (chapter 2, eq (5)) (*57*). Panels (c) and (d) show the variation of change in unfolding free energy, ΔG_D of Ferricyt *c* with GdnHCl concentration in the absence (o) and presence of 0.5 M GB (•) at pH 7.0 and 3.8, respectively. The insets of panels (c) and (d) show the variation of the urea unfolding midpoint, C_m of Ferricyt *c* as a function of GdnHCl in the absence (o) and presence of 0.5 M GB (•) at pH 7.0 and 3.8, respectively.

The urea unfolding midpoints, C_m (=$\Delta G_D/m_g$) for different concentration of GdnHCl were also calculated both in the absence and presence of GB (Table 10). At both pH 7.0 and pH 3.8, the ΔG_D and C_m values decrease linearly with GdnHCl concentration (Fig. 10c,d and Insets of Fig. 10c,d). However, in the presence of 0.5 M GB, the decrease in the values of ΔG_D and C_m with

GdnHCl concentration is less pronounced at pH 7.0 (Fig. 10c and Inset of Fig. 10c), while it is more pronounced at pH 3.8 (Fig. 10d and Inset of Fig. 10d). These findings indicate that the GB counteracts the denaturing action of GdnHCl at neutral pH while it shows a cumulative effect on the denaturing action of GdnHCl at mildly acidic pH.

Table 10. Dependence of the ΔG_D, m_g and C_m of Ferricyt *c* on GdnHCl concentration in the absence and presence of 0.5 M GB at pH 7.0 and pH 3.8 as monitored by Trp fluorescence (ex: 280; em: 365 nm)*.

Additive	Conc. (M)	pH 7.0			Conc. (M)	pH 3.8		
		C_m (M)	ΔG_D (kcal mol^{-1})	m_g (kcal mol^{-1} M^{-1})		C_m (M)	ΔG_D (kcal mol^{-1})	m_g (kcal mol^{-1} M^{-1})
GdnHCl	0.0	6.8	8.6	1.25	0.0	3.6	5.9	1.7
	0.2	6.2	7.9	1.28	0.2	3.4	5.5	1.7
	0.5	5.5	7.2	1.31	0.5	2.9	4.5	1.6
	0.75	5.0	6.8	1.35	0.75	2.9	4.0	1.4
	1.0	4.3	5.9	1.37	1.0	2.4	3.4	1.4
	2.0	2.6	3.5	1.36				
GdnHCl+	0.0	8.4	9.4	1.13	0.0	3.0	5.5	1.8
0.5 M GB	0.5	6.0	7.8	1.30	0.2	2.8	5.0	1.8
	1.0	4.6	6.4	1.39	0.5	2.8	4.2	1.5
	1.5	4.0	5.5	1.37	0.75	2.9	3.6	1.3
	2.0	3.4	3.6	1.08	1.0	2.3	2.8	1.2

*The uncertainties associated with ΔG_D, m_g, and C_m are ±0.5 (kcal mol^{-1}), ±0.2 (kcal mol^{-1} M^{-1}), and ±0.2 (M), respectively.

4.3 Discussion

Few earlier studies have shown that the collective motions of the M80-contaning Ω-loop control the CO dissociation from NCO (*51, 61*). The variations of log k_{diss} with GB, GdnHCl, and urea demonstrate how the collective motions of the Ω-loop of Ferrocyt *c* vary in response to these additives in the reaction milieu. Kinetic and thermodynamic studies of NCO and MbCO in the presence of different concentrations of GB or GdnHCl have provided evidence for internal motional constraints and entropy reduction of these proteins in the presence of GB or subdenaturing concentrations of GdnHCl. The probable explanation for the restricted dynamics of the NCO and MbCO in the presence of GB and subdenaturing concentrations of denaturant as well as the effect of GB on the structural fluctuations of the Ω-loop across the folding-unfolding transition of the Ferrocyt *c* are discussed. Thermal and chemical-denaturations studies of native Ferrocyt *c*, Ferricyt *c* and Mb at pH 7.0 and pH 3.8-4.5 in the presence of different concentrations of GB or TMAO have provided evidence that GB and TMAO increase the thermodynamic stability of the native proteins at neutral pH but decrease it at mildly acidic pH. The probable explanation why the GB and TMAO increase the thermodynamic stability of the

native proteins at neutral pH but decrease it at mildly acidic pH as well as the effect of these osmolytes on the GdnHCl-dependent thermodynamic stability of native proteins at pH 7.0 and pH 3.8-4.5 are discussed.

4.3.1 How could GB, urea, and GdnHCl restrict the internal dynamics of native proteins?

Fig. 2a and Fig. 2b show that as GB concentration is increased, the value of log k_{diss} (for NCO) and log k_{off} (for MbCO) decrease monoexponentially, which indicates that the GB constrains the internal dynamics of these proteins. Fig. 3b shows that as denaturant concentration is increased from 0.0 to 5.0 M GdnHCl or 9.5 M urea, the value of log k_{diss} of NCO initially decreases and then increases, showing a minimum at 2.5 M GdnHCl or 5.5 M urea. This finding suggests that the subdenaturing concentrations of GdnHCl and urea restrict the internal dynamics of Ferrocyt *c*. If the internal dynamics of protein is restricted in the presence of GB or subdenaturing concentrations of GdnHCl and urea, then the restricted dynamics should decrease the amplitude of structural fluctuations of the protein. Some earlier hydrogen exchange (HX) experiments have also shown that the osmolytes such as sugars decrease the structural fluctuations of native proteins (*37,59-60,62-65*). Since, both entropy and fluctuations have the same origin, therefore, the restricted dynamics in the presence of GB or subdenaturing amount of denaturant must alter the conformational entropy of the protein. The data in Table 2 clearly shows that relative to in the absence of additives, both the activation enthalpy and conformational entropy loss increases in the presence of 1.0 M GB and 2.5 M GdnHCl or 5.5 M urea. These results suggest that the GB and subdenaturing concentrations of urea and GdnHCl decrease the motional freedom of the native proteins, and thus restricts the internal dynamics of native proteins.

4.3.2 Effects of GB on the structural fluctuations of the M80-containing Ω-loop across the folding-unfolding transition of Ferrocyt c

Pioneering works by Englander and coworkers have shown that the subglobal unfolding units such as M80-containing Ω-loop of Cyt *c* can determine a limited set of folding pathways (*66-72*). Therefore, it is important to evaluate the effect of GB on the thermal motions of the M80-containing Ω-loop of Ferrocyt *c* across the folding-unfolding transition. As the denaturant concentration is increased from 0.0 to 5.0 M GdnHCl or 9.5 M urea, the log k_{diss} first decreases upto ~2.5 M GdnHCl or ~5.5 M urea and then increases (Fig. 3b). The linear decrease in log k_{diss} with denaturant concentration indicates that the structural fluctuations of the Ω-loop that

modulate the slow changes in structural dynamics of protein progressively decrease within the subdenaturing limit of denaturants. Recent studies have shown that within the subdenaturing limit of denaturants, the polyfunctional interactions between protein groups and denaturant can lower the conformational entropy and thus restrict the internal dynamics of protein (*51,54*). Since both GB and subdenaturing concentrations of GdnHCl or urea individually decrease the structural fluctuations of Ω-loop (Fig. 2a and Fig. 3b), the coexistence of the two in the reaction medium is expected to produce a cumulative effect on the constrained dynamics of NCO. In the subdenaturing limit of denaturant, the increase in the conformational entropy loss for CO dissociation reaction is more pronounced in the presence of GB than in the absence of GB (Table 2 and Fig. 3c,d). This finding indicates that the excluded volume interactions originated due to GB also contributes toward the constrained dynamics of NCO (*36*). En route from subdenaturing to denaturing conditions, the large-scale unfolding fluctuations dominate the dynamics (*49*), which increases the configurational entropy and decreases the activation enthalpy and activation entropy (Table 2). Remarkably, the extent of denaturant induced decrease in activation enthalpy and activation entropy are less in the presence of GB then in its absence (Table 1), indicates that GB opposes the structural fluctuations that cause the unfolding of the protein.

4.3.3 How could GB and TMAO modulate the thermodynamic stability of proteins at neutral pH and mildly acidic pH?

The current results show that at neutral pH, the protecting osmolytes can increase the thermodynamic stability of native Ferrocyt *c* (Fig. 3a and Fig. 5a,b), Mb (Fig. 5c), and Ferricyt *c* (Fig. 5e and Fig. 9c). This result is consistent with an earlier report where the protecting osmolytes (GB and TMAO) increase the thermal stability of α-lactalbumin, RNase-A and Lyz at neutral pH (*40, 42*). A recent report by Singh et al (2009) has shown that the effect of GB at acidic pH may vary from one protein to another (*42*). They showed that at acidic pH, GB decrease the thermal stability of α-lactalbumin, increase the thermal stability of RNase-A, and not greatly change the thermal stability of Lyz. The results from current study show that GB increases the thermodynamic stability of Ferricyt *c* at pH 7.0, however, the thermodynamic stability of the Mb at pH 7.0 is not greatly changed in the presence of GB (Fig. 5c). However, TMAO increases the thermodynamic stability of Mb at pH 7.0 (Fig. 5c). The results from current study also show that GB and TMAO decrease the thermodynamic stability of proteins at acidic pH 3.8-4.5 (Fig. 5d, Fig. 5f and Fig. 9c). How could GB and TMAO increase the thermodynamic

stability of native proteins at neutral pH but decrease it at mildly acidic pH? In general, the preferential exclusion of osmolytes stabilizes the proteins while the preferential binding of the osmolytes destabilizes the proteins (*73*). Our results suggest that in case of Ferricyt *c* and Mb, at neutral pH, the preferential exclusion effect of GB or TMAO may overcome the preferential binding effect, and thus stabilize the protein at pH 7.0. On the other hand, at mildly acidic pH, the preferential binding effect of GB or TMAO seems to overwhelm the preferential exclusion effect, and thus destabilize the proteins at pH 3.8-4.5.

4.3.4 GB and TMAO counteract the destabilizing actions of denaturants at neutral pH but these osmolytes show additive effect with denaturant at acidic pH

The denaturing action of guanidinium ions and urea molecules is generally based on their ability to bind to the protein (*49, 74-76*). Within the range of pH 7.0 to pH 3.8-4.5, the thermodynamic stability of native Ferrocyt *c* (Fig. 6f), native Ferricyt *c* (Fig. 7a,c and Fig. 10c,d) and Mb (Fig. 7b,d) decrease in the presence of denaturants. However, the inclusion of GB or TMAO results in the counteraction of the destabilizing action of the denaturants at neutral pH 7.0 (Fig. 6f, 7a,b and Fig. 10c) while it shows an additive effect on the denaturing action of GdnHCl at acidic pH 3.8-4.5 (Fig. 7c,d and Fig. 10d). Timasheff et al (1985, 1994) have reported that the TMAO counteracts the denaturing effect of urea mainly by shifting the equilibrium between preferential binding of urea and preferential exclusion of TMAO, which results in the enhanced hydration of the protein (*13,77*). Similarly, in case of Cyt *c* and Mb at pH 7.0, it is expected that the addition of GB or TMAO alters the balance between the preferential binding of denaturant and preferential exclusion of GB or TMAO, resulting in the increased hydration of the protein and helps in the counteraction of the destabilizing action of the denaturant.

4.3.5 Mechanism of osmolytes induced protein stabilization

Timasheff and co-workers (1981, 1990) have shown that the osmolytes which stabilize the proteins are preferentially excluded from the immediate vicinity of the protein domain, which is the major driving force for the stabilization of proteins (*78-79*). The pioneering work by Bolen (2001) has shown that the terms preferential exclusion of osmolyte and the preferential hydration of the protein are interchangeable and indicate the same phenomenon (*80*). By using the transfer model, Timasheff and coworkers (1994) and Bolen (2001) concluded that to stabilize the

proteins, the osmolytes mainly interact with the denatured state leaving the native state comparatively unaltered and functional (*13,80*).

A different study carried out by Bolen (2004) showed that there are three possible modes by which the osmolytes are preferentially excluded (*26*): (i) the solvophobic interaction between osmolyte and native and denatured states of protein, (ii) surface tension effect, *i.e.*, osmolytes that increase surface tension should also be excluded preferentially from the protein surface (*22, 81-83*), and (iii) excluded volume considerations (*84-86*). A recent theoretical study involving the MD simulations of a number of model peptides in aqueous solution of TMAO have shown that the entropic stabilization of proteins in a crowded environment is due to excluded volume interactions (*36*). Bolen et al (1998) have reported that the protecting osmolytes increase the stability of proteins by increasing the chemical potential of the denatured state and the uniform thermodynamic force acting on the peptide backbone results in the collateral effect of contracting the denatured state (*87*). The contraction decreases the conformational entropy of the denatured state while increasing the density of the hydrophobic groups (*87*). These two effects also contribute to the ability of the protecting osmolytes to force proteins to fold (*87*). Recently, Thirumalai et al (2008) studied the effects of TMAO on the stability of RNA hairpins and showed that TMAO preferentially interacts with the base through the formation of a single hydrogen bond (*88*). They further suggested that the effects of TMAO on the RNA secondary structure are likely to be small and the specific hydrogen bond interactions play an important role in the stabilization of the protein. Qin Zou et al (2002) have studied the effects of TMAO on cyclic dipeptides and show that TMAO increases the protein stability through the augmentation of water structure by raising the number of hydrogen bonds per water molecule, producing stronger water hydrogen bonds, and by long-range spatial arrangement of the solvent (*23*).

4.4 Conclusion

The kinetic and thermodynamic parameters measured for CO dissociation reaction of natively folded CO-liganded Ferrocyt *c* (NCO) and CO-replacement of carbonmonoxymyoglobin (MbCO) by hexacyanoferrate ion in the presence of different concentrations of GB at pH 7.0 indicate that the GB constrains the internal dynamics of these proteins at neutral pH. The kinetic and thermodynamic parameters measured for CO dissociation reaction of NCO under varying concentrations of GdnHCl or urea in the absence and presence of 1.0 M GB indicate that the GB and low concentrations of denaturants (urea and GdnHCl) restrict the internal dynamics of the

NCO-state at pH 7.0. Within the subdenaturing limit of denaturants, GB and GdnHCl or urea show a cumulative effect on the constrained dynamics of NCO. At relatively higher denaturant concentrations, the large-scale unfolding fluctuations dominate the dynamics and the inclusion of GB opposes the structural fluctuations that cause unfolding of the protein. Thermodynamic analysis of the thermal and GdnHCl-induced unfolding curves of proteins (Ferrocyt *c*, Ferricyt *c*, and Mb) measured in the absence and presence of GB or TMAO at pH 7.0 and at pH 3.8-4.5 indicates that GB and TMAO increase the thermodynamic stability of proteins at neutral pH, while decrease it at mildly acidic pH. Analysis of thermal and urea-induced unfolding curves of proteins (Ferrocyt *c*, Ferricyt *c*, and Mb) measured at different GdnHCl concentrations in the absence and presence of GB or TMAO suggests that GB and TMAO have counteracting and additive effects on the destabilizing action of denaturant at neutral pH 7.0 and mildly acidic pH 3.8-4.5, respectively.

4.5 References

1. Kuzmenkina, E.V., Heyes, C.D., and Nienhaus, G.U. (2005) *Proc. Natl. Acad. Sci. USA* **102**, 15471- 15476.
2. Yancey, P.H., and Somero, G.N. (1979) *Biochem. J.* **183**, 317–323.
3. Yancey, P.H., Clark, M.E., Hand, S.C., Bowlus, R.D., and Somero, G.N. (1982) *Science* **217**, 1214–1222.
4. Yancey, P.H., Blake, W.R., and Conley, J. (2002) *Comp. Biochem. Physiol.* **131B**, 667–676.
5. Venkatesu, P., Lee, M.J., and Lin, H.M. (2007) *Arch. Biochem. Biophys.* **466**, 106–115.
6. Strambini, G.B., and Gonnelli, M. (2008) *Biochemistry* **47**, 3322–3331.
7. Venkatesu, P., Lee, M.J., and Lin, H.M. (2009) *J. Phys. Chem. B* **113**, 5327–5338.
8. Timasheff, S.N. (2002) *Proc. Natl. Acad. Sci. USA* **99**, 9721–9726.
9. Bolen, D.W., and Baskakov, I.V. (2001) *J. Mol. Biol.* **310**, 955–963.
10. Niebuhr, M., and Koch, M.H.J. (2005) *Biophys. J.* **89**, 1978–1983.
11. Bennion, B.J., and Daggett V. (2003) *Proc. Natl. Acad. Sci. USA* **100**, 5142–5147.
12. Yancey, P.H., and Siebenaller, J.F. (1999) *J. Exp. Biol.* **202**, 3597–3603.
13. Lin, T.Y., and Timasheff, S.N. (1994) *Biochemistry* **33**, 12695–12701.
14. Baskakov, I., and Bolen, D.W. (1998) *Biophys. J.* **74**, 2658–2665.
15. Baskakov, I., Wang, A.J., and Bolen, D.W. (1998) *Biophys. J.* **74**, 2666–2673.
16. Wang, A.J., and Bolen, D.W. (1997) *Biochemistry* **36**, 9101–9108.

17. Tseng, H.C., and Graves, D.J. (1998) *Biochem. Biophys. Res. Commun.* **250**, 726–730.
18. Tatzelt, J., Prusiner, S.B., and Welch, W.J. (1996) *EMBO J.* **15**, 6363–6373.
19. Xie, G.F., and Timasheff, S.N. (1997) *Protein Sci.* **6**, 222–232.
20. Xie, G.F., and Timasheff, S.N. (1997) *Protein Sci.* **6**, 211–221.
21. Xie, G.F., and Timasheff, S.N. (1997) *Biophys. Chem.* **64**, 25–43.
22. Lin, T.Y., and Timasheff, S.N. (1996) *Protein Sci.* **5**, 372–381.
23. Zou, Q., Bennion, B.J., Daggett, V., and Murphy, K. (2002) *J. Am. Chem. Soc.* **124**, 1192–1202.
24. Wang, A.J., and Bolen, D.W. (1996) *Biophys. J.* **71**, 2117–2122.
25. Street, T.O., Bolen, D.W., and Rose, G.D. (2006) *Proc. Natl. Acad. Sci. USA* **103**, 13997-14002.
26. Bolen, D.W. (2004) *Methods* **34**, 312–322.
27. Attri, P., Venkatesu, P., and Lee, M.J. (2010) *J. Phys. Chem. B* **114**, 1471–1478.
28. Venkatesu, P., Lee, M.J., and Lin, H.M. (2008) *Biochem. Eng. J.* **38**, 326–340.
29. Ortiz-Costa, S., Sorenson, M.M., and Sola-Penna, M. (2008) *FEBS J.* **275**, 3388–3396.
30. Venkatesu, P., Lee, M.J., and Lin, H.M. (2007) *J. Phys. Chem. B* **111**, 9045–9056.
31. Frauenfelder, H., McMahon, B.H., Austin, R.H., Chu, K., and Groves, J.T. (2001) *Proc. Natl. Acad. Sci. U. S. A.* **98**, 2370–2374.
32. Fenimore, P.W., Frauenfelder, H., McMahon, B.H., and Parak, F.G. (2002) *Proc. Natl. Acad. Sci. U. S. A.* **99**, 16047–16051.
33. Fenimore, P.W., Frauenfelder, H., McMahon, B.H., and Young, R.D. (2004) *Proc. Natl. Acad. Sci. U. S. A.* **101**, 14408–14413.
34. Ansari, A., Jones, C.M., Henry, E.R., Hofrichter, J., and Eaton, W.A. (1992) *Science* **256**, 1796-1798.
35. Beece, D., Eisenstein, L., Frauenfelder, H., Good, D., Marden, M.C., Reinisch, L., Reynolds, A.H., Sorensen, L.B., and Yue, K.T. (1980) *Biochemistry* **19**, 5147–5157.
36. Cho, S.S., Reddy, G., Straub, J.E., and Thirumalai, D. (2011) *J. Phy. Chem. B* **115**, 13401-13407.
37. Wang, A., Robertson, A.D., and Bolen, D.W. (1995) *Biochemistry* **34**, 15096-15104.
38. Zhadin, N., and Callender, R. (2011) *Biochemistry* **50**, 1582-1589.
39. Santoro, M.M., Liu, Y., Khan, S.M.A., Hou, L.X., and Bolen, D.W. (1992) *Biochemistry* **31**, 5278–5283.

40. Singh, R.K., Haque, I., and Ahmad, F. (2005) *J. Biol. Chem.* **280**, 11035–11042.
41. Singh, L.R., Poddar, N.K., Dar, T.A., Kumar, R., and Ahmad, F. (2011) *Life Sciences* **88**, 117-125.
42. Singh, L.R., Dar, T.A., Rahman, S., Jamal, S., and Ahmad, F. (2009) *Biochim. Biophys. Acta*. **1794**, 929–935.
43. Schellman, J.A. (2002) *Biophys. Chem.* **96**, 91–101.
44. Courtenay, E.S., Capp, M.W., Anderson, C.F., and Record, M.T.Jr. (2000) *Biochemistry* **39**, 4455–4471.
45. Record, M.T.Jr., Zhang, W., and Anderson, C.F. (1998) *Adv. Protein Chem.* **51**, 281–353.
46. Frauenfelder, H., Parak, F., and Young, R.D. (1988) *Ann. Rev. Biophys. Biophys. Chem.* **17**, 451-479.
47. Schlichting, I., Berendzen, J., Phillips, G. N., and Sweet, R.M. (1994) *Nature* **371**, 808-812.
48. Bai, Y., Sosnick, T. R., Mayne, L., and Englander, S.W. (1995) *Science* **269**, 192-197.
49. Bhuyan, A.K. (2002) *Biochemistry* **41**, 13386–13394.
50. Varhac, R. (2013) *Biochem. Biophys. acta* **183**, 739-744.
51. Kumar, R., Prabhu, N.P., Yadaiah, M., and Bhuyan, A.K. (2004) *Biophys. J.* **87**, 2656–2662.
52. Kumar, R., and Bhuyan, A.K. (2009) *J. Biol. Inorg. Chem*. **14,** 11-21
53. Jain, R., Kaur, S., and Kumar, R. (2013) *J. Biochem.* **153**, 161–177
54. Kumar, S., Sharma, D., and Kumar, R. (2014) *Biochim. Biophys. Acta.: Prot. and Proteom.* **1844**, 641-655.
55. Olson, J.S. (1981) *Methods Enzymol* **76**, 631–651.
56. Kumar, R., and Bhuyan, A.K. (2005) *Biochemistry* **44**, 3024-3033.
57. Santoro, M.M., and Bolen, D.W. (1988) *Biochemistry* **27**, 8063-8068.
58. Hoang, L., Maity, H., Krishna, M.M.G., Lin, Y., and Englander, S.W. (2003) *J. Mol. Biol.* **331**, 37-43
59. Kim, Y.S., Jones, L.S., Dong, A.C., Kendrick, B.S., Chang, B.S., Manning, M.C., Randolph, T.W. and Carpenter, J.F. (2003) *Prot. Sci.* **12**, 1252-1261.
60. Butler, S.L., and Falke, J.J. (1996) *Biochemistry* **35**, 10595-10600.
61. Berghuis, A.M., and Brayer, G.D. (1992) *J. Mol. Biol.* **223**, 959–976.

62. Kendrick, B.S., Chang, B.S., Arakawa, T., Peterson, B., Randolph, T.W., Manning, M.C., and Carpenter, J.F. (1997) *Proc. Natl. Acad. Sci. USA* **94**, 11917-11922.
63. Cioni, P., Bramanti, E., and Strambini, G.B. (2005) *Biophys. J.* **88**, 4213-4222.
64. Morgan, J.D., and McCammon, J.A. (1983) *Biopolymers* **22**, 1579–1593.
65. Petsko, G.A., and Ringe, D. (1984) *Ann. Rev. Biophys. Bioeng.* **13**, 331-371.
66. Hoang, L., Bédard, S., Krishna, M.M.G., Lin, Y., and Englander, S.W. (2002) *Proc. Natl. Acad. Sci. USA* **99,** 12173–12178.
67. Bai, Y., Sosnick, T.R., Mayne, L., and Englander, S.W. (1995) *Science* **269,** 192-197.
68. Hoang, L., Maity, H., Krishna, M.M.G., Lin, Y., and Englander, S.W. (2003) *J. Mol. Biol.* **331**, 37-43.
69. Xu, Y., Mayne, L.C., and Englander, S.W. (1998) *Nature Struct. Biol.* **5**, 774-778.
70. Maity, H., Maity, M., Krishna, M.M., Mayne, L., and Englander, S.W. (2005) *Proc. Natl. Acad. Sci. USA* **102**, 4741-4746.
71. Maity, H., Maity, M., and Englander, S.W. (2004) *J. Mol. Biol.* **343**, 223-233.
72. Krishna, M.M., Maity, H., Rumbley, J.N., Lin, Y., and Englander, S.W. (2006) *J. Mol. Biol.* **359**, 1410-1419.
73. Gonnelli, M., and Strambini, G.B. (1995) *Biochemistry* **34**, 13847-13857.
74. Hibbard, L.S., and Tulinsky, A. (1978) *Biochemistry* **17**, 5460-5468.
75. Pike, A.C., and Acharya, K.R. (1994) *Protein Sci.* **3**, 706-710.
76. Dunbar, J., Yennawar, H.P., Banerji, S., Luo, J., and Farber, G.K. (1997) *Protein Science* **6**, 1727-1733.
77. Timasheff, S.N. (2002) *Biochemistry* **41**, 13473-13482.
78. Prakash, V., Loucheux, C., Scheuffle, S., Gorbunoff, J., Timasheff, S.N. (1981) *Arch. Biochem. Biophys.* **210**, 455-464.
79. Arakawa, T., Bhat R., and Timasheff, S.N. (1990) *Biochemistry* **29**, 1914-1923.
80. Bolen, D.W. (2001) *Methods Mol. Biol.* **168**, 17–36.
81. Kita, Y., Arakawa, T., Lin, T.Y., and Timasheff, S.N. (1994) *Biochemistry* **33**, 15178-15189.
82. Kaushik, J.K., and Bhat, R., (1998) *J. Phys. Chem. B* **102**, 7058-7066.
83. Kaushik, J.K., and Bhat, R. (2003) *J. Biol. Chem.* **278**, 26458-26465.
84. Davis-Searles, P.R., Morar, A.S., Saunders, A.J., Erie, D.A., and Pielak, G.J. (1998) *Biochemistry* **37**, 17048-17053.

85. Davis-Searles, P.R., Saunders, A.J., Erie, D.A., Winzor, D.J., and Pielak, G.J. (2001) *Annu. Rev. Biophys. Biomol. Struct.* **30**, 271-306.
86. Schellman, J.A. (2003) *Biophys. J.* **85**, 108-125.
87. Qu, Y., Bolen, C.L., and Bolen, D.W. (1998) *Proc. Natl. Acad. Sci. USA* **95**, 9268–9273.
88. Pincus, D.L., Hyeon, C., and Thirumalai, D. (2008) *J. Am. Chem. Soc.* **130**, 7364–7372.

Chapter 5

Effects of Chaotropic and Kosmotropic Salts on the Stability and Dynamics of Proteins

5.1 Introduction

Increasing evidences indicate that several factors such as, hydrophobic interactions (*1-2*), electrostatic interactions (*3-7*), and hydrogen bonding (*8-9*) contribute to protein stability. However, the relative contributions of each of these factors to protein stability are not completely resolved (*2*). In particular, the contributions of these factors to protein stability vary from one protein to another and also with the solution conditions under which the protein is exposed (*1-2, 7*). In general, cosolute such as salt ions modulates the protein stability by two ways; (i) by direct interaction with the protein, *i.e.,* binding, (*10*) and (ii) by involving effects on the solvent, *e.g.,* excluded volume effects (*11-12*). Recently, Tadeo et al (2007) have studied the thermal denaturation of protein L in the presence of various salts (NaF, Na_2SO_4, $NaNO_3$, $NaClO_4$, and NaSCN) concentrations and revealed that the salts ions modulate the protein stability by both mechanisms *i.e.,* excluded volume effects and preferential interactions (*13*).

The contributions of electrostatic and hydrophobic interactions to protein stability are generally evaluated by determining the stability of the protein in the presence of different concentrations of salts and osmolytes (*5,7,14,15*). Understanding the effect of salts and osmolytes are important for understanding the thermodynamic properties of biological systems. Few earlier reports indicate that at lower salt concentrations, the salt ions affect the protein stability by altering the electrostatic (Debye-Hückel) screening of Coulombic interactions (*9,16-17*). At relatively higher salt concentrations, the salt ions influence the protein stability by increasing the surface tension of solvent that eventually affect the hydrophobic interactions (*18-22*). The Hofmeister series characterizes some properties of ions as cosolvents in protein solutions and this series divides the ions in two groups: the kosmotropic and chaotropic ions (*23*). The Hofmeister series has consistent effects on the stability and structures of proteins. Anions have more pronounce effect than cations, and typically follow this order: $F^- \approx HPO_4^{2-} > SO_4^{2-} > CH_3COO^- > Cl^- > NO_3^- > Br^- > ClO_3^- > I^- > ClO_4^- > SCN$ (*23*). The cations usually follow this order: $NH_4^+ > K^+ > Na^+ > Li^+ > Mg^{2+} > Ca^{2+}$ (*23*). In the anions series, the species

left to the Cl^- are known as kosmotropes, which generally order the water structures and thus stabilize the protein structures (salting out effect) while those right to the Cl^- are referred to chaotropes, which generally break the water structures and thus destabilize the protein structures (salting-in effects) (*18-24*).

The contributions of electrostatic and hydrophobic interactions to the stability of proteins are generally determined by measuring the unfolding transitions of proteins as a function of salt concentration (*5,7,14-18*). Although, the effects of salts on the stability of proteins have been studied extensively (*14-24*), however, few studies are reported on the measurement of the relative contributions of the electrostatic and hydrophobic interactions to the stability and dynamics of proteins (*14, 17-18*). To understand the better the manner in which electrostatic and hydrophobic interactions control the stability of native proteins, this chapter analyzes the effects of chaotropic and kosmotropic salts on the thermal and chemical denatutations of native Cyt *c* and Mb at pH 7.0 and acid-denatured Lyz at pH 2.3. The results obtained indicate that at neutral pH, the kosmotropic anions increase while the chaotropic anions decrease the thermodynamic stability of the proteins. Furthermore, the effect of anions on the thermodynamic stability of these proteins follows the Hofmeister series ($SO_4^{2-} > Cl^- > Br^- > NO_3^- > I^- > ClO_4^-$). Water plays an important role in the stabilization of the native protein and in the control of its dynamics (*25*). Thermodynamic analysis of the thermal denturation curves of native Ferrocyt *c* measured in the presence of different concentrations of salts (NaCl, NaBr, NaI, Na_2SO_4, $NaNO_3$, and $NaClO_4$) indicates that water activity also plays important role in protein stability (*26-38*). The dynamic behavior of proteins in solution is of primary interest due to its concerned relationship with the structure and function of proteins (*29-30*). To determine the roles of electrostatic and hydrophobic interactions on the internal dynamics of proteins, this chapter evaluates the effects of chaotropic and kosmotropic salts on the structural fluctuations of the M80 containing Ω-loop of Cyt *c* by measuring the rate coefficients of CO association to native Ferrocyt *c* under conditions of varying concentrations of salts (NaCl, NaBr, NaI, Na_2SO_4, $NaNO_3$, and $NaClO_4$) at pH 7.0. This chapter results suggest that at low to intermediate salt concentrations, the ions arising from both chaotropic and kosmotropic salts restrict the internal dynamics of native proteins *via* (i) screening the protein charges electrostatically (*26, 31-35*), and (ii) by lowering the conformational entropy of proteins through binding interactions (*36-39*). At relatively higher

concentrations, the ions arising from chaotropic salts influence the internal dynamics of proteins according to Hofmeister series ($SO_4^{2-} > Cl^- > Br^- > NO_3^- > I^- > ClO_4^-$).

5.2 Results and discussion

5.2.1 CO association to Ferrocyt c

The ligation of CO to native Ferrocyt *c* (N-state) leads formation of Cyt-CO (Fe^{2+}-M80+CO → Fe^{2+}-CO+M80), which results in the loss of the intensity of the extinction coefficient at 550 nm (*40*). After the addition of the native protein in the CO-saturated and dithionite reduced buffer solution (pH 7) containing desired concentration of the salt, the N+CO→NCO reaction proceed. Fig. 1a shows a representative CO-association kinetic profile of native Ferrocyt *c* in the absence of salt ($\tau \approx 18$ min.), which indicates that the absorbance of the α-band (550 nm) decreases due to CO association to native protein.

5.2.2 Salt dependence of the log k_{ass}, $\Delta H_{ass}^{\ddagger}$ and $\Delta S_{ass}^{\ddagger}$

Fig. 1b shows the variation of the log k_{ass} of CO association reaction with various salts (NaCl, NaBr, NaI, Na_2SO_4, $NaNO_3$, and $NaClO_4$) concentrations at 25°C, pH 7.0. Fig. 1b clearly indicates that as the concentrations of the kosmotropic salts (*i.e.,* Na_2SO_4) are increased in the reaction medium, the values of log k_{ass} decrease mono-exponentially and plateau at ~0.5 M Na_2SO_4. However, when the concentrations of chaotropic salts (NaBr, NaI, $NaNO_3$, and $NaClO_4$) are increased from 0.0 to 2.0 M, the values of log k_{ass} initially decrease at low salts concentrations and then decrease, displaying the broad minimums around ~0.5 M of salts concentrations. The decrease in the values of log k_{ass} in the presence of kosmotropic and chaotropic (≤0.5 M) salts (Fig. 1b) indicate that kosmotropic salts at all concentrations and chaotropic salts at low concentrations (≤0.5 M) decrease the structural fluctuations of the Ω-loop of the protein. At relatively higher chaotropic salts concentrations (>1.0 M), the increase in log k_{ass} (Fig. 1b) can be interpreted to arise from protein destabilization action of the chaotropic salts. Notably, the increase in the values of log k_{ass} at higher concentrations of chaotropic salts are in accordance with the Hofmeister series effect *i.e.,* the increase in the value of log k_{ass} is more pronounced for $NaClO_4$ and is least for NaBr ($NaClO_4$ > NaI > $NaNO_3$ > NaBr) (Fig. 1b).

To further investigate the effect of various salts on the structural fluctuation of the protein, we have determined the salts dependence of the activation enthalpy ($\Delta H_{ass}^{\ddagger}$) and activation entropy ($\Delta S_{ass}^{\ddagger}$) of the CO association reaction of native Ferrocyt *c* at pH 7.0. The underlying principle is that if the kosmotropic salts at all concentrations and chaotropic salts at low concentrations (≤0.5 M) are really decreasing the structural fluctuations of the Ω-loop of the Ferrocyt *c* (Fig. 1b), then the activation energy or activation enthalpy for the CO-association reaction at those concentrations of kosmotropic and chaotropic salts will be comparatively higher. Fig. 1c represents the Eyring plots for the CO-association reaction of native Ferrocyt *c* in the absence and presence of ~0.5 M concentration of kosmotropic and chaotropic salts. The Eyring plots for the CO-association reaction of native Ferrocyt *c* in the absence and presence ~2.0 M concentration of chaotropic salts are given in Fig. 1d.

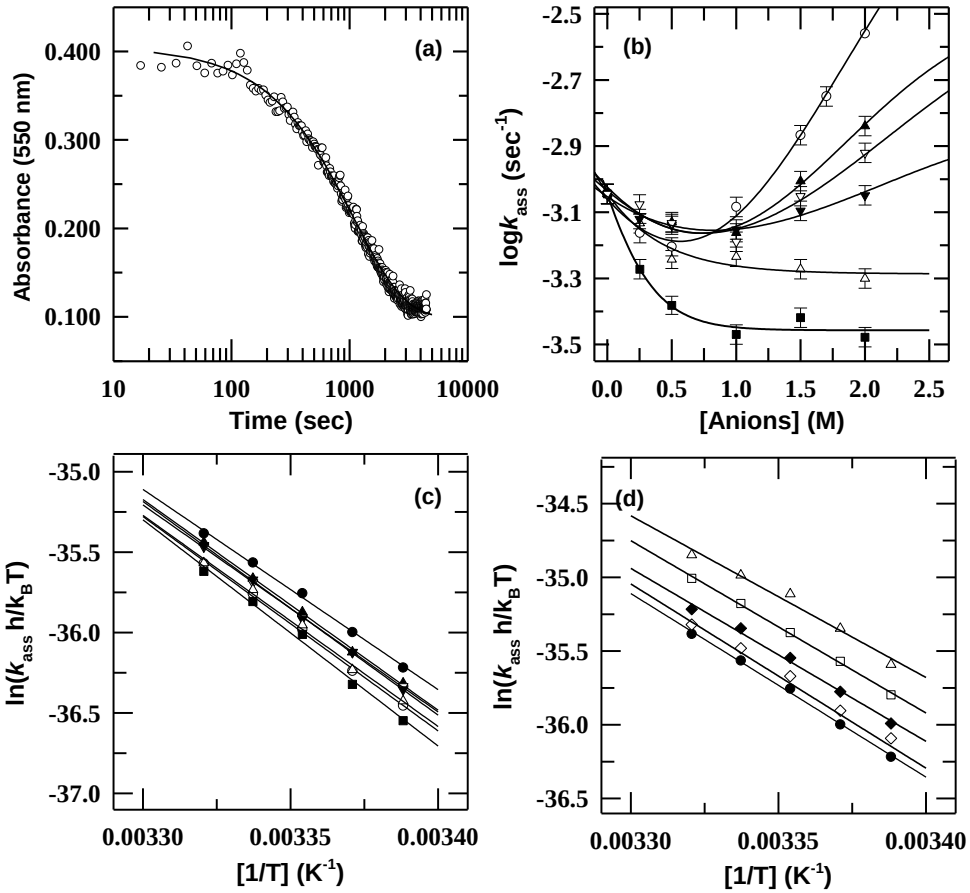

Fig. 1 (a) The slow single-phase association of CO to native Ferrocyt *c*, N+CO→NCO (τ =18 min., 0.0 M salt, 25 °C). The N+CO→NCO reaction was probed at 550 nm, the λ_{max} of the N-state spectrum. (b) Salt dependence of k_{ass} (▲, NaI; o, $NaClO_4$; ■, Na_2SO_4;∇, $NaNO_3$; ▼, NaBr; and Δ, NaCl) at 25(±1) °C, pH 7.0. The lines through the data have been drawn by inspection only. (c) Eyring plots for the CO association reaction, 50 mM phosphate buffer, pH 7, in the absence of salt (●); and in the presence of 0.5 M salt (▲, NaI; ○, $NaClO_4$; ■, Na_2SO_4; △, $NaNO_3$; ▼,

NaBr; ▽, NaCl). (d) Eyring plots for the CO association reaction, 50 mM phosphate buffer, pH 7.0, in the absence of salt (●); and in the presence of 2.0 M salt (◊, NaBr; ♦, $NaNO_3$; □, NaI; △, $NaClO_4$).

The Eyring plots in Fig 1c and Fig. 1d were analyzed by using the Eyring equation (eq (1)) (*41-42*), which helped in estimating the salts effect on the $\Delta H_{ass}^{\ddagger}$ and $\Delta S_{ass}^{\ddagger}$,

$$\ln(k_{ass}h/k_B T) = (\Delta S_{ass}^{\ddagger}/R) - (\Delta H_{ass}^{\ddagger}/RT) \qquad (1)$$

Clearly, relative to in the absence of salts, the $\Delta H_{ass}^{\ddagger}$ value for CO-association reaction increases in the presence of ~0.5 M concentration of kosmotropic and chaotropic salts (the values of $\Delta H_{ass}^{\ddagger}$ ~25.0, 26.7, 26.2, 25.7, 26.6, 26.3, and 28.1 kcal mol^{-1} in the absence and presence of ~0.5 M of $NaClO_4$, NaI, $NaNO_3$, NaBr, NaCl, and Na_2SO_4, respectively) (Table 1). As compared to in the absence of salts, the $\Delta H_{ass}^{\ddagger}$ values for CO-association reaction decrease in the presence of ~2.0 M concentration of chaotropic salts (the values of $\Delta H_{ass}^{\ddagger}$ ~25.0, 21.9, 24.9, 23.5, 23.4, in the absence and presence of ~2.0 M of $NaClO_4$, NaBr, $NaNO_3$ and NaI, respectively) (Table 1).

Table 1 Salt dependence of activation enthalpy ($\Delta H_{ass}^{\ddagger}$), activation entropy ($\Delta S_{ass}^{\ddagger}$) and conformational entropy loss ($\Delta\Delta S_{ass}^{\ddagger}$) for CO association reaction of Ferrocyt *c*.*

Salt	salt concentration	$\Delta H_{ass}^{\ddagger}$	$\Delta S_{ass}^{\ddagger}$	$\Delta\Delta S_{ass}^{\ddagger}$
control	0.0	25.0 (±0.8)	12.0 (±2.5)	0.0 (±0.0)
NaCl	0.5	26.3 (±1.2)	16.1 (±1.7)	4.1 (±1.3)
Na_2SO_4	0.5	28.1 (±1.4)	22.2 (±4.6)	10.3 (±2.1)
NaBr	0.5	26.6 (±0.4)	17.3 (±1.2)	5.4 (±1.4)
	2.0	24.9 (±0.3)	11.9 (±0.3)	0.1 (±0.01)
$NaNO_3$	0.5	25.7 (±0.2)	14.5 (±0.8)	2.6 (±1.8)
	2.0	23.5 (±1.2)	7.6 (±1.1)	-4.4 (±1.5)
NaI	0.5	26.2 (±0.5)	16.1 (±3.9)	4.2 (±0.8)
	2.0	23.4 (±0.6)	7.7 (±1.9)	-4.3 (±0.6)
$NaClO_4$	0.5	26.7 (±0.7)	17.4 (±2.3)	5.4 (±0.3)
	2.0	21.9 (±1.9)	3.2 (±0.3)	-8.7 (±2.3)

*$\Delta H_{ass}^{\ddagger}$, $\Delta S_{ass}^{\ddagger}$, and $\Delta\Delta S_{ass}^{\ddagger}$ are reported as kcal mol^{-1}, cal mol^{-1} K^{-1}, and cal mol^{-1} K^{-1}, respectively. The uncertainty (standard error) is indicated in parenthesis.

The values of $\Delta H_{ass}^{\ddagger}$ and $\Delta S_{ass}^{\ddagger}$ obtained from Eyring equation (eq (1)) are summarized in Table 1. The data in Table 1 clearly show that in the presence of low concentrations of kosmotropic and chaotropic salts (~0.5 M), the values of $\Delta H_{ass}^{\ddagger}$ and $\Delta S_{ass}^{\ddagger}$ increase, while in the presence of higher concentrations of chatropic salts (~2.0 M), the values of these thermodynamic parameters decrease. Notably, the decrease in the value of $\Delta H_{ass}^{\ddagger}$ and $\Delta S_{ass}^{\ddagger}$ in the presence of higher concentrations of chaotropic salts are in accordance with the Hofmeister series effect, where the

most destabilizing salt $NaClO_4$ decreases the values of $\Delta H_{ass}^{\ddagger}$ and $\Delta S_{ass}^{\ddagger}$ comparatively higher than the other chaotropic salts used in the present study (Table 1).

5.2.3 How could chaotropic and kosmotropic salts restrict the internal dynamics of Ferrocyt c?

The kinetic and thermodynamic studies of CO association reaction in the presence of various concentrations of kosmotropic and chaotropic salts provide evidence that the kosmotropes at all concentrations and chaotropes at low concentrations (≤0.5 M) restrict the internal dynamics of native Ferrocyt *c* at pH 7.0. How could kosmotropes at all concentrations and chaotropes at low concentrations (≤0.5 M) restrict the internal dynamics of Ferrocyt *c*? As also discussed in chapter 3, few earlier reports show that the collective motions of the M80 containing Ω-loop of Ferrocyt *c* control the CO association reaction (*37,43-45*). The variations of log k_{ass} with kosmotropic and chaotropic salts concentration demonstrate how the collective motions of the Ω-loop vary in response to these additives in the reaction milieu. Since, both entropy and fluctuations have the same origin, therefore, the restricted dynamics in the presence of kosmotropic and chaotropic (≤0.5 M) salts must alter the conformational entropy of the protein. The conformational entropy loss, $\Delta\Delta S_{ass}^{\ddagger}$ for native Ferrocyt *c* in the presence of salts relative to the entropy of the protein in the absence of salts was calculated and is summarized in Table 1. The data in Table 1 clearly shows that relative to in the absence of salts, both the activation enthalpy and conformational entropy loss increases in the presence of ~0.5 M salt concentrations, which suggest that low concentrations of kosmotropic and chaotropic salts decrease the motional freedom of the protein, and thus restricts the internal dynamics of native protein. Few previous reports have shown that at low to intermediate concentrations, the ions dissociated from chaotropic salts can constrain the internal dynamics of native proteins *via* screening the protein charges electrostatically (*26,31-35*), as well as by lowering the conformational entropy of proteins through binding interactions (*36-39*). It is possible and highly likely that the anions arising from chaotropic and kosmotropic salts can find target sites on Ferrocyt *c* because of predominance of cationic lysyl side chains on the protein surface. The resulting electrostatic interactions, be they ion-pair type or charge-screening type, can stabilize and restrict the internal dynamics of protein.

5.2.4 Effect of chaotropic and kosmotropic salts on the T_m and ΔH_m of native proteins at neutral pH in aqueous solution

To determine the effect of chaotropic and kosmotropic salts on the thermal stability of native proteins, thermal denaturations of native Ferrocyt *c*, Ferricyt *c*, and Mb were investigated in the presence of various concentrations of salts (NaCl, Na_2SO_4, NaBr, $NaNO_3$, NaI, and $NaClO_4$) at pH 7.0. Fig. 2a shows the representative heme absorption (550 nm) monitored normalized thermal denturation curves of native Ferrocyt *c* measured in the presence of different concentrations of NaI at pH 7.0. The representative far-UV (222 nm) and near-UV CD (282 nm) monitored normalized thermal unfolding curves of native Ferricyt *c* measured in the presence of different concentrations of $NaClO_4$ at pH 7.0 are shown in Fig. 2b and Fig. 2c, respectively. The far-UV CD (222 nm) monitored thermal unfolding curves of Ferricyt *c* were not successful in the presence of NaBr and NaI due to the increase in HT voltage in spectropolarimeter. Therefore, to determine the relative effect of these chaotropic salts on the thermal stability of Ferricyt *c*, the near-UV CD (282 nm) monitored thermal unfolding curves of protein were collected in the presence of different concentrations of NaBr, $NaClO_4$ and NaI at pH 7.0.

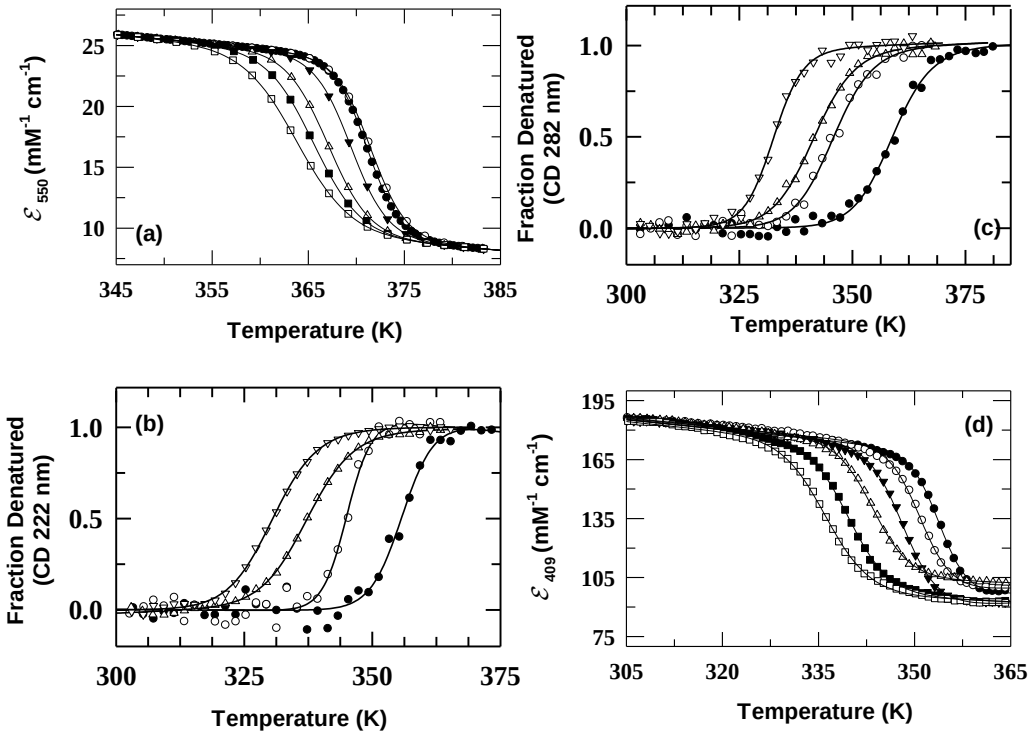

Fig. 2 (a) Representative heme absorption (550 nm) monitored thermal unfolding curves of Ferrocyt *c* represented as the change in excitation coefficient in the presence of 0.0 (●), 0.15 (○), 0.3 (▼), 0.6 (Δ), 0.9 (■), and 1.0 M (□) NaI. (b) The normalized far-UV CD (222 nm) monitored thermal unfolding curves of Ferricyt *c* in the presence of 0.0 (●), 0.75 (○), 1.5 (Δ) and 2.0 M $NaClO_4$ (▽), at pH 7.0. (c) The normalized near-UV CD (282 nm) monitored

thermal unfolding curves of Ferricyt *c* in the presence of 0.0 (●), 0.5 (○), 1.5 (Δ) and 2.0 M $NaClO_4$ (▽), at pH 7.0. (d) Representative visible (409 nm) monitored thermal unfolding curves of Mb, represented as the change in excitation coefficient in the presence of 0.0 (●), 0.15 (○), 0.3 (▼), 0.6 (Δ), 0.9 (■), and 1.0 M (□) NaI. The solid curves in panels (a), (b), (c) and (d) represent nonlinear least-squares fits of the data to Gibbs Helmholtz equation (*46*) (chapter 2, eqs (2) and (3)).

Fig. 2d presents the representative heme absorption (409 nm) monitored normalized thermal denturation curves of native Mb measured in the presence of different concentrations of NaI at pH 7.0. The thermal unfolding curves in Fig. 2a,b,c,d were analyzed for thermal denaturation midpoint (T_m), enthalpy of denaturation (ΔH_m), and heat capacity change (ΔC_p) by using a non-linear least squares method according to the Gibbs- Helmholtz equation (*46*) (chapter 2, eqs (2) and (3)). The resulting values of T_m, ΔH_m, and ΔC_p for thermal unfolding of native Ferrocyt *c*, Ferricyt *c* and Mb at various salts concentrations are provided in Table 2, Tables 3-4, and Table 5, respectively. Fig. 3a, Fig. 3b, and Fig. 3c shows the variation of T_m for native Ferrocyt *c*, Ferricyt *c* and Mb, respectively at different salts concentration. It is clear from Fig.3,b,c and Tables 2-5 that the chaoptropic salts (NaBr, $NaNO_3$, NaI, and $NaClO_4$) decrease the values of T_m while the kosmotropic salts (*i.e.*,Na_2SO_4) increase the values of T_m of the native proteins. NaCl shows the different behavior on the T_m values of native Ferrocyt *c* and Mb at pH 7.0. It slightly increases the value of T_m for native Ferrocyt *c* (Fig. 3a and Table 2) while decrease it for native Mb (Fig. 3c and Table 5). The increase and decrease in the value of T_m for various salts at pH 7.0 is according to the Hofmeister series ($SO_4^{2-} > Cl^- > Br^- > NO_3^- > I^- > ClO_4^-$), where $NaClO_4$ is the most destabilizing salt while Na_2SO_4 is the most stabilizing salt. These results are in consistent with the earlier reports which showed that the kosmotropic salts increase the thermal stability of the proteins while the chaotropic salts decrease the thermal stability of proteins (*13,47-48*).

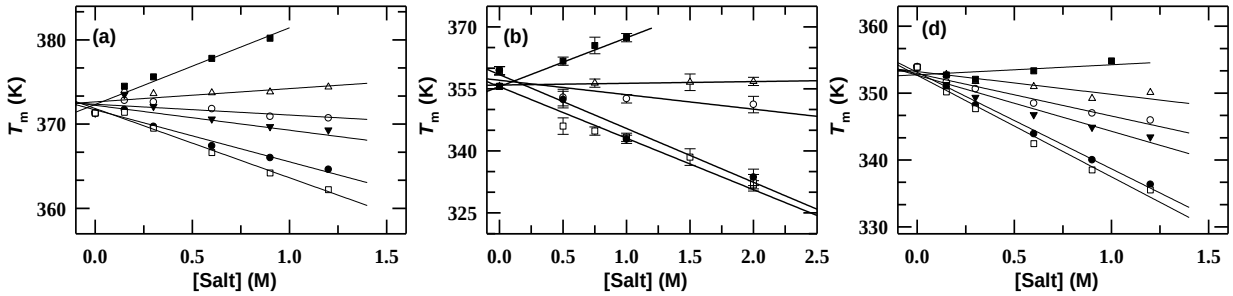

Fig. 3 (a) Variation of T_m for Ferrocyt *c* as function of different concentrations of various salts (Na_2SO_4 (■), NaCl (Δ), $NaNO_3$ (▼), NaBr (○), NaI (●), and $NaClO_4$ (□) pH 7.0. (b) Variation of T_m with different salt concentrations obtained from CD-222 nm monitored thermal unfolding of Ferricyt *c*, (Na_2SO_4 (■), NaCl (Δ), $NaClO_4$ (□)) and CD-282 nm monitored thermal unfolding of Ferricyt *c*, (NaBr (○), NaI (●), $NaClO_4$ (□)) at pH 7.0 (c) Variation of T_m for Mb as function of different concentrations of lyotropic salts (Na_2SO_4 (■), NaCl (Δ), $NaNO_3$ (▼), NaBr (○), NaI (●), $NaClO_4$ (□) pH 7.0. The solid lines in panels (a), (b) and (c) represent the linear least squares fit to the data.

Table 2. Salt dependence of the thermodynamic parameters (ΔH_m and T_m) for the absorbance-550 nm monitored thermal unfolding of Ferrocyt *c* at pH 7.0.

NaCl	ΔH_m	T_m	NaBr	ΔH_m	T_m	$NaNO_3$	ΔH_m	T_m
0.0	122.2	371.3	0.0	122.2	371.3	0.0	122.2	371.3
0.3	129.1	373.6	0.15	103.4	372.8	0.15	110.6	373.5
0.6	128.6	373.7	0.3	103.0	372.6	0.3	103.8	372.1
0.9	130.5	373.8	0.6	101.6	371.8	0.6	109.6	370.6
1.2	124.7	374.4	0.9	98.8	370.9	0.9	99.3	369.7
			1.2	98.8	370.7	1.2	106.1	369.3
Na_2SO_4	ΔH_m	T_m	$NaClO_4$	ΔH_m	T_m	NaI	ΔH_m	T_m
0.0	122.2	371.3	0.0	122.2	371.3	0.0	122.2	371.3
0.15	121.6	374.5	0.15	107.0	371.4	0.15	115.1	371.7
0.3	120.4	375.6	0.3	103.4	369.5	0.3	108.0	369.7
0.6	128.7	377.8	0.6	101.5	366.6	0.6	100.0	367.4
0.9	135.4	380.2	0.9	92.9	364.2	0.9	95.0	366.0
			1.2	85.0	362.2	1.2	90.0	364.6

The uncertainties of ΔH_m and T_m values reported here are ±5.0 kcal mol^{-1}, and ±0.5 *K* respectively.

Table 3. Salt dependence of the thermodynamic parameters (ΔH_m and T_m) for the CD-222 nm monitored thermal unfolding of Ferricyt *c* at pH 7.0.

NaCl	ΔH_m	T_m	Na_2SO_4	ΔH_m	T_m	$NaClO_4$	ΔH_m	T_m
0.0	72.1	355.6	0.0	72.1	355.6	0.0	72.1	355.6
0.75	74.4	356.4	0.5	71.3	361.7	0.75	90.2	344.8
1.5	67.0	356.6	0.75	71.6	365.5	1.5	70.0	338.5
2.0	77.7	356.8	1.0	69.6	367.4	2.0	60.0	331.8

The uncertainties of ΔH_m and T_m values reported here are ±5.0 kcal mol^{-1}, and ±0.5 *K* respectively.

Table 4. Salt dependence of the thermodynamic parameters (ΔH_m and T_m) for the CD-282 nm monitored thermal unfolding of Ferricyt *c* at pH 7.0.

NaI	ΔH_m	T_m	NaBr	ΔH_m	T_m	$NaClO_4$	ΔH_m	T_m
0.0	70.0	359.4	0.0	70.0	359.4	0.0	70.0	359.4
0.5	65.0	352.4	0.5	104.7	352.9	0.5	65.0	346.0
1.0	108.0	342.8	1.0	77.3	352.6	1.0	60.0	343.3
2.0	100.0	333.6	2.0	65.0	351.2	2.0	52.1	332.3

The uncertainties of ΔH_m and T_m values reported here are ±5.0 kcal mol^{-1}, and ±0.5 *K*, respectively.

Table 5. Salt dependence of the thermodynamic parameters (ΔH_m and T_m) for the absorbance-409 nm monitored thermal unfolding of Mb at pH 7.0.

NaCl	ΔH_m	T_m	NaBr	ΔH_m	T_m	$NaNO_3$	ΔH_m	T_m
0.0	109.8	354.0	0.0	109.8	354.0	0.0	109.8	354.0
0.15	112.0	352.8	0.15	102.9	351.8	0.15	102.0	351.0
0.3	101.0	351.8	0.3	99.2	350.7	0.3	98.0	351.1
0.6	100.0	350.8	0.6	92.8	348.5	0.6	88.1	346.7
0.9	95.0	347.8	0.9	88.0	347.1	0.9	76.7	344.5
1.2	102.0	349.4	1.2	84.4	345.8	1.2	74.5	343.1
Na_2SO_4	ΔH_m	T_m	$NaClO_4$	ΔH_m	T_m	NaI	ΔH_m	T_m
0.0	109.8	354.0	0.0	109.8	354.0	0.0	109.8	354.0
0.15	120.0	352.9	0.15	90.9	350.3	0.15	100.0	351.1
0.3	130.0	351.4	0.3	83.0	347.2	0.3	89.5	348.3
0.6	135.0	352.5	0.6	78.6	342.2	0.6	82.3	343.6
1.0	145.0	354.3	0.9	68.0	337.8	0.9	72.5	339.8
			1.2	60.5	334.2	1.2	66.0	336.3

The uncertainties of ΔH_m and T_m values reported here are ±5.0 kcal mol^{-1}, and ±0.5 *K* respectively.

5.2.5 Effect of chaotropic and kosmotropic salts on the ΔG_D and C_m of native protein

To determine the effect of chaotropic and kosmotropic salts on the thermodynamic stability of proteins, fluorescence monitored urea-induced equilibrium unfolding curves of Ferricyt *c* were measured in the presence of various concentrations of different salts (NaCl, Na_2SO_4, NaBr, $NaNO_3$, NaI, and $NaClO_4$) at pH 7.0. Fig. 4a shows the representative fluorescence monitored normalized urea-induced equilibrium unfolding curves of Ferricyt *c* measured in the presence of different concentrations of NaBr at pH 7.0. Two-state analysis (*49*) of the urea-unfolding curves in the absence and in the presence of different concentrations of chaotropic and kosmotropic salts provided the thermodynamic parameters, denaturation free energy (ΔG_D) and surface area exposed by the solvent (m_g). Table 6 summarized the values of ΔG_D and m_g calculated at various salts concentrations. From the ΔG_D and m_g values, the urea denaturation midpoints, C_m (=ΔG_D/ m_g) were obtained.

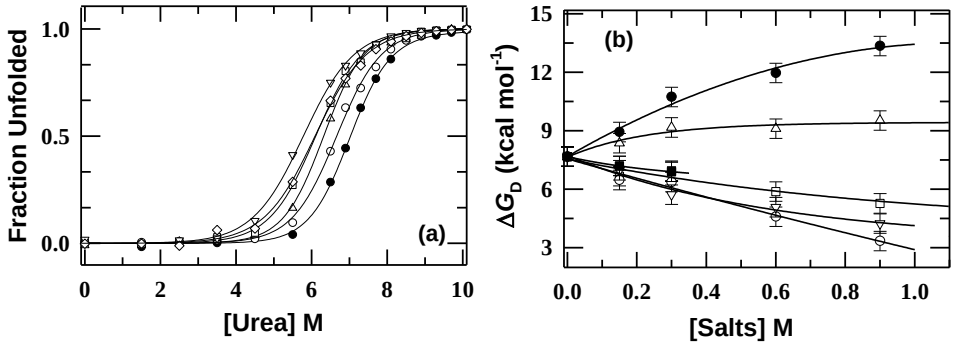

Fig. 4 (a) The representative urea unfolding curves of Ferricyt *c* in the absence and presence of different concentrations of NaBr; (●) 0.0; (○) 0.15; (Δ) 0.3; (□) 0.6; (◊) 0.9; and (▽) 1.2 M NaBr, pH 7.0, 25 °C. The solid lines in panel (a) represents the non-linear fit of the data to two-state equation (chapter 2, eq (5)) (*49*). (b) The variation of ΔG_D of Ferricyt *c* with different salt concentrations; (●) Na_2SO_4; (Δ) NaCl; (□) NaBr; (▽) NaI; (○) $NaClO_4$; and (■) $NaNO_3$, at pH 7.0. The solid lines in panel (b) are drawn by inspection only.

Fig. 4b represents the variation of ΔG_D with different salts concentration at pH 7.0. It is clear from Fig. 4a that with increase in the concentration of kosmotropic salts at neutral pH, the value of ΔG_D increases while it decreases in case of chaotropic salts. Further, the variation of ΔG_D with salts at pH 7.0 is in accordance with the Hofmiester series ($SO_4^{2-} > Cl^- > Br^- > NO_3^- > I^- > ClO_4^-$).

Table 6. Salt dependence of the thermodynamic parameters (ΔG_D, m_g and C_m) for the fluorescence monitored equilibrium unfolding of Ferricyt *c* at pH 7.0.

NaCl	ΔG_D	m_g	C_m	NaBr	ΔG_D	m_g	C_m	$NaNO_3$	ΔG_D	m_g	C_m
0.0	7.7	1.1	7.0	0.0	7.7	1.1	7.0	0.0	7.7	1.1	7.0
0.15	8.4	1.2	6.8	0.15	6.7	1.0	6.7	0.15	5.6	0.8	6.8
0.3	9.2	1.3	7.0	0.3	6.9	1.1	6.3	0.3	4.2	0.6	7.0
0.6	9.1	1.4	6.7	0.6	5.9	1.0	6.1				
0.9	9.5	1.4	6.8	0.9	5.3	0.9	6.1				
1.2	9.4	1.4	6.7	1.2	5.1	0.9	5.8				

Na_2SO_4	ΔG_D	m_g	C_m	$NaClO_4$	ΔG_D	m_g	C_m	NaI	ΔG_D	m_g	C_m
0.0	7.7	1.1	7.0	0.0	7.7	1.1	7.0	0.0	7.7	1.1	7.0
0.15	8.9	1.4	6.7	0.15	6.5	1.0	6.4	0.15	7.0	1.1	6.5
0.3	10.7	1.4	7.8	0.3	6.4	1.1	6.1	0.3	5.7	1.0	6.0
0.6	12.0	1.3	9.2	0.6	4.6	0.9	4.9	0.6	5.1	0.9	5.7
0.9	13.3	1.3	10.3	0.9	3.3	0.7	4.8	0.9	4.2	0.8	5.4

The uncertainties of ΔG_D, m_g and C_m values reported here are ± 1.0 kcal mol^{-1}, ± 0.2 kcal mol^{-1} M^{-1}, and ±0.5 M respectively.

5.2.6 Effect of chaotropic and kosmotropic salts on the ΔG_D and C_m of acid-denatured proteins

To determine the effect of chaotropic and kosmotropic salts on the acid-denatured proteins, the urea-induced equilibrium denaturation curves of Lyz in the presence of different concentrations of salts (NaCl, NaBr, NaI, and Na_2SO_4) were measured at pH 2.3, 25 °C. Fig. 5a shows the representative fluorescence monitored normalized urea-induced equilibrium denaturation curves of Lyz collected at different concentration of NaCl at pH 7.0, 25 °C. The urea-induced unfolding curves in Fig. 5a were analyzed by two-state equation (chapter 2, eq (5)) (*49*). Table 7 summarized the values of ΔG_D and m_g of acid-denatured Lyz calculated at various salts (NaCl, NaBr, NaI, and Na_2SO_4) concentrations at pH 2.3. From the ΔG_D and m_g values, the urea denaturation midpoints, C_m (=ΔG_D/ m_g) were obtained (Table 7). Fig. 5b shows the variation of ΔG_D with salts concentration. It is clear from Fig. 5b that with increase in the both chaotropic and kosmotropic salts concentrations, the value of ΔG_D of acid-denatured Lyz at pH 2.3 increase. Notably, the increase in the value of ΔG_D is more pronounced for Na_2SO_4 and NaI and least for NaCl and NaBr.

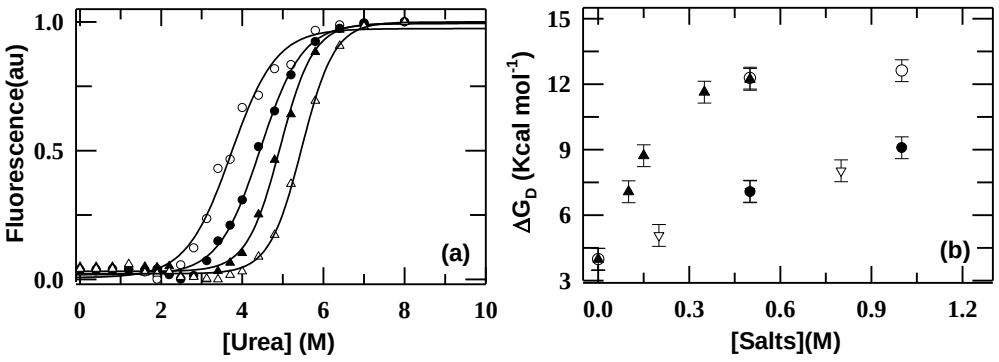

Fig. 5 (a) The representative urea unfolding curves of Lyz in the presence of 0.0 (○), 0.2, (●), 0.4 (▲), and 0.8 M NaCl (▽) pH 2.3, 25 °C. The solid lines in panel (a) represent the non-linear least square fit of the data to two-state equation (chapter 2, eq (5)) (*49*). (b) The variation of ΔG_D of Lyz with salt concentrations (▲) Na_2SO_4; (▽) NaBr; (○) NaI; and (▽) NaCl.

Table 7. Salt dependence of the thermodynamic parameters (ΔG_D, m_g and C_m) for the fluorescence monitored equilibrium unfolding of Lyz at pH 2.3.

NaCl	ΔG_D	m_g	C_m	Na_2SO_4	ΔG_D	m_g	C_m
0.0	4.0	1.1	3.7	0.0	4.0	1.1	3.7
0.2	5.1	1.1	4.4	0.1	7.1	1.3	5.5
0.5	7.1	1.4	4.9	0.15	8.7	1.5	5.8
0.8	8.0	1.5	5.5	0.35	11.6	1.6	7.3
				0.5	12.2	1.6	7.6
NaBr	ΔG_D	m_g	C_m	NaI	ΔG_D	m_g	C_m
0	4.0	1.1	3.7	0	4.0	1.1	3.7
0.5	7.1	1.5	4.7	0.5	12.3	1.6	7.7
1.0	9.1	1.6	5.7	1.0	12.6	1.6	7.9

The uncertainties of ΔG_D, m_g and C_m values reported here are ± 1.0 kcal mol^{-1}, ±0.2 kcal mol^{-1} M^{-1}, and ±0.5 M respectively.

5.2.7 Thermal denaturation of protein in different salts solutions with different water activity

To analyze the relative effect of salts on the stability of Ferrocyt *c*, the reciprocal form of the WT equation (eq (2)) was applied.

$$dlnK_{U,S}/dlna_W = \left[\Delta i - \left(X_W/X_Y\right)\Delta j\right] \qquad (2)$$

where $K_{U,S}$ (=[U]/[N]) is concentration ratio of unfolded protein (U) to native protein (N) in solution, a_W is water activity, and X_W and X_Y are molar fraction of water and cosolute, respectively. For the application of reciprocal form of the WT equation (eq (2)), a_W should be known as a function of cosolute concentrations. The values of a_W for different salts were estimated by using the relation, $\phi = -55.51/m \ln a_w$ where m is the molality of given salt. The experimental osmotic coefficients (ϕ) for various salts (Na_2SO_4, $NaNO_3$, NaBr, NaI, and $NaClO_4$) were obtained from literature (*50*). Fig. 6a shows the reciprocal WT plot for unfolding of Ferrocyt *c* at pH 7.0, in which the $\ln K_{U,S}$ of the protein is plotted against the $\ln a_W$ of salt solutions at 363.15 K. The slope which depends on the type of salt (*i.e.,* chaotropic or kosmotropic) was obtained for each salt from linear regression fits to eq (2) and it consists of Δi and the $(X_w/X_Y)\Delta j$. The effects of kosmotropic and chaotropic salts on the protein are indicated by the positive and the negative slopes (eq (2)), respectively. For Ferrocyt *c*, the sugars such as sucrose and kosmotropic salts such as Na_2SO_4 showed a positive slope while the chaotropic salts such as NaBr, NaI, $NaClO_4$, and $NaNO_3$ showed the negative slopes (Table 8). As explained earlier by Miyawaki et al, the second term for solute binding in eq (2), $(X_W/X_Y)\Delta j$ is negligible for non reducing sugars such as sucrose (*51-53*). Therefore, the hydration number change upon

protein unfolding, Δi, is determined from the slope of the plot based on eq (2) for sucrose, which is proved to be preferentially excluded from the protein surface and does not bind in the aqueous solution (*54-55*). Therefore, Δj is assumed to be zero for sucrose. The value of Δi thus determined, is 68.31 mol/ mol-protein for Ferrocyt *c* at pH 7. Once the value of Δi (eq (2)) is determined, the value of $(X_W/X_Y)\Delta j$ (binding term) can easily be determined from the slope in Fig. 6a (Table 8) and Δi. When the concentration of the salt is fixed, the Δj can easily be calculated from the $(X_W/X_Y)\Delta j$. The calculated Δj's at cosolute concentration of 1 mol/kg-solvent are summarized in Table 9. Among various salts used, the Δj is highest for $NaClO_4$ (5.17) and is least for Na_2SO_4 (-0.14).

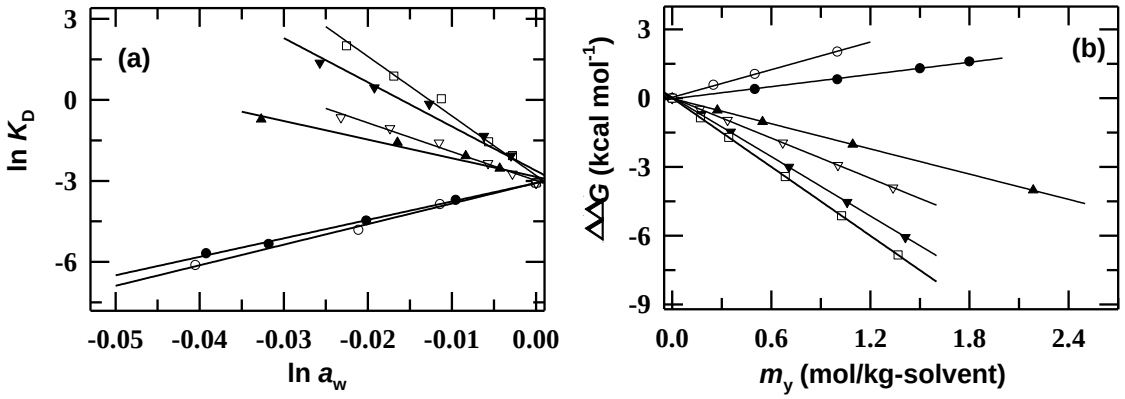

Fig. 6 (a) Reciprocal form of WT plot: Effect of water activity on unfolding ratio of Ferrocyt *c* in aqueous salt solutions (o, Na_2SO_4; ∇, $NaNO_3$; ▲, NaBr; ▼, NaI; and □, $NaClO_4$), and ●, sucrose; at pH 7.0, 363.15 K (b) $\Delta\Delta G$ is plotted as a function of salt and sugar concentration (m_y) (o, Na_2SO_4; ▲, NaBr; ∇, $NaNO_3$; ▼, NaI; □, $NaClO_4$ and ●, sucrose) obtained by thermal unfolding of Ferrocyt *c* at pH 7.0. The solid curves represent linear least-squares fitting.

Table 8. Slope of reciprocal WT plot (eq (2)).

Sucrose	Na_2SO_4	NaBr
68.31	76.16	-68.95
NaI	$NaNO_3$	$NaClO_4$
-163.76	-106.93	-220.44

Table 9. Number of change in bound-solute molecules upon protein unfolding, Δj at solute concentration of 1 mol/kg-solvent

Sucrose	Na_2SO_4	NaBr
0.00	-0.14	2.46
NaI	$NaNO_3$	$NaClO_4$
4.16	3.14	5.17

Green and Pace (*56-57*) proposed a linear extrapolation model (LEM) for $\Delta\Delta G$:

$$\Delta\Delta G = -m[m_Y] \qquad (3)$$

where m_Y is the concentration of cosolute (mol/kg-solvent), and m is termed as m-value. Various studies indicate that the m-value is positive for protein stabilizers and negative for protein destabilizers. The direct effect of lyotropic salt concentration on $\Delta\Delta G$ can be easily calculated in the present case by using eq (3), which is integrated as follows,

$$\Delta\Delta G = \Delta G_{U,S} - \Delta G_{U,0} = -RT\left(\Delta lnK_{U,S} - \Delta lnK_{U,0}\right)$$
$$= -RT\left[\Delta i - \left(X_W/X_Y\right)\Delta j\right] lna_W \qquad (4)$$

Eq (4) shows the role of water activity on protein stability by relating $\Delta\Delta G$ to $[\Delta i\text{-}(X_w/X_Y)\Delta j]$ and $\ln a_W$. It has also been shown that the net stability of protein is determined by a balance between Δi-term and Δj-term. The effect of salts concentration on thermal stability of Ferrocyt *c* is directly related by theoretical basis for the LEM model, eq (3) $\Delta\Delta G$ was calculated from eq (3) as a function of various salts concentrations. Fig. 6b shows a plot of $\Delta\Delta G$ against concentration of salts (m_Y). $\Delta\Delta G$ depends linearly on lyotropic salt concentration indicating the applicability of LEM model. The slope (m-value) determined for each salt from linear regression fits to eq (2) (Fig. 6b). The m-value is dependent on the type of salt used *i.e.*, the m-value is positive for kosmotropic salts (Na_2SO_4) and is negative for chaotropic salts (NaBr, NaI, $NaClO_4$, $NaNO_3$) (Table 10). These results are in agreement with an earlier report where the protein stabilizers such as sugars are shown to have positive m-values, where as the protein destabilizers such as alcohols are known to have negative m-values (*40, 42, 53*).

Table 10. The m-values of Ferrocyt *c* obtained in the presence of different salts and sucrose at pH7.

Sucrose	Na_2SO_4	NaBr
0.9	2.0	-1.83
NaI	$NaNO_3$	$NaClO_4$
-4.3	-2.9	-5.0

5.3 Conclusion

This chapter evaluates the effect of various chaotropic and kosmotropic salts on the structural fluctuations of the M80 containing Ω-loop of Ferrocyt *c* by measuring the kinetic and thermodynamic parameters for CO association reaction of native Ferrocyt *c* under conditions of different concentrations of various salts (NaCl, NaBr, NaI, Na_2SO_4, $NaNO_3$, and $NaClO_4$) at pH 7.0. The data obtained indicate that at low to intermediate concentrations, the ions dissociated from both chaotropic and kosmotropic salts restrict the internal dynamics of native proteins by electrostatic screening of the protein charges and by lowering the conformational entropy of proteins through

binding interactions. At relatively higher concentrations, the ions dissociated from chaotropic salts influence the internal dynamics of proteins according to Hofmeister series ($ClO_4^- > I^- > NO_3^- > Br^-$). To evaluate the effects of chaotropic and kosmotropic salts on the stability of native Cyt *c* and Mb at pH 7.0 and acid-denatured Lyz at pH 2.3, the thermal and urea-denaturation curves of the proteins were collected in the absence and presence of various salts at pH 7.0 and pH 2.3. The results obtained indicate that at neutral pH, the kosmotropic salts increase the thermodynamic stability of the proteins while the chaotropic salts decrease it. Furthermore, the effect of lyotropic salts on the thermodynamic stability of these proteins follows the Hofmeister series ($SO_4^{2-} > Cl^- > Br^- > NO_3^- > I^- > ClO_4^-$). The *m*-values were also determined from the slope of $\Delta\Delta G$ *vs* [salts] plot. The *m*-values were found to be most negative for $NaClO_4$ and least for Na_2SO_4, consistent with destabilization of proteins according to the Hofmeister series ($SO_4^{2-} > Br^- > NO_3^- > I^- > ClO_4^-$).

5.4 References

1. Jaenicke, R., and Bohm, G. (1998) *Curr. Opin. Struct. Biol.* **8**, 738-748.
2. Pace, C.N. (1995) *Methods Enzymol.* **259**, 538-554.
3. Karshikoff, A., and Ladenstein, R. (2007) In *Methods in Protein Structure and Stability Analysis: Conformational Stability, Size, Shape and Surface of Protein Molecules*; Uversky, V. N., Permyakov, E., Eds.; Nova Biomedical Books: New York, pp 71.
4. Perl, D., Holtermann, G., and Schmid, F.X. (2001) *Biochemistry* **40**, 15501-15511.
5. Jayaraman, S., Gantz, D.L., and Gursky, O. (2006) *Biochemistry* **45**, 4620-4628.
6. Benjwal, S., Jayaraman, S., and Gursky, O. (2005) *Biochemistry* **44**, 10218-10226.
7. Dominy, B.N., Perl, D., Schmid, F.X., and Brooks, C.L. (2002) *J. Mol. Biol.* **319**, 541-544.
8. Vogt, G., Woell, S., and Argos, P. (1997) *J. Mol. Biol.* **269**, 631-643.
9. Elcock, A.H., and McCammon, J.A. (1998) *J. Mol. Biol.* **280**, 731-748.
10. Timasheff, S.N. (1998) *Adv. Protein Chem.* **51**, 355-432.
11. Colonna-Cesan, F., and Sander, C. (1990) *Biophys. J.* **57**, 1103-1107.
12. Wills, P. R., Hall, D. R., and Winzor, D. J. (2000) *Biophys. Chem.* **84**, 217-225.
13. Tadeo, X., Pons, M., and Millet, O. (2007) *Biochemistry* **46**, 917-923.
14. Villa, A., Zecca, L., Fusi, P., Colombo, S., Tedeschi, G., and Tortora, P. (1993) *Biochem. J.* **295**, 827-831.
15. Apetri, A.C., and Surewicz, W.K. (2003) *J. Biol. Chem.* **278**, 22187-22192.

16. Perez-Jimenez, R., Godoy-Ruiz, R., Ibarra-Molero, B., and Sanchez-Ruiz, J.M. (2004) *Biophys. J.* **86**, 2414-2429.
17. Kumar, R., and Mauk, A.G. (2009) *J. Phys. Chem. B* **113**, 12400–12409.
18. Kumar, R., and Mauk, A.G. (2012) *J. Phys. Chem. B* **116**, 3795-3807.
19. Baldwin, R.L. (1996) *Biophys. J.* **71,** 2056-2063.
20. Cacace, M.G., Landau, E.M., and Ramsden, J.J. (1997) *Q. Rev. Biophys.* **30**, 241-277.
21. Von Hippel, P.H., and Wong, K.Y (1964) *Science* **145**, 577-580.
22. Pegram, L.M., and Record, M.T.Jr. (2008) *J. Phys. Chem. B* **112**, 9428-9436.
23. Hofmeister, F. (1888) *Arch. Exp. Pathol. Pharmakol.* **24**, 247-260.
24. Record, M.T. Jr., Anderson, C.F., and Lohman, T.M. (1978) *Q. Rev. Biophys.* **11**, 103-178.
25. Bellissent-Funel, M. (1999) Hydration Processes in Biology, IOS Press, Amsterdam.
26. Santoro, M.M., and Bolen, D.W. (1992) *Biochemistry* **31**, 4901-4907.
27. Tanford, C. (1969) *J. Mol. Biol.* **39**, 539–544.
28. Jenkins, W.T. (1998) *Protein Sci.* **7**, 376–382.
29. Petsko, G.A., and Ringe, D. (1984) *Annu. Rev. Biophys. Bioeng.* **13**, 331–371.
30. Karplus, M., and McCammon, J.A. (1983) *Annu. Rev. Biochem.* **52**, 263–300.
31. Makhatadze, G.I. (1999) *J. Phys. Chem. B* **103**, 4781-4785.
32. Rao, D.K., and Bhuyan, A.K. (2007) *J. Biomol. NMR* **39**, 187-196.
33. Yao, M., and Bolen, D.W. (1995) *Biochemistry* **34**, 3771-3781.
34. Mayr, L.M., and Schmid, F.X. (1993) *Biochemistry* **32**, 7994–7998.
35. Makhatadze, G.I., Lopez, M.M., Richardson, J.M., and Thomas, S.T. (1998) *Protein Sci.* **7**, 689–697.
36. Bhuyan, A.K. (2002) *Biochemistry* **41**, 13386–13394.
37. Kumar, R., Prabhu, N.P., Yadaiah, M., and Bhuyan, A.K. (2004) *Biophys. J.* **87**, 2656-2662.
38. Zarrine-Afsar, A., Mittermaier, A., Kay, L.E., and Davidson, A.R. (2006) *Protein Sci.* **15**, 162-170.
39. Kumar, R., and Bhuyan, A.K. (2009) *J. Biol. Inorg. Chem.* **14**, 11-21.
40. Jain, R., Sharma, D., and Kumar, R. (2013) *J. Biochem.* **154**, 341-354.
41. Kumar, R., and Bhuyan, A.K. (2005) *Biochemistry* **44**, 3024-3033.
42. Kumar, S., Sharma, D., and Kumar, R. (2014) *Biochim. Biophys. Acta.: Prot. and Proteom.* **1844**, 641-655.

43. Berghuis, A.M., and Brayer, G.D. (1992) *J. Mol. Biol.* **223**, 959–976.
44. Morgan, J.D., and McCammon, J.A. (1983) *Biopolymers* **22**, 1579–1593.
45. Banci, L., Bertini, I., Huber, J.G., Spyroulias, G.A., and Turano, P. (1999) *J. Biol. Inorg. Chem.* **4**, 21-31.
46. Kumar, R., Prabhu, N.P., Rao, D.K., and Bhuyan, A.K. (2006) *J. Mol. Biol.* **364**, 483-495.
47. Russell, A.E. (1973) *Biochem. J.* **131**, 335–342.
48. Komsa-Penkova, R., Koynova, R., Kostov, G., and Tenchov, B.G. (1996) *Biochim. Biophys. Acta.: Prot. and Proteom.* **1297**, 171-181.
49. Santoro, M.M., and Bolen, D.W. (1988) *Biochemistry* **27**, 8063-8068.
50. Hamer, W.J., and Wu, Y.J. (1972) *Phys. Chem. Ref. Data* **1**, 1047-1099.
51. Miyawaki, O. (2007) *Biochim. Biophys. Acta.: Prot. and Proteom.* **1774**, 928–935.
52. Miyawaki, O. (2009) *Biophysical chemistry* **144**, 46-52.
53. Miyawaki, O., and Tatsuno, M. (2011) *J. Biosci. Bioeng.* **111**, 198–203.
54. Lee, J.C., and Timasheff, S.N. (1981) *J. Biol. Chem.* **256**, 7193–7201.
55. Kendric, B.S., Chang, B.S., Arakawa, T., Peterson, B., Randorf, T.W., Manning, M.C., and Carpenter, J.F. (1997) *Proc. Natl. Acad. USA* **94**, 11917–11922.
56. Greene, R.F., and Pace, N. (1974) *J. Biol. Chem.* **249**, 5388–5393.
57. Pace, C.N. (1986) *Meth. Enzymol.* **131**, 266–280.

Chapter 6

Structural, Kinetic, and Thermodynamic Characterizations of Guanidinium and Sodium Cations-Induced Molten Globule States of Base-Denatured Cytochrome *c*

6.1 Introduction

The MG-state is a compact conformation that contains native-like secondary structure and fluctuating tertiary structure (*1-6*). Structural, kinetic, and thermodynamic studies show that the MG state is a major intermediate in protein folding (*3,5-21*) which typically populates at the late stages of folding (*5,6,22-25*). However, MG intermediates have also been detected at the early stages of folding of several proteins (*7,11,26-27*). The MG and other partially folded states of proteins have been found to play crucial role in human diseases. MG state is also important for protein function in the living cells. Few previous reports show that the intrinsically natively disordered proteins that resemble MG-like-state (*28-32*) can be involved in cell signaling and regulatory functions by their interactions with DNA and other proteins (*33-37*).

GdnHCl is one of the most powerful destabilizing salts commonly used to unfold native proteins. The effects of GdnHCl on protein stability are particularly complicated due to its ionic character. Therefore, a basic premise of the work is to examine the effect of ionic nature of GdnHCl on transformation of protein states. The exact mechanism by which GdnHCl acts upon proteins is still not clear. The ionic nature, and hence Coulombic effects, and chaotropic effect of the denaturant needs to be elaborated using a large number of proteins. There have been many cases reported where low concentrations of GdnHCl can stabilize proteins by committing $GdnH^+$ and Cl^- ions to screen charge-charge interactions in the native state of the protein (*38-41*). At lower concentrations of GdnHCl, the $GdnH^+$ ions also contribute to the native protein stability through more general but less discussed mechanism called protein stiffening (*39-41*). According to this, the interaction of $GdnH^+$ with the protein atoms by multiple non-covalent bonding leads to constraints on side-chain and main-chain dynamics in different parts of the protein, and thus stabilizes the protein entropically (*39-41*). However, there are fewer reports with reference to the effects of GdnHCl on the MG state of the proteins (*42-43*). The pioneering work by Goto and

coworkers has shown that GdnHCl at low concentrations (<1 M) refolds and stabilizes the acid-denatured proteins to MG states (*42*). Along the same line, we have studied the effect of GdnHCl on the base-denatured CO-liganded Ferrocyt *c* (Cyt-CO) and found that GdnHCl at low concentrations (≤0.2 M) also refolds and stabilizes the base-denatured Cyt-CO to MG state.

In the native state, the heme iron of Cyt *c* is axially coordinated by H18 and M80. At high pH, the M80 ligand to the iron in Ferricyt *c* is replaced by non-native lysyl ε-amino group (*44*), while in case of Ferrocyt *c* the Fe^{2+}-M80 contact persist even under extreme alkaline pH conditions (*44-45*). In strongly basic medium, the ligation of the lysyl ε-amino groups with the heme iron can compound the heme misligation problem (*46*), especially when the pH difference between the initial and final solutions affects the side-chain ionization. The non-native heme ligands do not interfere with inherent accelerated folding of Ferrocyt *c* (*47-48*), so this study uses Ferrocyt *c* for which the requirement for MG stabilization by itself abolishes the aforesaid ligation-related problems (*49*). Also the experiments with Ferrocyt *c* can be best performed at neutral to alkaline range of pH because low pH enhances autooxidation of the ferrous heme. Aqueous stability of Ferrocyt *c* is extremely high (~18 kcal mol^{-1} at 25 °C) and it hardly denatures even at the extreme of basic pH. To suppress the excessive stability of the protein, we test-tube engineered the protein by liganding the Fe^{2+} of heme with extrinsically added CO at pH ~12.6. Under these conditions the protein was fully denatured.

It is well known that the Cl^- arising from NaCl and GdnHCl refolds and stabilizes the acid-denatured protein to MG states by a charge screening mechanisms (*42*). Recently, it has been shown that the Na^+ arising from NaCl also transforms the alkali-denatured Ferricyt *c* and Cyt-CO to MG-states (*46, 49-51*). In this chapter we have shown that the $GdnH^+$ arising from GdnHCl (≤0.2 M) also transform the base-denatured Cyt-CO to MG state by making the electrostatic interactions to the negative charges of the protein. In addition, we have also compared the $GdnH^+$-induced alkali MG-state with the already known Na^+-induced alkali MG-state in terms of molecular compactness, and tertiary structures content, conformational and thermal stabilities, and also the restricted overall dynamics. The results obtained from this work suggest that the $GdnH^+$-induced MG state of the base-denatured protein is somewhat less stable as compared to the Na^+-induced MG state.

6.2 Results

6.2.1 Alkali-denatured Cyt-CO and its molecular compaction in the presence of guanidinium (≤0.2 M) and sodium cations

The fluorescence-monitored pH titration curves of Ferrocyt *c* in the absence and presence of CO reveal that the Ferrocyt *c* in the absence of CO remains folded under extreme alkaline conditions (pH 13) while it is steadily unfolded at pH above 12.6 in the presence of CO (Fig. 1a). The emission spectra in Fig. 1b provide three important informations. (i) The emission λ_{max} values for the base-denatured Cyt-CO (called U_B state, spectrum 4) and the denaturant-unfolded Cyt-CO at pH 7.0 (called the U-state, spectrum 6) are 361.5 and 368.5 nm, respectively. About 7.0 nm blue shift observed for the U_B-state suggests that W59 is in a relatively apolar surrounding, shielded from water. Remarkably, the emission intensity at pH 13 is at least 2.3-fold less relative to that at pH 7.0. This is possibly due to either quenching by hydroxyl ions or ionization of the phenolic hydroxyl group of tyrosine at alkaline pH. Further, when U_B-state is unfolded in the presence of 4.5 M GdnHCl, the emission intensity is found to be 1.2 fold less (spectrum 5) than the emission intensity of U-state (spectrum 6). However, the λ_{max} shifts to 366.5 nm. In spite of these effects of alkaline pH, the total observed fluorescence could still be used as a reliable marker of molecular compaction of alkaline Cyt-CO, because it is interesting to know if the emission is quenched, presumably because of increasing proximity of the fluorophores and the heme as the concentration of guanidinium (≤ 0.2 M) and sodium cations increases in the medium. (ii) Fig. 1a also shows guanidinium (≤ 0.2 M) and sodium cations driven molecular compaction of base-denatured Cyt-CO. The decrease in fluorescence emission due to W59 indole at ~0.2 M $GdnH^+$ (spectrum 3) or at ~0.2 M Na^+ (spectrum 2) concentration arises because molecular compaction brings W59 within the quenching proximity of the heme. Furthermore, in the presence of ~0.2 M GdnHCl or NaCl, the λ_{max} of U_B-state shifts to a longer wavelength showing a λ_{max} at 368 nm. This indicates that W59 in the compact protein is relatively more exposed to water. The U_B-state is denatured but still compact, and the MG-state is relatively more compact in accordance with the concept of chain compaction accompanying formation of the MG-state from the U_B-state.

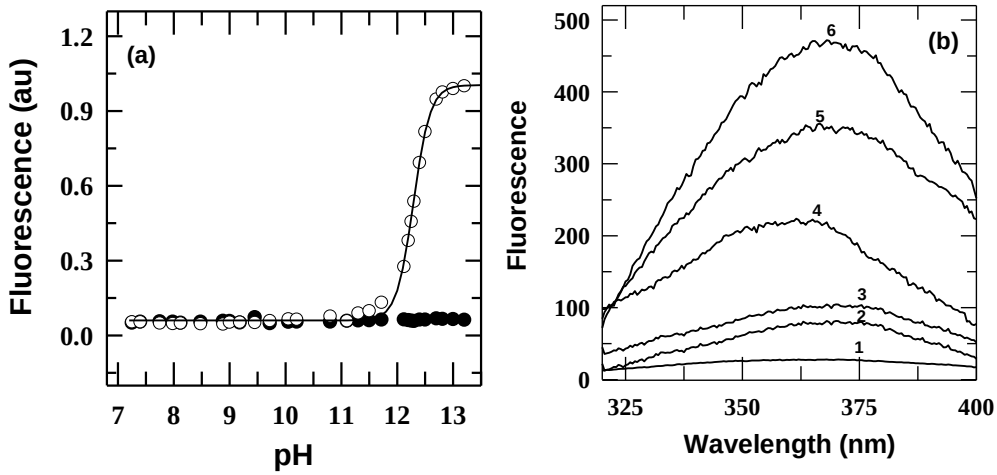

Fig. 1 Basic results indicating molecular compaction of the base-unfolded Cyt-CO in the presence of GdnHCl and NaCl (pH 12.6), 25 °C. (a) Fluorescence monitored alkaline pH-induced unfolding of Ferrocyt c. When CO is allowed to bind to the protein, it is fully unfolded at pH 12.5 (open circles), but in the absence of CO there is no unfolding (filled circles). The solid line in panel (a) is fits according to eq (4) (Chapter 2), which provided n~2.0, and C_m ~12.3 at 25 °C. (b) Fluorescence spectra for different states of Cyt-CO at 25°C. 1, pH 7.0, native; 2, pH 12.6, 0.2 M NaCl; 3, pH 12.6, 0.2 M GdnHCl; 4, pH 12.6, no salt; 5, pH, 12.6, 4.5 M GdnHCl; and 6, pH 7.0, 4.5 M GdnHCl.

6.2.2 GdnHCl-induced stabilization/folding and unfolding of the base-denatured Cyt-CO

Fig. 2 shows the fluorescence-monitored GdnHCl titration of base-denatured Cyt-CO at pH 12.6. Contrary to expectation, a remarkable behavior is observed: as the concentration of GdnHCl in reaction medium is increased, the fluorescence intensity initially decreases in a sharp cooperative manner (Fig. 2a), and then it increases relatively monotonously displaying a very weak unfolding transition (Fig. 2a).

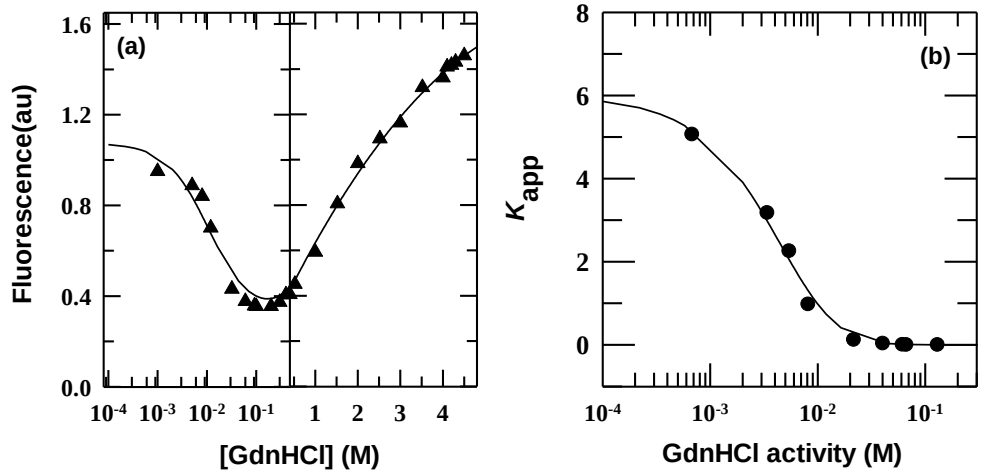

Fig. 2 (a)The GdnHCl-induced folding-unfolding transition of base denatured Cyt-CO at pH 12.6. The continuous line represents the fit to the experimental data by the use of eq (2). The fit yields m= 0.27(±0.01) kcal mol^{-1} M^{-1} and

$\Delta G°$=1.1(±0.02) kcal mol^{-1}. (b) In the presence of low concentrations of GdnHCl, guanidinium ions drive the $U_B \rightarrow$MG transition. The observable equilibrium constant, K_{app}, for the $U_B \rightleftharpoons$ MG is plotted against the molar activity of GdnHCl. The solid line is the fit to data according to eq (1) (see text). The fit yields Δn = 4.4, K_b = 51 M^{-1}, and K = 6.0. At 25°C, the value of K corresponds to the free energy of 1.07 kcal mol^{-1}.

GdnHCl-induced initial refolding transition (*i.e.*, $U_B \rightarrow$ MG transition) of base-denatured protein can be explained by the effects of $GdnH^+$ arising from GdnHCl, which binds to the negative charges of the protein, thus shielding the unfavorable repulsive forces. The number of $GdnH^+$ ions associated with the GdnHCl-induced refolding transition can be estimated for a model by assuming that the MG state interacts preferentially with the $GdnH^+$ ions and the binding constants for interaction of these cations with different binding sites offered by the MG state are comparable (*52*). The nonlinear least-squares fitting of the initial folding transition data (Fig. 2b) to the expression (1)

$$K_{app} = K(1 + K_b\, a_x)^{\Delta n} \qquad (1)$$

yields Δn = 4.4, K_b = 51 M^{-1} and K = 6.0, where Δn is the difference of the number of $GdnH^+$ ions bound to base-denatured and MG states, K_b is the binding constant, K is the true equilibrium constant for the GdnHCl-induced refolding transition in the absence of GdnHCl, and a_x is the molar activity of GdnHCl. At 298 K, the value of K corresponds to the free energy of 1.07 kcal mol^{-1}.

Starting at 0.25 M, increasing GdnHCl concentration caused unfolding of MG state (Fig. 2a) because the stabilizing effect of the $GdnH^+$ ions is overrun by its own unfolding action. The unfolding transition, MG $\rightleftharpoons$ U is apparently shallow (Fig. 2a). The GdnHCl titration data were fit to (*43*),

$$\Delta G = \Delta G° - RT \ln\left(\frac{1 + K^{u}_{bind}[GdnHCl]}{1 + K^{MG}_{bind}[GdnHCl]}\right)^{n} - m[GdnHCl] \qquad (2)$$

where K^{u}_{bind} and K^{MG}_{bind} are binding constants of $GdnH^+$ to the unfolded and the MG state, respectively, m is the equilibrium surface exposure of residues during unfolding, n is the number of $GdnH^+$ binding sites, and $\Delta G°$ is the free energy of unfolding in the absence of the denaturant. The fit yields m = 0.27(±0.01) kcal mol^{-1} M^{-1} and $\Delta G°$ = 1.1(±0.02) kcal mol^{-1}.

Fig. 3a shows the highly cooperative unfolding transition of the MG state stabilized by 0.3 M NaCl induced by GdnHCl. Therefore, a two-state analysis (*53*) was carried out to extract the thermodynamic parameters of the Na^+ cations-induced MG state. The fit yields denaturation free energy, $\Delta G°$=4.4(±1) kcal mol^{-1} and surface area exposed by solvent, m_g=2.0(±0.6) kcal

mol^{-1} M^{-1}. Fig. 3b compares the aromatic CD signals of native Ferrocyt *c* and base-denatured Cyt-CO in the presence of ~0.2 M GdnHCl and 0.2 M NaCl. Traditionally, the MGs are generally distinguished by a dramatic loss of near-UV CD signal (*54-55*). The 282 and 290 nm bands of native Ferrocyt *c* (pH 7 and 0.2 M GdnHCl) that arise from the coupling of the electric transition dipole moments of the W59 indole and the heme are not traceable in the GdnHCl-containing alkaline medium (pH 12.6 and 0.2 M GdnHCl), apparently indicating some loss of the tertiary structure.

The presence of a small amount of GdnHCl in alkali solutions obscured the peptide signals (CD 222 nm) due to an elevation of the HT voltage. The loss of 282 nm CD signal of the base-denatured protein with increasing concentration of GdnHCl up to 0.2 M is an indication of the $U_B \rightarrow$ MG transition (Fig. 3c). The nonlinear least-squares fitting of the $U_B \rightarrow$ MG transition data (Fig. 3c) to eq (1) yields Δn=1.5, K_b=300 M^{-1}, and K=2.96. At 25°C, the value of K corresponds to the free energy of 0.65 kcal mol^{-1}.

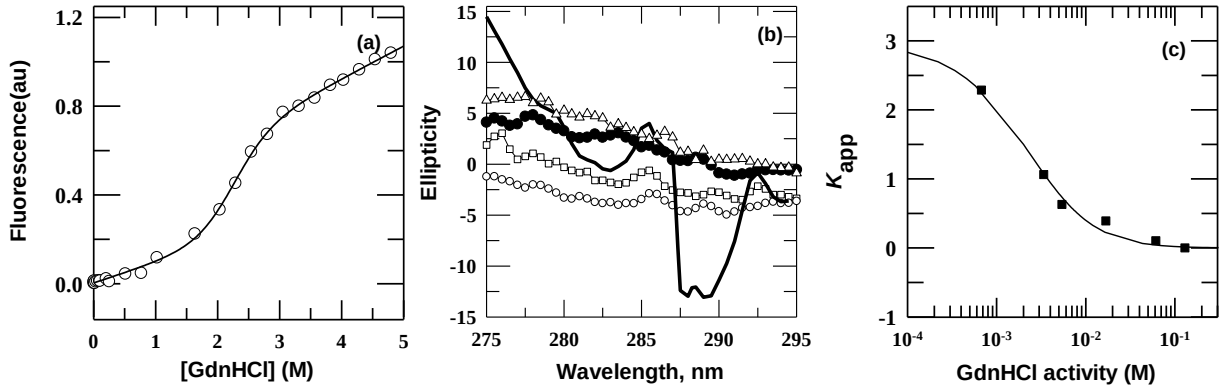

Fig. 3 (a) GdnHCl-induced equilibrium unfolding Cyt-CO at pH 12.6, 0.3 M NaCl, and 298 K. The solid line is the standard two-state fit to data (*53*). The fit yields $\Delta G°_D$ ~ 4.4 (±1) kcal mol^{-1} and m_g ~ 2.0 (±0.6) kcal mol^{-1} M^{-1}. (b) Near-UV CD spectra: native ferrocyt *c* at pH 7.0, 0.2 M GdnHCl, and 298 K (solid line); Cyt-CO at pH 12.6, 0.2 M GdnHCl, 298 K (□□□□□);Cyt-CO at pH 12.6, 0.2 M NaCl, 298 K (○○○○○); Cyt-CO at pH 12.6, no salt, 298 K (●●●●●); and Cyt-CO at pH 12.6, 4.0 M GdnHCl (△△△△△). (c) GdnHCl-induced $U_B \rightarrow$MG transition monitored by near-UV CD. The continuous line is the fit according to eq (1) (see text). The fit yields Δn=1.5, K_b=300 M^{-1}, and K=2.96. At 298 K, the value of K corresponds to the free energy of 0.65 kcal mol^{-1}.

6.2.3 NMR spectral features of alkali-denatured Ferricyt c in the presence of GdnHCl and NaCl

^{1}H NMR can be used to characterize MG state having increased internal mobility and side chain environmental averaging (*3, 54*). Selected regions of the basic NMR spectra presented in Fig. 4 reveal these properties. For the native state of Ferricyt *c* (pH 7.0, no salt), the resonances are

narrow and well dispersed (Fig. 4a,b (spectrum (i))). Whereas for the base-denatured state of the protein (pH 13, no salt), both the chemical shift dispersion and line shape are substantially lost (Fig. 4a,b (spectrum (iv))). However, the spectrum in the presence of ~0.3 M NaCl (Fig. 4a,b (spectrum (ii))) or ~0.15 M GdnHCl (Fig. 4a,b (spectrum (iii))), resembles to that of the base-denatured protein but the resonances are a little sharper (*56-59*).

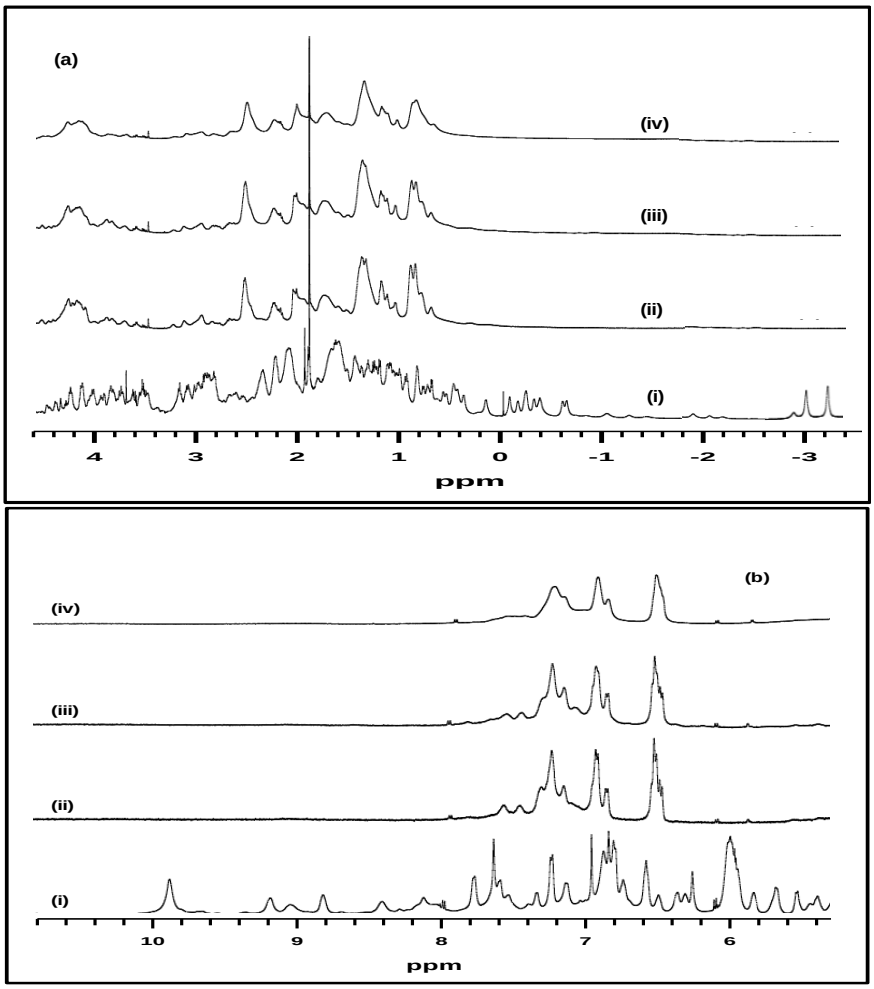

Fig. 4 NMR spectra (400 MHz). Panels (a) and (b): (i) Native state of Ferricyt *c*, pH 7.0, no salt; (ii) Na^+-induced MG state, pH 13.0, 0.3 M NaCl; (iii) $GdnH^+$-induced MG state, pH 13.0, 0.15 M GdnHCl; (iv) Base-unfolded state, pH 13.0, no salt. For clarity only selected regions of aromatic, aliphatic resonances are shown. All spectra were taken at 298 K.

Relative to resonances in the native state spectrum (Fig. 4a,b (spectrum (i))), the resonances in the NaCl and GdnHCl induced MG states spectra (Fig. 4a,b (spectrum (ii))), and (Fig. 4a,b (spectrum (iii))), respectively) are broad all over the aliphatic and aromatic regions. The finding that the GdnHCl or NaCl induced MG state resonances are still not markedly broad like that of the base-denatured state of the protein (pH 13, no salt), suggests that the MG-state interrogated

here is perhaps not excessively mobile and carries some traces of rigid tertiary structure involving both aliphatic and aromatic side chains.

6.2.4 GdnHCl and NaCl dependent kinetics of CO association to alkaline Ferrocyt c indicates that the MG state is stiff and dynamically constrained

Ferrocyt *c* can be driven to bind CO under mild destabilizing conditions when the CO is used in saturating concentration (~1.0 mM) (*48-49,60*). Intramolecular thermal collisions provide the energy for barrier crossing in the CO association reaction (*i.e.*, Ferrocyt *c*+CO → Ferrocyt *c*-CO) and the rate coefficient for CO association reaction, log k_{ass} is expected to decrease if the amplitudes of thermal fluctuations are reduced as a result of constraints on the collective modes of intramolecular motion (*40-41*). Fig. 5a typifies the kinetics of the CO association reaction of alkaline Ferrocyt *c* by monitoring the decrease in absorbance at 550 nm following the addition of a small volume of the protein solution to a CO-saturated aqueous alkaline solution (pH 12.6) containing ~0.03 M GdnHCl at 25 °C. Fig. 5b shows the kinetics of the single phase CO association reaction of native Ferrocyt *c* by same method at pH 7.0, 0.75 M GdnHCl, and 25 °C. The CO association kinetics results are well described by a monoexponential decay function and are consistent with a time constant, τ_{ass} of ~6.9 min at pH 12.6 and ~31 minute at pH 7. Fig. 5c shows the CO association kinetics of native Ferrocyt *c* by monitoring the decay of the peak height at about ―3.26 ppm (M80 CεH3 resonance) following the addition of a small volume of the protein solution to a CO-saturated aqueous native solution (pH 7) containing ~2.9 M GdnHCl at 25 °C. This NMR-monitored kinetic trace is fitted well to a monoexponential decay function with a time constant, τ_{ass} of ~20.5 min. Fig. 5d shows the GdnHCl-induced unfolding transition of alkaline Ferrocyt *c* (pH 12.6) at 25 °C. Fig. 5e and Fig. 5f show the logarithm of k_{ass} for alkaline (pH 12.6) and native (pH 7) Ferrocyt *c* as a function of GdnHCl concentration at 25 °C, respectively. Fig. 5e also shows the GdnHCl-dependent variation of k_{ass} for alkaline Ferrocyt *c* in the presence of ~0.3 M NaCl. A narrow minimum of log k_{ass} around 0.15–0.2 M GdnHCl is observed when the rate of CO association is measured for alkaline Ferrocyt *c* in the absence of NaCl (Fig. 5e). The rate-[GdnHCl] data in Fig. 5e provides an opportunity to analyze the dynamical behavior associated with the transitions from base-denatured state to the GdnHCl–induced MG and unfolded states.

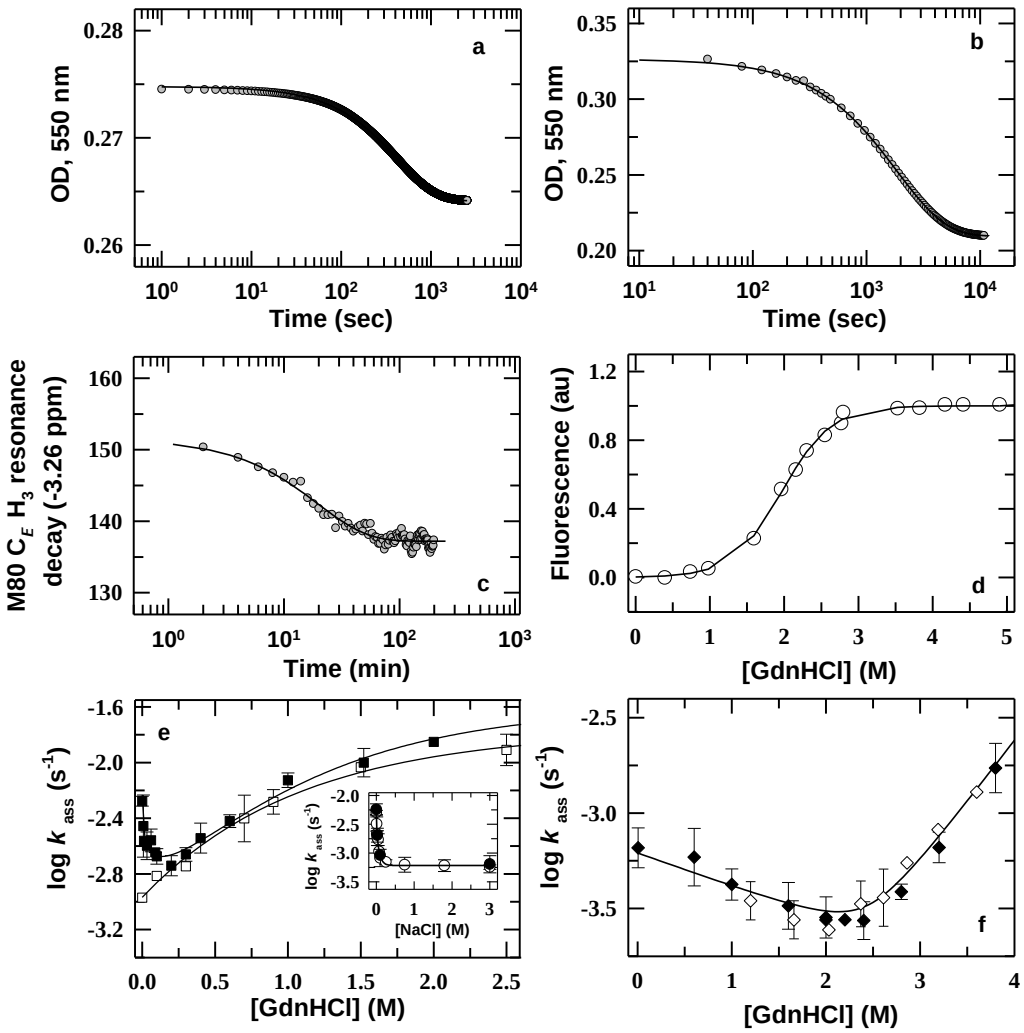

Fig. 5 Equilibrium stability and rate-denaturant/salt spaces for the CO association reaction of alkaline and native Ferrocyt *c*. Panels (a) and (b) represent the slow single-phase CO association kinetic traces of alkaline (τ=6.9 min, 0.03 M GdnHCl, pH 12.6, 298 K) and native (τ= 31 minute, 0.75 M GdnHCl, pH 7.0, 298 K) Ferrocyt *c*, respectively. Panel (c) shows the real-time NMR monitored mono-exponential decay of the peak height at -3.26 ppm (M80 $C_\varepsilon H_3$ resonance) during association of CO to native Ferrocyt *c* (τ=20.5 min, 2.9 M GdnHCl, pH 7.0, 298 K). In order to achieve a pseudo first order condition with respect to CO (saturating concentration), we have used a very low concentration of the protein (~50 μM) that rendered ^{1}D NMR acquisition more useful than ^{2}D acquisition. (d) GdnHCl-induced equilibrium unfolding of alkaline Ferrocyt *c* (pH 12.6) at 298 K. The solid line represents the iterated least-squares fit of the data to a two-state unfolding transition (*53*). The fit yields $\Delta G°_D$ ~3.53(±0.5) kcal mol^{-1} and m_g ~1.8(±0.2) kcal mol^{-1} M^{-1}. (e) Dependence of the rate of the CO association of alkaline Ferrocyt *c* on GdnHCl concentration in the absence (■) and in the presence (□) of ~0.3 M NaCl at pH 12.6, 298 K. Inset of panel (e) shows dependence of the rate of the CO association of alkaline Ferrocyt *c* (○, OD_{550} nm; •, NMR-monitored M80 $C_\varepsilon H_3$ resonance) on NaCl concentration at pH 12.6, 298 K. Panel (f) shows dependence of the rate of the CO association of native Ferrocyt *c* on GdnHCl concentration (♦, OD_{550} nm; ◊, NMR-monitored M80 $C_\varepsilon H_3$ resonance) at pH 7.0, 298 K. The lines through the data have been drawn by inspection only

When going from 0.0 to 0.2 M GdnHCl, the value of k_{ass} decreases 2(±0.3)-fold, and increases thereafter. The decrease suggests that at low GdnHCl concentrations (≤0.2 M), $GdnH^+$ ions tend

to block association of CO to Ferrocyt *c*. The increase in rate coefficients above 0.2 M GdnHCl can be interpreted to arise from MG state destabilization and structural unfolding that would facilitate CO association process. Inset of Fig. 5e shows the NaCl-dependent variation of k_{ass} for alkaline Ferrocyt *c* at 25 °C. As NaCl concentration is increased, k_{ass} decreases monoexponentially and plateau at ~0.2 M NaCl. Clearly, the internal dynamics of the Na^+ and $GdnH^+$ (≤0.2 M) ions-induced MG states are substantially constrained with respect to base-denatured and unfolded states.

To investigate these aspects further, we have determined the GdnHCl and NaCl dependence of the activation enthalpy and entropy of the CO association process. If the alkali-denatured protein is indeed stabilized at some concentration of GdnHCl or NaCl, then the energy barrier for CO association at that GdnHCl or NaCl concentration will be relatively higher. The analysis is based on the thermodynamic formulation of the conventional transition state theory, with the assumption that GdnHCl or NaCl has no effect at the transition state level. Any decrease in the entropy of the reactant state (Ferrocyt *c*+CO) must be compensated by an increase in the activation enthalpy of the CO association reaction. This follows from

$$\frac{H_{ass}}{RT} = \ln\left(\frac{\nu}{k_{ass}}\right) + \frac{S_{ass}}{R} \qquad (3)$$

where v is the vibrational frequency, and H_{ass} and S_{ass} are changes in enthalpy and entropy, respectively, between the reactant and transition states. By comparing eq (3) with the Arrhenius expression, $k_{ass} = A\exp(-E_a/RT)$, where A is the front factor and E_a is the activation energy, the following equalities are obtained.

$$E_a = H_{ass} \qquad (4)$$

$$\ln\left(\frac{A}{\nu}\right) = \frac{S_{ass}}{R} \qquad (5)$$

Fig. 6a shows the Arrhenius plots for the CO association reaction of alkaline Ferrocyt *c* in the presence of 0.0, 0.2, and 3.5 M GdnHCl. For comparison, the Arrhenius plots for the CO association reaction of alkaline Ferrocyt *c* (pH 12.6) in the presence of 0.2 M NaCl and 0.2 M GdnHCl are shown in Fig. 6b. Fig. 6b also shows Arrhenius plot for the CO association reaction of native Ferrocyt *c* (pH 7.0) in the presence of ~0.2 M GdnHCl. The activation energies and frequency factors are listed in Table 1. The data in Table 1 clearly show that in the presence of ~0.2 M GdnHCl or 0.2 M NaCl, the activation energy for the CO association reaction of alkaline

Ferrocyt *c* increases. We attribute this to reduced motional freedom in the MG state relative to that in the base-denatured and unfolded states (E_a = 19.2 (±0.3), 22.0 (±0.3), and 12.9 kcal mol^{-1} for the base-denatured, GdnH$^+$-induced MG and unfolded states, respectively). In terms of internal dynamics, the GdnH$^+$-induced MG state is more constrained relative to that of the base-denatured and unfolded states but less constrained relative to the Na$^+$-induced MG state (E_a = 22.8 kcal mol^{-1}, Fig. 6b) and native state (E_a = 25 kcal mol^{-1}, pH 7.0, Fig. 6b).

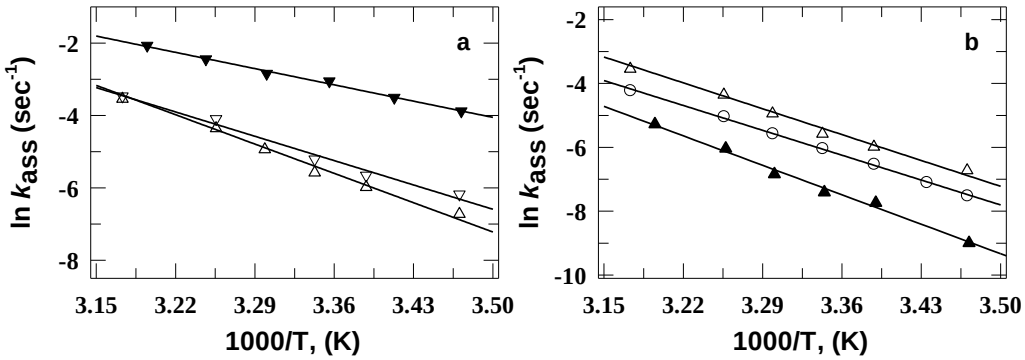

Fig. 6 Arrhenius plots for the CO association reaction in the presence of GdnHCl and NaCl. (a) Temperature dependence of the CO association rate of alkaline Ferrocyt *c* (pH 12.6) in the presence of 0.0 (∇, E_a = 19.2 (±0.3) kcal mol^{-1}), 0.2 (Δ, E_a = 22.0 (±0.3) kcal mol^{-1}), and 3.5 M GdnHCl (▼, E_a=12.9(±0.1) kcal mol^{-1}). (b) Temperature dependence of the CO association rate of alkaline Ferrocyt *c* (pH 12.6) in the presence of 0.2 M GdnHCl (Δ, E_a = 22 (±0.3) kcal mol^{-1}) and 0.2 M NaCl (o, E_a = 22.8 (±0.3) kcal mol^{-1}) and of native Ferrocyt *c* (pH 7.0) in the presence of ~ 0.2 M GdnHCl (▲, E_a = 25.0 (±0.3) kcal mol^{-1}).

The quantity ΔS_{ass}, defined as conformational entropy loss for the base-denatured protein in the presence of GdnHCl relative to the entropy of the base-denatured protein in the absence of denaturant was calculated according to (*40-41*)

$$\Delta S_{ass} = k_B \, ln \frac{A_x}{A_{ref}} \qquad (6)$$

Here, A_{ref} and A_x are the Arrhenius front factor for temperature dependence of the reactions in the absence and the presence of *x* concentration of GdnHCl. ΔS_{diss} is expressed in Boltzmann units (k_B). An increase of conformational entropy loss at ~0.2 M GdnHCl (Table 1) clearly shows that the decrease in CO association rate of alkaline Ferrocyt *c* is due to entropic stabilization of the base-denatured protein by GdnHCl. The substantial reduction in amplitudes of thermal motions in the presence of low concentrations of GdnHCl conceivably reduces the magnitude of global or subglobal unfolding motions, and is termed as "protein-stiffening effect" that stabilize structure by lowering the conformational entropy of the system (*39-40*).

Table 1. Activation energies (E_a), Frequency factor (A), and Entropy changes (ΔS_{ass}) for CO association of Ferrocyt *c* in 25 mM Tris-HCl, pH 7.0.*

		pH~12.6 (alkaline Ferrocyt *c*)			pH~7 (native Ferrocyt *c*)	
Additive	Additive concentration, M	$E_a(=H_{ass})$ kcal mol^{-1}	ln A s^{-1}	ΔS_{ass} k_B	$E_a(=H_{ass})$ kcal mol^{-1}	ln A s^{-1}
Control	0.0	19.2	27.0	0.0		
GdnHCl	0.2	22.0	31.4	+4.4	25.0	37.1
	3.5	12.9	18.4	-8.6		
NaCl	0.2	22.8	31.5	+4.5		

* Errors in values of E_a and ln A are <0.5 kcal mol^{-1} and 0.5 s^{-1}, respectively, and the corresponding errors in ΔS_{ass} is ~0.5. The errors values were determined from two or more independent measurements.

6.2.5 GdnHCl-dependence of intrapolypeptide diffusion rates of base-denatured Cyt-CO

When CO is photolyzed from base-unfolded Cyt-CO (pH 13), the side chains of the methionine (M65, and M80) and histidine (H26, and H33) residues make transient contacts with the heme iron via the vacant coordination site of the Fe^{2+} (*61-63*). The coordinates of amino acids to the heme iron are same at both alkaline and neutral pH because the side chains of the methionine (M65, and M80) and histidine (H26, and H33) residues also make transient contacts with the heme iron when the CO is photolysed from denaturant-unfolded Cyt-CO at pH 7 (*63-64*). Bimolecular CO recombination restores the initial state at longer times. When the intrapolypeptide ligand, say M binds to the Fe^{2+} of heme, this binding process involves first diffusive motions of the two contacting sites at a rate of k_{+M} to produce a heme-ligand contact loop (*63-64*). The side chain of the contacting residue M can now form a bond with the Fe^{2+} of heme at a rate k_{+b} or diffuse away at a rate of k_{-}. The binding of M to the Fe^{2+} of the heme can be depicted as below (*64*),

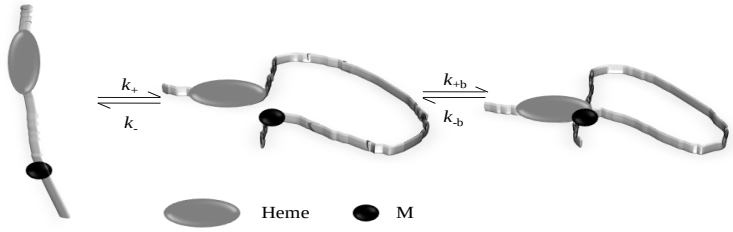

The steady-state approximation then gives the overall rate of binding, k_{+M}

$$k_{+M} = k_{+}\left[\frac{k_{+b}}{(k_{-} + k_{+b})}\right] \qquad (7)$$

Since the covalent binding, as approximated by the geminate rate (tens of nanoseconds) occurs very rapidly compared to chain diffusion that takes microseconds, so one can say $k_{+b} \gg k_{-}$. Hence, $k_{+M} \approx k_{+}$. Thus, the calculated values of ligand contact rates are actually the diffusion rates.

The intrapolypeptide diffusion rate of the contacting sites in a random coil configuration depends on the mean-squared distance between them (*65*). Thus the rate(s) of heme-ligand contact formation measured by CO photolysis from Cyt-CO can provide information about polypeptide compaction or expansion. Fig. 7a presents a typical kinetic trace showing changes in 421.5 nm absorbance at pH 12.7 in the 75 ns to 30 μs time range after CO photodissociation in the presence of 0.1 M GdnHCl. The data are best described by a 2-exponential fit with relaxation times of $\tau_1 \approx 320$ ns and $\tau_2 \approx 3.5$ μs. Bimolecular CO recombination that sets in after 50 μs is of no interest here. According to earlier studies (*62-64*), the fast and slow phases (λ_1 and λ_2, respectively) are assigned to transient binding of methionines (M80 and M65) and histidines (H26 and H33) to the heme iron of the photoproduct. Fig. 7b shows the GdnHCl dependence of the two observed rate constants, namely λ_1 and λ_2. In a 2-state approximation, $\lambda_1 = k_{+M} + k_{-M}$ and $\lambda_2 = k_{+H} + k_{-H}$, where the subscripts M and H refer to methionines and histidines, respectively. Under strongly refolding conditions (<1 M GdnHCl), the ratios k_{-M}/k_{+M} and k_{-H}/k_{+H} do not vary considerably (*62*), thus $\lambda_1 = a_1 k_{+M}$, and $\lambda_2 = a_2 k_{+H}$, where a_1 and a_2 are constants. The GdnHCl dependences of λ_1 and λ_2 should then provide qualitative estimates of the distance between two intrachain residues that make contact by diffusion.

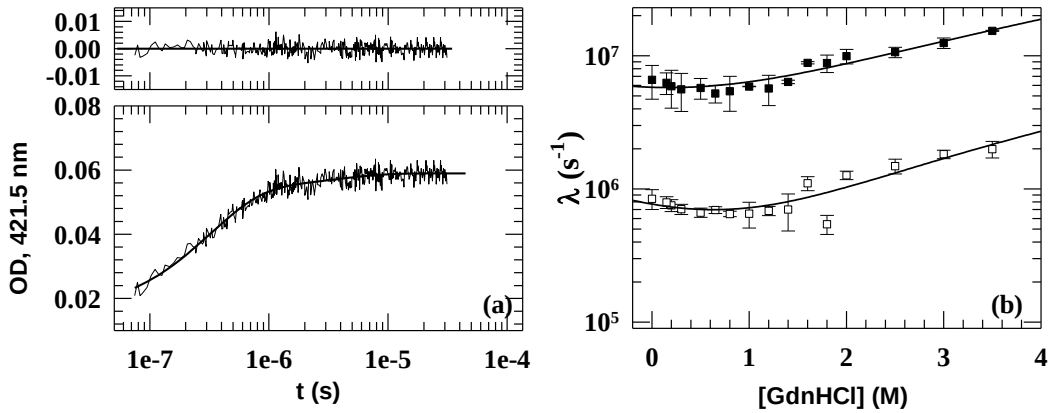

Fig. 7 Laser photolysis experiments for the measurement of intrapolypeptide diffusion rates. (a) Typical microsecond relaxation processes observed by heme optical absorption following photolysis of CO from Cyt-CO, pH 12.7, 298 K. The trace shown is for 0.1 M GdnHCl. The kinetics are described by two relaxations of time constants ≈0.32 and 3.5 μs. (b) GdnHCl dependence of the intrachain diffusion rates after photolysis of CO from

base-unfolded Cyt-CO (pH 13) at 25° C (transient binding of methionines, M65 and M80, (■) and histidines, H26 and H33 (□)).

As shown in Fig. 7b, both λ_1 and λ_2 respond little to the presence of GdnHCl in the 0-0.2 M range. This observation has two implications. (i) Under mild denaturing conditions, the chain contraction events within the initial relaxed state are not associated with any substantial surface burial, implying little structure formation. (ii) The diffusive motions of the incipient polypeptide are only marginally affected at low denaturant concentrations (≤0.2 M). This is presumably because (i) the intrachains diffusion of methionines (M80 and M65) (τ = 320 ns) and histidines (H26 and H33) (τ = 3.5 μs) are extremely fast, and (ii) the intrachains diffusion occurred with the incompletely relaxed heme. Therefore, even if a molecular compaction occurred in the GdnHCl-induced MG state of the base-denatured protein (Fig. 1b ang Fig. 2a,b), the marginally affected diffusive motions of the incipient polypeptide (≤0.2 M GdnHCl) are not sufficient to differentiate the distances of separation of the ligands from H18 in the base-unfolded and the MG state.

6.2.6 Thermal unfolding of the base-denatured protein in the presence of guanidinium (< 0.2 M) and sodium cations

To determine the thermal stability of Na^+ and $GdnH^+$-induced MG states, the thermal denaturation curves of base-denatured Ferricyt *c* were recorded (CD 282 nm) in the presence of variable concentrations of GdnHCl and NaCl. Fig. 8a shows that the 298 K spectrum of the MG state (0.3 M NaCl) retains pretty much native-like CD signals in the aromatic ellipticity band. However, the two negative peaks at 282 nm and 289 nm that arise from the tyrosyl side chains observed clearly in the native state of protein (*66-67*) are not fully retained in the spectrum of Na^+-induced MG state of the base-denatured protein (Fig. 8a). Signal intensity of the Na^+-induced MG state spectrum of the base-denatured protein at 298 K is gradually removed by decreasing NaCl concentration, exemplified by the spectra observed in the presence of 10 mM NaCl. Notably, at 353 K the base-denatured protein (pH 12.7) in the presence of 0.0 and 0.3 M NaCl is unfolded (Fig. 8a). Thermal denaturation of base-denatured protein shows substantially reversibility (*51*), hence, some of the basic principles of equilibrium thermodynamics can be used to interpret the thermal denaturation data.

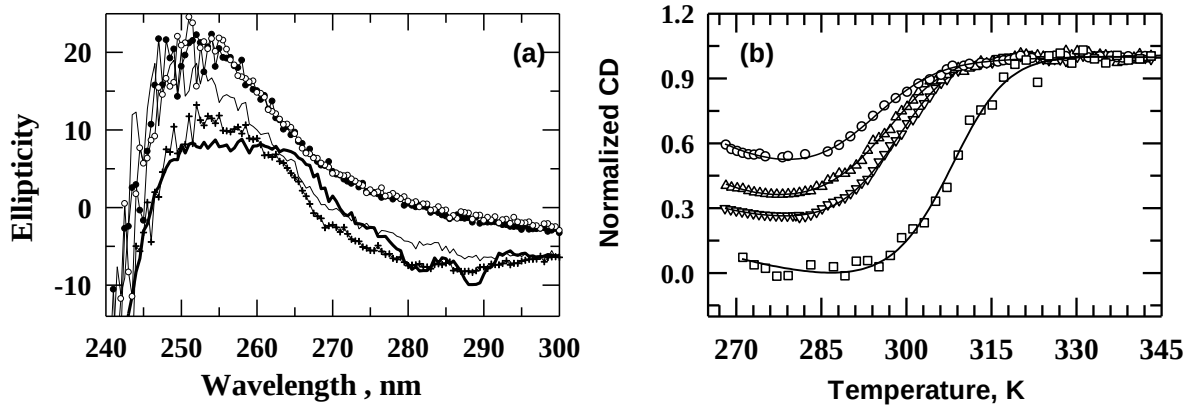

Fig. 8 Thermal transitions at pH 12.7 (a) Native Ferricyt *c* spectrum at pH 7.0, 0.1 M phosphate, 298 K (▬); alkaline Ferricyt *c* MG-state spectrum in 0.3M NaCl at 298 K (+++++) and 353 K (○○○○); and alkaline Ferricyt *c* MG-state spectrum in 10 mM NaCl at 298 K (—) and 353 K (●●●●). (b) Temperature dependence of normalized aromatic CD (282 nm) of base-denatured Ferricyt *c* in the presence of 0.0 M GdnHCl (○), 0.2 M GdnHCl (Δ), 0.2 M NaCl (∇) and 2.0 M NaCl (□). The solid lines are fits according to Gibbs Helmholtz equation (chapter 2, eqs (2) and (3)). The thermodynamic parameters derived from fits to 282-nm data are listed in Table 1 and Table 2, respectively.

Because the low temperature ellipticity values are dependent on GdnHCl (Fig.8a) and NaCl concentrations (Fig. 8a) but the high-temperature ones are not (Fig. 8a), therefore, the CD data were normalized according to

$$\theta = \frac{\theta_{\text{obs}} - (m_1 T + \theta_1)}{(m_2 T + \theta_2) - (m_1 T + \theta_1)} \tag{8}$$

where, θ_{obs} is the observed ellipticity, T is the temperature, m_1 and θ_1 are the slope and intercept, respectively, of the pretransition baseline for the 2.0 M NaCl curve, and m_2 and θ_2 are the slope and intercept of the post-transition baseline in the presence of a given concentration of GdnHCl or NaCl. Fig. 8b shows normalized thermal melts of the base-denatured protein monitored by the CD ellipticity at 282 nm in the absence of salt and in the presence of ~0.2 M GdnHCl, 0.2 M NaCl, and 2.0 M NaCl. The normalized thermal curves were analyzed by the Gibbs-Helmholtz equation (chapter 2, eqs (2) and (3)). Values of ΔH_{m} and T_{m} were also obtained from van't Hoff analysis (chapter 2, eq (1)) of thermal denaturation data (ln *k versus* 1/T) assuming that the temperature unfolding of alkali MG has two-state nature (*65-67*). Table 2 lists the T_{m}, ΔH_{m} and ΔC_{p} values. The T_{m} value for the unfolding of NaCl-induced MG state is found somewhat higher than that the unfolding of GdnHCl-induced MG state (Fig. 8b and Table 2) which indicates that

the thermal stability of the Na^+-stabilized MG state is slightly higher than the $GdnH^+$-stabilized MG state.

Table 2. Salt (GdnHCl and NaCl) dependence of the T_m, ΔH_m, ΔC_p, and $\Delta S^‡$ for thermal unfolding (CD 282 nm) of base-denatured Ferricyt *c**

	Gibbs-Helmholtz equation			van't Hoff equation		entropy-enthalpy compensation		
	T_m	ΔH_m	ΔC_p	T_m	ΔH_m	T_m	$\Delta H^‡$	$\Delta S^‡$
Control	289.0	17.4	1.1	291.5	25.9	292.1	25.7	-0.088
0.2 M GdnHCl	292.6	21.8	1.0	294.2	28.7	294.2	28.4	-0.096
0.2 M NaCl	296.1	28.9	1.0	296.8	32.2	297.2	30.9	-0.11
2.0 M NaCl	309.1	36.2	0.9	310.1	39.3	310.1	33.2	-0.12

* $\Delta H^‡$ and $\Delta S^‡$ are reported as kcal mol^{-1} and kcal mol^{-1} K^{-1}, respectively. The uncertainty of T_m values reported here is ±0.5 °C.

6.3 Discussion

Several experimental difficulties mainly due to heme autooxidation and extraordinary stability of Ferrocyt *c* have been overcome by working with the Cyt-CO under extremely basic condition (pH 12.6-12.7). The results presented show that both the sodium and guanidinium (≤0.2 M) cations stabilize the alkali-denatured Cyt-CO to MG-state at pH ~12.6-12.7, presumably by a charge screening mechanism. Interestingly, both guanidinium (≤0.2 M) and sodium cations substantially restrict overall motion and stiffen the polypeptide chain in the MG states. The anions-induced MG state of acid-denatured proteins are extensively studied, including the paradigmatic "Ferricyt *c*" (*16, 42-43, 52, 68-72*), and the cations-induced MG state of alkali-denatured Cyt-CO are expected to share at least qualitatively similar structural and dynamic properties. As reported earlier (*49*), the molecular compactness and secondary structure content of the alkali state are qualitatively comparable with those reported for the acid MG state of Ferricyt *c* (*3,71*). However, certain other properties of the alkali state of Ferrocyt *c* do not concur with the acid state (*49*).

6.3.1 Moderately rigid tertiary interactions in the cations-induced MG state of base-denatured Cyt-CO

The absence of the near-UV CD signal for the guanidinium and sodium cations-induced MG states of the base-denatured Cyt-CO (Fig. 3b) is tacitly assumed to be an indication of the loss of tertiary structure (*3, 54*), however, it need not always be so. The NMR spectra in Fig. 4 suggest

that the MG states interrogated here perhaps retained some traces of tertiary interactions. Both sodium and guanidinium cations promoted the growth of some aromatic and aliphatic resonances associated with tertiary interactions. Moderately rigid tertiary interactions, when present, as in the case of sodium cations-induced MG state of alkali-denatured Cyt-CO and β-lactamase not only contribute to molecular compaction, but also result in restricted environmental averaging for the side chains as indicated by the fairly narrow NMR lines (*49, 73*). The cooperativity observed for the GdnHCl-induced unfolding transition for the sodium cation-induced MG state of alkali-denatured Cyt-CO also points to the presence of ordered tertiary structure, since the steepness of denaturant-induced unfolding curves depends strongly on the content of rigid tertiary structure (*74-75*).

6.3.2 Folding and stabilization of the alkali-denatured protein by GdnHCl and NaCl

GdnHCl (≤0.2 M) and NaCl refold and stabilize the base-unfolded Cyt-CO to the MG states (Fig. 1b, Fig. 2). We conclude that $GdnH^+$ (≤0.2 M) and Cl^- refold and stabilize the base and acid denatured states, respectively to MG state is a general phenomenon. However, the possible mechanism of interaction of $GdnH^+$ with negative protein charge, and of Cl^- with the protein positive charges need not be the same. Since the pK_a of most carboxyls is ≥3.0, therefore, on decreasing the pH from 7.0 to 2.0, the protein becomes maximally positively charged (*55*). In acid medium (pH ≤2), where the net charges of Ferricyt *c* is +24, the Cl^- ions can shield the positive protein charges by Debye-Huckel or ion-pair or both types of interactions. In basic medium (pH >12.5), where the net protein charge of Ferricyt *c* is –17, the $GdnH^+$ ions are more likely to form ion-pairs with the anionic sites of the protein. Formation of Debye-Huckel type spheres will most likely be unfavorable due to large size of the $GdnH^+$ ions, therefore, the $GdnH^+$ ions stabilize the base-denatured protein only by ion-pair interactions. On the other hand, due to favorable size of Na^+ ions, they can stabilize the base-denatured protein by the formation of Debye-Huckel spheres as well as ion-pair interactions. Proteins in which $GdnH^+$ and Cl^- ions do not participate in charge-screening type of electrostatic interactions either due to the absence of relevant charge pairs or possibly for steric reasons, will not be stabilized by the electrostatic mechanism. Evidence for direct interactions between proteins and $GdnH^+$ comes from a number of studies, including x-ray crystallography (*76-77*) and isothermal calorimetry (*78*).

The $GdnH^+$ and Cl^- ions of GdnHCl are committed to screen the protein charges leading to stabilization in general (*42, 79-81*). However, GdnHCl can also contribute to the protein stability through the interaction of $GdnH^+$ with different groups of protein (*39-41*). The interactions of the $GdnH^+$ ions with different groups of protein can establish non-specific networks of intramolecular interactions, as observed in crystal structures of ribonuclease A with low concentrations of GdnHCl (*76*). These cross-linking interactions may serve to decrease the motional freedom in different parts of the protein, but increase the barriers to motions in the more compact conformers of the protein. Existing X-ray data for proteins have revealed that the B-factor for side-chain and main-chain atoms decrease significantly when $GdnH^+$ or urea bind to proteins (*76-77*). In an earlier study, GdnHCl, urea, and NaCl were used to establish that the GdnHCl stabilization originates from both entropic effect due to intramolecular protein cross-linking action of $GdnH^+$ and electrostatic effect due to the interaction of Cl^-, and $GdnH^+$ with charged groups of protein (*39-40*). In this perspective, $GdnH^+$-induced stabilization of the alkali denatured protein (Fig. 1b, and Fig. 2) would appear to originate from both the electrostatic and entropic effects. The relative contributions of these two effects- electrostatic shielding and conformational entropy to the free energy of stabilization of the MG state remain to be assessed.

6.3.3 Both guanidinium and sodium cations constrained overall dynamics of alkali-denatured protein

Thermal collisions due to collective motional mode of a subglobal structural unit (*i.e.,* M80-contaning Ω-loop) have been studied across the folding-unfolding transition of the alkaline Ferrocyt *c*. Spatial displacement of thermal fluctuations, and hence collisions between different groups of atoms each exhibiting collective motions is dramatically reduced as the base-denatured protein transforms to the guanidinium and sodium cations-induced MG states. This deduction is made from the kinetic and thermodynamic parameters measured for the CO association reaction of alkali-denatured Ferrocyt *c* at various GdnHCl and NaCl concentrations. The association of CO with alkali-denatured Ferrocyt *c* is an intramolecular thermally activated reaction that involves substantial energy barrier or steric requirements, and hence many collisions between the CO and protein groups, particularly the heme ring, are required before the reaction ensues. The value of log k_{ass} under a given solution condition then depends on the frequency of collisions

involving the CO and the heme side chains that exhibit highly collective motions. The rate constant for the CO association reaction, k_{ass}, decreases dramatically as the base-denatured protein undergoes to the MG states in the presence of 0.2 M GdnHCl or 0.2 M NaCl (Fig. 5e). Consequently, the activation energy for the reaction, E_a, also goes up (Table 1). In fact, the E_a values for the $GdnH^+$- and Na^+-induced MG states did not match to the native state (Table 1). This type of hindered collective motions is not commonly associated with the anion-induced MG state of acid-denatured protein. Because of dynamic disorder in the tertiary structure, the anion-induced MG state of acid-denatured protein is known to be highly mobile (*82*) with low energetic barriers for conformational fluctuations in the millisecond timescale (*83*). Absence of nonhelical hydrogen bonds due to a high degree of disorder in the side chain of majority of residues has been observed for the anion-induced MG state of Ferricyt *c* (*71*). In contrast, restricted mobility of aromatic side chains has also been observed for the anion-induced MG state of other proteins (*2,4*). The conclusion that the collective motions involving the side chains of the cation-induced MG state of the alkali-denatured protein are relatively restrained is consistent with the indications of organized tertiary structure discussed above.

Chain stiffness is atypical to dynamic properties of the MG state. Indeed, the polypeptide backbone in the anions-induced MG state of the acid-denatured protein is more mobile with respect to both native and unfolded states (*54*). Small but recognizable increase in the amplitude of local backbone fluctuations characterize the transition from the acid denatured state to the MG state of α-lactalbumin (*82*).Values of NMR measured backbone N–H order parameter, which provides an indication of the rigidity of the protein main chain, decreases significantly in the anions-induced MG state (*84*). Molecular dynamics simulations also reveal a significant increase of the fluctuations in the main-chain dihedral angles φ and ψ (*85*). A molecular interpretation of the chain stiffness in the cations-induced MG state of alkali-denatured protein is not clear at present. To sum up, the cations-induced MG state of alkali-denatured protein is distinguished by a substantial level of ordered tertiary interactions, restrained collective motions that cover larger length scales, and a stiff backbone, and it shares with other MGs the general property of being compact and with native-like secondary structure content.

6.3.4 Conformational stability and global m_g-value of the anions- and cations-induced MG states of the acid and base-denatured protein, respectively

A comparison with the Cl^--induced MG state of acid-denatured Ferricyt *c* analysis presented by Hagihara et al. (1993) indicates that the conformational stability and global m_g-value of the Cl^--stabilized MG state of acid-denatured Ferricyt *c* (2.04 kcal mol^{-1} and 1.61 kcal mol^{-1} M^{-1}, respectively (*42-43*)) is slightly higher than the $GdnH^+$-induced MG state of base-denatured Cyt-CO (1.1 kcal mol^{-1} and 0.27 kcal mol^{-1} M^{-1}, respectively). Fig. 3a shows the GdnHCl-induced unfolding transition of the Na^+-induced MG state of base-denatured Cyt-CO. The measured conformational stability and the global m_g-value of the Na^+-induced MG state of alkali-denatured Cyt-CO is substantially higher than the $GdnH^+$-induced MG state of this protein.

The global m_g-value of the Na^+-induced MG state of alkali-denatured Cyt-CO fairly matches with the GdnHCl unfolding of native Cyt-CO at pH 7.0 (*i.e.*, m_g ~2.0 and 2.1 kcal mol^{-1} M^{-1} for the Na^+-induced MG state of base-denatured Cyt-CO (pH 12.6) and native Cyt-CO (pH 7.0), respectively). This indicates a large amount of solvent exposure of amino acid residues accompanying the unfolding of the Na^+-induced MG state of base-denatured Cyt-CO. This suggests a significant hydrophobic core rather than patches of exposed and buried hydrophobic surfaces.

The Na^+-induced MG state of alkali-denatured Cyt-CO state is expected to be sufficiently stable, because it has a native-like secondary structure content, modest dynamics, and a compact molecular organization. Numerous non-structural supporting factors can determine the energetic stability of MGs. For example, time-averaged internalization of any uncompensated charge can reduce the stability, since charge burial in the low dielectric protein interior is energetically not preferred. The charge on the heme group of Cyt *c* itself provides an illustrative example. Ferricyt *c* A-state has a mixed spin ferric iron (*3*), meaning that a fraction of the A-state molecules carries a +ve charge, whereas the charge on the persistent low spin ferrous heme is zero due to pairing of all six *d*-orbital electrons. Thus the Ferricyt *c* A-state is less stable than the Ferrocyt *c* B-state. Charge density in relation to protein motions can also play a role. High frequency atomic fluctuations at the site of a protein charge can decrease the charge density by distorting the Debye-Huckel ion sphere. This result in weaker interactions of ions with the MG state compared to those with the initial pH-denatured state.

6.3.5 Thermal unfolding of the $GdnH^+$ and Na^+-induced MG states of base-denatured Ferricyt c

MGs most often do not exhibit a cooperative thermal unfolding transition (*7-8*). The thermal unfolding transition of the guanidinium and sodium cations-induced MG states of base-denatured protein reported here are rather cooperative (Fig. 8b), as reflected clearly by the sizable values of ΔH_m listed in Table 2. Thus, the cation-promoted stability proceeds with an increase in enthalpy. The thermal stability of Na^+- induced MG state is substantially higher than the $GdnH^+$-induced MG state of alkali-denatured protein (*i.e.*, midpoint thermal denaturation temperatures, T_m ~296.8 and 294.2 K for base-denatured Ferricyt *c* at 0.2 M NaCl and 0.2 M GdnHCl, respectively).

One more interesting observation is a decrease in $\Delta S^{\ddagger}$ associated with the folding transition of base-denatured protein by guanidinium and sodium cations (Table 2). Because the conformational entropy of the guanidinium and sodium cations-induced MG states cannot be higher than that in the base-denatured unfolded state, the observed entropy suppression must arise from the entropy of water. The change in the water entropy has been proposed to originate from the hydrophobic effect (*86*), which therefore appears to contribute considerably to forces stabilizing the $GdnH^+$ and Na^+-induced MG states of base-denatured protein. The MG state is thought to be stabilized by the same forces that are operative in the native state, *i.e.*, hydrophobic and hydrogen bond interactions (*43*), and we show a considerable influence of the hydrophobic effect.

6.4 Conclusion

This chapter reveals that both guanidinium (≤0.2 M) and sodium cations transform the base-denatured CO-liganded Ferrocyt *c* (Cyt-CO) to MG states by making the electrostatic interactions to the negative charges of the protein. Comprehensive spectroscopic (CD, fluorescence, NMR) studies suggest that the GdnHCl or NaCl-induced MG state is a molecular compact state containing native-like secondary structure and a disordered tertiary structure. Strategic experiments involving the measurement of the CO association to the alkaline Ferrocyt *c* (pH 12.6) in the presence of different concentrations of GdnHCl and NaCl indicate that the guanidinium-induced MG state is more constrained relative to that of the base-denatured and

unfolded states but less constrained relative to the sodium-induced MG state. Analyses of thermal (near-UV CD at 282 nm) denaturation curves of the base-denatured protein in the presence of 0.0, 0.2 M GdnHCl, and 0.2 M NaCl indicate that the base-denatured protein is indeed stabilized by both sodium and guanidinium cations. However, the cations-induced stabilizing effect is more pronounced for sodium as compared to the guanidinium.

6.5 References

1. Ptitsyn, O.B. (1995) *TIBS* **20**, 376–379.
2. Dolgikh, D.A., Gilmanshin, R.I., Brazhnikov, E.V., Bychkova, V.E., Semisotnov, G.V., Venyaminov, S.Y., and Ptitsyn, O.B. (1981) *FEBS Lett.* **136**, 311–315.
3. Ohgushi, M., and Wada, A. (1983) *FEBS Lett.* **164**, 21–24.
4. Dolgikh, D.A., Abaturov, L.V., Bolotina, I.A., Brazhnikov, E.V., Bychkova, V.E., Gilmanshin, R.I., Lebedev, Y.O., Semisotnov, G.V., Tiktopulo, E.I., and Ptitsyn, O.B. (1985) *Eur. Biophys. J.* **13**, 109–121.
5. Kuwajima, K., and Arai, M. (2000) in *Mechanisms of Protein Folding* (Pain, R. H., Ed.) 2nd ed. Oxford University Press, New York, pp 138-174.
6. Arai, M., and Kuwajima, K. (2000) *Adv. Protein Chem.* **53**, 209-282.
7. Kuwajima, K. (1989) *Proteins* **6**, 87–103.
8. Ptitsyn, O.B. (1992) *in: T.E. Creighton (Ed.)*, Freeman, New York, pp. 243–300.
9. Ghobadi, S., Safarian, S., Moosavi-Movahedi, A.A., and Ranjbar, B. (2001) *J. Biochemistry* **130**, 671–677.
10. Baldwin, R.L. (1993) *Curr. Opin. Struct. Biol.* **3**, 84–91.
11. Jenning, P.A., and Wright, P.E. (1993) *Science* **262**, 892–896.
12. Nakamura, S., and Kidokoro, S. (2005) *Biophys. Chem.* **113**, 161–168.
13. Nakamura, S., and Kidokoro, S. (2012) *J. Phys. Chem. B* **116**, 1927-1932.
14. Mukaiyama, A., Nakamura, T., Makabe, K., Maki, K., Goto, Y., and Kuwajima, K. (2013) *J. Mol. Biol.* **425**, 257-272.
15. Mukaiyama, A., Nakamura, T., Makabe, K., Maki, K., Goto, Y., and Kuwajima, K. (2013) *J. Mol. Biol.* **425**, 273-291.
16. Nakamura, S., Baba, T., and Kidokoro, S. (2007) *Biophys. Chem.* **127**,103-112.

17. Hamada, D., Kidokoro, S., Fukada, H., Takahashi, K., and Goto, Y. (1994) *Proc. Natl. Acad. Sci. USA* **91**, 10325-10329.
18. Kataoka, M., Hagihara, Y., Mihata, K., and Goto, Y. (1993) *J. Mol. Biol.* **229**, 591-596
19. Kataoka, M., Nishii, I., Fujisawa, T., Ueki, T., Tokunaga, F., and Goto, Y. (1995) *J. Mol. Biol.* **249**, 215-228.
20. Ptitsyn, O.B. (1987) *J. Protein Chem.* **6**, 273-293.
21. Kuwajima, K. (1992) *Biotechnol.* **3**, 462-467.
22. Colón, W., and Roder, H. (1996) *Nat. Struct. Biol.* **3**, 1019-1025.
23. Mok, K.H., Nagashima, T., Day, I.J., Hore, P.J., and Dobson, C.M. (2005) *Proc. Natl. Acad. Sci. USA* **102**, 8899-8904.
24. Sosnick, T.R., Mayne, L., Hiller, R., and Englander, S.W. (1994) *Nat. Struct. Biol*. **1**, 149-156.
25. Nishimura, C., Dyson, H.J., and Wright, P.E. (2002) *J. Mol. Biol.* **322**, 483-489.
26. Fujiwara, K., Arai, M., Shimizu, A., Ikeguchi, M., Kuwajima, K., and Sugai, S. (1999) *Biochemistry* **38**, 4455-4463.
27. Matthews, C.R. (1993) *Annu. Rev. Biochem*. **62**, 653-683.
28. Fink, A.L. (2005) *Curr. Opin. Struct. Biol.* **15**, 35–41.
29. Tompa, P. (2003) *Bioassays* **25**, 847–855.
30. Dyson, H.J., and Wright, P.E. (2002) *Curr. Opin. Struct. Biol.* **12**, 54–60.
31. Tompa, P. (2002) *Trends Biochem. Sci.* **27**, 527–533.
32. Uversky, V.N. (2002) *Eur. J. Biochem.* **269**, 2–12.
33. Nakayama, K.I., Hatakeyama, S., and Nakayama, K. (2001) *Biochem. Biophys. Res. Commun.* **282**, 853–860.
34. Dunker, A.K., Cortese, M.S., Romero, P., Iakoucheva, L.M., and Uversky, V.N. (2005) *FEBS J.* **272**, 5129–5148.
35. Kokai, E., Tantos, A., Vissi, E., Szoor, B., Tompa, P. Gausz, J., Alphey, L., Friedrich, P., and Dombradi, V. (2006) *Arch. Biochem. Biophys.* **451**, 59–67.
36. Radivojac, P., Vucetic, S., O'Connor, T.R., Uversky, V.N., Obradovic, Z., and Dunker, A. (2006) *Proteins: Struct. Funct. Genet.* **63**, 398–410.

37. Tompa, P., Banki, P., Bokor, M., Kamasa, P., Kovacs, D., Lasanda, G., and Tompa, K. (2006) *Biophys. J.* **91**, 2243–2249.
38. Santoro, M.M., and Bolen, D.W. (1992) *Biochemistry* **31,** 4901-4907.
39. Bhuyan, A.K. (2002) *Biochemistry* **41,** 13386–13394.
40. Kumar, R., Prabhu, N.P., Yadaiah, M., and Bhuyan, A.K. (2004) *Biophys. J.* **87**, 2656-2662.
41. Kumar, R., and Bhuyan, A.K. (2009) *J. Biol. Inorg. Chem*. **14,** 11-21.
42. Hagihara, Y., Aimoto, S., Fink, A.L., and Goto, Y.J. (1993) *J. Mol. Biol.* **231**, 180-184.
43. Hagihara, Y., Tan, Y., and Goto, Y. (1994) *J. Mol. Biol.* **237**, 336-348.
44. Wilson, M.T., and Greenwood, C. (1996) in *Cytochrome c: A multidisciplinary Approach* (Scott, R.A., and Mauk, A.G., Eds.) pp 611-634, University Science Books, Sausilito, CA.
45. Bhuyan, A. K., Rao, D. K., and Prabhu, N. P. (2005) *Biochemistry* **44**, 3034-3040.
46. Bhuyan, A.K. (2010) *Biochemistry* **49**, 7774-7782.
47. Kumar, R., and Bhuyan, A.K. (2005) *Biochemistry 44*, 3024-3033.
48. Bhuyan, A.K., and Kumar, R. (2002) *Biochemistry* **41**, 12821-12834.
49. Rao, D.K., Kumar, R., Yadaiah, M., and Bhuyan, A.K. (2006) *Biochemistry* **45**, 3412-3420.
50. Bhuyan, A.K. (2010) *Biochemistry* **49**, 7764-7773.
51. Kumar, R., Prabhu, N.P., Rao, D.K., and Bhuyan, A.K. (2006) *J. Mol. Biol.* **364**, 483-495.
52. Goto, Y., Takahashi, N., and Fink, A.L. (1990) *Biochemistry* **29**, 3480-3488.
53. Santoro, M.M., and Bolen, D.W. (1988) *Biochemistry* **27**, 8063-8068.
54. Ptitsyn, O.B. (1995) *Adv. Protein Chem.* **47,** 83-229.
55. Goto, Y., Calciano, L.J., and Fink, A.L. (1990) *Proc. Natl. Acad. Sci. USA* **87**, 573-577.
56. Assfalg, M., Bertini, I., Dolfi, A., Turano, P., Mauk, A.G., Rosell, F.I., and Gray, H.B. (2003) *J. Am. Chem. Soc.* **125**, 2913-2922.
57. Ferrer, J.C., Guillemette, J.G., Bogumil, R., Inglis, S.C., Smith, M., and Mauk, A.G. (1993) *J. Am. Chem. Soc.* **115**, 7507–7508.
58. Pollock, W.B.R., Rosell, F.I., Twitchett, M.B., Dumont, M.E., and Mauk, A.G. (1998) *Biochemistry* **37**, 6124–6131.
59. Russell, B.S., Melenkivitz, R., and Bren, K.L. (2000) *Proc. Natl. Acad. Sci. USA* **97**, 8312–8317.
60. Theorell, H., and Åkesson, A. (1941) *J. Am. Chem. Soc.* **63**, 1812-1827.

61. Choi, J., Jung, Y.O., Lee, J.H., Yang, C., Kim, B., and Ihee, H. (2008) *Chem. Phys. Chem.* **9**, 2708-2714.
62. Kumar, R., Prabhu, N.P., and Bhuyan, A.K. (2005) *Biochemistry* **44**, 9359-9367.
63. Jones, C.M., Henry, E.R., Hu, Y., Chan, C.K., Luck, S., Bhuyan, A.K., Roder, H., Hofrichter, J., and Eaton, W.A. (1993) *Proc. Natl. Acad. Sci. USA* **90,** 11860-11864.
64. Hagen, S.J., Carswell, C.W., and Sjolander, E.W. (2001) *J. Mol. Biol.* **305**, 1161-1171.
65. Hagen, S.J., Hofrichter, J., Szabo, A., and Eaton, W.A. (1996) *Proc. Natl. Acad. Sci. USA* **93**, 11615-11617.
66. Kuroda, Y., Kidokoro, S., and Wada, A. (1992) *J. Mol. Biol.* **223**, 1139-1153.
67. Strickland, E.H. (1974) *Crit. Rev. Biochem.* **2,** 113-175.
68. Hamada, D., Kidokoro, S., Fukada, H., Takahashi, K., and Goto, Y. (1994) *Proc. Natl. Acad. Sci. USA* **91**, 10325–10329.
69. Nakamura, S., and Kidokoro, S. (2005) *Biophys. Chem.* **113**, 161–168.
70. Goto, Y., and Nishikori, S. (1991) *J. Mol. Biol.* **222**, 679-686.
71. Jeng, M-F., and Englander, S.W. (1991) *J. Mol. Biol.* **221**, 1045-1061.
72. Nakamura, S., Seki, Y., Katoh, E., and Kidokoro, S. (2011) *Biochemistry* **50**, 3116-3126.
73. Goto, Y., and Fink, A.L. (1989) *Biochemistry* **28**, 945-952.
74. Ptitsyn, O.B., and Uversky, V.N. (1994) *FEBS Lett.* **341,** 15-18.
75. Uversky, V.N., and Ptitsyn, O.B. (1996) *Fold. Design.* **1**, 117-122.
76. Dunbar, J., Yennawar, H.P., Banerjee, S., Luo, J., and Farber, G.K. (1997) *Protein Sci.* **6**, 1272-1733.
77. Pike, A.C.W., and Acharya, R. (1994) *Protein Sci.* **3**, 706-710.
78. Makhatadze, G.I., and Privalov, P.L. (1992) *J. Mol. Biol.* **226**, 491-505.
79. Makhatadze, G.I. (1999) *J. Phys. Chem. B* **103**, 4781-4785.
80. Makhatadze, G.I., Lopez, M.M., Richardson, J.M., and Thomas, S.T. (1998) *Protein Sci.* **7**, 689–697.
81. Mayr, L.M., and Schmid, F.X. (1993) *Biochemistry* **32**, 7994–7998.
82. Chakraborty, S., Ittah, V., Bai, P., Luo, L., Haas, E., and Peng, Z. (2001) *Biochemistry* **40**, 7228-7238.
83. Kim, S., Bracken, C., and Baum, J. (1999) *J. Mol. Biol.* **294,** 551-560.

84. Redfield, C., Smith, R.A.G., and Dobson, C.M. (1994) *Nat. Struct. Biol*. **1**, 23-29.
85. Daggett, V., and Levitt, M. (1992) *Proc. Natl. Acad. Sci. USA* **89**, 5142-5146.
86. Kauzmann, W. (1959) *Adv. Protein Chem.* **14**, 1-57.

Chapter 7

Kinetic and Thermodynamic Studies on the Effects of SDS on the Native and Base-Denatured States of Horse Cytochrome *c*

7.1 Introduction

In general, under extreme acidic or basic pH conditions, the native proteins denature primarily due to electrostatic charge repulsions. Inclusion of salt in the acid- or base-denatured proteins can induce formation of MG-states (*1-8*) through the reduction of electrostatic repulsion between charged residues (*3, 9-12*). Few earlier reports suggest that the sugars, polyols, and low concentrations of GdnHCl stabilize and refold the highly positively charged acid-denatured state of Ferricyt *c* to MG states (*3, 8, 12-14*). Although, there is only little evidence available which shows that hydrophobic interactions also substantially contribute to the MG state stability, however, this is suggested by the positive heat capacity change for thermal denaturation of MG states of Ferricyt *c* (*5, 12, 15-16*) and apo-Mb (*11, 17*). Few recent reports had shown that the low concentrations of GdnHCl also transform the highly negatively charged base-denatured states of Ferricyt *c* and Cyt-CO to MG-states (*5, 18-19*).

Due to their transient lifetime, the MG-states are difficult to study under normal folding conditions at neutral pH. Few previous reports suggest that the submicellar concentrations of anionic surfactants such as sodium dodecyl sulfate (SDS) transform the native proteins to MG-states even at neutral pH (*20-23*). SDS is commonly known as a very potent protein denaturant and is routinely used in estimation of the molecular weight of proteins (*24-26*), as a micelle mimetic of membrane in studies of solution structure of membrane associated proteins (*27-35*), and to study environment of the heme in various heme proteins (*36*). The millimolar concentrations of SDS are sufficient to denature native proteins (*37-38*). Despite the everyday use of SDS in protein chemistry, the exact mechanism of action of SDS on proteins is not clearly understood. In particular, below submicellar concentration range, how SDS interacts with the native- and extreme pH-denatured states of proteins is less understood. There are fewer reports which show that the submicellar concentrations of SDS and the *n*-alkyl sulfates can transform the

acid-denatured states of proteins to MG states (*39-43*). Pioneering work by Keiderling and coworkers suggests that the decrease in electrostatic repulsion is the major driving force for the formation of MG-state at submicellar concentrations of SDS (*42*). Mazumdar and coworkers have revealed that both electrostatic and hydrophobic interactions contribute to the formation of MG-state in the presence of SDS (*41*).

This chapter evaluates the effects of submicellar concentrations of SDS on the native (pH 7.0) and base-denatured (pH 12.8(±0.2)) states of Cyt *c*. The work in this chapter reveals that (i) the interactions of the Na^+ ions arising from SDS (≤0.2 mM) with some anionic protein sites induce the molecular compaction in the base-denatured (pH ~12.8) state of Cyt *c* (U_B-state) (ii) the submicellar concentrations of SDS (≤0.4 mM) transform the U_B-state to MG state, which has native-like secondary structure but lacks tertiary structure, (iii) the base-denatured Cyt *c* (pH 12.8) exhibits cold denaturation at low SDS and NaCl concentrations and with increase in the SDS concentration, the thermal denaturation temperature increase and the cold denaturation temperature decrease (iv), the submicellar concentrations of SDS (≤0.5 mM) decrease the thermal stability of native Cyt *c* at pH 7.0, (v) kinetic and thermodynamic parameters measured for CO-association reaction of alkaline Ferrocyt *c* at pH 12.6 and CO-dissociation reaction of natively folded Cyt-CO (NCO) at pH 7.0 in the presence of various concentrations of SDS (≤0.6 mM) indicate that the submicellar concentrations of SDS constrain the internal dynamics of the base-denatured Cyt-CO at pH 12.6 and NCO at pH 7.0.

7.2 Results and discussion

7.2.1 *Submicellar concentrations of SDS induce the molecular compaction and expansion of base-denatured Ferricyt c*

In the native state of Cyt *c* (N-state), the single tryptophan W59 is typically buried in the hydrophobic core and almost no fluorescence is observed (fluorescence-silent) (*44*). However, upon denaturation, the tryptophan residue gets solvated and a dramatic increase in fluorescence occurs (*44-45*). The fluorescence intensity thus can be used as reliable indicator for molecular expansion and compaction. Fig. 1a presents the fluorescence monitored alkaline pH titration of Ferricyt *c* at 25 °C. The increase of fluorescence signal intensity of protein at pH ≥12.5 (Fig. 1a) shows molecular expansion of the base-denatured protein (*44-45*). Fig. 1b shows the effects of

SDS and NaCl concentrations on the fluorescence emission spectrum of base-denatured Ferricyt *c* at pH 12.8 (U_B-state). For comparison, Fig. 1b also presents fluorescence emission spectrum of native Ferricyt *c* at pH 7.0 (N-state). Fig. 1b clearly shows that the emission observed for the U_B-state (Fig. 1b, spectrum 4) decreases when ~0.2 mM SDS (Fig. 1b, spectrum 3) is included, which suggests a molecular compaction of protein chain due to interaction with SDS. In highly basic medium (pH ~12.8), where the net protein charge of Ferricyt *c* is ~ –20, the Na^+ ions can shield the negative protein charges of U_B-state by the Debye-Huckel or ion-pair or by both types of interactions. The SDS-induced molecular compaction of U_B-state thus can be attributed to arise from the interactions of the SDS-dissociated Na^+ ions with some anionic protein sites. When ~0.5 M NaCl is included in the U_B-state, the fluorescence emission intensity of the U_B-state (Fig. 1b, spectrum 4) also decreases significantly (B-state) (Fig. 1b, spectrum 2), which further supports that the interactions of Na^+ ions with some negatively charged groups of protein cause the molecular compaction of the base-denatured protein. Few recent reports have also shown that the interactions of the Na^+ ions dissociated from NaCl or SDS (≤0.2 mM) with some anionic protein sites lead to the molecular compaction of base-denatured Cyt-CO at pH 12.7 (*18, 36*). However, SDS is regarded as a salt with hydrophobic chain (*39*), therefore, the participation of hydrophobic moieties in the SDS (≤0.2 mM)-induced molecular compaction of base-denatured protein cannot be neglected. When ~0.5 mM SDS is included in the U_B-state (pH 12.8), the fluorescence emission intensity of protein increases (Fig. 1a, spectrum 5). The fluorescence enhancement of the U_B-state at high concentration of SDS can be attributed to the chain expansion, since the side chain of the single tryptophan 59 is moved away from the heme making the protein more fluorescent (*36*). The inclusion of ~0.5 mM SDS in the U_B-state also results in ~8.0-nm blue shift in the fluorescence emission spectrum of base-denatured protein, which suggests that the interactions with SDS are accompanied by positioning of the single Trp 59 side chains in an increasingly nonpolar environment (*36*). Fig. 1c shows fluorescence monitored normalized SDS titration of U_B-state (pH 12.8) in submicellar concentration range of SDS (≤0.6 mM). As concentration of SDS in reaction medium is increased, the fluorescence intensity initially decreases and then increases monotonously (Fig. 1c). Here, the initial molecular compaction transition (Fig. 1c) is attributed to Na^+ ions (arise from SDS)-mediated $U_B \rightarrow I_{SDS}$ transition, where the I_{SDS} is a structural intermediate. At low SDS concentrations, the Na^+ ions dissociated from SDS (or NaDS) bind to the negative charges of the protein, and thus shielding

the unfavorable repulsive forces. Although, the I_{SDS} intermediate is more compact than the U_B-state (Fig.1b and Fig. 1c), it is less compact than the B-state (Fig.1b).

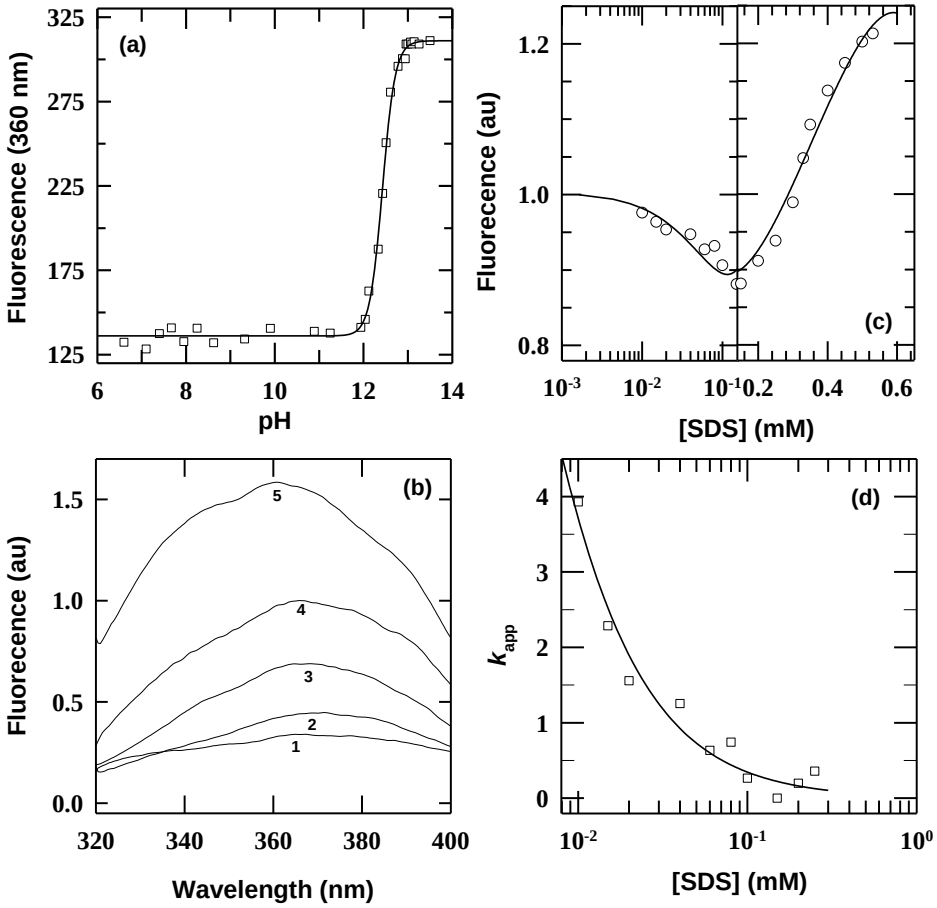

Fig. 1 (a) Fluorescence monitored alkaline pH titration of Ferricyt *c* at 25 °C. The alkaline pH-induced unfolding transition of Ferricyt *c* was best described by Henderson-Hasselbalch equation (chapter 2, eq (4)) (*5*), which provides the number of OH^- titrated ~3 and pH-midpoint ~12.5. (b) Fluorescence emission spectra for different states of Ferricyt *c* at 25°C indicating the molecular compaction of base denatured protein in the presence of low concentrations of SDS and NaCl; 1, pH 7.0, native state; 2, pH 12.8, 0.5 M NaCl (B-state); 3, pH 12.8, 0.2 mM SDS (I_{SDS}-state) 4, pH 12.8, no SDS (U_B-state); and 5, pH 12.8, 0.5 mM SDS (U-state). (c) The SDS-induced molecular compaction-expansion transition of base denatured Ferricyt *c* at pH 12.8 (○). The solid line through the data in panel (c) has been drawn by inspection only. (d) The base-denatured Ferricyt *c* transforms to MG_{SDS}-state in the presence of low concentrations of SDS. The observable equilibrium constant, K_{app}, for this transition is plotted against the SDS concentration. The solid line is the fit to data according to eq (1). The fit yields, Δn = 1.1, K_b = 500 M^{-1}, and K = 27. At 25°C, the value of K corresponds to the free energy of ~1.97 kcal mol^{-1} for SDS induced MG state of base-denatured Ferricyt *c*.

The number of Na^+ ions associated with the SDS-mediated $U_B \rightarrow I_{SDS}$ transition can be estimated for a model by assuming that the I_{SDS}-state interacts preferentially with the Na^+ ions and the binding constants for interaction of Na^+ ions with different binding sites offered by the I_{SDS}-state are comparable (*46*). The nonlinear least-squares fitting of the $U_B \rightarrow I_{SDS}$ transition data (Fig. 1d) to the expression (1)

$$K_{app} = K(1 + K_b [SDS])^{\Delta n} \quad (1)$$

yields Δn =1.1, K_b=500 M^{-1} and K=27, where Δn is the difference of the number of Na^+ ions bound to base denatured and the I_{SDS}-state, K_b is the binding constant, K is the true equilibrium constant for the SDS-induced $U_B \rightarrow I_{SDS}$ transition. The values of K_{app} in Fig. 1d were calculated from eq (2),

$$K_{app} = \left[(Y_{obs} - Y_{U_B}) / (Y_{I_{SDS}} - Y_{obs}) \right] \quad (2)$$

where Y_{obs} is the observed value of the signal, $Y_{I_{SDS}}$ and Y_{U_B} are the corresponding values for the SDS-induced I_{SDS}-state and base-denatured states, respectively (*46*). At 298 K, the value of K corresponds to the free energy of ~1.97 kcal mol^{-1}. At relatively higher SDS concentrations (≥ 0.2 mM), the hydrophobic interactions between the non-polar chains of surfactant and nonpolar groups of protein dominates (*39*), which subdue the molecular compaction effect of the Na^+ ions and thus expand the I_{SDS}-state (Fig. 1c).

7.2.2 Submicellar concentrations of SDS induce secondary structure in the base-denatured Ferricyt c

The far-UV CD spectrum of native Ferricyt *c* exhibits two negative bands at 208 nm and 220 nm (peptide bands), typical of proteins with well defined α-helical secondary structure. Fig. 2a shows the effects of SDS and NaCl concentrations on the far-UV CD spectrum of U_B-state at pH 12.8. For comparison, Fig. 2a also presents the far-UV CD spectrum of N-state at pH 7. U_B-state (Fig. 2a) shows a significant loss of secondary structure, which is indicated by ~70% loss of the MRE value of peptide bands in the far-UV CD spectrum of U_B-state at pH 12.8 (Fig. 2a). The inclusion of ~0.5 mM SDS in the U_B-state results in significant regain of the MRE value in the peptide bands of far-UV CD spectrum of U_B-state (Fig. 2a). This finding indicates that the submicellar concentrations of SDS induce the α-helical secondary structure in the U_B-state of Ferricyt *c* and thus transform the U_B-state to MG_{SDS}-state, where the MG_{SDS}-state is a SDS-induced refolded state of base-denatured Ferricyt *c*. When ~0.5 M NaCl is included in the U_B-state, the U_B-state regains the native-like peptide bands (negative bands at 208 nm and 222 nm) in the far-UV CD spectrum of U_B-state (Fig. 2a), indicating that NaCl induces the native-like α-helical secondary structure in the U_B-state of Ferricyt *c* and thus transforms the U_B-state to B-state, where the B-state is a Na^+ ions (dissociated from NaCl)-induced refolded state of base-denatured Ferricyt *c*. It

is also observed that the MRE value for the MG_{SDS}-state (Fig. 2a, cross line spectrum) is slightly higher than that of the B-state (Fig. 2a, plus line spectrum) and N-state (pH 7.0) (Fig. 2a, solid line spectrum) of Ferricyt *c*.

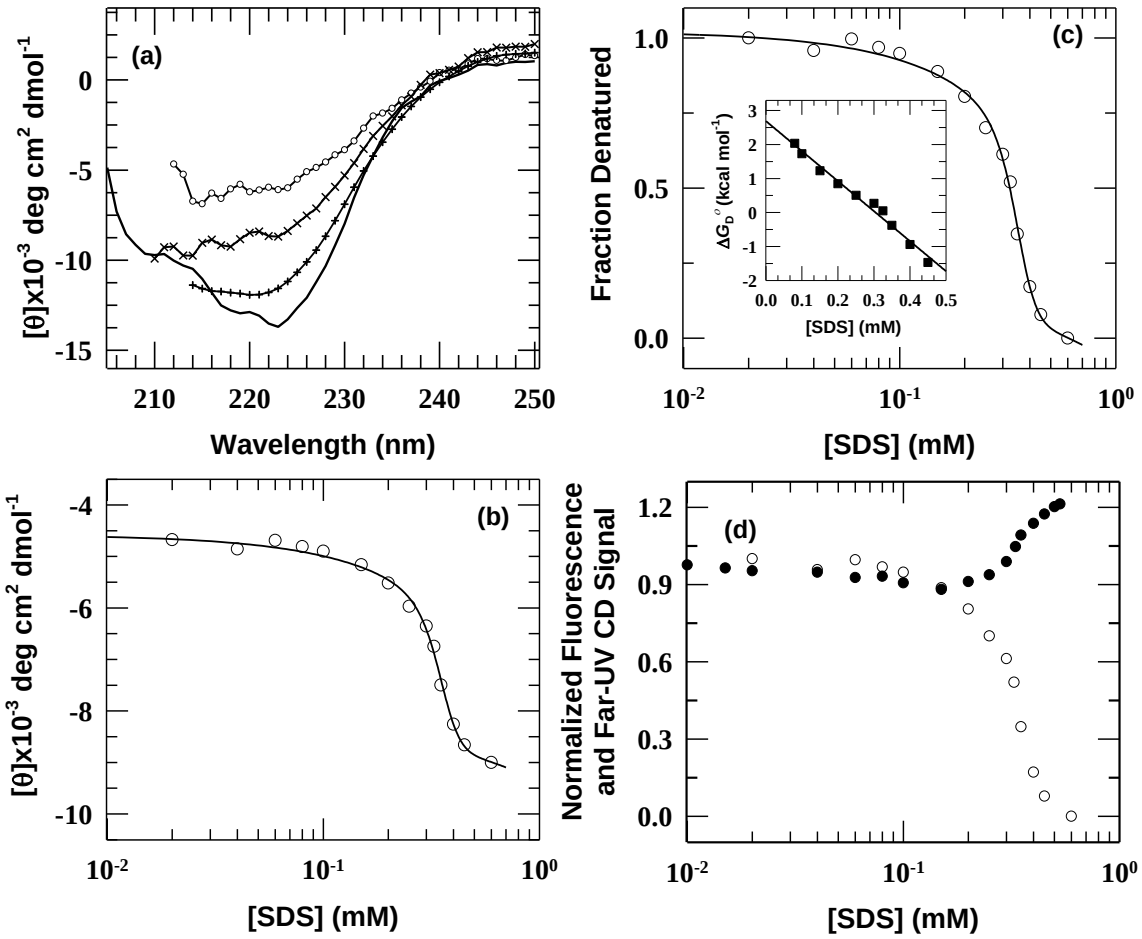

Fig. 2 (a) Far-UV CD spectra for different states of Ferricyt *c* at 25°C: pH 7.0, native state (solid line); pH 12.8, 0.5 M NaCl, B-state (++++), pH 12.8, 0.4 mM SDS, MG_{SDS}-state (××××); and pH 12.8, no SDS, U_B-state (○○○○). (b) Variation of the CD-222 nm intensity of base denatured Ferricyt *c* as a function of SDS concentration, indicating the formation of secondary structure with increasing concentration of SDS. The solid line through the data in panel (b) has been drawn by inspection only. (c) The normalized SDS-induced refolding transition (CD 222 nm) of base denatured Ferricyt *c* at pH 12.8. The solid line through the data in panel (c) has been drawn by inspection only. Inset of the panel (c) shows unfolding free energy changes in the transition region calculated from the equilibrium curve (panel (c)). The linear least-squares best fit of the data to eq (4) (*47*) provided, ΔG^o = 2.7 kcal mol^{-1}, and m = 8.2 kcal mol^{-1} M^{-1}. (d) Fluorescence (•) and far-UV CD (○, 222 nm) monitored normalized SDS titrations of base-denatured Ferricyt *c* at pH 12.8, 25 °C.

Fig. 2b shows the far-UV CD (CD 222 nm) monitored SDS titration of U_B-state (pH 12.8, 25° C) at submicellar concentration range of SDS (≤0.6 mM), which suggests that the submicellar concentrations of SDS refold and stabilize the U_B-state to MG_{SDS}-state. Clearly, the U_B-state acquires significant secondary structure in the presence of SDS (~0.4 mM). Few previous reports

have also shown that the submicellar concentrations of SDS enhance the α- helical secondary structure content of acid-denatured proteins at pH 2.0 (*55,74*), and thus transform the acid-denatured proteins to MG-states (*23*, *42*). Moosavi et al (2003) have studied the effect of *n*-alkyl sulfates on the structure of acid-denatured Ferricyt *c* at pH 2.0 and showed that the hydrophobic interactions play an important role in stabilizing the MG-state (*39*). Few earlier works by Keiderling and coworkers (2004, 2006) and Mazumdar et al (2003) have revealed that both electrostatic and hydrophobic interactions contribute to the stability of MG state in the presence of SDS (*41-43*). Fig. 2c shows the normalized far-UV CD monitored SDS (≤0.6 mM)-induced refolding transition of U_B-state at 25° C. The Gibbs free energy change, ΔG, for the two-state $U_B \rightarrow MG_{SDS}$ transition can be calculated by using the eq (3),

$$\Delta G = -RT \ln K = -RT \ln \left[(Y_{obs} - Y_{U_B}) / (Y_{MG_{SDS}} - Y_{obs}) \right] \qquad (3)$$

where, Y_{obs} is the observed value of CD signal, $Y_{MG_{SDS}}$ and Y_{U_B} are the corresponding values for the SDS-induced MG_{SDS}-state and base-denatured states, respectively (*46*). On the assumption of a linear dependence of ΔG on SDS concentration (*47*), the linear least-squares fit of the data (Inset of Fig. 2c) to eq (4),

$$\Delta G = \Delta G^o + m[\text{SDS}] \qquad (4)$$

finally provides, ΔG^o =2.7 Kcal mol^{-1} and *m* (slope reflecting the cooperativity of the transition) = 8.2 kcal mol^{-1} M^{-1}. Clearly, for the $U_B \rightarrow MG_{SDS}$ transition, the value of ΔG^o determined by far-UV CD (~2.7 Kcal mol^{-1}) (Fig. 2c) is slightly higher than those determined for the $U_B \rightarrow I_{SDS}$ transition by fluorescence (~1.97 Kcal mol^{-1}) (Fig. 1d). Furthermore, the far-UV CD monitored $U_B \rightarrow MG_{SDS}$ transition and the intrinsic fluorescence monitored $U_B \rightarrow I_{SDS}$ transition were not superimposable (Fig. 2d), which suggests that there may be an equilibrium intermediate involved in the SDS-induced folding transition of Ferricyt *c* at alkaline pH.

7.2.3 Base-denatured Ferricyt c does not acquire tertiary interactions in the presence of NaCl and submicellar concentrations of SDS

The near-UV CD spectrum of native Ferricyt *c* exhibits two negative bands at 280 nm and 290 nm (aromatic bands), typical of proteins with tertiary structure. These two negative bands can be attributed to the electronic transitions in the side chain of the single Trp 59 which has been confirmed by their disappearance in case of a single mutant Trp59F (*48*). Fig. 3a shows the

effects of SDS and NaCl concentrations on the near-UV CD spectrum of U_B-state at pH 12.8. For comparison, Fig. 3a also presents the near-UV CD spectrum of N-state at pH 7.0. Near UV-CD spectrum of U_B-state at pH 12.8 shows that the two negative bands between 280 nm and 290 nm are almost lost (Fig. 3a) suggesting that the tertiary structure interactions in the U_B-state of protein are significantly disrupted. Generally, the MGs are characterized by a loss of near-UV CD signal (*49-50*). The inclusion of low concentration of SDS (≤0.4 mM) and NaCl (0.5 M) does not result in the regain of the negative intensity of these two bands, which indicates that inclusion of SDS does not result in the formation of tertiary structure in base denatured Ferricyt *c*.

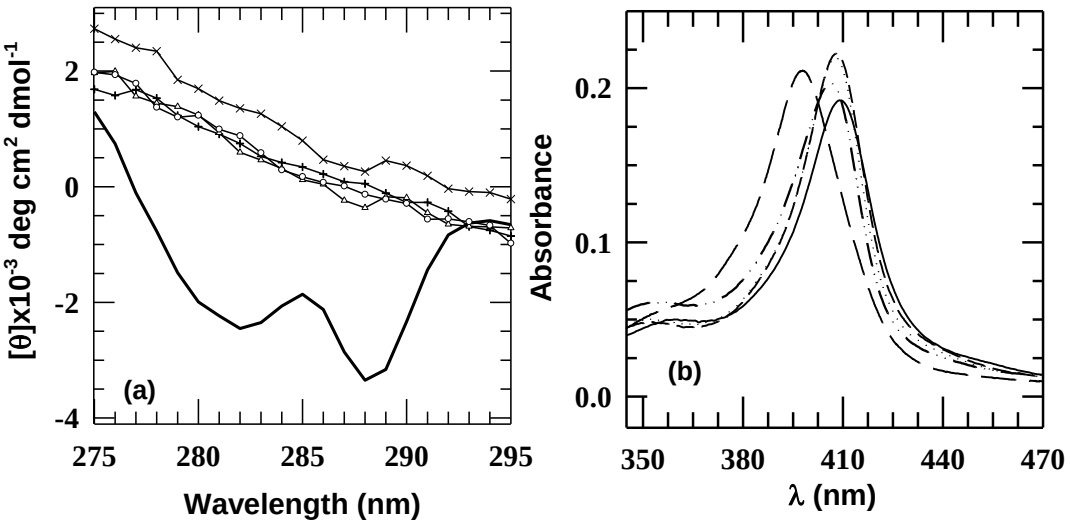

Fig. 3 (a) Near-UV CD spectra for different state of Ferricyt *c*: native state (solid line); pH 12.8, 0.5 M NaCl, B-state (++++), pH 12.8, 0.4 mM SDS, MG_{SDS}-state (××××); pH 12.8, 0.2 mM SDS, MG_{SDS}-state (ΔΔΔΔ); and pH 12.8, no SDS, U_B-state (○○○○). (b) UV-visible absorption spectra for different states of Ferricyt *c* in the Soret region: pH 7.0, native-state (solid line); pH 2.0, no SDS, U_A-state (long dash line); pH 12.8, no SDS, U_B-state (short dash line); pH 12.8, 0.2 mM SDS, MG_{SDS}-state (dotted line); and pH 12.8, 0.5 mM SDS, MG_{SDS}-state (dash double dot line).

7.2.4 Effects of submicellar concentrations of SDS on the Soret absorbance of base-denatured Ferricyt c

The UV-visible spectrum of native Ferricyt *c* in the Soret region shows a peak at ~409 nm (Fig. 3b). As pH is increased from pH 7.0 to pH 12.8, the Soret absorption peak shows a slight shift from 409 nm to 407 nm (Fig. 3b). However, when pH is decreased from pH 7.0 to pH 2.0, there is large shift in the Soret absorption peak from 409 nm to 394 nm (Fig. 3b), which is consistent with the earlier studies (*42*). Fig. 3b also shows the effects of submicellar concentrations of SDS on the Soret absorbance of base-denatured Ferricyt *c* at pH 12.8. As SDS concentration is increased from 0.0 to 0.5 mM, the absorbance peak of the base-denatured Ferricyt *c* decreases slowly with little shift from 407 nm to 405 nm, indicating no fundamental heme change in this

concentration range but the possibility of multiple heme microenvironment broadening the Soret band.

7.2.5 Effects of NaCl and submicellar concentrations of SDS on the internal dynamics of base-denatured Cyt-CO

Few recent reports show that the NaCl transform the base-denatured Cyt-CO to MG state at pH ~12.7 (*4, 18*). To determine the effects of NaCl and submicellar concentrations of SDS (≤0.5 mM) on the internal dynamics of base-denatured Cyt-CO, the kinetic and thermodynamic parameters for CO association to alkaline Ferrocyt *c* at pH 12.6 were measured in the presence of different concentrations of NaCl and SDS. Ferrocyt *c*+CO (≈1.0 mM)→Ferrocyt *c*-CO is basically Fe^{2+}−M80→Fe^{2+}−CO displacement reaction (*51-54*), and the collective motions of the M80-contaning Ω-loop control this CO-association reaction (*51-54*). If the amplitudes of thermal fluctuations decrease due to constraints on the collective modes of intramolecular motion (*51*), the speed of CO association reaction will slow down. Fig. 4a shows representative kinetic profile of CO association to alkaline Ferrocyt *c* at pH 12.6 in the absence of NaCl and SDS measured by monitoring the decrease in absorbance at 550 nm, 25 °C. The CO association kinetics is well described by a single exponential rate expression with a time constant, τ_{ass} of ~2.5 min at pH 12.6, 25 °C. Fig. 4b shows the fluorescence monitored normalized SDS titration of alkaline Ferrocyt *c* collected at pH ~12.6, 25 °C. Fig. 4c shows the common logarithm of k_{ass} for alkaline Ferrocyt *c* as a function of SDS (≤0.5 mM) and NaCl concentrations (Inset of Fig. 4c) at pH 12.6, 25 °C. Given the midpoint of SDS-titration of alkaline Ferrocyt *c* (C_m = 0.36 mM SDS) (Fig. 4b), these data provide an opportunity to analyze the dynamical behavior of alkaline Ferrocyt *c* in the subdenaturing and denaturing limits.

As SDS concentration is increased from 0.0 to 0.5 mM, the value of Log k_{ass} initially decreases, showing a broad minimum around 0.1-0.2 mM, and then increases (Fig. 4c). The initial decrease in the Log k_{ass} suggests that the motional freedoms or internal motions of alkali-denatured protein are reduced at lower concentrations of SDS (≤0.2 mM) that tend to block the CO association to protein. The increase in the Log k_{ass} in the presence of higher SDS concentration (≥0.2 mM) is attributed to the destabilization of alkali-denatured protein that facilitates the CO-association process. As NaCl concentration is increased, Log k_{ass} decrease

monoexponentially and plateau at ~1.0 M NaCl (Inset of Fig. 4c), which suggests that NaCl also constrains the internal dynamics of alkali-denatured protein.

To investigate these aspects further, we have determined the SDS and NaCl dependence of the activation enthalpy ($\Delta H^{\ddagger}_{ass}$) and activation entropy ($\Delta S^{\ddagger}_{ass}$) of the CO association process. If the internal dynamics of base-denatured protein is indeed constrained at some concentration of SDS or NaCl, then the $\Delta H^{\ddagger}_{ass}$ at that SDS or NaCl concentration will be relatively higher. Fig. 4d shows the Eyring plots for the CO association reaction of alkaline Ferrocyt *c* in the absence of additive and in the presence of 0.1 and 0.5 mM SDS, and 1.0 M NaCl. Fig. 4d also shows the Eyring plots for the CO association to native Ferrocyt *c* in the absence of additive at pH 7.0. Eyring plots were analyzed by linear least-squares analysis (Fig. 4d) (eq (5)) of the temperature dependent k_{ass} (*55*).

$$\ln(k_{ass}h/k_{B}T) = (\Delta S^{\ddagger}_{ass}/R) - (\Delta H^{\ddagger}_{ass}/RT) \qquad (5)$$

Table 1 summarizes the values of $\Delta H^{\ddagger}_{ass}$ and $\Delta S^{\ddagger}_{ass}$ for alkaline Ferrocyt *c* in the absence of additive and in the presence of 0.1 and 0.5 mM SDS, and 1.0 M NaCl. For comparison, Table 1 also summarizes the values of $\Delta H^{\ddagger}_{ass}$ and $\Delta S^{\ddagger}_{ass}$ for native Ferrocyt *c* at pH 7.0. Clearly, relative to in the absence of additives, the values of $\Delta H^{\ddagger}_{ass}$ for base-denatured protein are found higher at ~0.1 mM SDS and 1.0 M NaCl (Table 1). However, the $\Delta H^{\ddagger}_{ass}$ values for base-denatured protein at ~0.1 mM SDS and 1.0 M NaCl did not match to the $\Delta H^{\ddagger}_{ass}$ value measured for native protein at pH 7.0 (Table 1). These results clearly indicate that the internal dynamics of base-denatured protein at ~0.1 mM SDS and 1.0 M NaCl are more constrained relative to that in the absence of SDS and NaCl but are relatively less constrained than the native state (Table 1).

Table 1. SDS-dependent activation enthalpy ($\Delta H_{ass}^{\ddagger}$), activation entropy ($\Delta S_{ass}^{\ddagger}$) and conformational entropy loss ($\Delta\Delta S_{ass}^{\ddagger}$) for CO association reaction of Ferrocyt *c*.*

Additive	Additive concentration	$\Delta H_{ass}^{\ddagger}$	$\Delta S_{ass}^{\ddagger}$	$\Delta\Delta S_{ass}^{\ddagger}$
Control (pH 12.6)	0.0	19.5 (±0.2)	-4.0 (±0.3)	0.0
SDS (mM)	0.1	22.5 (±0.4)	2.7 (±0.4)	6.7 (±0.1)
	0.5	12.8 (±0.4)	-23.2 (±0.4)	-19.2 (±0.1)
NaCl (M)	1.0	22.0 (±0.1)	2.1 (±0.4)	6.1 (±0.1)
Control (pH 7.0)	0.0	26.0 (±0.1)	12.3 (±0.8)	16.3 (±0.5)

*$\Delta H^{\ddagger}_{ass}$, $\Delta S^{\ddagger}_{ass}$, and $\Delta\Delta S^{\ddagger}_{ass}$ are reported as kcal mol^{-1}, cal mol^{-1} K^{-1}, and cal mol^{-1} K^{-1}, respectively. The uncertainty (standard error) is indicated in parenthesis.

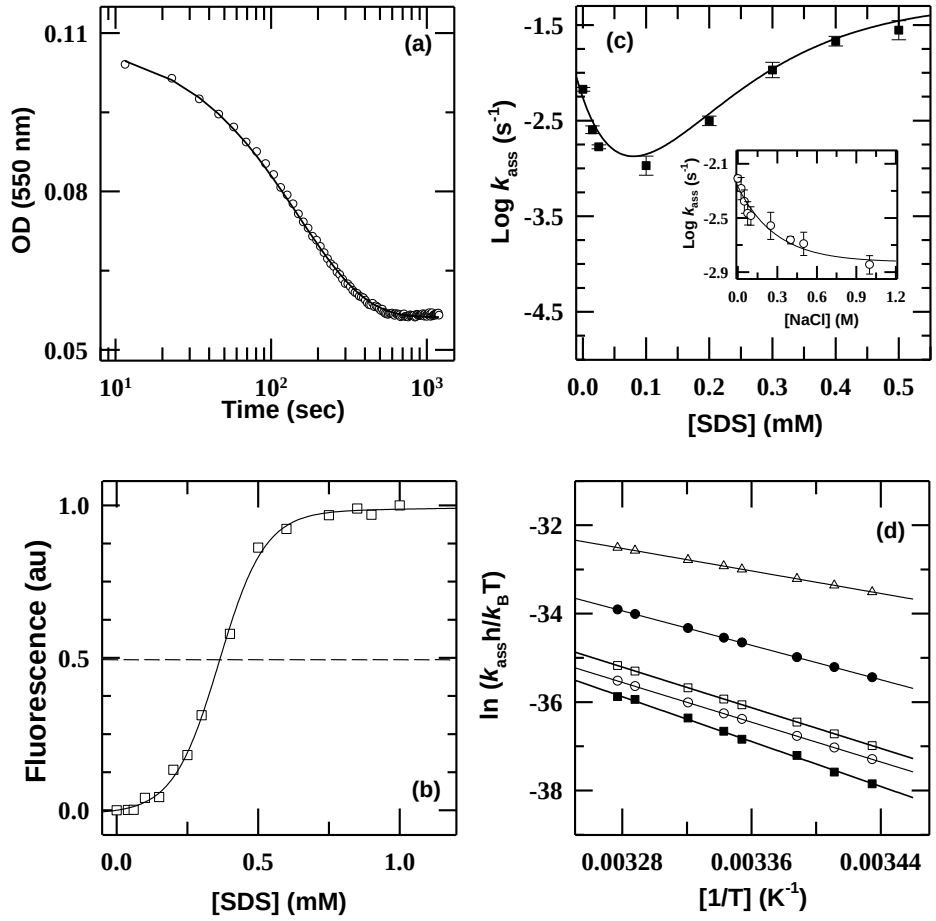

Fig. 4 (a) The slow single-phase CO association kinetic trace of alkaline Ferrocyt *c* (τ = 2.5 min, 0.0 mM SDS, pH 12.6, 25 °C). (b) SDS-titration of alkaline Ferrocyt *c* at 25 °C, pH 12.6. The solid line through the data in panel (b) has been drawn by inspection only. (c) Dependence of the rate of the CO association of alkaline Ferrocyt *c* (pH 12.6) with SDS (■) and NaCl (○) at 25 °C. The lines through the data have been drawn by inspection only. (d) SDS and NaCl concentrations dependence of the Eyring plot for the CO association reaction of alkaline Ferrocyt *c* at pH 12.6. Eyring plots were analyzed by linear least-squares analysis (Fig. 4d) (eq (5) (see text)) of the temperature dependence of k_{ass} (without SDS (●), $\Delta H^{\ddagger}_{ass}$ =19.5 kcal mol^{-1}; 0.1 mM SDS (○), $\Delta H^{\ddagger}_{ass}$ =22.5 kcal mol^{-1}; 1.0 M NaCl (□), $\Delta H^{\ddagger}_{ass}$ =22.0 kcal mol^{-1}; 0.5 mM SDS (Δ), $\Delta H^{\ddagger}_{ass}$ =12.8 kcal mol^{-1}. For comparison, panel (d) also shows Eyring plot for CO association reaction of native Ferrocyt *c* at pH 7.0 (■), $\Delta H^{\ddagger}_{ass}$ =26.0 kcal mol^{-1}.

7.2.6 Effects of submicellar concentrations of SDS on the internal dynamics of natively folded Cyt-CO (NCO-state) at pH 7.0

To evaluate the effects of submicellar concentrations of SDS (≤0.5 mM) on the internal dynamics of natively-folded compact state of Ferrocyt *c*, the rate coefficient of CO-dissociation (log k_{diss}) from the NCO-state were measured in the presence of various concentrations of SDS at pH 7.0, 25 °C. Fig. 5a presents the fluorescence monitored normalized SDS titration of native Ferrocyt *c* at pH 7.0, 25 °C (SDS denaturation midpoint of native Ferrocyt is ~1.3 mM). Fig. 5b shows the variation of Log k_{diss} as a function of SDS concentration (≤0.5 mM) at 25 °C, pH 7.0.

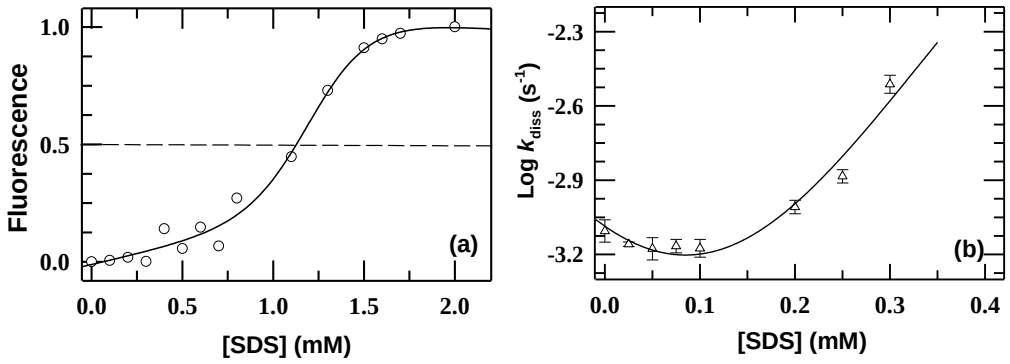

Fig. 5 (a) SDS-titration of native Ferrocyt *c* at 25 °C, pH 7.0. The solid line through the data in panel (a) has been drawn by inspection only. (b) Dependence of the rate of the CO dissociation of NCO at pH 7.0, 25 °C.

As the final concentration of SDS (≤0.5 mM) in the reaction medium is increased starting from strongly native like conditions, Log k_{diss} initially decreases, showing a broad minimum around 0.05-0.1 mM, and then increases (Fig. 5b). The decrease of Log k_{ass} at 0.1 mM SDS indicates that subdenaturing concentrations of SDS reduce the motional freedom of the protein and thus constrain the internal dynamics of the native protein at pH 7.0.

7.2.7 Effects of submicellar concentrations of SDS on the heat and cold denaturations of base-denatured proteins

The pH-denatured proteins can show cold denaturation process in the presence of low concentrations of salt (*18, 56*). Fig. 6a shows that when temperature is increased from -1 °C to 60 °C, the negative ellipticity in the far-UV CD spectrum of the base denatured Ferricyt *c* (0.01 M NaCl) is significantly lost, indicating the thermal denturation of base-denatured protein. This aspect allows us to determine the effects of submicellar concentrations of SDS on the heat and cold denaturations of base-denatured Ferricyt *c* at pH 12.8. An earlier report showed that the thermal denaturation of base-denatured Ferricyt *c* in the presence of low concentrations of NaCl (0.01 M NaCl) exhibits substantial reversibility (*18*). Fig. 6b shows that the thermal denaturation of base-denatured Ferricyt *c* shows partial reversibility (~80%) in the presence of ~ 0.4 mM SDS, pH 12.8. Fig. 6c shows the far-UV CD (222 nm) monitored normalized thermal unfolding curves for the base-denatured Ferricyt *c* at pH 12.8 in the presence of ~0.01 M NaCl, and ~0.05, 0.3, 0.5, and 0.6 mM SDS. Since the low temperature ellipticity values are dependent on SDS concentration while the high-temperature ones are not, so, the thermal denaturation data for base-denatured protein were normalized by using eq (6)

$$\theta = \frac{\theta_{obs} - (m_1 T + \theta_1)}{(m_2 T + \theta_2) - (m_1 T + \theta_1)} \quad (6)$$

where, θ_{obs} is the observed ellipticity, T is the temperature, m_1 and θ_1 are the slope and intercept, respectively, of the pre transition baseline, and m_2 and θ_2 are the slope and intercept of the post-transition baseline in the presence of a given concentration of SDS. The normalized thermal unfolding curves in Fig. 6c were analyzed by the Gibbs-Helmholtz equation (chapter 2, eqs (2) and (3)). Table 2 lists the T_m, ΔH_m and ΔC_p values for base-denatured Ferricyt *c* obtained at ~0.01 M NaCl, and ~0.05, 0.3, 0.5, and 0.6 mM SDS. At low SDS and salt concentrations, the base-denatured protein undergoes cold denaturation (Fig. 6c). With increasing SDS concentration, the low temperature unfolding transition becomes less obvious (Fig. 6c). The T_m values for the thermal unfolding of base denatured Ferricyt *c* increase with increasing concentration of SDS (≤0.6 mM) (Table 2), which indicates that the submicellar concentrations of SDS increases the secondary structure thermal stability of the base-denatured protein. Qi xu et al (2004) have also shown that the submicellar concentrations of SDS influence the secondary structure thermal stability of the acid-denatured Ferricyt *c* (*42*).

Fig. 6d presents the temperature dependent stability curves of base-denatured Ferricyt *c* in the presence of different SDS concentrations at submicellar level. These stability curves were calculated according to eq (7) or eq (8),

$$\Delta G = -RT \ln K_{app} = -RT \ln \left(\frac{\theta(T) - (m_1 T + \theta_1)}{(m_2 T + \theta_2) - \theta(T)} \right) \quad (7)$$

$$\Delta G = \Delta H_m \left(1 - \frac{T}{T_m} \right) + \Delta C_p \left(T - T_m - T \ln \left(\frac{T}{T_m} \right) \right) \quad (8)$$

The midpoint temperature, T_c for the low temperature denaturation at different SDS concentrations as read from the stability curves are also listed in Table 2. It is observed that even very small concentration of SDS has a profound effect on the temperature dependent stability curve. In all cases, addition of SDS makes the stability curves wider and raises the maxima (Fig. 6d). Fig. 6d and Table 2 clearly indicate that as SDS concentration is increased, the thermal denaturation temperature increase and the cold denaturation temperature decrease. Cold denaturation process typically occurs when the native protein is destabilized by either extremes of pH or denaturants (*55-56*). Cold denaturation phenomenon is typically based on the thermodynamic principles of protein stability (*56-57*) and generally arises due to decrease of hydrophobic interactions in proteins as temperature is lowered (*58*). However, few previous

reports reveal that both hydrophobic and hydrophilic interactions are accountable for cold denaturation (*59-60*).

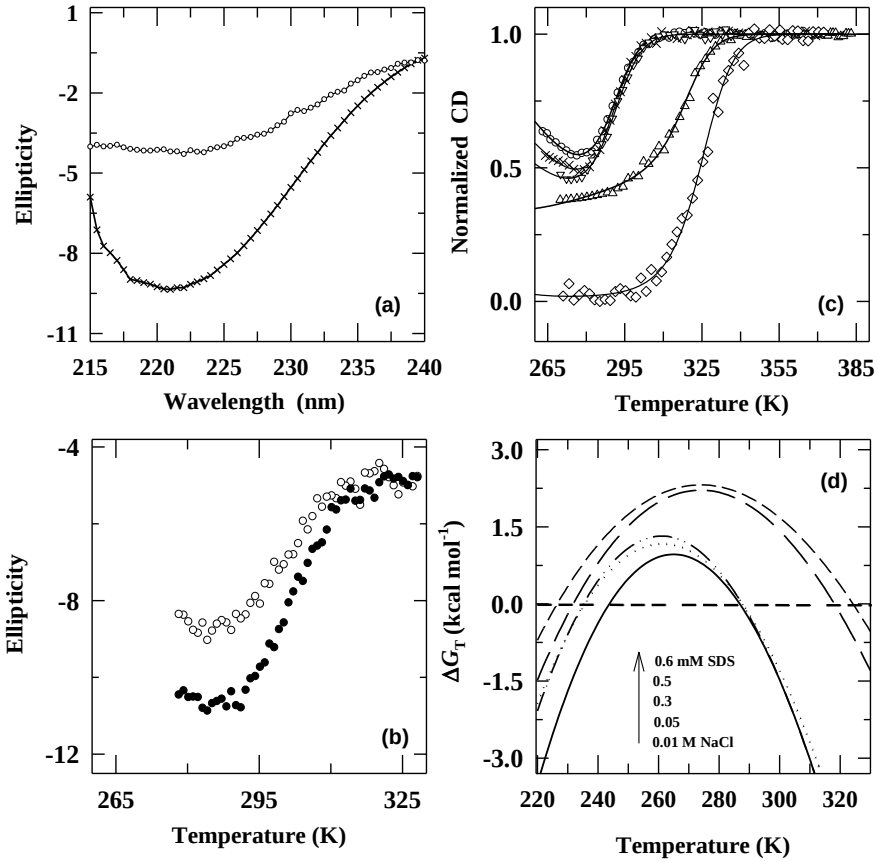

Fig. 6 (a) Far-UV CD spectra of base-denatured Ferricyt *c* (pH 12.8, 0.01 M NaCl) at −1.0 (⁎⁎⁎⁎) and 60.0 °C (○○○○). (b) Reversibility of thermal transitions of base-denatured Ferricyt *c* (pH 12.8, 0.4 mM SDS) monitored at CD 222 nm: (•) heating from 5 °C to 55 °C; and (○) cooling from 55 °C to 5 °C. (c) CD-222 nm monitored thermal unfolding curves of base denatured Ferricyt *c*, pH~12.8: 0.01 mM NaCl (○), 0.05 mM SDS (×), 0.3 mM SDS (∇), 0.5 mM SDS (Δ), and 0.6 mM SDS (◊). The solid curves in panel (c) represent the non-linear fit of the data to Gibb's Helmholtz equation (chapter 2, eqs (2) and (3)). (d) Temperature dependent stability curves of the base-denatured Ferricyt *c* (pH 12.8) in the presence of 0.01 mM NaCl (solid line), 0.05 mM SDS (dotted line), 0.3 mM SDS (dash double dot line), 0.5 mM SDS (long dash line), and 0.6 mM SDS (short dash line).

Table 2. SDS dependence of the T_m, ΔH_m, ΔC_p and T_c for thermal unfolding (CD 222 nm) of base-denatured Ferricyt *c*.*

Additive	Conc.	T_m	ΔH_m	ΔC_p	T_c
NaCl	0.01 M	286.8	25.0	1.1	243
SDS	0.05 mM	287.7	28.0	1.0	234
SDS	0.3 mM	288.1	30.0	0.9	234
SDS	0.5 mM	318.2	31.0	0.7	231
SDS	0.6 mM	324.3	29.0	0.5	226

* T_m, ΔH_m and ΔC_p are reported as K, kcal mol^{-1} and kcal mol^{-1} K^{-1}. The uncertainty in the values of T_m, ΔH_m and ΔC_p are ±0.5 K, ±2.0 kcal mol^{-1} and ±0.2 kcal mol^{-1}K^{-1}, respectively.

7.2.8 Effects of submicellar concentrations of SDS on the thermal stability of native Ferricyt c

Thermal unfolding transition of Ferricyt *c* probed by the far-UV CD at 222 nm can typically provide the secondary structure thermal stability of Ferricyt *c* (6*1-62*). Fig. 7 present the far-UV CD (222 nm) monitored normalized thermal unfolding curves of native Ferricyt *c* measured in the absence and presence of ~0.25 and 0.5 mM SDS at pH 7.0. The thermal unfolding curves of native Ferricyt *c* were analyzed for T_m, ΔH_m, and ΔC_p by using a non-linear least squares method according to Gibbs-Helmholtz equation (chapter 2, eqs (2) and (3)) (*5*). The resulting T_m, ΔH_m, and ΔC_p values at different SDS concentrations are provided in Table 3. As SDS concentration is increased from 0.0 to 0.5 mM, the value of T_m for native Ferricyt *c* decreases by ~19 °C, indicating that the submicellar concentrations of SDS decrease the secondary structure thermal stability of native Ferricyt *c* at pH 7.0.

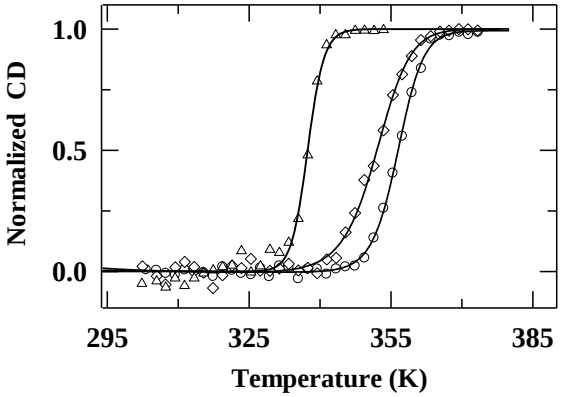

Fig. 7 Far-UV CD (222 nm) monitored thermal unfolding curves of native Ferricyt *c* at pH ~7.0: 0.0 (○), 0.25 mM SDS (◊), and 0.5 mM SDS (Δ).The solid curves represent the non-linear fit of the data to Gibb's Helmholtz equation (chapter 2, eqs (2) and (3)).

Table 3 SDS dependence of the T_m, ΔH_m and ΔC_p for thermal unfolding (CD 222 nm) of native Ferricyt *c**

SDS (mM)	T_m	ΔH_m	ΔC_p
0	356.4	76.7	1.3
0.25	351.8	56.2	1.3
0.5	337.6	80.0	1.4

* T_m, ΔH_m and ΔC_p are reported as K, kcal mol^{-1} and kcal mol^{-1} K^{-1}. The uncertainty in the values of T_m, ΔH_m and ΔC_p are ±0.5 K, ±2.0 kcal mol^{-1} and ± 0.2 kcal mol^{-1}K^{-1}, respectively.

7.3 Conclusion

This chapter analyzes the effect of submicellar concentrations of SDS (≤0.6 mM) on the structural, kinetic, and thermodynamic properties of native and base-denatured states of horse Cyt *c*. The major finding in this chapter is that the submicellar concentrations of SDS (≤0.4 mM) refold and stabilize

the base-denatured Ferricyt *c* to MG_{SDS}-state, which resembles the generic properties of MG-state. Single Trp59 fluorescence experiments show that the base-denatured Ferricyt *c* undergoes molecular compaction in the presence of 0.2 mM SDS. Far-UV and near-UV CD experiments reveal that the fully populated MG_{SDS}-state (0.4 mM SDS) acquires significant content of secondary structure without gaining the tertiary structure. Collective motions of the M80 containing Ω-loop of Ferrocyt *c* control the CO association with alkaline Ferrocyt *c* at pH 12.6 and CO-dissociation from the natively-folded Cyt-CO (NCO-state) at pH 7.0. Kinetic and thermodynamic parameters measured for CO association reaction of alkaline Ferrocyt *c* at pH 12.6 and CO dissociation reaction of NCO at pH 7.0 in the presence of different concentrations of SDS indicate that subdenatuaring concentrations of SDS (≤ 0.2 mM) restrict the internal dynamics of base-denatured and native states of Ferrocyt *c*. Analysis of the CD-222 nm monitored thermal denaturation curves of base-denatured Ferricyt *c* at pH 12.8 and native Ferricyt *c* at pH 7.0 measured in the presence of different concentrations of SDS (≤0.6 mM) indicates that the submicellar concentrations of SDS (≤0.6 mM) increase the secondary structure thermal stability for the base-denatured protein but decrease it for the native protein.

7.4 References

1. Arai, M., and Kuwajima, K. (2000) *Adv. Protein Chem.* **53**, 209-282.
2. Ptitsyn, O.B. (1995) *Adv. Protein Chem.* **47**, 83-229.
3. Goto, Y., and Fink, A.L. (1989) *Biochemistry* **28**, 945-952.
4. Rao, D.K., Kumar, R., Yadaiah, M., and Bhuyan, A.K. (2006) *Biochemistry* **45**, 3412-3420.
5. Kumar, R., Prabhu, N.P., Rao, D.K., and Bhuyan, A.K. (2006) *J. Mol. Biol.* **364**, 483-495.
6. Bhuyan, A.K. (2010) *Biochemistry* **49**, 7774-7782.
7. Bhuyan, A.K. (2010) *Biochemistry* **49,** 7764-7773.
8. Nakamura, S., Seki, Y., Katoh, E., and Kidokoro, S. (2011) *Biochemistry* **50**, 3116-3126.
9. Kuwajima, K. (1989) *Proteins* **6**, 87–103.
10. Goto, Y., and Nishikori, S. (1991) *J. Mol. Biol.* **222**, 679-686.
11. Griko, Y.V., and Privalov, P.L. (1994) *J. Mol. Biol.* **235**, 1318-1325.
12. Kamiyama, T., Sadahide, Y., Nogusa, Y., and Gekko, K. (1999) *Biochim. Biophys. Acta* **1434**, 44–57.

13. Davis-Searles, P.R., Morar, A.S., Saunderes, A.J., Erie, D.A. and Pielak, G.J. (1998) *Biochemistry* **37**, 17048-17053.
14. Saunderes, A.J., Davis-Searles, P.R., Allen, D.L., Pielak, G.J., and Erie, D.A. (2000) *Biopolymers* **53**, 293-307.
15. Hamada, D., Kidokoro, S., Fukada, H., Takahashi, K., and Goto, Y. (1994) *Proc. Natl. Acad. Sci. USA* **91**, 10325-10329.
16. Kuroda, Y., Kidokoro, S., and Wada, A. (1992) *J. Mol. Biol.* **223**, 1139-1153.
17. Nishii, I., Kataoka, M., Tokunaga, F., and Goto, Y. (1994) *Biochemistry* **33**, 4903–4909.
18. Jain, R., Kaur, S., and Kumar, R. (2013) *J. Biochem.* **153**, 161–177.
19. Hagihara, Y., Tan, Y., and Goto, Y. (1994) *J. Mol. Biol.* **237**, 336-348.
20. Markus, G., and Karush, F. (1957) *J. Am. Chem. Soc.* **79**, 3264–3269.
21. Moriyama, Y., Kawasaka, Y., and Takeda, K. (2003) *J. Colloid Interf. Sci.* **257**, 41–46.
22. Das, T.K., Mazumdar, S., and Mitra, S. (1998) *Eur. J. Biochem.* **254**, 662-670.
23. Naeem, A., and Khan, R.H. (2004) *Int. J. Biochem. Cell Biol.* **36**, 2281-2292.
24. Shapiro, A.L., Vinuela, E., and Maizel, J.V. (1967) *Biochem. Biophys. Res. Commun.* **28**, 815–820.
25. Weber, K., and Osborn, M. (1969) *J. Biol. Chem.* **244**, 4406–4412.
26. Shirahama, K., Tsujii, K., and Takagi, T. (1974) *J. Biochem.* **75**, 309–319.
27. Robinson, N., and Tanford, C. (1975) *Biochemistry* **14** 369–378.
28. Reynolds, J.A., and Tanford, C. (1970) *Proc. Natl. Acad. Sci. USA* **66**, 1002–1007.
29. Patil, S.M., Xu, S., Sheftic, S.R., and Alexandescu, A.T. (2009) *J. Biol. Chem.* **284**, 11982–11991.
30. Ulmer, T.S., Bax, A., Cole, N.B., and Nussbaum, R.L. (2005) *J. Biol. Chem.* **280**, 9595–9603.
31. Ulmer, T.S., and Bax, A. (2005) *J. Biol. Chem.* **280**, 43179–43187.
32. Coles, M., Bicknell, W., Watson, A.A., Fairlie, D.P., and Craik, D.J. (1998) *Biochemistry* **37**, 11064–11077.
33. Chandra, S., Chen, X., Rizo, J., Jahn, R., and Sudhof, T.C. (2003) *J. Biol. Chem.* **278**, 15313–15318.
34. Jarvet, J., Zdunek, J., Damberg, P., and Graslund, A. (1997) *Biochemistry* **36**, 8153–8163.

35. Gangabadage, C.S., Najda, A., Bogdan, D., Wijmenga, S.S., and Tessari, M. (2008) *J. Phys. Chem. B* **112**, 4242–4245.
36. Bhuyan, A.K. (2009) *Biopolymers* **93**, 186–199.
37. Turro, N.J., Lei, X., Ananthapadmanabhan, K.P., and Aronson, M. (1995) *Langmuir* **11**, 2525–2533.
38. Gelamo, E.L., and Tabak, M. (2000) *Spectrochim. Acta A* **56**, 2255–2271.
39. Moosavi-Movahedi, A.A., Chamani, J., Goto, Y., and Hakimelahi, G.H. (2003) *J. Biochem.* **133**, 93–102.
40. Prasanna Kumari, N.K., and Jagannadham, M.V. (2011) *Colloids Surf. B. Biointerfaces* **82**, 609-615.
41. Chattopadhyay, K., and Mazumdar, S. (2003) *Biochemistry* **42**, 14606-14613.
42. Xu, Q., and Keiderling, T.A. (2004) *Protein Science* **13**, 2949–2959.
43. Xu, Q., and Keiderling, T.A. (2006) *Proteins: struc., func. and bioinf.* **63**, 571-580.
44. Vanderkooi, J.M., and Erecinska, M. (1975) *Eur. J. Biochem.* **60**, 199-207.
45. Tsong, T.Y. (1974) *J. Biol. Chem.* **249**, 1988-1990.
46. Goto, Y., Takahashi, N., and Fink, A.L. (1990) *Biochemistry* **29**, 3480-3488.
47. Pace, C.N. (1975) *CRC Crit. Rev. Biochem.* **3**, 1-43.
48. Davies, A.M., Guillemette, J.G., Smith, M., Greenwood, C., Thurgood, A.G.P., Mauk, A.G., and Moore, G.R. (1993) *Biochemistry* **32**, 5431-5435.
49. Ptitsyn, O.B. (1995) *TIBS* **20**, 376–379.
50. Goto, Y., Calciano, L.J., and Fink, A.L. (1990) *Proc. Natl. Acad. Sci. USA* **87**, 573-577.
51. Kumar, R., Prabhu, N.P., Yadaiah, M., and Bhuyan, A.K. (2004) *Biophys. J.* **87** 2656-2662.
52. Banci, L., Bertini, I., Huber, J.G., Spyroulias, G.A., and Turano, P. (1999) *J. Biol. Inorg. Chem.* **4**, 21-31.
53. Morgan, J.D., and McCammon, J.A. (1983) *Biopolymers* **22**, 1579-1593.
54. Berghuis, A.M., and Brayer, G.D. (1992) *J. Mol. Biol.* **223,** 959-976.
55. Miksovská, J., Day, J.H., and Larsen, R.W. (2003) *J. Biol. Inorg. Chem.* **8**, 621-625.
56. Privalov, P.L. (1990) *Crit. Rev. Biochem. Mol. Biol.* **25**, 281–305.
57. Privalov, P.L. (1979) *Adv. Protein Chem.* **33**, 167-241.
58. Murphy, K.P., and Freire, E. (1992) *Adv. Protein Chem.* **43**, 313–361.
59. Makhatadze, G.I., and Privalov, P.L. (1995) *Adv. Protein Chem.* **47**, 307–425.

60. Spolar, R.S., Livingstone, J.R., and Record, M.T. (1992) *Biochemistry* **31**, 3947–3955.
61. Allen, D.L., and Pielak, G.J. (1998) *Prorein Sci.* **7**, 1262-1263.
62. Uchiyama, S., Oshima, A., Nakamura, S., Hasegawa, J., Terui, N., Takayama, S.J., Yamamoto, Y., Sambongi, Y., and Kobayashi, Y. (2004) *J. Am. Chem. Soc.* **126**, 14684-14685.

Chapter 8

Analysis of the pH-Dependent Stability and Folding Dynamics of Proteins

8.1 Introduction

From long ago, biochemists are interested to study the pH-dependence of thermodynamic stability of proteins. In general, the proteins have maximum conformational stability near neutral pH or near their isoelectric points (*1-2*). At extremely acidic or basic pH values, the conformational stability of proteins decreases significantly. Linderstrom-Lang in 1924 for the first time suggested a probable reason for the decreased thermodynamic stability of the proteins at extremely acidic or basic pH values (*2*). At extremely acidic pH values, the protonations of protein groups can lead to the unfavorable electrostatic interactions among the positively charged groups of proteins, which results in the decrease of thermodynamic stability of proteins. Similarly, at extremely basic pH values, the deprotonations of basic amino acid groups can produce the unfavorable electrostatic interactions among the negatively charged groups of proteins, and thus decrease the thermodynamic stability of proteins (*1-3*).

Increasing evidences indicate that the ionizable amino acid groups of proteins play important roles in protein solubility, folding, stability, binding ability, and catalytic activity (*4-9*). Generally, the pH of reaction medium changes the thermodynamic stability of proteins by altering the charges of ionizable amino acid groups of proteins through protonations and deprotonations (*3*). The pH dependence of thermodynamic stability reflects the contribution of electrostatic interactions, which are of great importance for protein structure and function (*10-11*). From the last few decades, there is a fundamental interest in developing theoretical models for the correct assessment of electrostatic interactions involving conformational changes (*12-15*) and their contribution to protein stability (*12, 16-20*). The pK_a values of the ionizable residues are the basis for understanding the pH-dependent characteristics of proteins (*21*). The electrostatic free energy contribution of an ionizable group is related to its pK_a in the folded and unfolded states (*17, 22-23*). Any electrostatic effect from an ionizable group will lead to a pKa shift between the folded and unfolded states (*17, 22-23*). The pK_a values of proteins can be computed by a number of ways such as by the utilization of the free energies from molecular

dynamic simulations or by numerical solutions of the linearized-Poisson-Boltzmann equation (*19, 24-28*).

Ionic interactions among the charged residues play crucial roles in stability and folding of proteins (*10, 29-32*). Campos et al (2010) have recently studied the effect of pH on structure of prion protein (PrP) by computational methods and demonstrated that the low pH (pH ~2.0) can trigger the misfolding in PrP (*33*). Recent pH-dependent theoretical and experimental investigations on PrP have revealed that the low pH triggered misfolding transition of PrP could be reversed by increasing the pH back to 7.0 (*34-35*). The pH dependence of thermodynamic stability of proteins has been widely studied (*17,25,29-32,36-58*), however, the pH dependence of folding kinetics of proteins has received lesser attention (*49-56*). Fersht and coworkers have analyzed the pH-dependency on folding and unfolding kinetics of CI-2 and barnase (*56*). Raleigh and coworkers have shown that the comparison of pH-dependent protein stability profiles and folding rates can provide the information about the development of electrostatic interactions in the transition state of folding (*49,53,55*).

This chapter investigates the pH dependence of stability of horse Cyt *c* and hen Lyz and folding dynamics of horse Cyt *c*. Two-state thermodynamic analysis of the thermal and chemical denaturant (urea or GdnHCl)-induced unfolding transitions of Ferricyt *c*, Ferrocyt *c* and Lyz measured at several different pH values, ranging from pH 3.0 to pH 13.0 demonstrates that Cyt *c* and Lyz have maximum thermodynamic stability between pH 8.0-9.5 and pH ~4.0, respectively. The theoretically predicted electrostatic unfolding energies of Ferricyt *c* and Lyz over the pH range from 0.0 to 14.0 also suggest that the Ferricyt *c* and Lyz have maximum stability at pH ~8.0 and pH ~4.0, respectively. At relatively higher basic pH values (pH>10), the unfavorable interactions among the negatively charged groups while at acidic pH (pH<5.0), the unfavorable interactions among the positively charged groups decrease the thermodynamic stability of Cyt *c*. In stopped flow experiments, denaturant-unfolded Ferrocyt *c* in refolding buffer at pH 7.0 and pH 12.7 refold rapidly to the native-state. In order to probe the development of electrostatic interactions in the transition state of folding, this chapter compares the pH-dependent stability profiles and folding rates of Ferrocyt *c*. Between pH 7.0 and pH 12.7, the activation free energy barrier for folding of Ferrocyt *c* varies less than 1.0 kcal mol^{-1}, while the folding free energy which is estimated by GdnHCl-induced unfolding experiments of Ferrocyt *c* varies more than 9.0 kcal mol^{-1}. This finding reveals that on changing the pH from pH 7.0 to pH 12.7, the large

change in thermodynamic stability of protein is not strongly reflected in the refolding rates. The classic Wyman-Tanford (WT) linkage relation was used to estimate the β^{pH}-value (*i.e.*, $\Delta\nu^{\ddagger}(pH)/\Delta\nu(pH)$ ratio, where $\Delta\nu^{\ddagger}$ (pH), and $\Delta\nu$ (pH) are the differences in the number of protons bound to the transition and unfolded states, and folded and unfolded states, respectively) for folding of Ferrocyt *c* between pH 7.0 and pH 12.7. The β^{pH}-value was found to be less than 0.1, indicating that the electrostatic interactions are weakly formed in the transition state for folding.

8.2 Results and Discussion

8.2.1 pH-induced unfolding of Cyt c

Because of excitation energy transfer from lone Trp59 to the heme, the native state of Cyt *c* is fluorescence-silent (*59*). Unfolding results in increase in heme-tryptophan distance due to molecular expansion (*59-60*). Fig. 1a shows the fluorescence-monitored normalized alkaline pH-titrations of Ferricyt *c* and Ferrocyt *c* at 25 °C which clearly indicates that between pH 7.0 and pH 13.5, Ferrocyt *c* possesses similar structural integrity but the Ferricyt *c* is almost denatured at pH >12.6. Fig. 1b presents the fluorescence-monitored normalized acidic pH-titration of Ferricyt *c*, which indicates that Ferricyt *c* is significantly denatured at pH <2.5. The pH-induced normalized unfolding transitions of Ferricyt *c* (Fig. 1a and Fig. 1b) were analyzed by using the transformed Henderson-Hasselbalch equation (chapter 2 eq (4)) (*61*). The fit of data in Fig. 1a to eq (4) (chapter 2) provides the number of OH^- titrated ~3.0 and pH-midpoint ~12.5. Similarly, the fit of data in Fig. 1b to eq (4) (chapter 2) gives the number of H^+ titrated ~3.0 and pH-midpoint ~2.5.

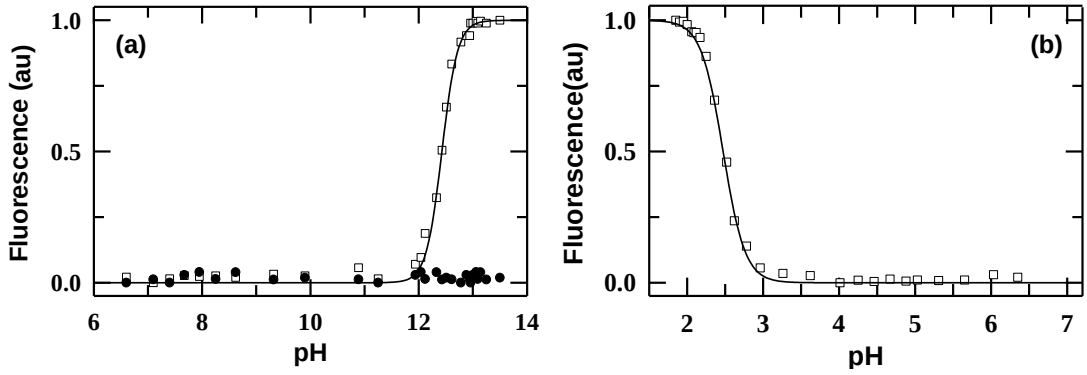

Fig. 1. (a) Fluorescence monitored alkaline-pH titration of Ferricyt *c* (□) and Ferrocyt *c* (●), 25 °C. (b) Fluorescence monitored acidic-pH titration of Ferricyt *c* (□), 25 °C. The solid lines represent the fit of the data to Handerson Hasalbalch equation (chapter 2, eq (4)) (*61*).

8.2.2 pH-dependent global and local (Fe^{2+}-M80 bond) stability of Cyt c in water-denaturant solutions

Denaturant-induced equilibrium unfolding transition of Cyt *c* probed by the excitation energy transfer from the lone Trp59 to the iron of heme can typically provide the global stability of Cyt *c* (*60,62-64*). Fig. 2a and Fig. 2b show the fluorescence-monitored pH-dependent normalized denaturant-unfolding curves of Ferricyt *c* and Ferrocyt *c*, respectively measured at several different pH values at 25 °C. Denaturant-induced equilibrium unfolding transition of Ferrocyt *c* measured by monitoring the heme absorption at 550 nm (α-band) can typically provide the local stability of the Fe^{2+}-M80 bond of Ferrocyt *c* (*63,65*).

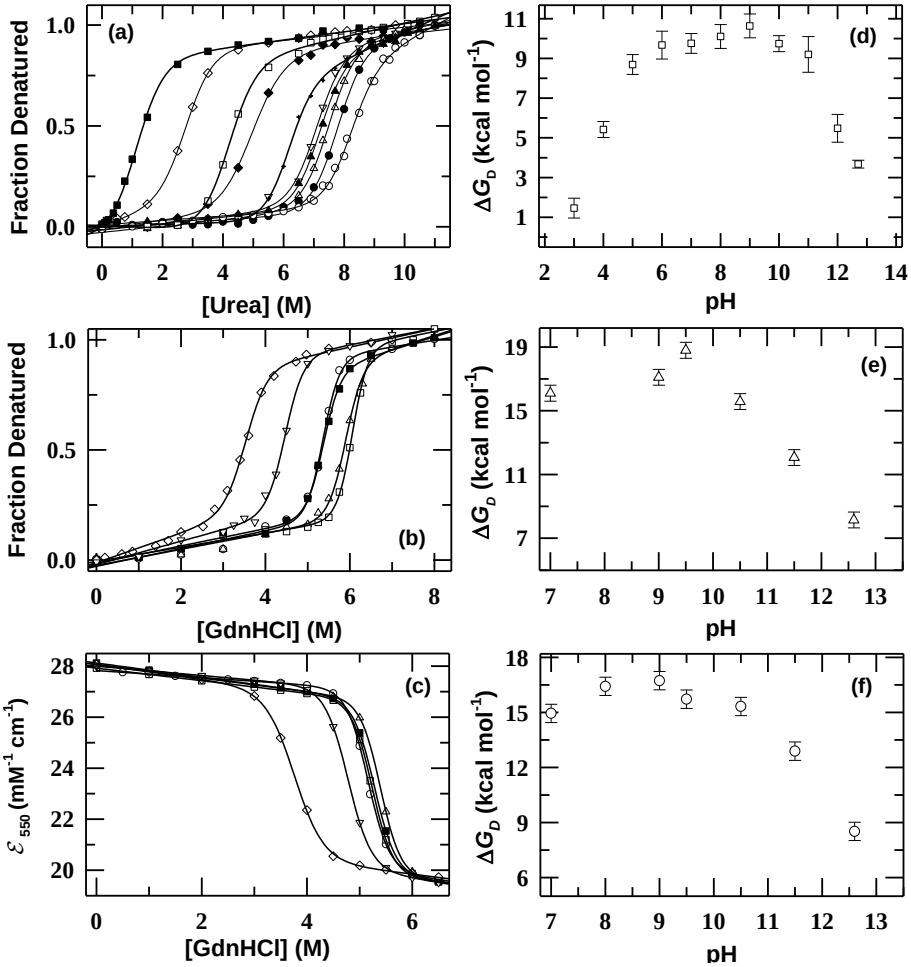

Fig. 2. (a) Fluorescence monitored normalized urea-induced equilibrium unfolding curves of Ferricyt *c* at different pH values ranging from pH 3 to pH 13; pH 3 (■), pH 4 (□), pH 5 (+), pH 7 (▲), pH 8 (●), pH 9 (○), pH 10 (Δ), pH 11 (∇), pH 12 (♦), and pH 12.7 (◊). (b) Fluorescence monitored normalized GdnHCl-induced equilibrium unfolding curves of Ferrocyt *c* measured at pH 7 (○), pH 9 (Δ), pH 9.5 (□), pH 10.5 (■), pH 11.5 (∇) and pH 12.6 (◊). (c) The absorbance monitored GdnHCl-induced equilibrium denaturation curves of Ferrocyt *c* represented as change in extinction coefficient at 550 nm measured at pH 7 (○), pH 9 (Δ), pH 9.5 (□), pH 10.5 (■), pH 11.5 (∇) and pH 12.6 (◊) (25 °C). The solid lines in panels (a), (b), and (c) represents the non-linear fit of the data to two-state equation (chapter 2, eq (5)) (*66*). (d) Variation of ΔG_D obtained from fluorescence monitored urea-induced equilibrium

unfolding curves of Ferricyt *c* with pH. (e) Variation of ΔG_D obtained from fluorescence monitored GdnHCl-induced equilibrium unfolding curves of Ferrocyt *c* with pH. (f) Variation of ΔG_D obtained from heme absorption (550 nm) monitored GdnHCl-induced equilibrium denaturation curves of Ferrocyt *c* with pH.

Fig. 2c shows the heme absorption (550 nm) monitored normalized GdnHCl–induced unfolding curves of Ferrocyt *c* measured at several different pH values at 25 °C. Two-state analysis of the denaturant-induced unfolding curves of Ferricyt *c* (Fig. 2a and Table 1) and Ferrocyt *c* (Fig. 2b,c and Tables 1-2) (*66*) at different pH values yields the denaturation free energy, ΔG_D and surface area exposed by solvent, m_g (Tables 1-2) for global and local changes of protein. The denaturant unfolding midpoints, C_m ($=\Delta G_D/m_g$) at different pH values were also calculated (Tables 1-2).

The available data from the two probes (W59 fluorescence and absorbance 550 nm) employed suggest that the equllibrium unfolding of Ferrocyt *c* involves only the native and the unfolded states without accumulation of structural intermediates to any detectable level. This conclusion is reached only within the limit and the resolution of equilibrium unfolding experiments. There are perhaps several short lived partially unfolded forms of Ferrocyt *c*, and at least one of these states is identifiable by stopped-flow NMR hydrogen exchange measurements under moderate to strongly destabilizing conditions (*67*). As pH is increased from pH 3.0 to pH 13.0, the values of ΔG_D (based on Trp59 fluorescence and heme absorption (550 nm)) initially increases, reaches a maximum at pH 9.0-9.5 and then decreases (Fig. 2d,e,f). Clearly, relative to neutral pH, the values of ΔG_D (based on Trp59 fluorescence and heme absorption (550 nm)) are found to be more at alkaline pH 9.0-9.5 (Fig. 2d,e,f and Tables 1-2), which suggests that the Cyt *c* has maximum global and local (Fe^{2+}-M80 bond) stabilities at alkaline pH ~9.0. This result is consistent with an earlier report that showed that the yeast iso-2 Ferricyt *c* has maximum global stability between pH 9.0 and 10.0 (*68*). The increase in stability of the yeast iso-2 Ferricyt *c* at high pH has been attributed to the pH-induced conformational changes of the protein (*68*).

At relatively higher basic pH (pH >10.0), the deprotonations of basic amino acid groups of Cyt *c* result in the unfavorable interactions amongst the negatively charged groups. As a consequence, the ΔG_D values (based on Trp59 fluorescence and heme absorption (550 nm)) are decreased at extreme alkaline pH conditions (Fig. 2d,e,f and Tables 1-2). Between pH 3.0 and pH 6.0, the protonations of acidic amino acid groups of Ferricyt *c* also lead to the unfavorable interactions amongst the positively charged groups, which result in decrease of the ΔG_D value of Ferricyt *c* (based on Trp 59 fluorescence) at extreme acidic pH (Fig. 2d and Table 1). Table 1 and Table 2 show the pH dependence of m_g-values of Ferricyt *c* and Ferrocyt *c*, respectively. For

both Ferricyt *c* and Ferrocyt *c*, the m_g-values are not greatly changed up to pH ~11.5 but above this pH the m_g-values are slightly decreased (Tables 1-2). Decrease of the m_g values at alkaline pH relative to neutral pH 7.0 are likely due to relatively small solvent accessible area in the denatured state of protein at pH ≥11.5. Deviation from two-state folding can also lead to lower m_g-values (*69*). Thus, it is also possible that the folding of Cyt *c* is not two-state at extreme alkaline pH.

Table 1. Dependence of the ΔG_D, m_g, and C_m on pH for Ferricyt *c* and Ferrocyt *c*, as monitored by Trp fluorescence (ex: 280; em: 365/360 nm)*.

Ferricyt *c*				Ferrocyt *c*			
pH	C_m (M)	ΔG_D (kcal mol^{-1})	m_g (kcal mol^{-1} M^{-1})	pH	C_m (M)	ΔG_D (kcal mol^{-1})	m_g (kcal mol^{-1} M^{-1})
3	1.1	1.5	1.30	7.0	5.4	16.1	3.0
4	4.2	5.4	1.30	9.0	5.9	17.1	2.9
5	6.1	8.7	1.42	9.5	6.1	18.8	3.1
6	7.0	9.7	1.38	10.5	5.4	15.6	2.9
7	7.2	9.8	1.36	11.5	4.5	12.1	2.7
8	7.8	10.1	1.30	12.7	3.5	8.1	2.3
9	8.2	10.6	1.30				
10	7.5	9.7	1.30				
11	7.1	9.2	1.30				
12	5.0	5.5	1.10				
12.7	2.8	3.7	1.12				

*The uncertainties associated with ΔG_D, m_g, and C_m are ±0.5 (kcal mol^{-1}), ±0.2 (kcal mol^{-1} M^{-1}), and ±0.2 (M), respectively.

Table 2. Dependence of the ΔG_D, m_g and C_m on pH, monitored by absorbance (550 nm) for Ferrocyt *c*.

pH	C_m (M)	ΔG_D (kcal mol^{-1})	m_g (kcal M^{-1} mol^{-1})
7	5.2	14.9	2.9
8	5.5	16.4	3.0
9	5.4	16.7	3.1
9.5	5.2	15.7	3.0
10.5	5.3	15.3	2.9
11.5	4.8	12.9	2.7
12.7	3.7	8.5	2.3

*The uncertainties associated with ΔG_D, m_g, and C_m are ±0.5 (kcal mol^{-1}), ±0.2 (kcal mol^{-1} M^{-1}), and ±0.2 (M), respectively.

8.2.3 pH-dependent global stability of Lyz in water-denaturant solutions

Fig. 3a shows the fluorescence monitored normalized GdnHCl-unfolding curves of Lyz measured at six different pH values, in the range from pH 7.0 to pH 13.0. The fluorescence monitored normalized GdnHCl-unfolding curves of Lyz measured at five different pH values, in the range from pH 7 to pH 2 is shown in Fig. 3b. The G_D and m_g values at different pH were calculated by two-state analysis (chapter 2, eq (5)) of the GdnHCl-induced unfolding curves of

Lyz (*66*) (Table 3). The C_m (= $\Delta G_D/m_g$) values were also calculated at different pH values and are plotted in Fig. 3d as a function of pH (Table 3). It is clear from Fig. 3c and Fig. 3d that as the pH of the solution is increased from pH 2.0 to pH 13, the values of ΔG_D and C_m initially increase up to pH ~4 and then decrease. This finding indicates that the Lyz has maximum thermodynamic stability at pH ~4.0. An earlier report shows that the Lyz produced by the bacteriophage T4 is also maximally stable near pH ~5.0 (*3*). Relative to pH 7.0, at extreme acidic (pH ≤4) or basic pH (pH >11), the value of m_g increased significantly (Table 3). This indicates a relatively more solvent accessible area of protein in the acidic- or basic-conditions than that of the native pH conditions.

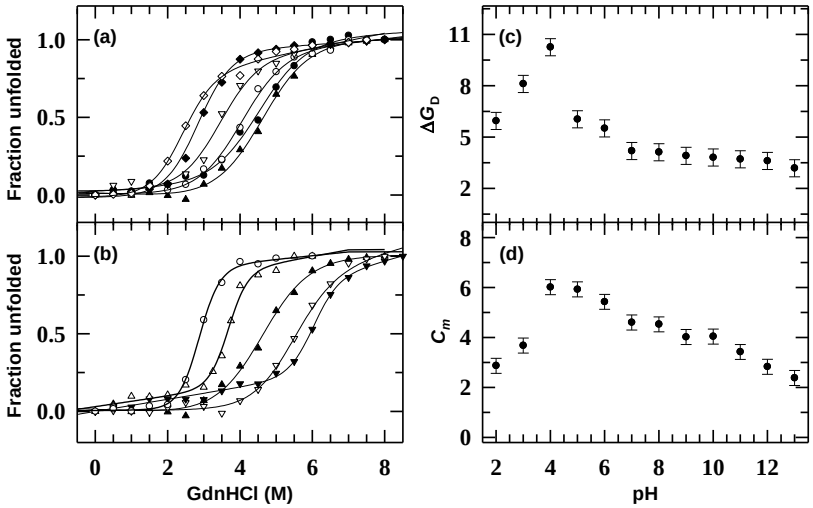

Fig. 3. (a) Fluorescence monitored normalized GdnHCl-induced equilibrium unfolding curves of Lyz at different pH values ranging from pH 7.0 to 13 ; pH 7 (▲), pH 8 (●), pH 9 (○), pH 11 (∇), pH 12 (♦), and pH 13 (◊), (b) fluorescence monitored urea-induced equilibrium unfolding curves of Lyz at various pH values from pH 2.0 to pH 7.0; pH 7 (▲), pH 6 (∇), pH 4 (▼), pH 3 (Δ), and pH 2 (○). The solid lines in panels (a) and (b) represents the non-linear fit of the data to two-state equation (chapter 2, eq (5)) (*66*). (c) and (d) Variation of ΔG_D and C_m, respectively, obtained from GdnHCl induced equilibrium unfolding curves of Lyz at different pH values.

Table 3. Dependence of the ΔG_D, m_g and C_m on pH for Lyz, as monitored by Trp fluorescence (ex: 280; em: 365 nm)*.

pH	C_m (M)	ΔG_D (kcal mol^{-1})	m_g (kcal mol^{-1} M^{-1})
2	2.9	5.9	2.1
3	3.7	8.1	2.2
4	6.0	10.3	1.7
5	5.9	6.0	1.0
6	5.4	5.5	1.0
7	4.6	4.2	0.9
8	4.5	4.1	0.9
9	4.0	3.9	1.0
10	4.0	3.8	0.9
11	3.4	3.7	1.1
12	2.8	3.6	1.3
12.7	2.4	3.2	1.3

*The uncertainties associated with ΔG_D, m_g, and C_m are ±0.5 (kcal mol^{-1}), ±0.2 (kcal mol^{-1} M^{-1}), and ±0.2 (M), respectively.

8.2.4 pH-dependent secondary structure and Fe^{2+}-M80 linked thermal stability of Cyt c in aqueous solutions

Thermal unfolding transition of Cyt *c* probed by the far-UV CD at 222 nm can typically provide the secondary structure thermal stability of Cyt *c* (*70-71*). Fig. 4a and Fig. 4b present the far-UV CD (222 nm) monitored normalized thermal unfolding curves of Ferricyt *c* and Ferrocyt *c*, respectively measured at several different pH values. Thermal denaturation transition of Ferrocyt *c* probed by the use of heme absorption at 550 nm (α-band) can typically provide the stability of the Fe^{2+}-M80 bond of Ferrocyt *c* (*72-74*). Fig. 4c presents the heme absorption (550 nm) monitored normalized thermal denaturation curves of Ferrocyt *c* measured at several different pH values. The thermal unfolding curves were analyzed for thermal denaturation midpoint (T_m), enthalpy change (ΔH_m), and heat capacity change (ΔC_p) by using a non-linear least squares method according to Gibbs-Helmholtz equation (chapter 2, eqs (2) and (3)) (*61*). The resulting T_m, ΔH_m, and ΔC_p values at different pH values are provided in Table 4 and Table 5. By using the eq (3) (chapter 2) and the corresponding T_m, ΔH_m, and ΔC_p values, the ΔG_T values from pH 3.0 to pH 12.7 were estimated for Ferricyt *c* at 25 °C (Table 4). Fig. 4d and Fig. 4f show the variation of resulting T_m values for Ferricyt *c* and Ferrocyt *c*, respectively, with pH. As pH is increased from pH 3.0 to pH 13.0, the values of T_m (based on CD (222 nm) and heme absorption (550 nm)) initially increase, displaying a maximum at pH ~8.0-9.0, and then decreases (Fig. 4d,f and Tables 4-5).

Relative to pH 7.0, the values of T_m (based on CD (222 nm) and heme absorption (550 nm)) are found to be higher at alkaline pH ~8.0-9.0 (Fig. 4d,f and Tables 4-5), which suggests that the Cyt *c* has maximum secondary structure and Fe^{2+}-M80 linked thermal stabilities at alkaline pH ~8.0-9.0. Fig. 4e shows the variation of ΔG_T (based on CD at 222 nm) with pH for Ferricyt *c* at 25 °C. As pH is increased from pH 3.0 to pH 12.7, the ΔG_T value initially increase, showing a maximum at pH ~8.0, and then decrease (Fig. 4e and Table 4). This finding suggests that the Ferricyt *c* has maximum thermodynamic stability at alkaline pH ~8.0. Between pH 3.0 and pH 6.0, the protonations of protein groups of Ferricyt *c* lead the unfavorable interactions amongst the positively charged groups, which in turn decrease the T_m and ΔG_T values (based on CD) of protein at extreme acidic pH (Fig. 4d,e and Table 4). At relatively higher basic pH (pH >10.0), the deprotonations of basic amino acid groups of Cyt *c* also lead the unfavorable interactions amongst the negatively charged groups. As a consequence, the secondary structure

and Fe^{2+}-M80 link thermal stabilities of protein are decreased at extreme alkaline pH (Fig. 4f and Tables 4-5). Interestingly, between pH 10.0 and pH 13.0, the decrease in the T_m value for the Fe^{2+}-M80 link disruption is found to be less than the decrease in the T_m value for the secondary structure disruption (Fig. 4f and Tables 4-5). This finding suggests that at extreme alkaline pH, the thermal unfolding of Ferrocyt *c* deviates from its two-state behavior.

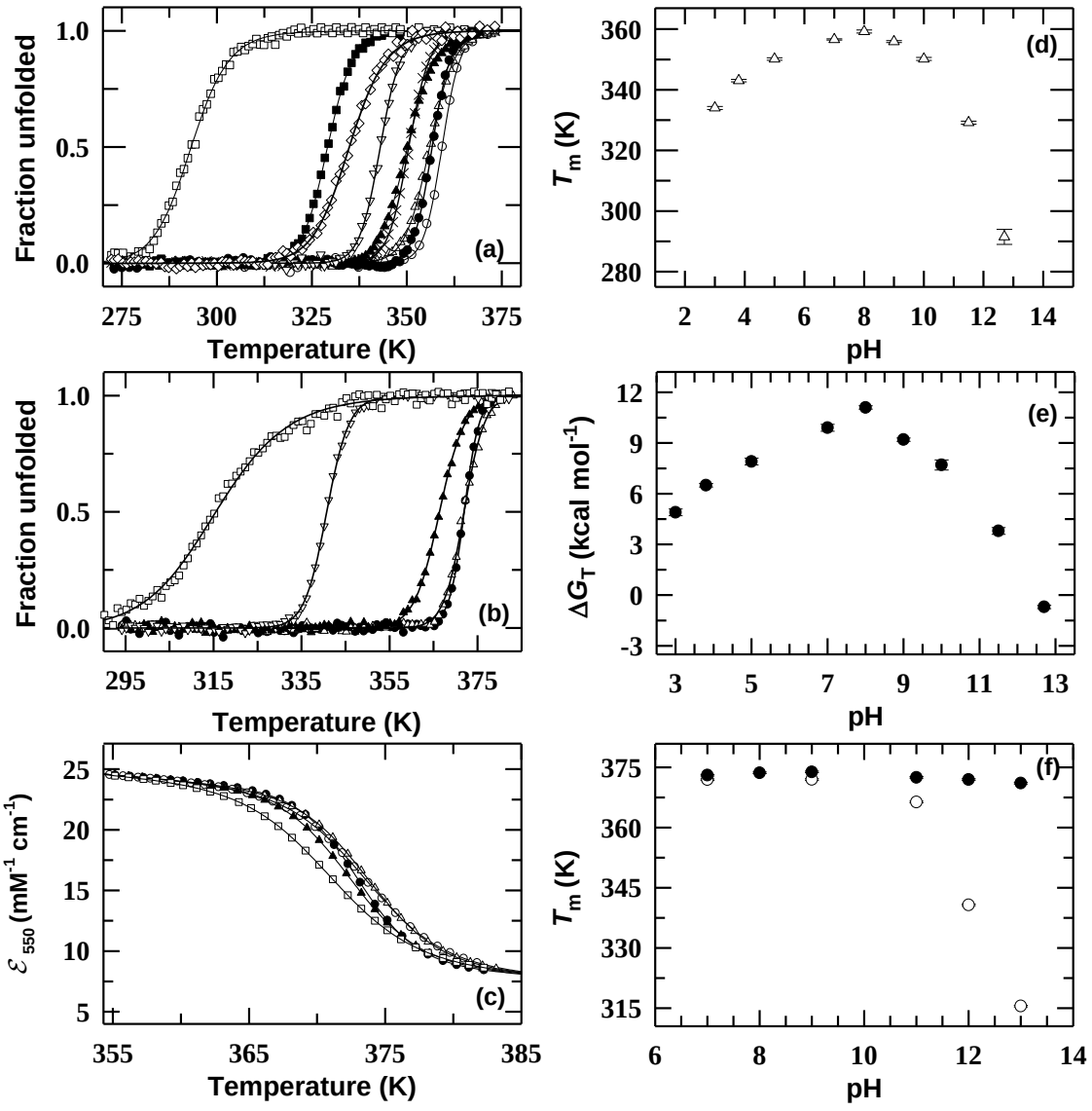

Fig. 4. Panel (a) shows the far-UV CD (222 nm) monitored normalized thermal unfolding curves of Ferricyt *c* measured at pH 12.7 (□), pH 11.5 (■), pH 10 (▲), pH 9 (Δ), pH 8 (○), pH 7 (●), pH 5 (×), pH 3.8 (▽), and pH 3.0 (◊). (b) Far-UV CD (222 nm) monitored thermal unfolding curves of Ferrocyt *c* collected at pH 7 (●), pH 9 (Δ), pH 11 (▲), pH 12 (▽), and pH 13 (□). (c) Heme absorption monitored thermal denaturation curves of Ferrocyt *c* represented as changes in extinction coefficient at 550 nm collected at pH 7 (●), pH 8 (○), pH 9 (Δ), pH 11 (▲), and pH 13 (□). The solid lines in panels (a), (b), and (c) represent the non-linear fits of the data to Gibbs-Helmholtz equation (chapter 2, eqs (2) and (3)) (*61*). Panel (d) represents the variation of T_m (based on CD at 222 nm) with pH

for thermal unfolding of Ferricyt *c*. Panel (e) represents the variation of ΔG_T (based on CD at 222 nm) with pH for thermal unfolding of Ferricyt *c*. Panel (f) represents the variation of T_m (based on CD at 222 nm (○) and heme absorption at 550 nm (●)) with pH for thermal unfolding of Ferrocyt *c*.

Table 4. CD monitored (222 nm) pH dependence of the T_m, ΔH_m, ΔG_T and ΔC_p for thermal unfolding of Ferricyt *c* and Ferrocyt *c*.

Ferricyt *c*					Ferrocyt *c*		
pH	T_m (K)	ΔH_m (Kcal mol^{-1})	ΔG_T (Kcal mol^{-1})	ΔC_p (Kcal mol^{-1} K^{-1})	pH	T_m (K)	ΔH_m (Kcal mol^{-1})
3	334.0	70.0	4.9	1.3	7	371.9	138.5
3.8	343.0	80.0	6.5	1.3	9	372.0	118.9
5	350.2	90.0	7.9	1.4	11	366.4	93.6
7	356.6	100.5	9.9	1.3	12	340.7	91.7
8	359.2	106.0	11.1	1.3	13	315.5	24.2
9	355.9	95.0	9.2	1.3			
10	350.2	85.0	7.7	1.2			
11.5	329.2	60.0	3.8	1.2			
12.7	291.5	30.0	-0.7	1.1			

*The uncertainties of T_m, ΔH_m, ΔG_T and ΔC_P values reported here are ±0.5 °C, ±2.0 kcal mol^{-1}, ±0.5 kcal mol^{-1} and 0.2 kcal mol^{-1} K^{-1}, respectively.

Table 5. pH dependence of the T_m and ΔH_m for thermal unfolding of Ferrocyt *c* monitored by absorbance (550 nm)

pH	T_m (K)	ΔH_m (Kcal mol^{-1})
7	373	105.8
8	373.6	112
9	373.8	108.1
11	372.5	110.5
12	372	114.8
13	371.1	89.1

*The uncertainties of T_m, and ΔH_m values reported here are ±0.5 °C, and ±2.0 kcal mol^{-1}, respectively.

8.2.5 pH dependent secondary structure thermal stability of Lyz in aqueous solutions

Fig. 5a shows the far-UV CD (222 nm) monitored normalized thermal unfolding curves of Lyz measured at seven different pH values, ranging from pH 7.0 to pH 12.5. Fig. 5b presents the far-UV CD (222 nm) monitored normalized thermal unfolding curves of Lyz measured at six different pH values, ranging from pH 2.0 to pH 7.0. The thermal unfolding curves were analyzed for T_m and ΔH_m by using van't Hoff equation (chapter 3, eq (1)) (*75*). Table 6 summarizs the values of T_m and ΔH_m measured at different pH values, ranging from pH 2.0 to pH 13.0. Fig. 5c and Fig. 5d show the variation of T_m and ΔH_m, respectively with pH. As pH is increased from pH 2.0 to pH 13.0, the values of T_m and ΔH_m initially increase, displaying a maximum at pH ~4.0, and then decrease (Fig. 5c,d and Table 6). This finding suggests that Lyz has maximum structural thermal stability at pH ~4.0. Graziano et al (2000) studied the pH dependence of the thermal stability of α-amylase inhibitor tendamistat and found that the α-

amylase inhibitor tendamistat also has maximum thermal stability at pH ~4.0 (*76*). Lyz exhibits maximum thermal stability at pH ~4.0 owing to reduced aggregation (*77*).

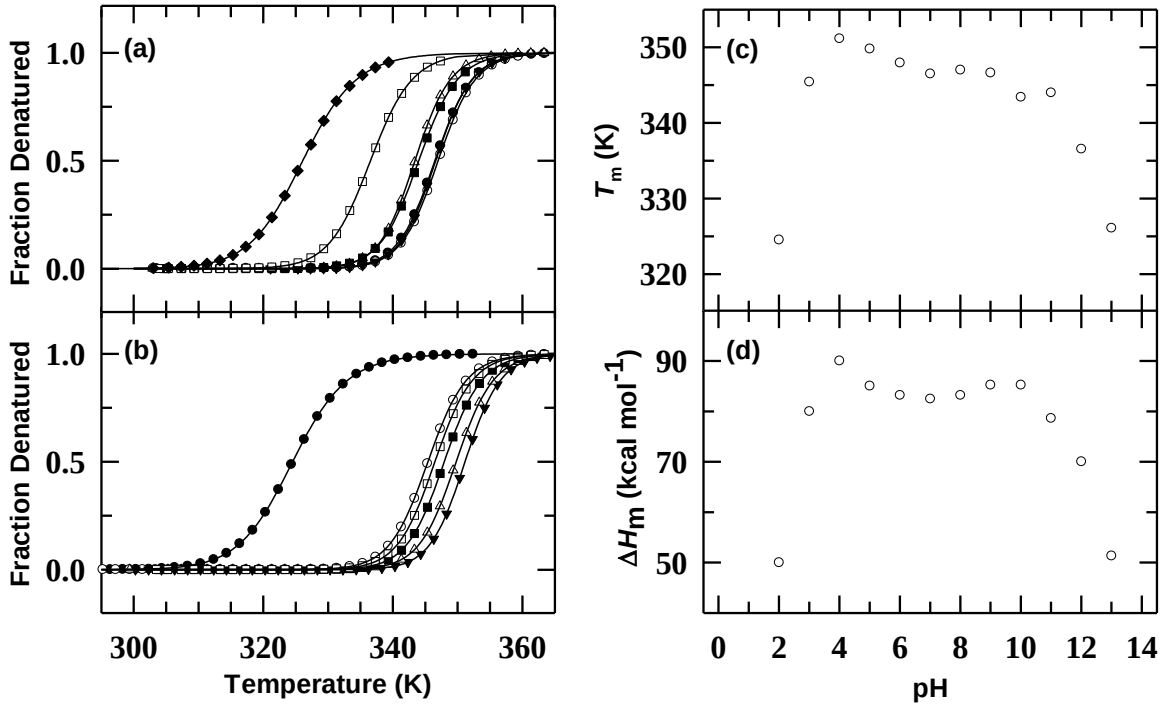

Fig. 5. Panel (a) shows the far-UV CD (222 nm) monitored normalized thermal unfolding curves of Lyz collected at pH 7.0 (●), pH 8 (○), pH 9 (▼), pH 10 (Δ), pH 11 (■), pH 12 (□) and pH 13 (♦). Panel (b) shows the far-UV CD (222 nm) monitored normalized thermal unfolding curves of Lyz collected at pH ~2 (●), pH 3 (○), pH 4 (▼), pH 5 (Δ), pH 6 (■), and pH 7 (□). The solid lines in panels (a) and (b) represents the non-linear fit of the data to van't Hoff equation (chapter 2, eq (1)) (*75*). Panels (c) and (d) show the variation of T_m and ΔH_m with pH, respectively.

Table 6. CD (222 nm) monitored pH dependence of the T_m and ΔH_m for thermal unfolding of Lyz.

pH	T_m (K)	ΔH_m (Kcal mol^{-1})
2	324.5	50
3	345.4	80
4	351.1	90
5	349.8	85
6	348.0	83.2
7	346.5	82.5
8	347	83.2
9	346.6	85.2
10	343.4	85.2
11	344	78.6
12	336.5	70
13	326.1	51.3

*The uncertainties of T_m, and ΔH_m values reported here are ±0.5 °C, and ±2.0 kcal mol^{-1}, respectively.

8.2.6 Effect of pH on the folding-unfolding kinetics of Ferrocyt c

In stopped-flow experiments, the GdnHCl-unfolded Ferrocyt *c* (U-state) in native buffer at pH 7.0 refolds rapidly to native-state (N-state) (*78-80*). Fig. 6a and Fig. 6b show the representative refolding kinetic profiles for U-state to N-state conversion measured at pH 7.0 and pH 12.7, respectively. These refolding kinetic profiles were best described by a two-exponential fit with rate constants, k_{f1} ~280 s^{-1} and k_{f2} ~36 s^{-1} at pH 7.0 (1.0 M GdnHCl) (Fig. 6a and Table 7) and k_{f1} ~77 $s^{-1}$and k_{f2} ~18 s^{-1} at pH 12.7 (1.0 M GdnHCl) (Fig. 6b and Table 7). About ten percent of the observed amplitude is due to the slower minor phase, which is most likely due to the fraction of oxidized protein. It is to be noted that between pH 7.0 and pH 12.7, the activation folding energy barrier ($\Delta G_D^{\circ\ddagger} = -RT \ln(hk_f/k_BT)$) varies less than ~1.0 kcal mol^{-1} ($\Delta G_D^{\circ\ddagger}$ values are ~14.2 and 15.0 kcal mol^{-1} at pH 7 and 12.7, respectively (Table 7)) while the folding free energy (ΔG_D°), which is estimated by the GdnHCl-induced equilibrium unfolding measurements of Ferrocyt *c* (Fig. 2b,e and Table 1) varies more than 9.0 kcal mol^{-1} (ΔG_D° values are ~16.1 and 8.1 kcal mol^{-1} at pH 7 and pH 12.7, respectively) (Fig. 2b,e and Table 1). This finding demonstrates that the large disparity in thermodynamic stability of protein at pH 12.7 relative to pH 7.0 is not greatly reflected in the refolding rates.

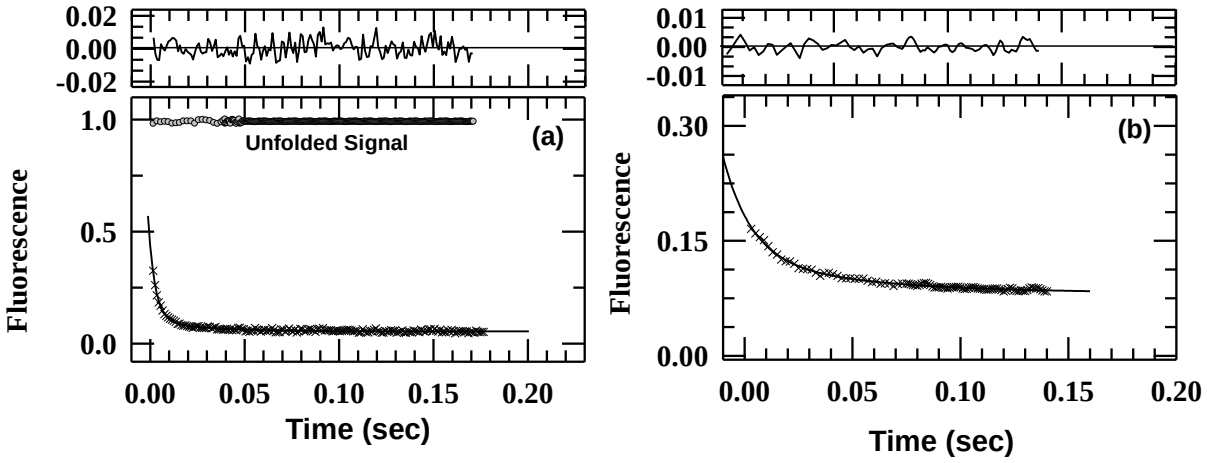

Fig. 6. (a) A representative stopped flow kinetic trace of Ferroyt *c* (pH 7) for refolding in the presence of 1.0 M GdnHCl (~~xxxx~~), showing the recovery of the fluorescence signal with respect to the fluorescence signal of the unfolded protein (••••), during the burst kinetic phase. This refolding kinetic trace was best described by a two-exponential fit with rate constants, k_{f1} ~280 s^{-1} and k_{f2} ~36 s^{-1}(residual shown). (b) A representative stopped flow kinetic trace of Ferrocyt *c* (pH 12.7) for the refolding in the presence of 1.0 M GdnHCl. This refolding kinetic trace was best described by a two-exponential fit with rate constants, k_{f1} ~77 $s^{-1}$and k_{f2} ~18 s^{-1} (residual shown).

Table 7. Values of k_{f1}, ln $k_{f1,}$ and $\Delta G_D^{\circ\ddagger}$ for Ferrocyt *c* folding kinetics at pH 7.0 and 12.7, 25 °C.

	pH 7.0	pH 12.7
k_{f1} (s^{-1})	280	77
ln k_{f1} (s^{-1})	5.63	4.34
$\Delta G_D^{\circ\ddagger}$ (K cal mol^{-1})	14.2	15.0

8.2.7 Quantitative measurement of the development of the electrostatic interactions in the transition state of Ferrocyt c folding

Fig. 7 shows the variation of the natural logarithm of apparent equilibrium constant (ln K_{app}) with pH. Between pH 7.0 and pH 12.7, there is very small change in the natural logarithm of the refolding rates (<1.0 unit) of Ferrocyt *c* (Fig. 6a,b and Table7) while within this range of pH, there is large change in the ln K_{app} of Ferrocyt *c* (Fig. 7). This comparison suggests that the pH-dependent ionic interactions have significant effect on the overall stability of protein but have very little effect on the folding kinetics of Ferrocyt *c*. The classic WT linkage relations can be used to measure the development of electrostatic interactions in transition state of folding (*23, 81*).

$$\frac{\partial \Delta G^{\circ}}{\partial \mathrm{pH}} = 2.303RT\Delta\nu(\mathrm{pH}) \qquad (1)$$

$$\frac{\partial \Delta G^{\circ\ddagger}}{\partial \mathrm{pH}} = 2.303RT\Delta\nu^{\ddagger}(\mathrm{pH}) \qquad (2)$$

where, the terms ΔG° and $\Delta G^{\circ\ddagger}$ are the apparent free energy of folding and activation folding free energy barrier, respectively. The terms $\Delta\nu$(pH), and $\Delta\nu^{\ddagger}$ (pH) represent the difference in the number of protons bound to the folded and unfolded states, and transition and unfolded states, respectively. In accordance with few earlier studies (*17,49,53,55*), the development of electrostatic interactions in the transition state for folding can be quantitatively measured by comparison of the ratio:

$$\beta^{\mathrm{pH}} = \left[\frac{\Delta\Delta G^{\circ\ddagger}(\mathrm{pH}_2,\mathrm{pH}_1)}{\Delta\Delta G^{\circ}(\mathrm{pH}_2,\mathrm{pH}_1)}\right] = \left[\frac{\Delta G^{\circ\ddagger}(\mathrm{pH}_2) - \Delta G^{\circ\ddagger}(\mathrm{pH}_1)}{\Delta G^{\circ}(\mathrm{pH}_2) - \Delta G^{\circ}(\mathrm{pH}_1)}\right] = \left[\frac{\int_{\mathrm{pH}_1}^{\mathrm{pH}_2} \Delta\nu^{\ddagger}(\mathrm{pH})d\mathrm{pH}}{\int_{\mathrm{pH}_1}^{\mathrm{pH}_2} \Delta\nu(\mathrm{pH})d\mathrm{pH}}\right] \qquad (3)$$

$$= [\ln k_f(\mathrm{pH}_2) - \ln k_f(\mathrm{pH}_1)]/[\ln K(\mathrm{pH}_2) - \ln K(\mathrm{pH}_1)] \qquad (4)$$

Value of β^{pH} between neutral pH 7.0 and alkaline pH 12.7 was estimated by using eq (5),

$$= [\ln k_f(\mathrm{pH}\ 12.7) - \ln k_f(\mathrm{pH}\ 7.0)]/[\ln K(\mathrm{pH}\ 12.7) - \ln K(\mathrm{pH}\ 7.0)] \qquad (5)$$

The β^{pH} value calculated between pH 7.0 and pH 12.7 for folding of Ferrocyt *c* is ~0.098.

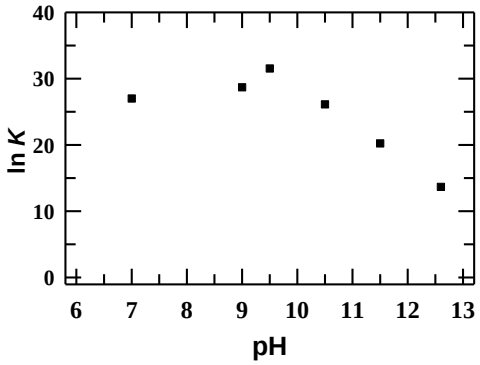

Fig. 7. The variation of the natural logarithm of apparent equilibrium constant (ln K_{app}) of Ferrocyt *c* with pH at 25 °C.

Few other investigators have also calculated the β^{pH} or $\Delta\nu^{\ddagger}(pH)/\Delta\nu(pH)$ values for other proteins (barnase, CTNL9, NTL9, and CI-2)) and correlated these β^{pH} values to the development of electrostatic interactions in the transition state for folding (*49,53-56*). The observation of larger β^{pH} values for barnase (~0.5) and CTNL9 (~0.6) were attributed to a better development of electrostatic interactions in the transition states for folding of barnase and CTNL9 (*53-55*). On the other hand, the observation of lower β^{pH} values for CI-2 (~0.25) and NTL9 (~0.3) were attributed to a weaker development of electrostatic interactions in the transition states for folding of these two proteins (*49, 56*). Between the pH 7.0 and 12.7, the β^{pH} value estimated for folding of Ferrocyt *c* is less than 0.1, which demonstrates that the electrostatic interactions are very weakly formed in the transition state for folding of Ferrocyt *c*.

8.2.8 Ionization of native and denatured states of Ferricyt c and Lyz as a function of pH

The characterization of the pH-dependent stability of proteins requires the consideration of the ionization of its native and denatured states. It is clear from Table 4 that when pH is changed, the value of T_m for thermal unfolding of Ferricyt *c* also changes. At acidic pH, the positive charge on both the native and the denatured states increases. There is also a change in $\Delta\nu$ (pH), which is the difference in number of protons bound to the denatured and the native states. The value of $\Delta\nu$ (pH) at each pH was determined by applying the eq (6) to the data in Table 4 and Table 6.

$$\Delta\nu(\mathrm{pH}) = \frac{\Delta H_m}{2.3RT_m^2} \cdot \frac{\delta T_m}{\delta \mathrm{pH}} \qquad (6)$$

The $\delta T_m/\delta$pH term was calculated by fitting a second-order polynomial to plots of T_m versus pH curves and evaluating the first derivative at each T_m value (*82*). Fig. 8a shows the variation of $\Delta\nu$ (pH) of Ferricyt *c* and Lyz with pH (eq (6)) at 25 °C. The value of $\Delta\nu$(pH) for Ferricyt *c* can also be determined by considering the classic WT linkage relationship (eq (1)). The value of $\Delta\nu$ (pH) by using eq (1) was calculated by using the data in Table 1 (urea-unfolding of Ferricyt *c*) and Table 4 (thermal unfolding of Ferricyt *c*). Fig. 8a and Fig. 8b show the variation of $\Delta\nu$(pH) with pH obtained by using eq (1) for thermal and urea-unfolding of Ferricyt *c*, respectively. At pH ~9.0, the value of $\Delta\nu$ (pH) becomes zero for both Lyz and Ferricyt *c* (Fig. 8a,b), indicating that there is no change in the number of the bound proton upon unfolding. Between pH 2.0 and pH 3.0, the values of $\Delta\nu$ (pH) observed for Lyz and Ferricyt *c* are about 1.0 (Fig. 8a) and 2.0 (Fig. 8a and Fig. 8b), indicating that about one and two protons are taken up upon unfolding of Lyz and Ferricyt *c*, respectively.

Raleigh and coworkers (2002) studied the pH-dependent stability and folding kinetics of the ribosomal C-terminal domain of L9 (*55*). They have shown that for ribosomal protein L9, $\Delta\nu$(pH) is almost zero at pH 8.0, indicating that there is no change in the number of the bound protons upon unfolding at pH ≥8.0 (*55*). Between pH 6.0 and pH 5.0, $\Delta\nu$(pH) is about 1.5, indicating one to two protons are taken up upon unfolding (*55*). Pielak and coworkers (1994) also studied the ionization of the native and denatured states of yeast iso-1 Ferricyt *c* as function of pH (*82*). They have shown the maximum value of $\Delta\nu$ (pH)(≈2.4) at pH 3.5, which decreases with increasing value of pH and passes through zero near pH 6.5 (*82*). They further demonstrated that between pH 5.0 and pH 3.0 at least two groups (more specifically, His 26 and His 18, and one of heme propionates) take up protons upon denaturation (*82*).

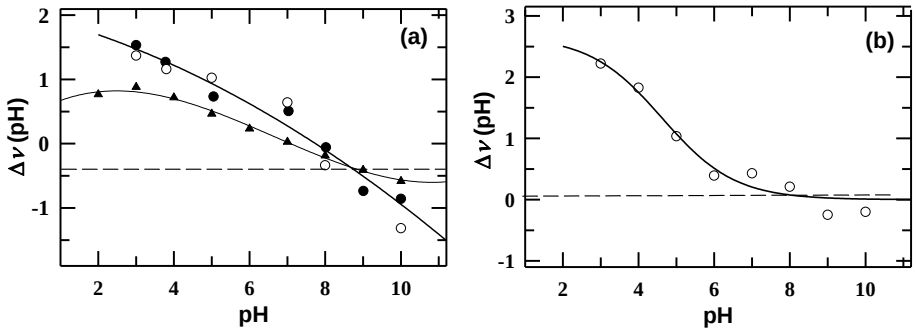

Fig. 8. (a) Variation of $\Delta\nu$ (pH) of Ferricyt *c* (● (eq (6)) and ○ (eq (1))) and Lyz (▲ (eq 6)) with pH by using the thermodynamic parameters obtained from CD 222nm-monitored thermal unfolding of proteins at different pH

values. (b) Variation of Δν (pH) of Ferricyt *c* with pH calculated by eq (1) using the thermodynamic parameters obtained from the equilibrium unfolding of Ferricyt *c* collected at different pH values.

8.2.9 pH- dependence of the intrachain diffusion rates of CO-liganed Ferrocyt c

The biphasic microsecond relaxation following CO photolysis is the hallmark of heme-polypeptide dynamics in the denaturant-unfolded Cyt-CO at pH 7.0. According to few previous studies (*83-85*), following CO photolysis from the GdnHCl-unfolded protein at pH 7.0, the side chains of the methionine (M65 and M80) and histidine (H26 and H33) residues make transient contacts with the Fe^{2+} of heme. Fig. 9a shows the observed changes in 423 nm absorption from 0.2 μs to 45 μs after photodissociation of CO from the GdnHCl (5.0 M)-unfolded CO-liganded Ferrocyt *c* at pH 10. The kinetic data are best fitted as two exponential relaxation processes with rate constants of $\lambda_1 \approx 5.7\times10^5$ s^{-1} ($\tau_1 \approx$ 1.6 μs) and $\lambda_2 \approx 1.6\times10^5$ s^{-1}($\tau_2 \approx$ 6.2 μs). The fast ($\tau_1 \approx$ 1.6 μs) and slow ($\tau_2 \approx$ 6.2 μs) relaxation processes are related to the transient binding of the methionine (M65 and M80) and histidine (H26 and H33), respectively to Fe^{2+} of the photoproduct (Fig. 9a) (*83-85*). The microsecond relaxation processes rates measured after the photodissocition of CO from the GdnHCl-unfolded cyt-CO at different pH values, ranging from pH 7.8 to pH 13.0, are plotted as a function of pH in Fig. 9b. When pH is increased from pH 7.8 to pH 13.0, both λ_1 and λ_2 initially remain almost constant up to pH ~11.0 and then gradually increase (Fig. 9b). This indicates that the diffusive motions of the incipient polypeptide are only marginally affected from pH 7.0 to pH 11.0. The gradual increase of λ_1 and λ_2 above pH 11.0 is due likely from base-induced expansion of the denaturant unfolded Cyt-CO, which in results decrease the intrachains contractions rates of the methionine (M80 and M65) and histidine (H26 and H33) to the Fe^{2+} of heme (*73, 83*).

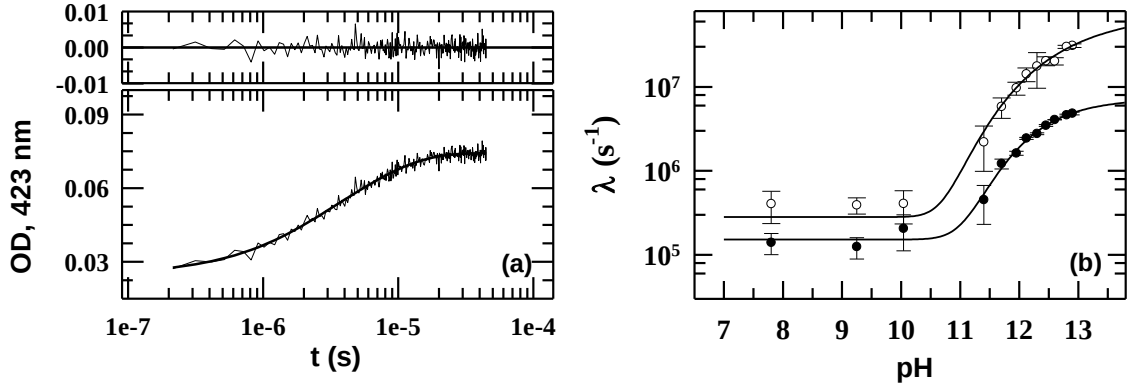

Fig. 9. (a) The observed changes in 423 nm absorption from 0.2 μs to 45 μs after photodissociation of CO from the GdnHCl (5.0 M)-unfolded Cyt-CO at pH 7.0. (b) pH-dependence of the intrachain diffusion rates after photolysis of

CO from denaturant-unfolded Cyt-CO (5.0 M GdnHCl) at 25 °C (transient binding of methionines, M65 and M80 (open circles) and histidines, H26 and H33 (filled circles)).

8.2.10 Theoretical estimation of the pH-dependent stability of proteins

For large biological systems, it is very difficult to obtain the pK_a values experimentally, therefore, several software have been developed to predict the pK_a values on the basis of protein structure (*86-88*). PROPKA 3.1 is one of the popular pK_a predicting software and is better than the other software mainly because of its speed and accuracy (*86-88*). The PROPKA 3.1 predicts the pK_a values of the ionizable residues in a protein by determining the perturbation to the model pK_a value, pK_{model}, caused due to the desolvation penalty (DS), back bone and side chain hydrogen bonds (HB), and interactions with the other charged groups (CC), in protein environment (*21, 89-90*). The pK_a and pK_{model} values corresponding to the ionizable groups of horse Ferricyt *c* (PDB: 1HRC) and hen Lyz (PDB: 2LYZ) as predicted by PROPKA 3.1 are given in Table 8.

Table 8. The pK_a values for all the ionizable amino acid residues of the horse Cyt *c* (PDB: 1HRC) and Lyz (PDB: 2LYZ) calculated by using the PROPKA 3.1 program (*21*).

PDB: 1 HRC						**PDB: 2 LYZ**					
Group	**pK_a***	**Model -pK_a***	**Group**	**pK_a***	**Model -pK_a***	**Group**	**pK_a***	**Model -pK_a***	**Group**	**pK_a***	**Model -pK_a***
ASP 2 A	2.90	3.80	LYS 5 A	10.80	10.50	Asp 18 A	4.08	3.8	LYS 1 A	11.25	10.50
ASP 50 A	3.79	3.80	LYS 7 A	10.30	10.50	Asp 48 A	2.81	3.80	LYS 13 A	11.60	10.50
ASP 93 A	3.76	3.80	LYS 8 A	10.39	10.50	Asp 52 A	4.93	3.80	LYS 33 A	10.15	10.50
GLU 4 A	4.79	4.50	LYS 13 A	10.62	10.50	Asp 66 A	2.3	3.80	LYS 96 A	10.15	10.50
GLU 21 A	3.87	4.50	LYS 22 A	10.61	10.50	Asp 87 A	2.28	3.80	LYS 97 A	10.45	10.50
GLU 61 A	3.54	4.50	LYS 25 A	10.36	10.50	Asp101 A	4.43	3.80	LYS 116 A	10.17	10.50
GLU 62 A	4.69	4.50	LYS 27 A	10.00	10.50	Asp 119 A	3.49	3.80	ARG 5 A	11.87	12.50
GLU 66 A	4.79	4.50	LYS 39 A	10.20	10.50	GLU 7 A	3.58	4.50	ARG 14 A	12.42	12.50
GLU 69 A	4.43	4.50	LYS 53 A	10.48	10.50	GLU 35 A	6.95	4.50	ARG 21 A	12.46	12.50
GLU 90 A	3.64	4.50	LYS 55 A	10.02	10.50	C^- 129 A	2.19	3.20	ARG 45 A	11.81	12.50
GLU 92 A	4.53	4.50	LYS 60 A	10.33	10.50	HIS 15 A	6.42	6.50	ARG 61 A	12.47	12.50
GLU 104 A	4.32	4.50	LYS 72 A	9.53	10.50	CYS 6 A	99.99	99.99	ARG 68 A	12.55	12.50
C^- 104 A	3.25	3.20	LYS 73 A	10.43	10.50	CYS 30 A	99.99	99.99	ARG 73 A	12.32	12.50
HIS 18 A	2.02	6.50	LYS 79 A	10.24	10.50	CYS 64 A	99.99	99.99	ARG 112 A	12.19	12.50
HIS 26 A	6.43	6.50	LYS 86 A	10.99	10.50	CYS 76 A	99.99	99.99	ARG 114 A	12.15	12.50
HIS 33 A	6.57	6.50	LYS 87 A	9.44	10.50	CYS 80 A	99.99	99.99	ARG 125 A	12.48	12.50
CYS 14 A	13.89	9.00	LYS 88 A	10.63	10.50	CYS 94 A	99.99	99.99	ARG 128 A	12.47	12.50
CYS 17 A	10.59	9.00	LYS 99 A	11.46	10.50	CYS 115 A	99.99	99.99	N^+ 1 A	7.45	8.00
TYR 48 A	13.68	10.00	LYS 100 A	10.47	10.50	CYS 127 A	99.99	99.99			
TYR 67 A	15.41	10.00	N^+ 1 A	7.95	8.00	TYR 20 A	9.24	10.00			
TYR 74 A	11.19	10.00	HEM NA A	-2.44	5.00	TYR 23 A	10.10	10.00			
TYR 97 A	11.14	10.00	HEM NC A	3.59	5.00	TYR 53 A	11.87	10.00			
ARG 38 A	11.81	12.50	HEM CGA A	4.13	4.50						
ARG 91 A	12.12	12.50	HEM CGD A	3.03	4.50						

*****Here pK_a and Model-pK_a represent the pK_a values of the native and the denatured state of protein, respectively.

The pH dependent electrostatic free energies ΔG^{el} (pH) in the native state, ΔG_N^{el} (pH) and in the denatured state, ΔG_D^{el} (pH) of Ferricyt *c* and Lyz were calculated by using the following relation (*17*):

$$\Delta G^{ele} \text{ (pH)} = - \text{RT} \sum_{i=1}^{N} \ln \left\{1 + \exp\left[-2.3\gamma(i) \text{ (pH-p}K_i)\right]\right\} \qquad (7)$$

where, γ (i) = +1 or -1 for a basic or acidic group, respectively and pK_i is the pK_a value of the i^{th} ionizable group of the protein in the native (pK_a) and denatured (pK_{model}) states obtained from PROPKA 3.1 (Table 8). Table 9 summarizes the values of ΔG_N^{el} (pH) and ΔG_D^{el} (pH), calculated at different pH, ranging from pH 0.0 to pH 14.0. The pH dependent term for protein stability, ($\Delta\Delta G_{ND}^{el}$) can be determined by using eq (8) (*12*).

$$\Delta\Delta G_{ND}^{el} \text{ (pH)} = \Delta G_N^{el} \text{ (pH)} - \Delta G_D^{el} \text{ (pH)} \qquad (8)$$

Fig. 10a and Fig. 10b show the variation of $\Delta\Delta G_{ND}^{el}$ obtained for Ferricyt *c* and Lyz, respectively, as a function of pH. As pH is increased from pH 0.0 to pH 14.0, the value of $\Delta\Delta G_{ND}^{el}$ first decreases and then increases showing a minimum at pH values at pH ~8.0 in case of Ferricyt *c* whereas, the corresponding minimum in case of Lyz appears at pH ~4.0. The theoretical predication of pH dependent stability of Ferricyt *c* and Lyz thus indicates that the Ferricyt *c* and Lyz are maximally stable at pH ~8.0 and pH ~4.0, respectively. By using the pH-dependent stability term, $\Delta\Delta G_{ND}^{el}$(pH), the total free energy of folding, ΔG_{ND}(pH) can be determined by using eq (9),

$$\Delta G_{ND} \text{ (pH)} = \Delta G_{ND}^{neu}\text{(pH)} + \Delta\Delta G_{ND}^{el} \text{ (pH)} \qquad (9)$$

where ΔG_{ND}^{neu} (pH) is the pH-independent folding energy of hypothetical protein with all neutral residues. Only the theoretical calculations or experimental measurements cannot predict the pH-independent term accurately (*17, 19*). However, it is possible to calculate it using the values of the ΔG_{ND}^{neu}(pH) at experimentally determined denaturation midpoints $pH_{1/2}$ in the acidic and alkaline regions (*12*). The zero experimental points for ΔG_{H2O} are observed at pH 2.5 and pH 12.5 for the acidic and alkaline denaturations, respectively for Ferricyt *c* (Fig. 1). To determine the ΔG^{neut} term, we have taken the average of the calculated $\Delta\Delta G_{ND}^{el}$ values at the acidic and alkaline pH midpoints.

The pH-dependent charges of the folded and unfolded protein *i.e.*, Q_F and Q_U respectively, can be calculated by using the following relations (*22*):

$$Q_U = \sum_{i=1}^{n} q_U^i \quad \text{and} \quad Q_F = \sum_{i=1}^{n} q_F^i \tag{10}$$

$$\text{where, } q_U^i \text{ or } q_F^i \text{ (for an acidic group)} = \frac{-1}{1+ 10^{pK_a^i - pH}}$$

$$q_U^i \text{ or } q_F^i \text{ (for a basic group)} = \frac{1}{1+ 10^{pH - pK_a^i}}$$

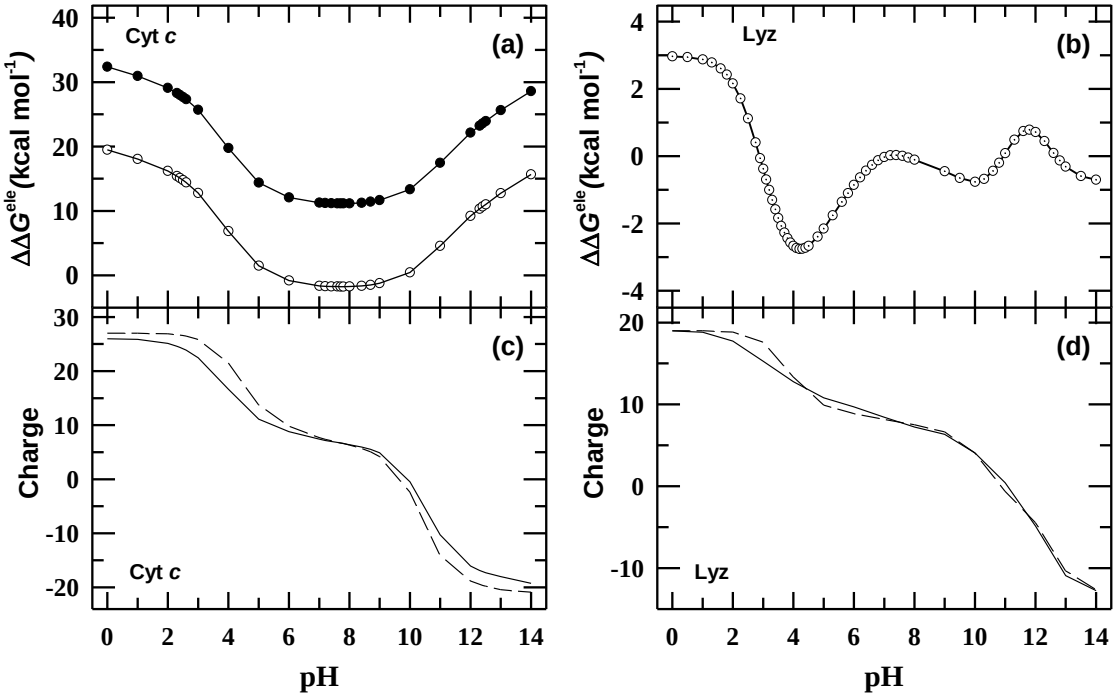

Fig. 10. Panel (a) shows the variations of $\Delta\Delta G^{ele}$ (●) and ΔG_{ND} (○) as a function of pH for Ferricyt *c*. Panel (b) shows the variation of $\Delta\Delta G^{ele}$ (v) as a function of pH for Lyz. Panels (c) and (d) show the variation of charges of the folded (—) and the unfolded (- - -) states of Ferricyt *c* and Lyz, respectively, as a function of pH.

To calculate the charges of the folded protein, the perturbed protein pK_a values were used, while the charges of the unfolded state were calculated by using the pK_{model} values. The calculated values of the Q_U and Q_F at different pH values are provided in Table 9. Fig. 10c and Fig. 10d show the variation of charges (Q_U and Q_F) with the pH for Ferricyt *c* and Lyz, respectively. The pH where the Q_U and Q_F become zero reflects the isoelectric point of the unfolded and folded states of protein (*22*). In case of Ferricyt *c*, the isoelectric point comes out to be ~10.0 (Fig. 10c). Interestingly, the Ferricyt *c* also has maximum stability near its isoelectric point (Fig. 2, Fig. 4, Table 1, Table 4). The isoelectric point of Lyz comes out to be ~10.5 (Fig. 10d). Notably, Lyz is not maximally stable near its isoelectric point (Fig. 3,5, and Tables 3,6). According to few earlier

reports, a protein is maximum stable near to its isoelectric point where the net charge on the protein is zero (*2*). However, a large number of proteins having acidic and basic isoelectric points are found to be maximum stable at neutral pH (*3*). This finding suggests that in addition to the overall charge, some other factors are also important in determining the folding energy of the globular proteins. For example, the Lyz produced by the bacteriophage T4 is a rather basic protein with an isoelectric point above 10.0 yet is most stable near to pH 5.0 (*3*). The maximum thermal stability of Lyz at pH ~4.0 is attributed to the reduced aggregation. On the other hand, its thermal stability is affected at other pH due to increased aggregation and reduced native helical content (*77*).

Table 9. The pH dependence of the electrostatic energies and charges in the native state, $\Delta G_N^{el}(\mathrm{pH})$ and Q_N, respectively, and in the denatured state, $\Delta G_D^{el}(\mathrm{pH})$ and Q_D, respectively calculated by using electrostatic model.

	Cyt *c*					Lyz				
pH	ΔG_N^{el} **(pH)**	ΔG_D^{el} **(pH)**	$\Delta\Delta G_{ND}^{el}$	Q_N	Q_D	ΔG_N^{el} **(pH)**	ΔG_D^{el} **(pH)**	$\Delta\Delta G_{ND}^{el}$	Q_N	Q_D
0	-339.85	-359.33	19.48	25.99	27.00	-291.91	-294.87	2.97	18.98	19.00
1	-304.26	-322.31	18.05	25.87	26.99	-265.95	-268.82	2.88	18.82	18.98
2	-269.17	-285.36	16.19	25.12	26.86	-240.70	-242.86	2.16	17.72	18.83
2.3	-258.94	-274.33	15.40	24.60	26.72	-233.54	-235.15	1.61	17.05	18.66
2.4	-255.58	-270.67	15.09	24.38	26.66	-231.22	-232.59	1.37	16.80	18.58
2.5	-252.25	-267.02	14.77	24.14	26.58	-228.93	-230.05	1.12	16.55	18.48
2.6	-248.96	-263.38	14.43	23.87	26.48	-226.68	-227.52	0.85	16.30	18.36
3	-236.23	-249.01	12.78	22.44	25.84	-218.02	-217.64	-0.38	15.28	17.59
4	-209.16	-216.02	6.85	16.64	21.46	-198.78	-196.12	-2.67	12.79	13.36
5	-190.44	-191.94	1.50	11.12	13.74	-182.71	-180.55	-2.16	10.81	9.88
6	-177.05	-176.24	-0.81	8.79	9.81	-168.69	-167.83	-0.86	9.71	8.86
7	-165.99	-164.36	-1.63	7.40	7.66	-156.20	-156.17	-0.03	8.42	8.16
7.2	-163.99	-162.30	-1.69	7.18	7.35	-153.93	-153.95	0.02	8.14	8.03
7.4	-162.05	-160.32	-1.73	6.98	7.08	-151.73	-151.76	0.03	7.87	7.90
7.6	-160.16	-158.41	-1.74	6.79	6.83	-149.61	-149.61	0.00	7.63	7.77
7.7	-159.23	-157.48	-1.75	6.70	6.71	-148.57	-148.55	-0.02	7.52	7.70
7.8	-158.32	-156.57	-1.75	6.60	6.58	-147.55	-147.50	-0.05	7.42	7.63
8	-156.54	-154.80	-1.74	6.40	6.32	-145.54	-145.43	-0.11	7.24	7.48
8.4	-153.15	-151.51	-1.64	5.95	5.67	-141.65	-141.41	-0.24	6.94	7.18
8.7	-150.78	-149.30	-1.49	5.52	5.03	-138.85	-138.50	-0.34	6.69	6.93
9	-148.63	-147.40	-1.24	4.89	4.15	-136.16	-135.71	-0.45	6.35	6.63
10	-144.90	-145.33	0.44	-0.48	-2.38	-128.78	-128.02	-0.76	4.06	4.03
11	-152.31	-156.86	4.56	-10.31	-14.11	-125.67	-125.75	0.08	0.43	-0.62
12	-171.00	-180.24	9.23	-16.06	-18.86	-128.36	-129.07	0.71	-4.87	-4.43
12.3	-177.79	-188.12	10.33	-16.89	-19.46	-130.79	-131.24	0.44	-6.96	-6.15
12.4	-180.12	-190.80	10.68	-17.10	-19.63	-131.79	-132.12	0.33	-7.65	-6.78
12.5	-182.48	-193.51	11.02	-17.29	-19.80	-132.89	-133.10	0.21	-8.31	-7.43
13	-194.60	-207.32	12.73	-18.00	-20.46	-139.56	-139.24	-0.32	-10.92	-10.34
14	-220.12	-235.80	15.68	-19.25	-20.93	-156.16	-155.46	-0.70	-12.75	-12.66

8.3 Conclusion

This chapter analyzes the effects pH on the stability of Cyt *c* and Lyz and folding kinetics of Cyt *c* all across the acidic- and alkaline pH-unfolding transitions of the proteins. Thermal and chemical denaturant (urea or GdnHCl)-induced unfolding experiments were used to measure the thermodynamic stabilities of Ferricyt *c*, Ferrocyt *c* and Lyz at several different pH values, ranging from pH 3.0 to pH 13.0. Ferricyt *c* is maximally stable between pH 8.0 and pH 9.0 with $\Delta G_T° \approx 11.1$ kcal mol^{-1} and $\Delta G_D° \approx 10.6$ kcal mol^{-1} at 25 °C. Ferrocyt *c* is also found to be maximally stable between pH 8.0 and pH 9.0 with $\Delta G_D° \approx 16.6$ kcal mol^{-1} at 25 °C. At relatively higher basic pH (pH >10), the unfavorable interactions among the negatively charged groups decrease the thermodynamic stability of protein. The Lyz is found to be maximally stable at pH 4.0 with $\Delta G_D° \approx 10.3$ kcal mol^{-1} at 25 °C. The classic Wyman-Tanford linkage relation was used to estimate the $\Delta\nu$ (pH) value. Between pH 2.0 and pH 3.0, the values of $\Delta\nu$(pH) observed for Lyz and Ferricyt *c* are about 1.0 and 2.0, indicating that about one and two protons are taken up upon unfolding of Lyz and Ferricyt *c*, respectively. In stopped-flow experiment, the dilution of denaturant unfolded Ferrocyt *c* (6.5 M GdnHCl) in refolding buffer at pH 7.0 and pH 12.7 result in rapid refolding of unfolded protein to the native-state. Between pH 7.0 and pH 12.7, the activation folding free energy of Ferrocyt *c* varies less than 1.0 kcal mol^{-1}, while the folding free energy varies by more than 9.0 kcal mol^{-1}. This comparison provides two important informations, (i) the large disparity in thermodynamic stability is not strongly reflected in the refolding rates, and (ii) the pH-dependent ionic interactions contribute significantly to the thermodynamic stability of protein but have little effect on folding kinetics of Ferrocyt *c*. By using the classic WT linkage relation, the β^{pH}-value for Ferrocyt *c* folding was calculated between pH 7.0 and pH 12.7, which is less than 0.1, indicating that the electrostatic interactions are weakly formed in the transition states for folding.

8.4 References

1. Matthew, J.B., and Gurd, F.R.N. (1986) *Methods Enzymol.* **130,** 413- 436
2. Linderstrom-Lang, K.U. (1924) *C. R. Trav. Lab. Carlsberg* 15, 70-95.
3. Anderson, D.E., Becktel, W.J., and Dahlquist, F.W. (1990) *Biochemistry* **29,** 2403-2408.

4. Raquet, X., Lounnas, V., LamotteBrasseur, J., Frere J.M., and Wade, R.C. (1997) *Biophys. J.* **73**, 2416–2426.
5. Nielsen, J.E., and Mccammon, J.A. (2003) *Protein Sci.* **12,** 1894–1901.
6. Lamotte-Brasseur, J., Lounnas, V., Raquet, X., and Wade, R.C. (1999) *Protein Sci.* **8**, 404–409.
7. Lamotte-Brasseur, J., Dubus, A., and Wade, R.C. (2000) *Proteins* **40**, 23–28.
8. Warshel, A. (1981) *Biochemistry* **20**, 3167–3177.
9. Warshel, A. (1981) *Acc. Chem. Res.* **14**, 284–290.
10. Perutz, M.P. (1978) *Science* **201**, 1187-1191.
11. Warshel, A. (1978) *Proc. Natl. Acad. Sci. USA*, **75**, 5250-5254.
12. Shosheva, A., Miteva, M., Christova, P., and Atanasov, B. (2003) *Eur. Biophys. J.* **31**, 617–625.
13. You, T., Bashford, D. (1995) *Biophys. J.* **69**, 1721-1733.
14. Alexov, E., and Gunner, M. (1997) *Biophys. J.* **72**, 2075-2093.
15. Rabenstein, B., and Knapp, E.W., (2001) *Biophys. J.* **80**, 1141-1150.
16. Warshel, A. (1991) *Annu. Rev. Biophys. Biophys. Chem.* **20**, 267–298.
17. Yang, A.S., Honig, B. (1993) *J. Mol. Biol.* **231**, 474–495.
18. Yang, A.S., and Honig, B. (1994) *J. Mol. Biol.* **237**, 602–614.
19. Antoziewicz, J., McCommon, J., and Gilson, M. (1994) *J. Mol. Biol.* **238**, 415–436.
20. Schaefer, M., Sommer, M., and Karplus, M. (1997) *J. Phys. Chem. B* **101**, 1663–1668.
21. Li, H., Robertson, A.D., and Jensen, J.H. (2005) *Proteins: Structure, Function, and Bioinformatics* **61**, 704–721.
22. Bosshard, H.R., Marti, D.N., and Jelesarov, (2004) *I. J. Mol. Recognit.* **17**, 1–16.
23. Tanford, C. (1970) *Chem. Adv. Prot.* **24**, 1–95.
24. Antosiewicz, J., McCammon, J.A., and Gilson, M.K. (1996) *Biochemistry* **35**, 7819–7833.
25. Bashford, D., and Karplus, M. (1990) *Biochemistry* **29**, 10219–10225.
26. Ullmann, G.M., and Knapp, E.W. (1999) *Eur. Biophys. J. Biophys. Lett.* **28**, 533–551.
27. Yang, A.S., Gunner, M.R., Sampogna, R., Sharp, K., and Honig, B. (1993) *Proteins* **15**, 252–265.
28. Mehler, E.L. and Guarnieri, F. (1999) *Biophys. J.* **77**, 3–22.
29. Hendsch, Z.S., and Tidor, B. (1994) *Protein Sci.* **3**, 211-226.

30. Barlow, D.J., and Thornton, J.M. (1983) *J. Mol. Biol.* **168**, 867-885.
31. Kumar, S. and Nussivov, R. (1999) *J. Mol. Biol.* **293**, 1241-1255.
32. Honig, B., and Nicholls, A. (1995) *Science* **268**, 1144-1149.
33. Campos, S.R., Machuqueiro, M., Baptista, A.M. (2010) *J. Phys. Chem. B* **7**, 12692-12700.
34. Vila-Viçosa, D., Campos, S.R., Baptista, A.M., and Machuqueiro, M. (2012) *J. Phys. Chem. B* **116**, 8812–8821.
35. Bjorndahl, T.C., Zhou, G.P., Liu, X., Perez-Pineiro, R., Semenchenko, V., Saleem, F., Acharya, S., Bujold, A., Sobsey, C.A., and Wishart, D.S. (2011) *Biochemistry* **50**, 1162-1173.
36. Durr, E., Jelesarov, I., and Bosshard, H.R. (1999) *Biochemistry* **38**, 870-880.
37. Blasie, C.A., and Berg, J.M. (1997) *Biochemistry* **36**, 6218-6222.
38. Gilson, M.K., Rashin, A., Fine, R., Honig, B.H. (1995) *J. Mol. Biol.* **183**, 503-516.
39. Hollecker, M., and Creighton, T.E. (1982) *Biochim. Biophys. Acta* **701**, 395-404.
40. Horovitz, A., Serrano, L., Avron, B., Bycroft, M., and Fersht, A.R. (1990) *J. Mol. Biol.* **216**, 1031-1044.
41. Lumb, K.J., and Kim, P.S. (1995) *Science* **268**, 436-439.
42. Pace,C. N., Laurents, D.V., and Thomson, J.A. (1990) *Biochemistry* **29**, 2564-2572.
43. Sali, D., Bycroft, M., and Fersht, A.R. (1991) *J. Mol. Biol.* **220**, 779-788.
44. Schaller, W., and Robertson, A.D. (1995) *Biochemistry* **34**, 4714-4723.
45. Spector, S., Wang, M., Carp, S.A., Robblee, J., Hendsch, Z.S., Fairman, R., Tidor, B., and Raleigh, D.P. (2000) *Biochemistry* **39**, 872-879.
46. Kohn, W.D., Kay, C.M., and Hodges, R.S. (1997) *J. Mol. Biol.* **267**, 1039-1052.
47. Strop, P., and Mayo, S.L. (2000) *Biochemistry* **39**, 1251-1255.
48. Waldburger, C.D., Schildbach, J.F., and Sauer, R.T. (1995) *Nature Struct. Biol.* **2**, 122-128.
49. Luisi, D.L., and Raleigh, D.P. (2000) *J. Mol. Biol.* **299**, 1091–1100.
50. Cavagnero, S., Debe, D.A., Zhou, Z.H., Adams, M.W.W., and Chan, S.I. (1998) *Biochemistry* **37**, 3369-3376.
51. LoÂ pez-Arenas, L., SolõÂs-Mendiola, S., and HernaÂndez-Arana, A. (1999) *Biochemistry* **38**, 15936-15943.

52. SolõÂs-Mendiola, S., GutieÂrrez-GonzaÂ lez, L.H., Arroyo-Reyna, A., Padilla-ZuÂnÄ iga, J., Rojo-DomõÂnguez, A., and HernaÂndez-Arana, A. *Biochim. Biophys. Acta* **1388**, (1998) 363-372.
53. Horng, J-.C., Cho, J-.H., and Raleigh, D.P. (2005) *J. Mol. Biol.* **345**, 163–173.
54. Tissot, C., Vuilleumier, S., and Fersht, A.R. (1996) *Biochemistry* **35**, 6786-6794.
55. Satoshi, S., and Raleigh, D.P. (2002) *J. Mol. Biol.* **318**, 571-582.
56. Tan, Y.J., Oliveberg, M., Fersht, A. (1996) *J. Mol. Biol.* **264**, 377-389.
57. Tan, Y.J., Oliveberg, M., Davis, B., and Fersht, A.R. (1995) *J. Mol. Biol.* **254**, 980-992.
58. Oliveberg, M., Arcus, V.L., and Fersht, A.R. (1995) *Biochemistry* **34**, 9424-9433.
59. Vanderkooi, J.M., and Erecinska, M. (1975) *Eur. J. Biochem.* **60**, 199-207.
60. Tsong, T.Y. (1974) *J. Biol. Chem.* **249**, 1988-1990.
61. Kumar, R., Prabhu, N.P., Rao, D.K., and Bhuyan, A.K. (2006) *J. Mol. Biol.* **364** (2006) 483–495.
62. Bhuyan, A.K., and Kumar, R. (2002) *Biochemistry* **41**, 12821-12834.
63. Kumar, R., and Bhuyan, A.K. (2005) *Biochemistry* **44**, 3024-3033.
64. Sanchez, K.M., Schlamadinger, D.E., Gable, J.E., and Kim, J.E. (2008) *J. Chem. Ed.* **85,** 1253–1256.
65. Latypov, R.F., Maki, K., Cheng, H., Luck, S.D., and Roder, H. (2008) *J. Mol. Biol.* **383,** 437-453.
66. Santoro, M.M., and Bolen, D.W. (1988) *Biochemistry* **27**, 8063-8068.
67. Bhuyan, A.K, and Udgaonkar, J.B. (2001) *J.Mol. Biol.* **312**, 1135-1160.
68. Osterhout, J.J., Muthukrishnan, Jr.T.K., and Nall, B.T. (1985) *Biochemistry* **24,** 6680-6684.
69. Whitten, S.T., Wooll, J.O., Razeghifard, R., Moreno E, B.G., and Hilser, V.J. (2001) *J. Mol. Biol.* **309,** 1165-1175.
70. Allen, D.L., and Pielak, G.J. (1998) *Prorein Science* **7**, 1262-1263.
71. Uchiyama, S., Oshima, A., Nakamura, S., Hasegawa, J., Terui, N., Takayama, S.J., Yamamoto, Y., Sambongi, Y., and Kobayashi, Y. (2004) *J. Am. Chem. Soc.* **126**, 14684-14685.
72. Varhac, R., M. Antalik, M., and Bano, M. (2004) *J. Biol. Inorg. Chem.* **9**, (2004) 12-22.
73. Jain, R., Sharma, D., and Kumar, R. (2013) *J. Biochem.* **154**, 341–354.
74. Kumar, S., Sharma, D., Kumar, R., (2014) *BBA- Prot. and Proteom.* **1844**, 641-655.

75. Santoro, M.M., and Bolen, D.W. (1992) *Biochemistry* **31**, 4901-4907.
76. Grazianoa, G., Catanzanoa, F., and Baronea, G. (2000) *Thermochim. Acta* **345**, 59-66.
77. Venkataramani, S., Truntzer, J., and Coleman, D.R. (2013) *J. Pharmacy & BioAllied Sci.* **5**, 148-153.
78. Yadaiah, M., Kumar, R., and Bhuyan, A.K. (2007) *Biochemistry* **46,** 2545-2551.
79. Bhuyan, A.K. (2002) *Biochemistry* **41**, 13386-13394.
80. Kumar, R., Prabhu, N.P., Yadaiah, M., and Bhuyan, A.K. (2004) *Biophys. J.* **87,** 2656-2662.
81. Wyman, J.Jr. (1964) *Advan. Protein Chem.* **16**, 223-245.
82. Cohen, D.S., and Pielak, G.J. (1994) *Protein Science* **3**, 1253-1260.
83. Kumar, R., Prabhu, N.P., and Bhuyan, A.K. (2005) *Biochemistry* **44**, 9359-9367.
84. Jones, C.M., Henry, E.R., Hu, Y., Chan, C.K., Luck, S., Bhuyan, A.K., Roder, H., Hofrichter, J., and Eaton, W.A. (1993) *Proc. Natl. Acad. Sci. USA* **90,** 11860-11864.
85. Hagen, S.J., Carswell, C.W., and Sjolander, E.W. (2001) *J. Mol. Biol.* **305**, 1161-1171.
86. Davies, M.N., Toseland, C.P., Moss, D.S., and Flower, D.R. (2006) *BMC Biochem.* **7,** 18.
87. Lee, A.C., and Crippen, G.M. (2009) *J.* Chem. Inf. Model **49**, 2013-2033.
88. Stanton, C.L., and Houk, K.N., (2008) *J. Chem. Theory Comput.* **4**, 951-966.
89. Bas, D.C., Rogers, D.M., and Jensen, J.H. (2008) *Proteins* **73**, 765-783.
90. Olsson, M.H.M., Søndergaard, C.R., Rostkowski, M., and Jensen, J.H. (2011) *J. Chem. Theory Comput*. **7**, 525–537.

List of Publications

Papers in SCI/referred journals

1. **Rishu Jain,** Sandeep Kaur and Rajesh Kumar, "Guanidine hydrochloride-induced alkali molten globule model of horse ferrocytochrome *c*" (2013) ***Journal of Biochemistry*** 153 (2), 161-177.

2. **Rishu Jain,** Deepak Sharma and Rajesh Kumar, **"**Effects of alcohols on the stability and low-frequency local motions that control the slow changes in structural dynamics of ferrocytochrome *c*" (2013) ***Journal of Biochemistry*** 154 (4), 341-354.

3. Rajesh Kumar*****, **Rishu Jain** and Rajesh Kumar, **"**Viscosity-dependent structural fluctuation of the M80-containing Ω-loop of horse ferrocytochrome *c*" (2013) ***Chemical Physics*** 418, 57-64.

4. **Rishu Jain,** Deepak Sharma, Sandeep Kumar and Rajesh Kumar, "Factor defining the effects of glycine betaine on the thermodynamic stability and internal dynamics of horse cytochrome *c*" (***Biochemistry, Revision submitted, bi-2014-00356c.R1***).

5. **Rishu Jain,** and Rajesh Kumar, "Analysis of the pH-dependent stability and folding kinetics of horse cytochrome *c*" (2014) **(*BBA - Proteins and Proteomics, Revision Requested, BBAPRO-S-14-00075*).**

6. **Rishu Jain,** Deepak Sharma and Rajesh Kumar, "Structural, kinetic, and thermodynamic characterizations of SDS-induced molten globule state of a highly negatively charged cytochrome *c*" (2014) (***Journal of Biochemistry, Revision Requested- JB-14-02-0031***).

Papers/ posters in Conferences

1. **Rishu Jain,** Deepak Sharma and Rajesh Kumar,"Thermodynamic analysis of effect of alcohols on thermal stability of horse ferrocytochrome *c*" International symposium on protein folding and dynamics, **NCBS-2012**, Bangalore.

2. **Rishu Jain,** and Rajesh Kumar, "Guanidine hydrochloride-induced folding and stabilization of alkali denatured carbonmonoxycytochrome *c*" International symposium on protein folding and dynamics, **NCBS-2012**, Bangalore.

3. Sandeep Kaur, **Rishu Jain** and Rajesh Kumar, "Effect of osmolytes on the stability and motional dynamics of horse ferrocytochrome *c*" National conference on advances in chemical engineering **(A chemE-2011),** Thapar University, Patiala.

4. **Rishu Jain** and Rajesh Kumar, **"**Effect of neutral salts on the stability and dynamics of horse cytochrome *c*" National Conference on emerging trends in Chemistry-Biology interface **(ETCBI– 2011)**, Kumaun University, Nainital.

5. Sandeep Kumar**, Rishu Jain** and Rajesh Kumar, "Iron release from diferric ovotransferrin in the absence of chelators involves six kinetic steps at acidic pH" 6^{th} National conference on thermodynamics of Chemical and Biological systems **(NCTCBS– 2011),** MDU, Rohtak.

6. **Rishu Jain** and Rajesh Kumar, "Entropic stabilization of ferrocytochrome *c* by subdenaturing concentrations of methanol" Functional materials for sustainable energy and advanced technologies **(MRSI-AGM-2012)**, Thapar University, Patiala.

7. **Rishu Jain,** and Rajesh Kumar, "The size of anions and crowding agents control the local dynamics of a native-like compact state of horse ferrocytochrome *c*" National conference on innovative molecules for sustainable future, **(NCIMSF-2013),** Thapar University, Patiala.